Application and Refinement of COSMO-RS-ES for calculating phase equilibria of electrolyte systems at high concentrations in mixed and non-aqueous solvents

Vom Promotionsausschuss der
Technischen Universität Hamburg
zur Erlangung des akademischen Grades
Doktor-Ingenieur (Dr.-Ing.)

genehmigte Dissertation

von
Simon Müller

aus
Zeven

2020

DOI: https://doi.org/10.15480/882.2994
ORCID: https://orcid.org/0000-0003-1684-6994

1. Gutachterin: Prof. Dr.-Ing. Irina Smirnova
2. Gutachter: Apl. Prof. Dr. rer. nat. Kai Olaf Leonhard
Vorsitzender des Prüfungsausschusses: Prof. Dr.-Ing. Maksym Dosta

Datum der mündlichen Prüfung: 07.08.2020

Danksagung

Ich blicke dankbar auf die Jahre als Doktorand am Institut für Thermische Verfahrenstechnik an der Technischen Universität Hamburg zurück. Es war mir eine Freude mit so einer Vielzahl von Nationalitäten zusammenzuarbeiten. Ich habe mich sehr wohl gefühlt und es genossen, immer wieder verschiedene Sprachen zu hören und interessante kulinarische Spezialitäten probieren zu dürfen.

Es war für mich eine Zeit des Wachsens, in der Frau Prof. Dr.-Ing. Irina Smirnova mir stets mit ihrer Unterstützung zur Seite stand und durch ihre zielführende Betreuung zu einer erfolgreichen Dissertation verholfen hat. Vielen Dank dafür, dass ich neue Ideen ausprobieren durfte und Sie immer ein offenes Ohr hatten, wenn es mal knifflig wurde.

Herrn Apl. Prof. Dr. rer. nat. Kai Leonhard möchte ich für die detaillierte Begutachtung der Dissertation danken. Die Diskussionen und Anregungen haben mir sehr geholfen. Herrn Prof. Dr.-Ing. Maksym Dosta danke ich herzlich für die Übernahme des Prüfungsvorsitzes.

Mit meinen Bürokollegen Wienke, Victor, Andrés, Razan und/oder den anderen Mitgliedern der Gruppe Molekulare Methoden Sven, Deni, Ralena, Oliver, Jan Philipp, und Xihua durfte ich oft lachen. Vielen Dank an alle Mitarbeiter für die gute Zeit und die wertvollen Gespräche und Diskussionen. Wenn ich mal bei der Bürokratie nicht weiterwusste, war Steffi stets da, um mir mit Geduld zu helfen oder mich beim Mittagessen nicht alleine in der Küche sitzen zu lassen. Danke für deine Zeit und dein offenes Ohr, auch in schwierigen Zeiten. Im Labor hat mich Marianne auch tatkräftig und kompetent unterstützt.

Vielen Dank auch den Studierenden und studentischen Hilfskräften, die mich während meiner Arbeit begleitet haben und maßgebend zum Erfolg der Arbeit beigetragen haben.

Meiner Familie und meinen Freunden möchte ich danken für die Unterstützung und die Motivation, die mir über die Jahre geholfen hat, mich immer wieder aufzubauen. Vor allem aber möchte ich meiner Frau Mery danken, für ihre Liebe, dass sie mir auch in den stressigen Zeiten zur Seite gestanden hat und mich ab und zu zur richtigen Zeit auch mal abgelenkt hat.

Abstract

For an efficient process design to save resources and time or for a first estimation during the beginning phase of the development, predictive thermodynamic models are a key tool. COSMO-RS is an efficient method that allows prediction of thermodynamic properties without the need for binary interaction parameters which in many cases have to be adjusted to experimental data. The electrolyte extension of this model, namely COSMO-RS-ES, has been shown to be a very versatile model being capable of predicting very diverse phase equilibria in electrolyte systems. The model employs an especially modified COSMO-RS model to describe the short-range interactions of the different species combined with the Pitzer-Debye-Hückel model to describe the long-range ionic interactions.

In this work, the model was successfully extended to be able to calculate solubilities of inorganic solvents in mixed-solvent and completely non-aqueous systems. Some systematic deviations could be found, which could be attributed to the short-range or the long-range part of the model respectively.

By including Gibbs free energies of transfer of ions into the training set of the model, the short-range description of the ionic interactions was improved, allowing for a better prediction of salt solubilities in a wide range of solvents. To also improve the long-range interactions of the model, the influence of using the solution properties such as permittivity and density was assessed leading to several important observations for this part of the model. As other models include a Born term to describe the ion solvation better, which so far is not considered within the COSMO-RS-ES model, this possibility is investigated. Furthermore, the model is enhanced to explicitly describe the effect of ion-pairing which becomes prominent for systems with a very low permittivity. With these developments, the predictive capabilities of the model are greatly advanced.

Two completely non-aqueous liquid-liquid equilibrium systems and four solid-liquid equilibria are measured and modelled with COSMO-RS-ES leading to a better understanding of how the model works for these complex systems.

Finally, the model is reparametrized from the ground up to allow prediction of pKa values, applying the model to free solvation energies for the first time.

Table of contents

Table of contents ..... **vii**

Symbols and abbreviations ..... **x**

1 Introduction **1**

2 Fundamentals **3**

2.1 Thermodynamic principles 3

2.2 Electrolyte systems 5

2.2.1 The behavior of ions in solution 5

2.2.2 Electrostriction, dielectric saturation and dielectric decrement 10

2.2.3 Activity coefficients in electrolyte solutions 14

2.2.4 Calculation of thermodynamic properties in electrolyte systems 15

2.3 Modeling of intermolecular interactions 18

2.3.1 The Born model 20

2.3.2 COSMO 21

2.3.3 COSMO-RS 22

2.3.4 Pitzer-Debye-Hückel model 26

2.3.5 COSMO-RS-ES 29

2.3.6 Modeling of ion-pairing 31

3 State of the art **35**

3.1 Modeling of phase equilibria of electrolyte systems 35

3.2 Liquid-liquid equilibria in completely non-aqueous electrolyte systems 40

4 Objectives **43**

5 Computational details and experimental methods **45**

5.1 Computational details 45
5.1.1 COSMO-RS-ES details 45
5.1.2 Procedure for model parameterization and evaluation 46
5.1.3 Database used for model parameterization and evaluation 49
5.2 Experimental methods 51
5.2.1 Preparation of chemicals 51
5.2.2 Method for the measurement of the liquid-liquid phase equilibria 51
5.2.3 Analytical methods 52

6 Results and discussion 55

6.1 Extension of COSMO-RS-ES: highly concentrated, mixed-solvent systems 56
6.2 Refinement of COSMO-RS-ES: the SR term 63
6.2.1 Parameterization A: Including Gibbs free energies of transfer 65
6.3 Refinement of COSMO-RS-ES: the LR term 70
6.3.1 Sensitivity of the long-range term towards its input parameters 70
6.3.2 The influence of the closest approach parameter 72
6.3.3 The influence of the permittivity and the dielectric decrement 75
6.3.4 Summary and important considerations for the improvement of the long-rang term 88
6.4 Refinement of COSMO-RS-ES: the interplay of SR and LR interactions 90
6.4.1 Evaluation of the description of ion-pairing by Fuoss and by Bjerrum 93
6.4.2 Parameterization B: Inclusion of ion-pairing according to Bjerrum 95
6.5 Experimental and computational analysis of non-aqueous LLE 105
6.6 Application of COSMO-RS-ES for calculating free solvation energies and pKa values 111

7 Conclusions 121

8 Appendix 127

8.1 Complementary evaluations 127
8.1.1 Solubility products 127
8.1.2 Infinite dilution activity coefficients for hydrocarbons 128
8.1.3 Evaluation conformer equilibrium 129
8.1.4 Evaluation of relative importance in the terms of the SLE calculation 130
8.2 Solving Bjerrum's integral 131
8.3 Experimental data for non-aqueous phase equilibria 132
8.4 Dataset used with COSMO-RS-ES for training and evaluation 134
8.4.1 MIAC (aqueous) dataset at 298.15 K 134
8.4.2 MIAC (organic) dataset at 298.15 K 135
8.4.3 LLE dataset 136
8.4.4 SLE dataset at 298.15 K 138
8.4.5 Gibbs free energy of transfer of ions dataset at 298.15 K 143
8.4.6 Dielectric decrement dataset at 198.15 K 148

9 Bibliography 151

10 Relevant publications 179

11 Student theses 181

12 Curriculum Vitae ..... Error! Bookmark not defined.

Symbols and abbreviations

Latin symbol	Meaning
$\mathbf{a}$	closest approach distance
$\boldsymbol{A}$	Helmholtz free energy / Area
$\boldsymbol{A_{\varphi}}$	Debye-Hückel parameter
$\boldsymbol{b}$	Closest approach parameter
$\mathbf{c}$	Molar concentration
$\mathbf{d}$	Distance
$\boldsymbol{e}$	Charge of the electron
$\mathbf{E}$ / $\mathbf{e}$	Energy
$\boldsymbol{\vec{E}}$	Electric field
$\boldsymbol{f(x)}$	Function of x
$\boldsymbol{f_{\mathbf{corr}}}$	Model parameter
$\mathbf{F}$	Force / value of the objective function
$\boldsymbol{g}$	Kirkwood g-factor / radial distribution function
$\mathbf{\Delta g^{\circ}_{f,i,aq}}$	Standard aqueous Gibbs formation energy for species i
$\boldsymbol{G}$	Gibbs free energy
$\boldsymbol{\Delta G_f}$	Formation energy
$\mathbf{\Delta G^{o}_{solv}}$	Solvation energy
$\boldsymbol{H}$	Enthalpy
$\boldsymbol{I}$	Ionic strength
$\boldsymbol{k_B}$	Boltzmann constant
$\boldsymbol{K}$	Partition ration
$\boldsymbol{K_{SP}}$	Solubility product
$\mathbf{m}$	molal concentration
$\boldsymbol{M}$	Cation / molecular mass
$\boldsymbol{n}$	Amount of substance
$\boldsymbol{N_A}$	Avogadro constant
$\boldsymbol{P}$	Pressure / probability
$\mathbf{r}$	Radius
$\boldsymbol{R}$	Universal gas constant
$\boldsymbol{S}$	Entropy / solvent
$\boldsymbol{T}$	Temperature
$\mathbf{u}$	Potential energy
$\boldsymbol{U}$	Internal energy
$\boldsymbol{V}$	Volume
$\boldsymbol{w}$	Weighting factor
$\boldsymbol{x}$	Mole fraction / model parameter
$\boldsymbol{X}$	Anion / surface fraction of a segment
$\boldsymbol{z}$	Charge

Greek symbol	Meaning
$\boldsymbol{\alpha}$	Dissociation degree / activity / parameter
$\boldsymbol{\alpha'}$	Misfit constant
$\boldsymbol{\Gamma}$	Segment activity coefficient
$\boldsymbol{\gamma}$	Activity coefficient
$\boldsymbol{\epsilon}$	Relative permittivity
$\boldsymbol{\epsilon_\infty}$	Permittivity in the vacuum
$\boldsymbol{\Theta}$	Fraction of molecules not irrotationally bound
$\boldsymbol{\lambda}$	Ionic conductivity
$\boldsymbol{\lambda_B}$	Bjerrum length
$\boldsymbol{\lambda_D}$	Debye length
$\boldsymbol{\mu}$	Chemical potential / dipole moment
$\boldsymbol{\nu}$	Molar volume / stoichiometric coefficient
$\boldsymbol{\xi}$	Generic measure of concentration
$\boldsymbol{\rho}$	Density
$\boldsymbol{\sigma}$	Screening charge density
$\boldsymbol{\tau}$	Relaxation time / function of interaction energies
$\boldsymbol{\phi}$	Volume fraction / osmotic coefficient
$\boldsymbol{\Psi}$	Electrostatic potential

Subscript	Meaning
$\pm$	Mean ionic value
∞	Infinite frequency
0	In vacuum
A	Association
an	Anion
acc	Hydrogen bond acceptor
av	Average
cat	Cation
corr	Local charge correlations
coord	Coordination
don	Hydrogen bond donor
DP	Datapoints
eff	Effective
hal	Halide
HB **/ hb**	Hydrogen bonds
i	Species i
ij	Contact between species *i* and *j*
I, ***J***	Segment type indices
IJ	Contact between segments of type *I* and *J*
int	Interaction
IP	Ion pair
m	Measured
mf	Misfit
min	Minimum
norm	Normalized
om	Organic molecule
pa	Polyatomic anion
pc	Polyatomic cation
r	Relative
s	Solvent
salt	Salt property
sf	Salt-free
solv	Solvation
tr	Transfer
$\boldsymbol{w \rightarrow s}$	From water to solvent

Superscript	Meaning
+	Reference state / positively charged
-	Negatively charged
(c)	Molar concentration
(m)	Molal concentration
(x)	Mole fraction
∞	Infinite dilution
⊥	Orthogonal
0	Standard
α	Related to phase alpha
β	Related to phase beta
calc	calculated
cloud	Ionic cloud
comb	Combinatorial
el	Electrostatic
exp	Experimental
E	Excess
lit	Literature value
LR	Long-range
MSD	Mean signed deviation
O	Organic-rich phase
res	Residual
RMSE	Root mean square error
s	Solvent
S	Salt-rich phase
SR	Short-range
T	Related to the temperature
w	Water

Abbreviation	Meaning
2SIP	Solvent-separated ion pairs
AAD	Average absolute deviation
ARD	Average relative deviation
AIOMFAC	Aerosol Inorganic–Organic Mixtures Functional-groups Activity coefficient model
aq	Aqueous
CIP	Contact ion pairs
CPA	Cubic Plus Association EOS
COSMO	Conductor like Screening MOdel
COSMO-RS	COSMO for Realistic Solvation
COSMO-RS-ES	COSMO for Realistic Solvation in Electrolyte Solutions
COSMO-SAC	COSMO Segment Activity Coefficient
DES	Deep eutectic solvent
DFT	Density functional theory
DMSO	Dimethyl sulfoxide
EOS	Equation of state
EXAFS	Extended X-ray absorption fine structure
g^E-models	Excess Gibbs free energy models
IDAC	Infinite dilution activity coefficient
IEFPCM	Integral equation formalism polarizable continuum model
LIFAC	Li Functional groups Activity coefficient model
LLE	Liquid-liquid equilibrium
MIAC	Mean ionic activity coefficient
MSA	Mean spherical approximation
MX	Salt with cation M and anion X
NRTL	Non-random two-liquid model
org	Organic
PDH	Pitzer-Debye-Hückel model
pKa	Negative logarithm of the dissociation constant
RSK	Redlich-Soave-Kwong EOS
SAFT	Statistical Associating Fluid Theory
SLE	Solid-liquid equilibrium
SSIP	Solvent-shared ion pairs
UNIQUAC	UNIversal Quasichemical model
UNIFAC	UNIversal quasichemical Functional-group Activity Coefficients model
VLE	Vapor-liquid equilibrium

1 Introduction

There is hardly another chemical species with more impact on the thermodynamics of a mixture than the electrolyte. Its dissociation into highly charged ions in fluid phases causes a reorientation of the surrounding polar molecules, i.e. modifying its structure (cf. Figure 2.1) and making the description of these systems more challenging than others. In other words, as people with lifelong experience on electrolytes have stated[1]: 'Life is too short for electrolytes'.

It is this difficulty that firstly lead the development of thermodynamic models into more simple and dilute solutions of aqueous electrolytes.[2] This situation is very similar when it comes to assessing the available experimental data for electrolytes. Most measured data include water at least as one of the solvents. These reasons explain why the development of thermodynamic models for electrolytes so far has not focused much on highly concentrated nor on non-aqueous systems.

In most cases, traditional thermodynamic models undergo large modifications to be able to be applied to electrolyte systems.[3] Although some exceptions exist, most of these models require binary interaction parameters to accurately describe the thermodynamics of these complex systems. Of the available g^E-models, one of the most widely applicable predictively for electrolyte systems are LIFAC[4] and AIOMFAC[5]. However, since these models are based on group contribution methods, they are confined to the use of components for which parameters are available.

The issue concerning the availability of parameters in many cases also applied to systems composed of neutral components until COSMO-RS was developed by Klamt[6,7]. By describing the thermodynamics of mixtures as a function of the polarity of the molecules calculated from quantum chemistry, the model is able to describe many systems predictively without the need for binary interaction parameters.

Although COSMO-RS has previously been applied successfully for delocalized ions such as ionic liquids[8] and in some DESs[9], modifications of the model are necessary for the description of highly charged ions[10–13] such as for example the alkaline halide salts. To address these issues, in previous work[14] by Gerlach, COSMO-RS was modified to be able

to truly predict the phase equilibria in electrolyte solutions. It was shown that the new model COSMO-RS in Electrolyte Solutions (COSMO-RS-ES) is capable of calculating and even predicting aqueous MIACs, LLEs and VLEs for a wide variety of systems quite accurately.

The objective of this work is to evaluate and further develop COSMO-RS-ES with a special focus on the improvement of the calculation of highly concentrated and non-aqueous systems. For this goal a large database of literature data is gathered. The model is analyzed systematically to improve its different contributions and their interplay with each other to extend the predictive applicability of the model to a wider range of thermodynamic equilibria

The results of this work have partially been published by Müller et al.[15], Müller et al.[16] and Kröger et al.[17].

2 Fundamentals

This chapter summarizes the theoretical basis of this work. It especially introduces details of electrolyte systems and describes the models implemented.

2.1 Thermodynamic principles

Any two phases α and β in a heterogeneous closed system are said to be in equilibrium when thermal, mechanical and chemical equilibrium equality exists between these[3]:

$$P^{\alpha} = P^{\beta} \tag{2.1}$$

$$T^{\alpha} = T^{\beta} \tag{2.2}$$

$$\mu_i^{\alpha} = \mu_i^{\beta} \tag{2.3}$$

While the pressure P and the temperature T are state variables closely related to the actual experimental measurement of thermodynamic equilibria, the chemical potential μ_i is a mathematical function introduced by Gibbs to describe the change in energy in a mixture as the number of moles of a substance i changes. It is therefore linked to the other thermodynamic potentials, namely the internal energy U, the enthalpy H, the Helmholtz free energy A and the Gibbs free energy G, as follows[3]:

$$\mu_i \equiv \left(\frac{\partial U}{\partial n_i}\right)_{\mathrm{S,V,n_j}} = \left(\frac{\partial H}{\partial n_i}\right)_{\mathrm{S,P,n_j}} = \left(\frac{\partial A}{\partial n_i}\right)_{\mathrm{T,V,n_j}} = \left(\frac{\partial G}{\partial n_i}\right)_{\mathrm{T,P,n_j}} \tag{2.4}$$

Because the chemical potential is a state function it can be described as a value at a specific reference state μ_i^{+} and a term describing the difference with respect to this reference state[3]:

$$\mu_i(T, P, \boldsymbol{x}) = \mu_i^{+}(T, P, \boldsymbol{x}^{+}) + RT\ ln\ a_i(T, P, \boldsymbol{x}) \tag{2.5}$$

Where the activity a_i is defined as the product of the mole fraction x_i and the activity coefficient γ_i:

$$a_i = x_i \cdot \gamma_i(T, P, \boldsymbol{x})$$

The activity coefficient describes the non-ideality of the mixture and consequently its value is unity for ideal mixtures. It can be defined based on other concentration units, however unless stated otherwise throughout this work, the mole fraction is used.

The chemical potential of one species is however not independent of the chemical potential of the other species in a mixture. They are connected through the Gibbs-Duhem relation[3]:

$$\sum_i n_i d\mu_i = SdT - VdP \tag{2.6}$$

Of which the right-hand side becomes zero in an isobaric and isothermal system.

When considering any two liquid phases α and β at thermodynamic equilibrium, it is possible to equate the chemical potential for a species i from Eq. (2.5) for both phases. Choosing the same reference state shows that the activity of every species in the different phases is equal:

$$x_i^\alpha \gamma_i^\alpha = x_i^\beta \gamma_i^\beta \tag{2.7}$$

Following this relation, it is possible to define the partition ratio of a species i in both phases:

$$K_i^{\alpha\beta} = \frac{x_i^\alpha}{x_i^\beta} = \frac{\gamma_i^\beta}{\gamma_i^\alpha} \tag{2.8}$$

2.2 Electrolyte systems

This chapter introduces to the specialties of how ions behave in solution in contrast to neutral molecules. Its effects on the structure of the liquid and the therefore existing modeling implications are discussed.

2.2.1 The behavior of ions in solution

Polar neutral molecules already exhibit certain ordering in solution, particularly when hydrogen bonds exist. (cf. Figure 2.1 left). However, this ordering is not as pronounced as in the case of charged species. When electrolytes are solubilized in a polar liquid, they tend to dissociate into highly charged ions keeping the overall charge of the mixture electroneutral. Although this process is dynamic, on a time-averaged scale the solvation can be described quasi-statically.[18] This reorientation leads to very large electrical fields interacting over much longer distances than neutral molecules and changing the local structure of the solvating molecules around it.[19]

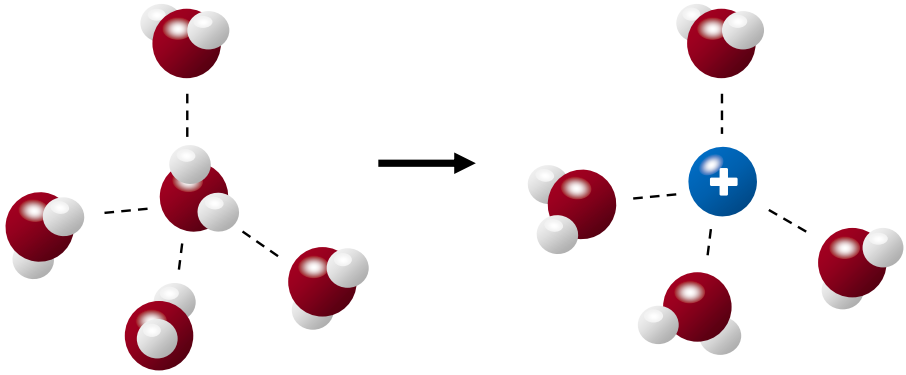

Figure 2.1: Example of the change in the structure of liquid water brought about by the introduction of a cation into the solution

Ionic solvation and pairing

The particular structure around a solvated ion forms the so-called solvation shell. Depending on the ion charge and size this shell can include one to several layers of solvent molecules. In mixtures of solvents the solvation shell can be filled with different molecules and in different ratios than the ratios of the bulk concentration. This preferential solvation is due to the more energetically favorable interaction of one solvent with the ion in comparison to the interaction with other solvents.[20] In condensed phases it is the

solvation shell that is most often used to define the quantity of the radii of the different ions. The radius can be defined as the distance between the ion and the first solvation shell. Although the definition of a radius of an atom is generally not a trivial task as approximations have to be made concerning the partitioning of the distance between the different atoms, in crystals the distance between the ions can be measured quite accurately[20]. It is possible to determine the radii e.g. from crystallographic data[21,22], from diffraction methods[23] or from solvation energies[24]. The radii from the solvation energies are usually calculated using the equation proposed by Born[20](cf. section 2.3.1).

Depending on the type of ion, the charge and the interaction with the different solvents, the radius of an ion might be assigned different values.[20] Table 2.1 shows three sets of radii of ions. As can be observed, the values can vary significantly although the relative size to each other and the trend expectedly remains similar.

Table 2.1: Different sets of ionic radii of alkali and halide ions.

	Radii of ions [Å]		
	from the Born equation[24]	**from measurements in solution**[23]	**from crystallographic measurements**
Li^+	1.46	0.71	0.74 [22]
Na^+	1.87	0.97	1.02 [22]
K^+	2.33	1.41	1.38 [22]
Rb^+	2.52	1.50	1.49 [22]
Cs^+	2.75	1.73	1.70 [22]
F^-	1.39	1.24	1.33 [22]
Cl^-	1.86	1.80	1.81 [25]
Br^-	2.00	1.98	1.96 [25]
I^-	2.23	2.25	2.20 [25]

The preferential solvation of an ion can also be analyzed as a function of the electrolyte concentration rather than the solvent composition. At low electrolyte concentrations and high permittivities, ions are usually dissociated mainly interacting with the available solvent. However, as the concentration increases, the interaction of one of the ions can be

more preferential towards the solvent than towards the other ion.[26] Especially at these high concentrations and in low permittivities ions tend to form ion-pairs and to be solubilized as such.[1,27] Conductivity measurements[28], dielectric spectroscopy[29] and EXAFS measurements[30] all suggest the existence of ion-pairs. One widely accepted definition of the possible types of ion-pairing divides them into solvent-separated, solvent-shared and contact ion pairs as shown in Figure 2.2. Neutral ion-pairs are considered to behave similar to neutral dipolar molecules[20], even forming higher order ion-pairs as the concentration increases further.[27]

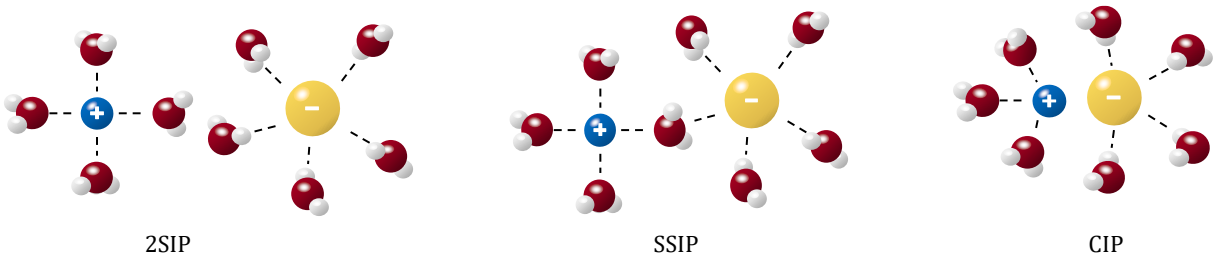

Figure 2.2: Types of ion pairs[27]: solvent-separated (2SIP), solvent-shared (SSIP) and contact ion pairs (CIP).

Following the observations by Eigen & Tamm[27], ion-pairing happens in steps from free ion-pairs to solvent-separated ion-pairs to solvent-shared ion-pairs to contact ion-pairs. For a 1:1 electrolyte (MX) ion-pairing can be described as the following reaction sequence[20]:

$$M^+_{free\ ion} + X^-_{free\ ion} \rightleftharpoons M^+(SS)X^- \rightleftharpoons M^+(S)X^- \rightleftharpoons M^+X^- \tag{2.9}$$

In many cases it can be simplified by observing only the association as a one step process between the free ions and the contact ion pair. By applying the law of mass action the molar concentration based association constant $\mathrm{K_A^{(c)}}$ can be calculated as follows[20]:

$$\mathrm{K_A^{(c)}} = \frac{(1-\alpha)\gamma_{IP}^{(c)}}{c\left(\alpha\gamma_{\pm}^{(c)}\right)^2} \tag{2.10}$$

Where α refers to the fraction of dissociated ions, c refers to the molar concentration of electrolyte, $\gamma_{IP}^{(c)}$ and $\gamma_{\pm}^{(c)}$ are the molar concentration based activity coefficients of the ion-pairs and of the free ions respectively.

Effects on the solubility of other solutes

Depending on its effects on the original structure of neutral solvents, the ions can be classified into two groups: chaotropes and kosmotropes. While chaotropes break the structure of the solvent, kosmotropes do the opposite increasing and stabilizing the local structure of the solvents.[19] This effect on the solution might affect the interaction of the solvent with other solutes. Chaotropes are said to increase the ability to solubilize other molecules causing "salting-in' while kosmotropes decrease the ability to solubilize other molecules leading to salting-out.

The effects on the solubility of other molecules have been studies extensively in the past due to its possibility to influence phase equilibria e.g. for a process to be more effective or viable in the first place. Already in the 19th century, Hofmeister started the first attempt at categorizing this effect.[31]

Figure 2.3 shows a summarized representation of the Hofmeister series of ions. The idea is that by keeping one ion constant and changing the counterion, the Hofmeister series predicts the trend of the effect of the salt on the ability of a solution to solubilize other solutes. And although the concepts of chaotropicity, kosmotropicity and the Hofmeister series were initially introduced for the influence of ions in water solutions only, it has been shown that similar effects might be observed in non-aqueous solutions as well.[32,33]

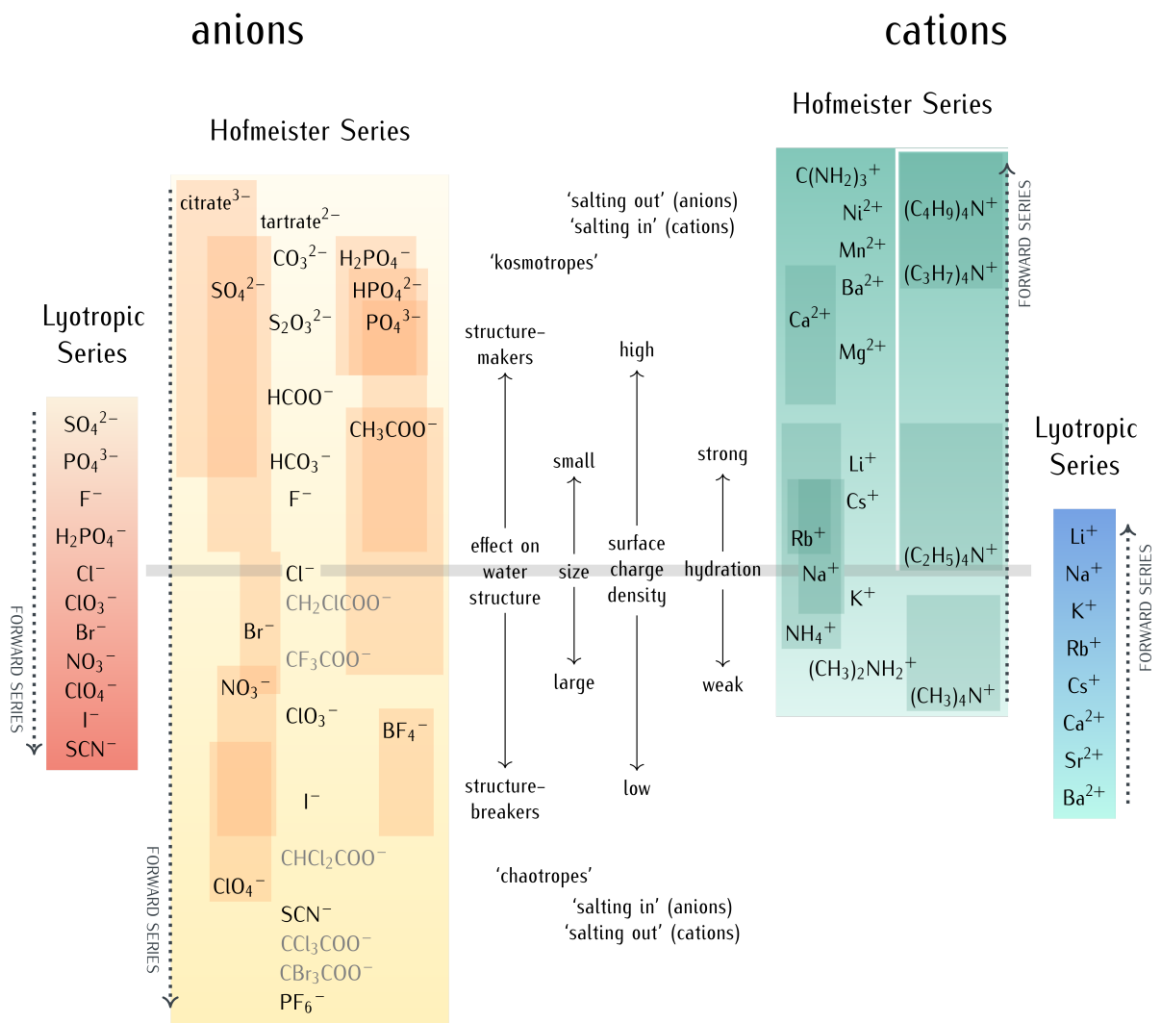

Figure 2.3: The effect of electrolytes on the solvation ability of solvents might be expressed as the Hofmeister series. To reflect the fact that different publications report different ordering of the Hofmeister series, the individual ions are enclosed in rectangles reflecting the values available in literature (used with permission from Mazzini[34])

2.2.2 Electrostriction, dielectric saturation and dielectric decrement

The strong interactions of the ions with the solvent causes the physical properties to behave differently than with other mixtures of species. With respect to the density, ions are capable of constraining the solvation shell causing a higher local density through the principle of electrostriction.[18] Electrostriction refers to the contraction of a substance due to an influence of an electric field, in this case the ions influence on the solvating molecules. To what extent this happens depends on the charge density of the ion, i.e. its electrical field and on the compressibility and the pressure derivative of the permittivity of the solvent.[35]

Closely related to this is the phenomenon of dielectric decrement because of the effect of dielectric saturation.[36] Due to the reorientation of dipoles caused by the solvation of ions and the strong interaction the ions hold on the molecules, the molecules lose the capability of orientational polarizability which results in a change in the measured dielectric constant of the mixture.[37] In most systems with a high permittivity the change in the measured dielectric constant is negative leading to a decrease of even more than 50%.[38] Figure 2.4 b) shows an example of this behavior. The decrease starts in a linear fashion for low electrolyte concentrations while as the concentration increases the effect becomes less pronounced. In systems with low permittivities due to the formation of ion-pairs, which can be considered to act similarly as dipoles in the mixture, the permittivity might increase with salt concentration.[39,40] There is however a difficulty with the measurement of the dielectric constant of these systems which is due to the effect of the kinetic depolarization.

Kinetic depolarization

In general, when measuring the static permittivity in conducting mixtures, a spectrum of the complex permittivity is measured at several oscillating fields on different frequencies as shown by Bucher et al[41]. Then a relaxation model is fitted to the data to extrapolate the permittivity to zero frequency to get the value of the static permittivity ϵ_{r} or to very high frequencies to estimate the value of the permittivity at infinite frequency ϵ_{∞}. The value of the static permittivity is also commonly known as the dielectric constant.[40,42] The problem with conducting mixtures of ions is that besides having to be adjusted by a conductivity contribution because of the ion drift, ions move due to the changing field at the moment of measuring. Therefore, there are more than one competing electrical field influencing

the orientational polarization and thus influencing the results of the measurement: namely the field applied to measure and the field from ions in the mixture. This effect that influences the measured value, called kinetic depolarization, is depicted in Figure 2.4 a).

Therefore the measured permittivity ϵ_{m} can be divided into the actual (thermodynamically relevant) permittivity ϵ_r and a contribution due to the kinetic depolarization $\epsilon_{kin.depol.}$ [43,44]:

$$\epsilon_{\mathrm{m}} = \epsilon_r + \epsilon_{kin.depol.} \tag{2.11}$$

With:

$$\epsilon_{kin.depol.} = -p\left(1 - \frac{\epsilon_\infty}{\epsilon_r}\right)\frac{\tau\lambda}{\epsilon_0} \tag{2.12}$$

Where p is a theoretical constant depending on the condition applied to the description of the friction of the ions with the surrounding molecules. For no-slip condition p = 1 and for perfect slip condition p = $\frac{2}{3}$. ϵ_∞ is the permittivity at infinite frequency, τ is the characteristic relaxation time of the solvent and λ is the ionic conductivity.

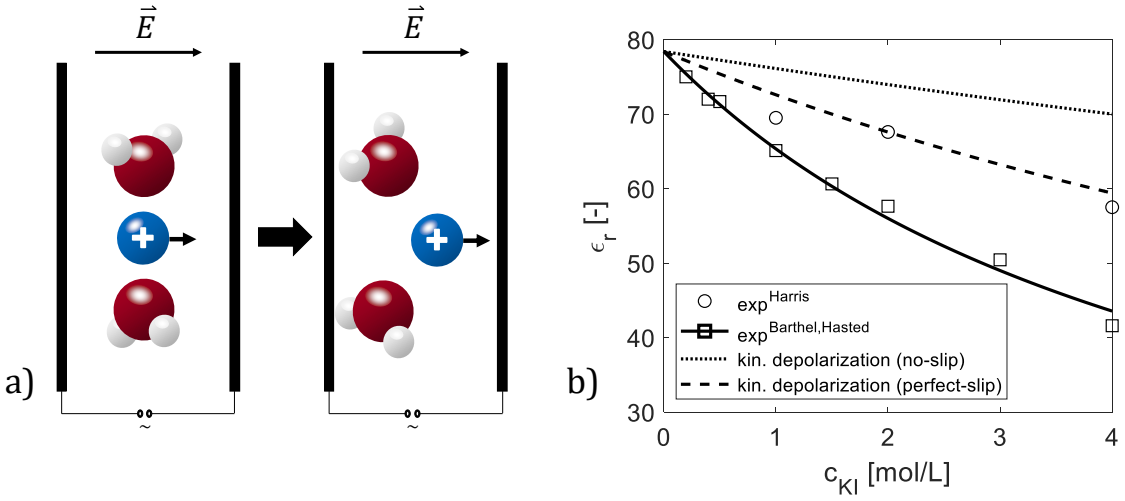

Figure 2.4: a) The effect of kinetic depolarization is the change in polarization of a mixture because of the reorientation of the dipoles in an electric field due to the movement of ions. b) Example of the influence of the concentration of potassium iodide on the dielectric constant of the mixture. The dashed and the dotted line show the effect of kinetic depolarization when applied to the measurements of Barthel et al.[45] and Hasted et al.[46] The values by Harris & O'Konski[47] deviate from the other values.

The real value should lie in between these two assumptions. In Figure 2.4 b), the shown experimental values of Barthel et al.[45] and Hasted et al.[46] agree with each other quite well.

The dashed and the dotted line show these values corrected for kinetic depolarization with both assumptions described above. The values by Harris & O'Konski[47] deviate from the other values largely, however fall into the area of the corrected values. The problem with the dielectric decrement data found in literatures is that some may have the correction for the dielectric decrement already included or not, but this is not necessarily mentioned.

Modeling the dielectric decrement

Many models have been proposed to describe the effect of dielectric decrement, some of which are more correlative just describing the phenomenon and others, which are more theoretically founded. Maribo-Mogensen gives an overview of some of the available models.[48] In light of the effect of kinetic depolarization the question about what is the correct thermodynamic permittivity value is difficult to respond. This is probably the reason why already Hückel experimented adjusting his dielectric decrement model either to the measured data or to the activity coefficients.[49]

Here we present a summary of three models to calculate the dielectric decrement that are quite different from each other and somewhat represent the broadness of available models.

The model by Simonin et al.[50] as extended by Inchekel et al.[51] and Zuber et al.[52] is a simple phenomenological model used to correlate the dielectric decrement data without a thorough theoretical background.

$$\epsilon_{\mathrm{r}} = \frac{\epsilon_{r,sf}}{1 + \Sigma_i \alpha_i \xi_i} \tag{2.13}$$

Where $\epsilon_{r,sf}$ corresponds to the salt-free permittivity, ξ_i corresponds to a measure of concentration and α_i to a parameter for the species i which could be an ion or a salt.

The model by Pottel[37] as applied by Zuber et al.[52,53] and Fürst et al.[54,55], is based on theoretical considerations of a simplified solvation model. As shown in Figure 2.6, if applied to multisolvent systems, with this model an electrolyte solution is considered as a mixture of 2 pseudo-species. The first pseudo-species consists of the solvents with a permittivity of $\epsilon_{r,sf}$ in which the second species consisting of ions with a solvation shell with a radius of $r_{i,solv}$ and a permittivity of $\epsilon_{r,solv} = 2$ is immersed:

$$\epsilon_{\mathrm{r}} = 1 + (\epsilon_{\mathrm{r,sf}} - 1)\frac{1 - \phi_{ions}}{1 + \left(\frac{\phi_{ions}}{2}\right)} \tag{2.14}$$

With the volume fraction of the ions ϕ_{ions} defined as:

$$\phi_{ions} = \frac{N_{\mathrm{A}}\pi}{6}\sum_{i}^{\text{ions}} \frac{n_i(2 \cdot r_{i,solv})^3}{V} = \frac{4N_{\mathrm{A}}\pi\rho}{3M}\sum_{i}^{\text{ions}} x_i {r_{i,solv}}^3 \tag{2.15}$$

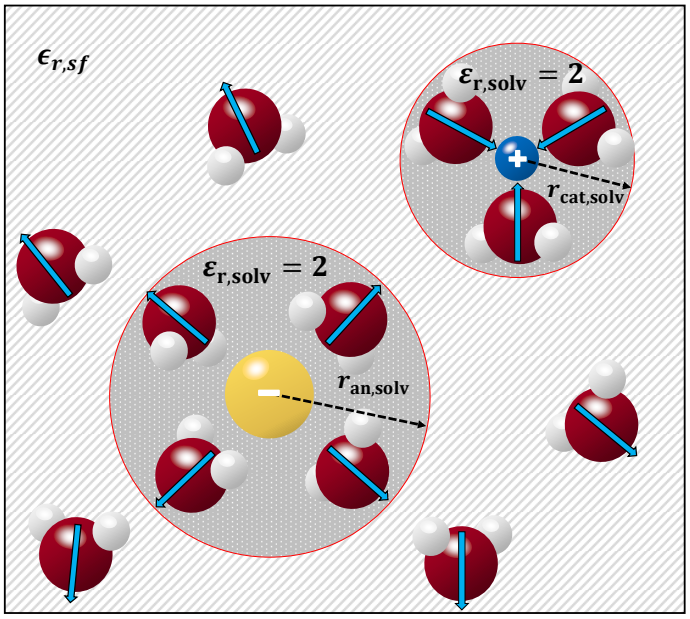

Figure 2.5: The model of Pottel[37,52,53] considers an electrolyte solution as a mixture of 2 pseudo-species. The first of the pseudo-species consists of the solvents with a permittivity of $\epsilon_{r,sf}$ in which the second species consisting of ions with a solvation shell with a radius of $r_{i,solv}$ and a permittivity of $\epsilon_{r,solv} = 2$ is immersed. (Figure adapted from Franks[37])

The model by Maribo-Mogensen et al.[48] is a thorough model based on the papers by Onsager[56], Kirkwood[57] and Fröhlich[58]. With his first publication[59] he showed successfully how to calculate permittivities of neutral mixtures as a function of composition, pressure and temperature using an equation of state by adjusting one parameter for every pure component. To extend the model to electrolyte solutions, he introduced the effect of dielectric decrement by adding the parameter Θ_i to describe the fraction of molecules not irrotationally bound to an ion. As the fraction of molecules bound to an ion would not add to the overall permittivity ϵ_r due to the cancelling of the dipole moments $\mu_{i,0}$, similar as shown in Figure 2.6:

$$\frac{(2\epsilon_r + \epsilon_\infty)(\epsilon_r - \epsilon_\infty)}{\epsilon_r(\epsilon_\infty + 2)^2} = \frac{N_A}{9\epsilon_0 k_B T v}\sum_i x_i \Theta_i g_i \mu_{i,0}^2 \quad (2.16)$$

Where ϵ_∞ is the permittivity at infinite frequency calculated from the Clausius-Mosotti relation[60], v is the molar volume of the mixture, $\mu_{i,0}$ is the dipole moment and g_i is Kirkwood's g-factor calculated from a geometrical model using association probabilities calculated with Wertheim's theory.

2.2.3 Activity coefficients in electrolyte solutions

Through statistical mechanics it can be shown that the thermodynamics of a system are closely related to the amount of existing microstates[61]. As explained in section 2.2.1, introducing highly charged ions into a mixture changes the structure, i.e. the available states in a great manner. Thus, having a large effect on the thermodynamics.

The dissolution of a solid salt solvate can be described in the most general form as follows:

$$M_{\nu_{cat}}X_{\nu_{an}} \cdot nY(solid) \leftrightharpoons M_{\nu_{cat}}X_{\nu_{an}}(solubilized) + \nu_{cat}M^{z+} + \nu_{an}X^{z-} + nY \quad (2.17)$$

The solid salt solvate is solubilized in the liquid phase into undissociated $M_{\nu_{cat}}X_{\nu_{an}}(solubilized)$, dissociated ions $\nu_{cat}M^{z+}, \nu_{an}X^{z-}$ and the solubilized solvent prior forming part of the solid crystal. For a non-solvate salt dissociating completely this simplifies to:

$$M_{\nu_{cat}}X_{\nu_{an}} \leftrightharpoons +\nu_{cat}M^{z+} + \nu_{an}X^{z-} \quad (2.18)$$

This means that the chemical potential of a completely dissociated salt can be described in the following way:

$$\mu_{salt} = \nu_{cat}\mu_{cat} + \nu_{an}\mu_{an} \quad (2.19)$$

After introducing eq. (2.5) and (2.6) it might be rewritten as:

$$\mu_{salt} = \nu_{cat}(\mu_{cat}^{+} + RT\ln x_{cat}\gamma_{cat}) + \nu_{an}(\mu_{an}^{+} + RT\ln x_{an}\gamma_{an}) \quad (2.20)$$

However, as single-ion properties are elusive and they do not exist in nature as bare ions without the counterion, it is common practice to introduce the mean ionic mole fraction $x_\pm$ and the mean ionic activity coefficient $\gamma_\pm^+$ (MIAC) as follows:

$$\gamma_{\pm} = (\gamma_{cat}^{\nu_{cat}} \gamma_{an}^{\nu_{an}})^{1/(\nu_{cat}+\nu_{an})} \tag{2.21}$$

$$x_{\pm} = (x_{cat}^{\nu_{cat}} x_{an}^{\nu_{an}})^{1/(\nu_{cat}+\nu_{an})} \tag{2.22}$$

With this definition and by summing the chemical potential of the ions at the reference state, the chemical potential of a complete dissociating salt in solution with respect to the reference state + might be described very similarly to eq. (2.5):

$$\mu_{salt} = \mu_{salt}^{+} + RT \ln x_{\pm}\gamma_{\pm} \tag{2.23}$$

A common reference state for neutral components is the pure component at system pressure and temperature. However, the electrolyte behaves very differently in solution than it does in its pure solid or liquid form. Therefore, commonly for electrolytes the reference state of hypothetical ideal solution at unit concentration at system pressure and temperature are taken employing the asymmetric convention:

$$\lim_{x_{\pm}\to 0} \gamma_{\pm} = 1 \tag{2.24}$$

Unless otherwise noted, the reference state of the electrolyte is assumed to be the one just defined allowing to drop the superscript +.

2.2.4 Calculation of thermodynamic properties in electrolyte systems

To calculate phase equilibria of electrolyte solutions it is necessary to observe the constraints of electroneutrality.

In the case of liquid-liquid equilibria, equation (2.7) applies all the same with the only difference that for the ions instead of using the single-ion activity coefficients, the electrolyte is observed as a species with concentration $x_{\pm}$ and mean ionic activity coefficient $\gamma_{\pm}$ as defined in section 2.2.3.

The Gibbs free energy of transfer of an ion describes the energy necessary to transfer one ion at infinite dilution from water to another solvent. It therefore describes the difference in the chemical potential of one ion at infinite dilution between these two states and can therefore be calculated as follows:

$$\Delta G_{tr,ion\ w\to s}^{0} = \mu_{ion,s}^{\infty} - \mu_{ion,w}^{\infty} \tag{2.25}$$

With equation (2.5) if a common reference state is chosen, this might be reformulated as[62]:

$$\Delta G^{0}_{tr,ion\ w\to s} = RT \ln\left(\frac{\gamma^{\infty}_{ion,s}}{\gamma^{\infty}_{ion,w}}\right) \tag{2.26}$$

The Gibbs free energy of transfer of a salt is the sum of the Gibbs free energy of transfer of the ions:

$$\Delta G^{0}_{tr,salt\ w\to s} = \nu_{cat}\Delta G^{0}_{t,cat\ w\to s} + \nu_{an}\Delta G^{0}_{t,an\ w\to s} \tag{2.27}$$

To calculate the solid-liquid-equilibria there are several possibilities. If the same ansatz is used as with neutral molecules, the melting temperature and the melting enthalpy would be needed to calculate the solubility of a salt in different solvents. In this work, the solubilities are calculated using the solubility product, as the aim is to enable an easy applicability. It is usually much easier to measure a value for the solubility of an electrolyte in one solvent or to find the value in literature than to measure its melting temperature and enthalpy. Which would also not be easily applicable if the electrolyte decomposes at high temperatures.

Equation (2.20) can be rearranged putting the chemical potential of the solid and the chemical potentials at reference state to the left and at the same time introducing the solubility product in a reference solvent K_{SP} to:[15]

$$\frac{\mu_{salt(solid)} - \nu_{cat}\mu^{+}_{cat} - \nu_{an}\mu^{+}_{an}}{RT} = (\nu_{cat} + \nu_{an}) \ln(x_{\pm}\gamma_{\pm}) \equiv \ln K_{SP} \tag{2.28}$$

As the solubility product is only a function of temperature and reference state, it is possible to calculate the solubility in any solvent using the solubility product of the reference solvent (+). This is under the constraints of keeping the reference state, the temperature and the nature of the solid phase the same.

Mathematically this can be expressed by equating the chemical potential of the electrolyte in the solvent s and in the reference solvent (water) as follows:

$$\mu_s = \mu^{\infty}_s + RT\ ln\ x_{\pm,s}\gamma_{\pm,s} = \mu_w = \mu^{\infty}_w + RT\ ln\ x_{\pm,w}\gamma_{\pm,w} \tag{2.29}$$

By introducing equations (2.25) and (2.27) it can be written to:

$$(\nu_{cat} + \nu_{an})\, ln\, x_{\pm,s}\gamma_{\pm,s} + \frac{\Delta G^0_{tr,salt\ w\to s}}{RT} = (\nu_{cat} + \nu_{an})\, ln\, x_{\pm,w}\gamma_{\pm,w} = \ln K_{SP,w} \tag{2.30}$$

Figure 2.6 shows a visualization of the calculation approach for the solubility determination. First an experimental solubility in the reference solvent water ($x_{\pm,w}$) is used combined with a model to calculate the activity coefficient at that concentration ($\gamma_{\pm,w}$). Then the solubility product in water might be calculated. Using the model again it is possible to calculate the Gibbs free energy of transfer $\Delta G^0_{tr,salt\ w\to s}$ and the activity coefficient of the salt $\gamma_{\pm,s}$ to finally be able to determine the solubility in the other solvent $x_{\pm,s}$.

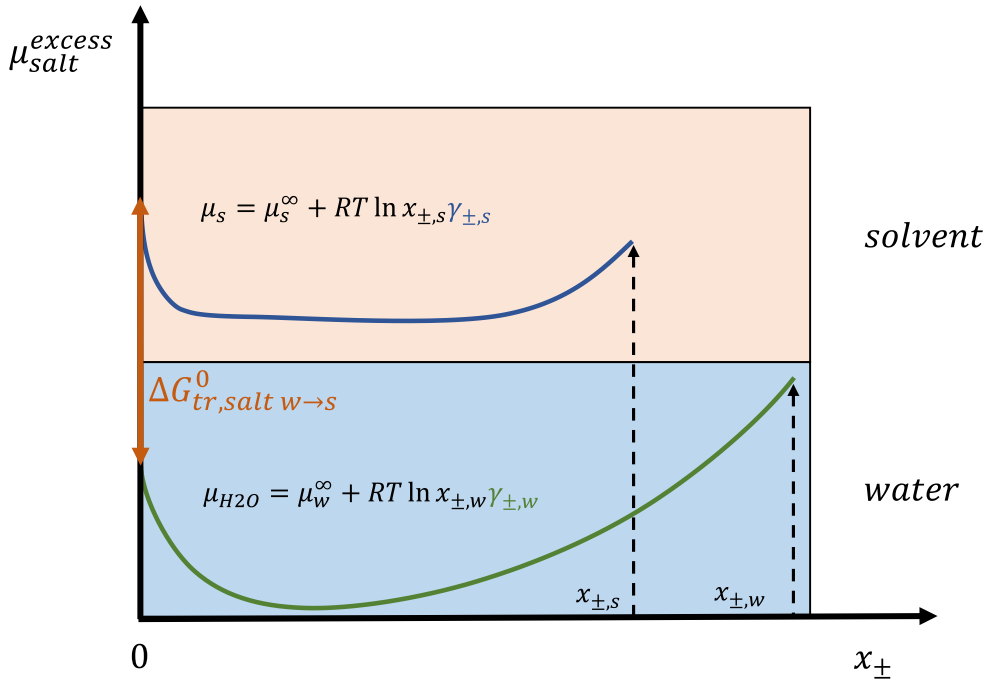

Figure 2.6: Visualization of the calculation of the solubility of an electrolyte in solvent $x_{\pm,s}$ from the solubility in the reference solvent water $x_{\pm,w}$ by means of a g^E-model to compute the activity coefficients.

2.3 Modeling of intermolecular interactions

The way how molecules interact with each other through the forces that govern their contacts will define how they will behave at certain compositions, temperature and pressure. And it is this behavior that dictates how the thermodynamics evolve at different conditions. These forces are usually expressed as the derivative of the interatomic or intermolecular potentials[3] with respect to the distance r:[3]

$$F = -\frac{du}{dr} \tag{2.31}$$

One group of potentials widely used e.g. in molecular dynamics is the potential proposed by Mie[63]:

$$u(r) = u_{min}\left[\frac{n}{n-m}\left(\frac{n}{m}\right)^{\frac{m}{n-m}}\right]\left[\left(\frac{d}{r}\right)^{n} - \left(\frac{d}{r}\right)^{m}\right] \tag{2.32}$$

Where u_{min} is the minimum of the potential, n is the exponent for the repulsive term , m is the exponent for the attractive term and d is the distance for which the potential vanishes as shown in Figure 2.7. The widely used Lennard-Jones potential is a special case of the Mie potential with fixed exponents: $n = 12, m = 6$.

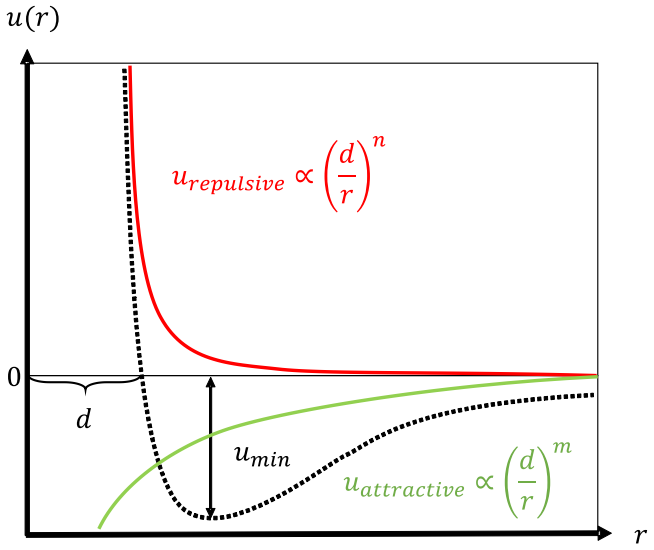

Figure 2.7: Example of an intermolecular potential $u(r)$ with its repulsive and attractive terms as a function of the distance r.

As equation (2.32) already suggests, the potential can have different exponents with relation to the distance r. This shows that forces can interact very differently being orders of magnitude larger or smaller than others at the same distance. There is no clear distinction, but intermolecular forces can be divided into short-range and long-range varying according to their dependence on the distance r[64]. Although it is not possible to assign a definitive proportionality of the intermolecular potential to a specific interaction, it is possible to estimate their order of magnitude as shown in Table 2.2.

Table 2.2:Proportionality of the intermolecular potential with respect to the distance[3,64].

Interaction type	$\boldsymbol{u(r)} \propto$
ion -ion	$1/r$
ion – dipole	$1/r^2$
dipole - dipole	$1/r^3$
dipole – induced dipole	$1/r^6$
induced dipole – induced dipole	$1/r^6$
repulsion	$1/r^{12}$

On some level, the majority of interactions can be called electrostatic, however they commonly are classified into electrostatic forces, induction forces, dispersion forces, repulsion forces and specific or quasi-chemical.[3]

Electrostatic forces are the ones occurring between species with highly localized charges (e.g. ions, dipoles, multipoles). Induction forces arise between species with highly localized charges interacting with their own induced dipoles. Dispersion forces exist when the oscillating electron clouds of two neighboring molecules synchronize creating an attractive force between 2 induced dipoles.[3] Specific or quasi-chemical forces might include for example hydrogen bonds[3] and ion-pairing[65]. The repulsion forces are mainly based on the Pauli exclusion principle.[64]

While for polar molecules, i.e. with a strong dipole moment, in most cases electrostatic forces ($u(r) \propto \frac{1}{r^{2-3}}$) are more relevant to the description of the attractive intermolecular forces, for nonpolar molecules, the dispersion forces tend to dominate ($u(r) \propto \frac{1}{r^6}$).[3] And for both cases the relative magnitude is smallest for the induction forces.[3]

2.3.1 The Born model

The solvation model by Born was one of the first which employed the idea of calculating solvation energies by treating the solvent implicitly, which also is the foundation for continuum solvation models like COSMO. Under the neglection of the pressure-volume work, he proposed to equate the solvation energy of an amount of n_i mols of an ion i with radius r_i and charge z_i to the difference of charging energy in the ideal gas phase and in a solution of permittivity ε_r:

$$\Delta G_{solv,i}^{Born} = \frac{n_i z_i^2 e^2 N_A}{8\pi\varepsilon_0 r_i}\left(\frac{1}{\epsilon_r} - 1\right) \tag{2.33}$$

Where N_A is the Avogadro constant, e the charge of an electron and ε_0 the vacuum permittivity.

The model can also be applied to describe the solvation energy difference for a salt between one mixture and a reference mixture (+) with different dielectric constants as follows:

$$\Delta G_{solv,salt}^{Born} = \frac{e^2 N_A}{8\pi\varepsilon_0}\left(\frac{1}{\epsilon_r} - \frac{1}{\epsilon_r^+}\right)\sum_{ions}\frac{(n_i - n_i^+)z_i^2}{r_i} \tag{2.34}$$

It is possible to describe the difference in solvation energy of an ion due to the dielectric decrement with this equation. By taking the infinite dilution (∞) as reference mixture, the derivative with respect to the amount of substance according to equation (2.4) allows to calculate a contribution to the activity coefficient of an ion due to the change of permittivity as follows[66]:

$$\ln\gamma_i^{\mathrm{Born}} = \frac{1}{RT}\frac{N_\mathrm{A}e^2}{8\pi\epsilon_0}\left[\left(\frac{1}{\epsilon_\mathrm{r}} - \frac{1}{\epsilon_\mathrm{r}^\infty}\right)\frac{z_i^2}{r_i} - \left(\sum_{\mathrm{ions}}\frac{n_i z_i^2}{r_i}\right)\frac{1}{\epsilon_\mathrm{r}^2}\left(\frac{\partial\epsilon_\mathrm{r}}{\partial n_i}\right)_{\mathrm{T,V,n_{j\neq i}}}\right] \tag{2.35}$$

The value of this contribution to the activity coefficient vanishes when no dielectric decrement is being considered, while the value of $\frac{\partial\epsilon_\mathrm{r}}{\partial n_i}$ depends on the model used to describe the effect in question.

2.3.2 COSMO

The COnductor-like Screening MOdel (COSMO) is a model developed by Klamt and Schüürmann[67] allowing to estimate the interaction between a solute described by its electronic charge distribution projected on its cavity surface immersed in a solvent solely described by its permittivity. This makes COSMO an apparent surface charge dielectric continuum model.[68]

The cavity is approximated through a set of small segments with a specific surface charge density enabling to describe the distribution as a set of point charges at a specific radius from the atom center.[69] As the potential at every point on the surface depends on all of the assigned charges, the calculation of the charges in normal polarizable continuum models becomes a computationally expensive iterative calculation.[70] However, Klamt and Schüürmann[67] proposed to exchange the exact boundary condition for an ideal conductor (i.e. $\epsilon = \infty$). By introducing this approach instead of the exact boundary condition, the potential vanishes at the contact from the cavity with the conductor. This allows the calculation of analytical gradients decreasing the algorithmical complexity to calculate geometries efficiently. A comparison to IEFPCM shows that COSMO delivers almost equal results at much lower computational cost[71].

To return from the ideal conductor to a finite permittivity, a scaling[69] was introduced as a function of the permittivity. This scaling function alludes to the multipole extension for the calculation of solvation energies in a homogeneous dielectric[72]:

$$f(\epsilon) = \frac{\epsilon - 1}{\epsilon + x} \tag{2.36}$$

With x lying between zero and unity, set to 0.5 in some implementations.[69]

To calculate the input for the COSMO model approximate quantum mechanical methods are usually employed as calculating the charge distribution of larger molecules is not otherwise explicitly solvable. DFT (Density Functional Theory) is one of the most applied methods in conjunction with polarizable continuum models and this also holds true for the use with the COSMO model.[69]

COSMO has been successfully applied to correlate Henry coefficients[73,74] and partition coefficients[75,76]. However, the need for a better description of the solvent's properties

besides just the permittivity and its interactions with solutes at different concentrations and temperatures lead to the development of COSMO-RS[77].

2.3.3 COSMO-RS

The COnductor like Screening MOdel for Realistic Solvation (COSMO-RS[6]) which in contrast to COSMO is a g^E-model, allows the calculation of complete phase equilibria.

The main step from COSMO to COSMO-RS is the replacement of the ideal conductor by an ensemble of pairwise independently interacting segments by the use of statistical thermodynamics. By introducing the independent interactions, all three-dimensional information and steric effects are lost. And although this is a large simplification, it allows to circumvent the mathematical complications of describing the complete molecules in an efficient way that has proven quite accurate.[6]

The surface charge density distribution employed in COSMO-RS is taken from the charge distribution calculated by the COSMO model (σ_J^{COSMO}). However, a smoothing of the charge distribution is done as first step according to:

$$\sigma_I = \frac{\sum_J \sigma_J^{COSMO} \frac{r_J^2 r_{\mathrm{av}}^2}{r_J^2 + r_{\mathrm{av}}^2} \exp\left(-\frac{d_{IJ}^2}{r_J^2 + r_{\mathrm{av}}^2}\right)}{\sum_J \frac{r_J^2 r_{\mathrm{av}}^2}{r_J^2 + r_{\mathrm{av}}^2} \exp\left(-\frac{d_{IJ}^2}{r_J^2 + r_{\mathrm{av}}^2}\right)} \tag{2.37}$$

Where d_{IJ} is the euclidean distance between the segments I and J, r_I is the radius of the segment and r_{av} is a parameter of the model.

The transition from ideal conductor to real solution can be described by a thought experiment. In the ideal conductor the electrostatic potential of the interacting screening charges of a molecule vanish.

If a group of molecules is put into a close volume without removing the ideal conductor a situation arises as depicted in Figure 2.8, in which the ideal conductor is depicted as the gray lines in between the molecules. Under the assumption that the slight deformations of the cavity necessary to reach a closely packed structure with about the right liquid density are negligible, the change in energy going to this state is also negligible.[70]

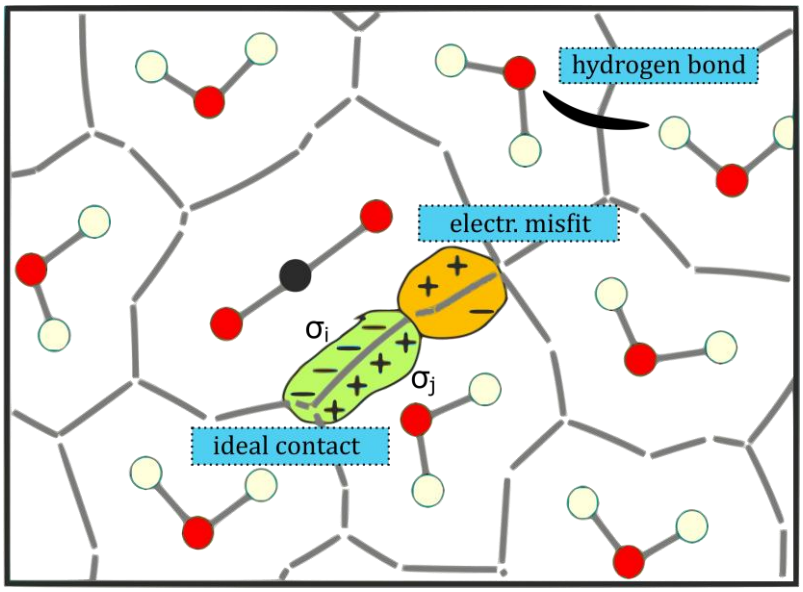

Figure 2.8: Thought experiment showing a group of interacting molecules separated by the ideal conductor depicted as the gray line between the cavities. The electrostatic misfit energy (orange) arises for the interaction of two segments with different charge. The ideal contact (green) occurs when the contacting segments are of same magnitude but opposite sign. Hydrogen bonds (black) might arise when two opposite highly charged segments interact with each other. (adapted from Klamt[70] with permission of Elsevier Science & Technology Journals; permission conveyed through Copyright Clearance Center, Inc.)

Initially the interactions between the cavities are non-existent due to the presence of the ideal conductor. However, as the conductor is removed, the charges on the cavity calculated from the COSMO model start to interact with each other. Several possibilities may arise. Possibly a segment on the first molecule with screening charge σ_I has the same but opposite net charge from the second molecule σ_J leading to an ideal contact. If the charges are however different, an energy arises due the difference of this contact with respect to the ideal conductor. Assuming the contact is non-polarizable for neither of the molecules segments, the electrostatic misfit energy can be defined like so:[6,70]

$$e_{misfit} = \frac{\alpha'}{2}(\sigma_I + \sigma_J)^2 \tag{2.38}$$

Where σ_I and σ_J are the screening surface charge densities of the two segments in contact. α' is a constant that could be calculated through electrostatics from an approximation of the self-energy of a circular charged disc. However, the theoretical value is not taken here because in the real solvent the molecules would readjust their electrons to an

energetically favorable configuration. This electronic polarizability correction is introduced empirically as the value of α' is adjusted to experimental data.[6]

As can be seen from (2.38) the electrostatic misfit energy is a function of the contacting screening surface charge densities. The screening surface charge density σ is the single most important 'descriptor' used to calculate interaction energies within the COSMO-RS framework. Although other descriptors like local shape index, local polarizability, molecule polarizability would be possible[70], to the authors knowledge, in the published versions of COSMO-RS no other descriptor is used besides the type of atom the contacting segment belongs to. There is however a correction to the misfit energy proposed by Klamt[7] that seeks to regain some of the lost three-dimensional information. Instead of equation (2.38) the following is proposed:

$$e_{misfit} = \frac{\alpha'}{2}(\sigma_I + \sigma_J)\left[(\sigma_I + \sigma_J) + f_{\mathrm{corr}}(\sigma_I^{\perp} + \sigma_J^{\perp})\right] \tag{2.39}$$

$$\sigma_I^{\perp} = \sigma_{I,\mathrm{corr}} - 0.816 \cdot \sigma_I \tag{2.40}$$

So, for each segment σ_I an additional $\sigma_{I,corr}$ is calculated with the averaging expression from equation (2.37) with an averaging radius r_{av} twice as large. Where $\sigma_I^{\perp}$represents the linear independent portion of $\sigma_{I,corr}$ with respect to σ_I and f_{corr} is a model parameter. This correction adds information of the surrounding of each segment to the calculation of the misfit energy accounting for local charge correlations.[7]

Besides the electrostatic misfit energy, an additional hydrogen bonding term was proposed. This followed the need for including the description of strong attractive interactions between unlike charged segments with a charge density above a certain threshold value of σ_{HB}:

$$e_{HB} = c_{HB}(T) \cdot min(0; \sigma_{don} + \sigma_{HB}) \cdot max(0; \sigma_{acc} - \sigma_{HB}) \tag{2.41}$$

Where σ_{don} and σ_{acc} are the hydrogen bond donor and acceptor segments respectively; calculated by $\sigma_{don} = min(\sigma_I, \sigma_J)$ and $\sigma_{acc} = max(\sigma_I, \sigma_J)$. While $c_{HB}(T)$ is a temperature dependent parameter calculated by:

$$c_{HB}(T) = c_{HB} \cdot max\left(0; 1 - c_{HB}^{T} + c_{HB}^{T}\frac{298.15\mathrm{K}}{T}\right) \tag{2.42}$$

Where c_{HB} and c_{HB}^{T} are model parameters.

Other interaction energies would be possible, for example the van der Waals dispersion energy introduced by Klamt & Eckert[78] to fine-tune the performance of the model for one haloalkane. However, neglecting this contribution, the interaction energy between two segments with an effective area of a_{eff}, can be calculated as follows:

$$E_{\text{int}} = a_{eff}\left(e_{misfit} + e_{HB}\right) \tag{2.43}$$

Figure 2.9 shows a plot of the interaction energies to understand how these behave:

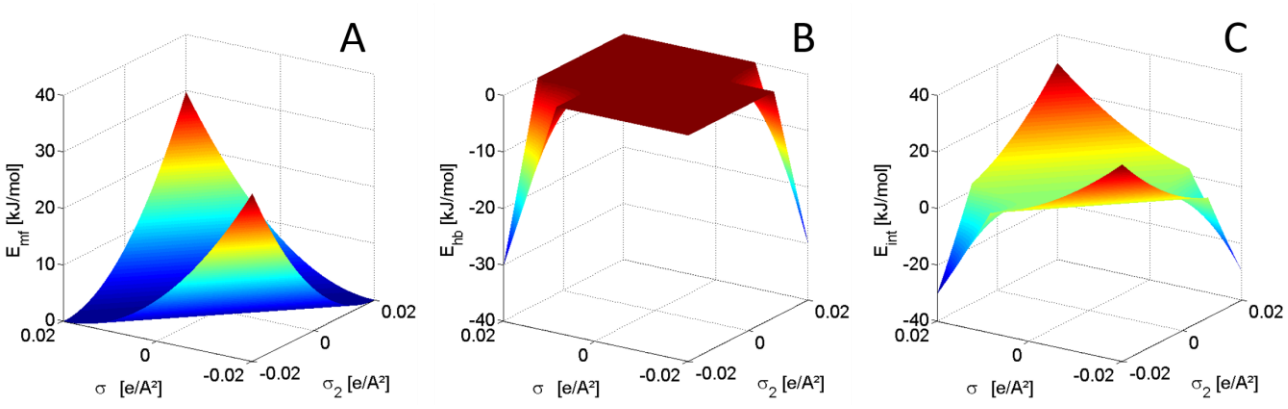

Figure 2.9: Energy terms of COSMO-RS and its dependence on the charge density of the contacting segments σ and σ_2.(A) electrostatic misfit energy as calculated by equation (2.38),(B) hydrogen-bonding energy as calculated by equation (2.41) and (C) total interaction energy as calculated by equation (2.41).

Now that we have an expression for calculating the interaction of 2 segments, the next step is to combine this with statistical thermodynamics to be able to calculate the properties of the mixture. For this let us introduce the central equation of COSMO-RS, the COSMOSPACE equation[79]:

$$\frac{1}{\Gamma_I} = \sum_J \tau_{IJ} \cdot \Gamma_J \cdot X_J \tag{2.44}$$

where Γ_I is the activity coefficient for segment I, $X_J$is the surface fraction of segment J in the mixture of segments and τ_{IJ} is a symmetrical function of the interaction energies E_{IJ} between two segments I and J like:

$$\tau_{IJ} = \tau_{JI} = \exp\left(-\frac{E_{int}(\sigma_I, \sigma_J) - 0.5\left(E_{int}(\sigma_I, \sigma_I) + E_{int}(\sigma_J, \sigma_J)\right)}{k_B T}\right) \tag{2.45}$$

In order to calculate the residual activity coefficient γ_I^{res} for a molecule i a sum of the activity coefficients of the segments on this molecule Γ_i weighted by the relative amount of the area of this segment on molecule i is necessary:

$$\ln(\gamma_I^{res}) = \sum_i \frac{A_I^i}{a_{eff}} \cdot [\ln \Gamma_i - \ln \Gamma_i^{+}] \tag{2.46}$$

To account for different sizes in the interacting molecules a combinatorial term is included to calculate the activity coefficient of a molecule i:

$$\ln \gamma_i^{COSMO-RS} = \ln \gamma_i^{res} + \ln \gamma_i^{comb} \tag{2.47}$$

One combinatorial term (also used with COSMO-SAC[80] and UNIFAC[81]) is the Staverman-Guggenheim expression[70]:

$$ln\, \gamma_i^{comb} = ln\frac{\phi_i}{x_i} + \frac{z_{coord}}{2}\frac{\theta_i}{\phi_i} + I_i + \frac{\phi_i}{x_i}\sum_j x_j I_j \tag{2.48}$$

With:

$$\theta_i = \frac{x_i q_i}{\sum_j x_j q_j}; \quad \phi_i = \frac{x_i r_i}{\sum_j x_j r_j}; \quad I_i = \frac{z_{coord}}{2}[(r_i - q_i) - (r_i - 1)]; q_i = \frac{A_i}{A_{norm}}; r_i = \frac{V_i}{V_{norm}}$$

Where z_{coord} the coordination number, x_i the mole fraction, A_i the surface area and V_i the volume of molecule i. A_{norm} and V_{norm} are normalization values equal for every molecule, i.e. model parameters.

2.3.4 Pitzer-Debye-Hückel model

The development Pitzer introduced to the Debye-Hückel model was based on the following equation for the osmotic coefficient ϕ:[82]

$$\phi - 1 = -\frac{1}{6}\sum_i \sum_j c_i c_j \int_0^\infty \frac{\partial u_{ij}}{\partial r} g_{ij}(r) 4\pi r^3 dr \tag{2.49}$$

Where c_i is the numeric concentration of ions i per unit of volume, u_{ij} is the interaction potential and g_{ij} is the radial distribution function of ions *i* and *j*. Once the right-hand side

is known, it is possible to calculate the activity coefficient of the ion through the Gibbs-Duhem equation.[83]

The potential used is based on the hard core and the Coulombic potential in a dielectric continuum:

$$u_{ij}\begin{cases}\infty & if\ r < a\\ \dfrac{z_i z_j e^2}{4\pi\epsilon_o\epsilon_r r} & if\ r \geq a\end{cases} \tag{2.50}$$

Where the closest approach distance α is the sum of r_i and r_j.

Equal as with the Debye-Hückel theory, the potential of mean force is assumed to be directly proportional to the electrostatic potential of the ion cloud in the dielectric continuum for radii larger than the closest approach distance a not taking into account the hard-core potential:[82]

$$g_{ij}(r) = \exp\left(-\frac{\Psi_i^{cloud}\cdot z_j e}{k_B T}\right) \approx 1 - \frac{\Psi_i^{cloud}\cdot z_j e}{k_B T} + \frac{1}{2}\left(\frac{\Psi_i^{cloud}\cdot z_j e}{k_B T}\right)^2 + \cdots \tag{2.51}$$

Where Ψ_i^{cloud} is the electrostatic potential of a cloud of ions with reference to a central ion.

By integrating the electrostatic part of equation (2.49)(2.50) only from the closest approach distance to infinity it is possible to get an expression for the electrostatic contribution to the osmotic coefficient of the solvent after introducing the molality based ionic strength $I^{(m)}$ as follows:

$$\phi^{el} = -\frac{2I^{(m)}}{\sum_i m_i} A_\varphi \left(\frac{\left(I^{(m)}\right)^{0.5}}{1 + bI^{(m)0.5}}\right)$$
$$\text{With } A_\phi = \frac{1}{3}(2\pi N_A \rho_s)^{1/2}\left(\frac{e^2}{4\pi\varepsilon_0\varepsilon_r k_B T}\right)^{3/2},\ b = \frac{a}{I^{(\mathrm{m})0.5}\lambda_\mathrm{D}} = a\left(\frac{2N_A\rho_S}{M_S}\frac{e^2}{\epsilon_0\epsilon_r k_B T}\right)^{0.5} \tag{2.52}$$

Where m_i is the molality of species i, b is the so called closest approach parameter, ρ_s is the solvent density, λ_D is the Debye length, a is the closest approach distance and M_s is the solvent molecular mass. In most applications of the Pitzer-Debye-Hückel model the closest approach parameter is set to a fixed value of 14.9[84–87]. However, as shown above, it is possible to explicitly calculate this value as a function of the closest approach distance

a and the Debye length which is a measure as to how far the central ion interacts with other ions. Both lengths are shown in Figure 2.10.

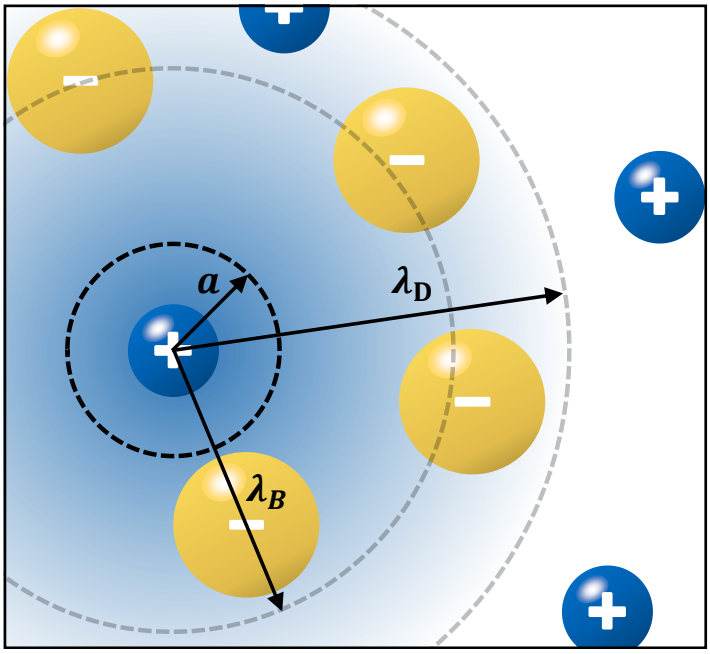

Figure 2.10: Depiction of the important distances regarding electrolyte models: the closest approach distance α, the Debye length λ_D and the Bjerrum length λ_B.

Now by connecting equation (2.52) with the excess Gibbs free energy G^E by:

$$\phi^{el} - 1 = -\frac{1}{M_s RT \sum_i m_i}\left(\frac{\partial G^E}{\partial n_s}\right)_{T,P,n_i \neq n_s} \tag{2.53}$$

it is possible to integrate with respect to the amount of solvent n_s assuming a small electrolyte concentration and changing to mole fraction based ionic strength $I^{(x)}$ to get a function for the excess Gibbs free energy as follows:[84]

$$\frac{G^{E,el}}{RT} = -\left(\sum_i n_i\right)\frac{4}{b}\frac{A_\phi}{M_s^{1/2}} I^{(x)} \ln\left(1 + bI^{(x)^{1/2}}\right) \tag{2.54}$$

Now by deriving with respect to the species i it is possible to get an expression for the activity coefficient also valid for the ions:

$$\ln(\gamma_i^{PDH}) = -\frac{A_\phi}{\sqrt{M_s}}\left\{\frac{2z_i^2}{b}\ln\left(1 + bI^{(x)^{1/2}}\right) + \frac{z_i^2 I^{(x)^{1/2}} - 2I^{(x)^{3/2}}}{1 + bI^{(x)^{1/2}}}\right\} \tag{2.55}$$

2.3.5 COSMO-RS-ES

COnductor like Screening MOdel for Realistic Solvation in Electrolyte Systems (COSMO-RS-ES) is a predictive electrolyte model developed by Gerlach et al.[14] that combines the power of COSMO-RS (cf. section 2.3.3) to account for the short-range interactions with the term developed by Pitzer based on the Debye-Hückel theory (cf. section 2.3.4) to describe long-range interactions in electrolyte systems.

The short-range contribution and the long-range contribution are connected similarly to other electrolyte g^E-models as follows:

$$\ln(\gamma_i^{COSMO-RS-ES}) = \ln(\gamma_i^{SR,COSMO-RS}) + \ln(\gamma_i^{LR,PDH}) \tag{2.56}$$

For the purpose of extending the COSMO-RS theory for electrolyte systems, the energy interaction equation (2.43) was made dependent on the type of contact. Whereas for the contact between neutral molecules the original COSMO-RS interaction equation was employed, different equations were developed for the contact between the following species: cations, halides, polyatomic anions, water and organic molecules. The misfit energy was multiplied by a misfit factor and the hydrogen bonding energy was replaced by specific ionic interaction energy terms as shown in Table 2.3.[14]

The long-range Pitzer-Debye-Hückel model requires the input parameters of the density and the permittivity. For this, under the assumption that the electrolytes have no influence on these parameters and in accordance to the derivation of the model, the salt-free permittivity (ϵ_{sf}), salt-free molar mass (M_{sf}) and salt-free density (ρ_{sf}) are employed. The mixture of solvents is represented as a single pseudo solvent using the following mixing rules neglecting excess volume effects:

$$M_{sf} = \sum_{solvents} x_{i,sf} M_i \tag{2.57}$$

$$\rho_{sf} = \frac{M_{sf}}{\sum_{solvents} \frac{x_{i,sf} M_i}{\rho_{i,sf}}} \tag{2.58}$$

$$\epsilon_{sf} = \frac{M_{sf}}{\rho_{sf}} \sum_{solvents} \frac{x_{i,sf} M_i}{\rho_{i,sf}} \epsilon_{i,sf} \tag{2.59}$$

Table 2.3: Interaction energy equations for ionic interactions in the short-range contribution of COSMO-RS-ES.[14]

Type of contact	Misfit factor	Ionic interaction energy term	
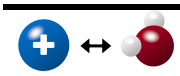 cation – H_2O	A_1	$E^{ion}_{cat-H_2O} = \frac{a_{eff}}{2} B_1 \sigma_{cat}\, max(0, \sigma_{H_2O})$	(2.60)
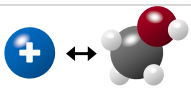 cation – org. mol.	A_2	$E^{ion}_{cat-om} = \frac{a_{eff}}{2} B_2 \sigma_{cat}\, max(0, \sigma_{om})$	(2.61)
 cation - halide	0	$E^{ion}_{cat-hal} = \frac{a_{eff}}{2} B_3\, min\big(0, \sigma_{cat}(1 - D_1\lvert\sigma_{cat}\rvert^{E_1})\big)\ \sigma_{hal}$	(2.62)
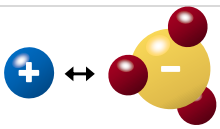 cation – polyat. an.	0	$E^{ion}_{cat-pa} = \frac{a_{eff}}{2} B_4\, min\big(0, \sigma_{cat}(1 - D_1\lvert\sigma_{cat}\rvert^{E_1})\big)\, max\big(0, \sigma_{pa}\big)^{E_2}$	(2.63)
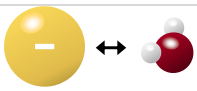 halide - H_2O	A_3	$E^{ion}_{hal-H_2O} = \frac{a_{eff}}{2} B_5\, min\big(0, \sigma_{H_2O}\big)\, max(0, \sigma_{hal} - C_1)$	(2.64)
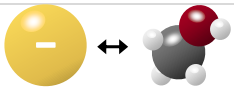 halide – org. mol.	A_4	$E^{ion}_{hal-om} = \frac{a_{eff}}{2} B_6\, min(0, \sigma_{om})\, max(0, \sigma_{hal} - C_2)^{E_3}$	(2.65)
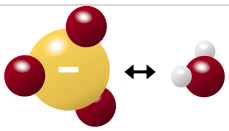 polyat. an. - H_2O	A_5	$E^{ion}_{pa-H_2O} = \frac{a_{eff}}{2} B_7\, min\big(0, \sigma_{H_2O}\big)\, max\big(0, \sigma_{pa}\big)$	(2.66)
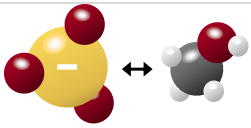 polyat. an. - org. mol.	A_6	$E^{ion}_{pa-om} = \frac{a_{eff}}{2} B_8\, min(0, \sigma_{om})\, max\big(0, \sigma_{pa} - C_3\big)$	(2.67)

2.3.6 Modeling of ion-pairing

The modeling of ion-pairing can be approached from different angles, considering single step or multistep association and within several theoretical frameworks.[27] In the following, the models by Bjerrum and Fuoss are presented. Whereas their derivation is somewhat similar, as can be observed from Figure 2.11, their behavior is quite different for very high permittivities ($\epsilon > 65$). Both models assume a single step association of free ions expressed by the following reaction:

$$M^+_{free\ ion} + X^-_{free\ ion} \rightleftharpoons M^+X^- \tag{2.68}$$

Both models provide a molar concentration-based association constant, which in the limit of ionic infinite dilution can be transformed into a mole-fraction based association constant like so:

$$\mathrm{K_A} = \mathrm{K_A^{(c)}}\frac{\rho_{sf}}{M_{sf}} \tag{2.69}$$

Where ρ_{sf} and M_{sf} are the density and the molar mass of the salt-free solvent respectively.

Ion-pairing according to Bjerrum

The first to develop a theory to calculate the ion-pairing degree was Bjerrum. It is based on the Debye-Hückel theory and therefore describes ions as charges in a dielectric continuum. According to Bjerrum the probability of finding a paired ion P_{IP} between the distances of r and $r + dr$ in a dilute electrolyte solution can be calculated as:[88]

$$P_{IP} = c_i 4\pi r^2 \exp(-\frac{\mathrm{u_{ij}^{el}}}{k_B T})dr = c_i 4\pi r^2 \exp(-\frac{\frac{z_i z_j e^2}{4\pi\varepsilon_0\varepsilon_s r}}{k_B T})dr \tag{2.70}$$

Where c_i is the concentration of ions i per unit of volume, $\mathrm{u_{ij}^{el}}$ is the electrostatic potential energy according to Coulomb's law. For two ions z_i and z_j with opposite charges, the probability P_{IP} has a minimum at a distance of λ_B:

$$\lambda_B = -\frac{z_i z_j e^2}{8\pi\varepsilon_0\varepsilon_s k_B T} \tag{2.71}$$

At the Bjerrum length λ_B the energy required to separate both ions is equal to four times the thermal energy of a one-dimensional translational motion ($2k_BT$). With this theory, the ion-pair is defined as two ions of opposite charges with a distance from each larger

than the closest approach distance a and smaller than the Bjerrum length λ_B (cf. Figure 2.10).[27] The molar concentration based association constant for two oppositely charged ions is therefore calculated from the integral of equation (2.70) as follows[28]:

$$\mathrm{K_A^{(c)}} = N_A \int_0^{2\pi} d\varphi \int_0^{\pi} \sin(\theta)\, d\theta \int_a^{\lambda_B} \exp\left(-\frac{z_i z_j e^2}{4\pi\varepsilon_0\varepsilon_s k_B T r}\right) r^2 dr \tag{2.72}$$

Which can be rearranged into[27]:

$$\mathrm{K_A^{(c)}} = 4\pi N_A \int_a^{\lambda_B} \exp\left(\frac{2\lambda_B}{r}\right) r^2 dr \tag{2.73}$$

As the solution of this integral is only possible numerically, several correlations have been proposed in literature. These correlations are usually only valid for a certain range of permittivities. During this work a correlation was developed valid for the complete permittivity range (cf. section 8.2 in the appendix). Two literature correlations and the one developed in this work are shown in Figure 2.1.

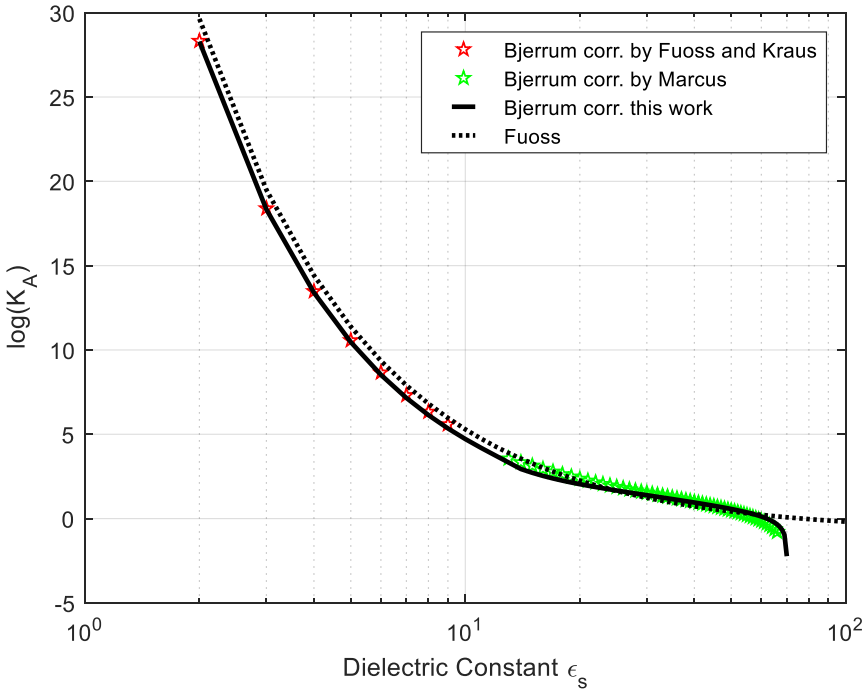

Figure 2.11: Dependency of the association constant with regards to the permittivity for a fixed closest approach distance of 5 Å as calculated by the Bjerrum model (solid line), calculated by the Fuoss model[89] (dashed line). The correlations for the Bjerrum model by Fuoss and Kraus[28] and by [Marcus: personal communication][90], only valid for a specific permittivity range, are also shown here for comparison with the correlation developed in this work valid for the complete permittivity range.

Ion-pairing according to Fuoss

In contrast to Bjerrum's wider definition of an ion-pair, Fuoss[89] decided to only consider ion pairs at a distance r = a between their centers, where a is the closest approach distance. Modeling the cation as a charged conducting sphere and the anion as a point charge allowed to penetrate the cations sphere, the following can be derived from the simplified Poisson-Boltzmann equation for the potential energy at a distance a:[89]

$$u_{ij}^{el} = \frac{z_i z_j e^2}{4\pi\varepsilon_0\varepsilon_s a}\left(\frac{1}{a\lambda_D^{-1}+1}\right) \tag{2.74}$$

Assuming that only the associated ions contribute to the potential energy allows to drop the part in parenthesis related to the ion cloud of the potential energy in equation (2.74). Which at the end produces a potential energy equal to the one between two point charges, however with the boundary condition of ideal conductor within the cation radius. If the transition state between free and paired ions is neglected, it is possible to calculate the association constant as:

$$K_A^{(c)} = \left(N_A \int_0^{2\pi} d\varphi \int_0^{\pi} \sin(\theta)\, d\theta \int_0^{a} r^2 dr\right) \cdot \exp\left(-\frac{z_i z_j e^2}{4\pi\varepsilon_0\varepsilon_s k_B T a}\right) \tag{2.75}$$

Which then after integration leads to:

$$K_A^{(c)} = \frac{4}{3}\pi a^3 N_A \exp\left(-\frac{z_i z_j e^2}{4\pi\varepsilon_0\varepsilon_s k_B T a}\right) \tag{2.76}$$

In contrast to the solution proposed by Bjerrum, the calculation of the association constant with the model by Fuoss is non-iterative allowing a faster calculation without the need for correlations aimed at the resolution of the integral.

3 State of the art

3.1 Modeling of phase equilibria of electrolyte systems

Many equations of state and g^E-models have been extended to describe electrolyte thermodynamics. Most models have achieved this by addition of long-range electrostatic terms. However, the majority of these models, especially the g^E-models, have been applied only to correlate data. Since the main topic of this work is a predictive model for strong electrolytes, the literature discussed in this section is focused on models that have been or that could be applied predictively; if possible, in multi-solvent systems. There exist two ways to parametrize the models with respect to the electrolytes: either with salt-specific parameters or with ion-specific parameters. The models mentioned here, are all ion specific as this gives the model a predictive character applicable to ion combinations originally not in the training data set.

Equations of state (EOS)

The EOS applied to electrolytes can be grouped by type into cubic, cubic plus association, SAFT and other.

The first equations of state developed for electrolytes where of the cubic type. Simon[91] combined the RSK EOS with a modified Debye-Hückel term and Born term, describing the dielectric decrement of the salts by an empirical model in aqueous and alcoholic systems. Fürst & Renon[55] also combined the RSK with the mean spherical approximation (MSA) and a Born term, including the effect of the dielectric decrement with the model by Pottel (cf. 2.2.2) in aqueous systems. They were able to correlate most of the parameters as a function of the ionic sizes, which allows for a prediction of parameters for other ions. The model was developed further[54,92,93] and applied to mixed-solvent systems to even calculate LLEs. Cubic equations of state have also been combined with the g^E-model LIFAC to calculate phase equilibria assuming non-volatile electrolytes.[94–96]

The cubic plus association EOS all combine either the PR or the RSK EOS with the association term from the SAFT theory. All the reviewed models include a Born term. Wu

& Prausnitz[97], who applied the model to calculate solubilities of gases in electrolyte solutions. and Inchekel et al.[51] use the MSA term to describe the electrolyte interactions however only in aqueous systems. The latter includes the model of Pottel (cf. 2.2.2) to describe the dielectric decrement. The group around Kontogeorgis developed the similar eCPA model based on the Debye Hückel theory and a new way to calculate the permittivity of the mixture of the solvents implicitly describing the dielectric decrement.[48] The model was later combined with a Huron-Vidal mixing rule based on NRTL to be able to calculate phase equilibria in mixed solvent systems (SLE, LLE, VLE).[98] Although some predictivity is lost, because binary parameters are needed, the EOS allows extrapolating to other conditions quite accurately. The model has even been applied to challenging electrolytes like the Tetra-butyl-ammonium halides successfully.[99] Recently, an ion-specific version of the model has been published[100,101], but for multisolvent-systems still binary parameters are necessary.

The majority of EOS based on SAFT are combined with the MSA model to describe the electrolyte interactions. SAFT-VRE based on the variable range potential has been applied successfully to aqueous electrolytes at different conditions and to the salting-out behavior of alkane-water mixtures.[102–105] Later a Born term was added to be able to represent solvation energies accurately[106,107]. ePC-SAFT was first developed by Cameretti et al.[108] including a Debye Hückel term, which was then extended by Held to a wide variety of strong[109] and weak electrolytes[110]. By the introduction of ion-ion dispersion the model was improved further and tested on more than 100 aqueous electrolytes[111] being applied to LLE calculations[112,113] even with organic electrolytes[114]. Rozmus et al.[115] show with ePPC-SAFT that by improving the underlying solvent model the properties of the electrolytes also were represented better. Ahmed et al.[66] described the dielectric decrement explicitly with ePPC-SAFT and showed that by adjusting binary interaction parameters between solvents they were able to predict the salt effect on mixed-solvent VLEs. SAFT2[116,117] was even shown to predict the salt effect on mixed-solvent VLEs[118,119].

The ePHSC[120] and the Q-electrolattice[53,121] EOS are recent examples which do not fit in any of the other types. While both use the MSA term to describe the ionic interactions, the latter one includes a Born term and explicitly takes dielectric decrement into account by the model of Pottel being applied to 78 different aqueous strong electrolytes and even to non-aqueous systems[53].

Although all these EOS allow predicting phase equilibria, in the rare cases they were extended to mixtures of solvents, binary interaction parameters or solvent-specific parameters were introduced into the model reducing the predictive capacity of these approaches. The very recent group-contribution-based approaches SAFT-γ Mie[122,123] and eGC-PPC-SAFT[124] have the largest potential for further developments in this field.

g^E-models

Whereas several EOS can be considered predictive and a lot of effort is put into a good and consistent parameterization, in most cases the g^E-models in literature are employed in a correlative manner. In recent years, almost no experimental article has been published that does not fit the data with a model.

The existing models which are applied predictively can be grouped by type into NRTL-based, UNIQUAC-based, UNIFAC -based and COSMO-RS-based, depending on which model was employed to describe the short-range interactions.

NRTL is one of the most used models to fit experimental phase equilibrium data. Its electrolyte version eNRTL was first published by Cruz & Renon[125] and widely developed by the group of Chen[85–87,126–136]. However, the first one to implement a predictive ion-specific version of the model was Liu[137,138]. The model combines NRTL with an especially modified Debye-Hückel approach for local composition models, a Born term and accounts for the dielectric decrement in the mixture with a predictive empirical model being able to represent some aqueous MIACs of alkali halides. Kuramochi[139] developed a similar model adding only the Pitzer-Debye-Hückel term instead. His model is able to correlate aqueous MIACs for more than 40 salts and predict the MIACs in mixed salt systems.

Contrasted with the NRTL-based models discussed, which were all utilized only with aqueous salt systems, extended UNIQUAC for electrolytes models have been also applied to mixed solvents. The development of extended UNIQUAC already started quite early[140,141] adding a Debye-Hückel term and a composition dependent middle-range (MR) ternary term which hindered the predictive application of the model. The developments hereafter split into two groups. The first group discarded the MR-term and were able to successfully calculate aqueous mixed salt SLEs[142–146], mixed solvent VLEs[147], LLEs[148], SLEs[149] and even mixed salts in mixed solvent systems.[150] The second group kept the MR-term in form of a Pitzer-like virial term but only using binary interaction parameters. By

this, the number of parameters for each binary interaction is larger allowing for a better fit whilst keeping the predictivity. LIQUAC, a model from the group lead by Prof. Gmehling was the first model of this type to be developed. It has been shown to be able to calculate mixed solvent VLEs[151,152], later expanded to aqueous SLEs[153,154] and mixed solvent LLEs[155,156] and SLEs[156–158]. The mixed solvent electrolyte model (MSE) as published by Wang[159] is similar to LIQUAC. The SR term is the same as LIQUAC, the MR term is also similar having a more complex temperature dependency. However, the LR term is a modified Pitzer-Debye-Hückel with explicit permittivity and density dependence on all species. The permittivity is calculated by a model developed by the same authors[160] which takes dielectric decrement and ion-pair formation into account in an empiric manner. The density dependence is calculated by a model based on a modification of the SR and the MR term including a pressure dependence fitted only for this purpose. Initially the model was shown to be able to calculate mixed solvent VLEs and SLEs.[159] Later the model was also shown capable of calculating mixed salt hydrate temperature dependent SLEs[161], mixed solvent LLEs[162], VLEs with speciation[162] and acid-base equilibria[163].

Models based on UNIFAC are even more predictive than the models described before, because if the right combination of functional groups is available, the system can be calculated. As with UNIQUAC, the models developed based on UNIFAC can be divided into two groups. The first models did not employ a MR-term and were mainly applied to mixed-solvent VLEs.[164–166] All the models after these employed a Pitzer-like virial term. Although some other groups have worked on UNIFAC-based models[167–170] and even expanded the application range to polymer containing aqueous electrolyte LLEs[171], LIFAC and AIOMFAC are among the most widely developed. LIFAC[172], a model also created by the group lead by Prof. Gmehling, has seen a series of improvements leading to it being capable of calculating mixed-solvent LLEs, osmotic coefficients, non-aqueous VLEs[155], mixed-solvent SLEs.[4,157,158] Similarly, the closely related AIOMFAC[173] has seen various developments[5,174–176] improving the model to calculate MIACs, mixed-solvent LLEs, mixed solvent SLEs and even non-aqueous SLEs successfully.

So far, all the discussed models include binary interaction parameters. Models based on COSMO-RS are of the most predictive ones as this type of parameters is not necessarily needed. The interactions are described as functions of the polarity of the molecules.

In the past COSMO-RS based models have been widely applied to ionic liquids. However, the literature is not as abundant for inorganic electrolytes. Hsieh & Lin[12] were the first ones to propose a modified COSMO-RS model. They combine the Pitzer-Debye-Hückel term with ion-specific sigma profiles and interaction energy equations depending on the type of interaction. The model was adjusted using aqueous MIACs at 25 °C and was shown capable of predicting aqueous VLEs at other temperatures, mixed-salt aqueous osmotic coefficients and mixed-solvent MIACs with one universal parameter set. Wang et al. also combine COSMO-RS with a Pitzer-Debye-Hückel term using however an electrolyte sigma profile. As this publication is more of a proof of concept only temperature dependent aqueous MIACs for NaCl were predicted. Ingram et al.[10] modified the commercially available version of COSMO-RS by addition of the same LR term, by adjusting the monoatomic cation radii and the hydrogen bonding energy. By this approach, the model was able to predict mixed-solvent MIACs and even calculate the LLE n-butanol + water + NaCl more accurately than the LIQUAC model. Furthermore, it could predict electrolyte induced phase separation. Gerlach et al.[14] developed COSMO-RS-ES (cf. section 2.3.5) by expanding the concept of Hsieh & Lin[12]. The interaction energy equations are also implemented depending on the type of interactions, however, differentiating between monoatomic cation, halide, polyatomic anion, water and organic molecules. The model was shown to calculate aqueous MIACs, mixed solvent LLEs, salt-induced, phase separation, mixed-solvent VLEs and expanded to gas solubility in complex aqueous media with speciation.[177]

Another different approach, COSMO-RS-PDHS, was developed by Toure et al.[11,178] In his model, he also described the LR interactions using a Pitzer-Debye-Hückel model. The solvation of ions is treated explicitly by an equilibrium reaction between the differently solvated ions. For this approach several quantum chemistry calculations are necessary for every cluster containing one central ion and zero or more surrounding solvent molecules. Which makes this approach computationally expensive and difficult to expand to mixed-solvent systems. Nevertheless, the model successfully predicts several aqueous alkali-halide MIACs until very high concentrations.

3.2 Liquid-liquid equilibria in completely non-aqueous electrolyte systems

In literature a variety of data is available for mixtures of organic solvents and ionic liquids. However, very few experimental data exist for non-aqueous liquid-liquid equilibrium of at least two organic solvents and an inorganic electrolyte, particularly if the partitioning of the electrolyte is of interest.

Eckfeldt and Lucasse[179] measured the influence of several electrolytes (NaCl / NaBr / NaI / $NaNO_3$ / NaSCN) on mixtures of methanol and cyclohexane at concentrations lower than 1 wt-% electrolyte between temperatures of 25 and 60 °C. This was done by preparing several ternary mixtures and changing the temperature to find the point at which the mixture became homogeneous. Unfortunately, only the distribution of the solvents into both phases was considered. The influence of the salt on the temperature dependent miscibility gap was quite large, however the partitioning of the electrolyte could not be addressed using this experimental setup.

Andrade et al.[180] measured the system consisting of ethyl stearate, ethanol, glycerol and NaCl. However, he could not find any measurable influence of the salt upon the liquid-liquid equilibrium at the low salt concentrations measured (50 mg/L). Although the salt concentration in both phases was measured using conductometry, it is not possible to calculate the partitioning of the salt due to its detection only in one of the phases.

Dong et al.[181–183] measured the quaternary LLE of benzene, cyclohexane, dimethylformamide and different electrolytes (NaSCN / KSCN / NH_4SCN). Only the concentration of the solvents was measured with a GC method. They calculated the partitioning of the salt based on the partitioning of the measured dimethylformamide concentration in both phases probably because dimethylformamide is the solvent with the highest affinity towards the ions. The same method for calculating the salt partitioning was applied to measure the system with KSCN by Song et al.[184]

In summary, to the authors knowledge, there is no available data for non-aqueous liquid-liquid equilibrium systems for which all the concentrations of the solvents and the concentration of the electrolyte in both phases have been measured. There is however important information to be gathered from the measurements in the literature. As

Eckfeldt and Lucasse[179] remark, keeping the water concentration as low as possible is very important while measuring non-aqueous phase equilibria, as it can have a very large impact on the results. This must be taken care of during the complete experimental procedure and becomes even more important when handling more hygroscopic salts as the ones measured in this work.

4 Objectives

Examining the state of the art in electrolyte thermodynamics shows that the majority of models in the literature are correlative. Of the systems that are applicable predictively due to an ion-specific parameterization (cf. section 3.1), the majority employs binary interaction parameters to describe the different interactions between the ions and the solvents more accurately.

COSMO-RS-ES belongs to the most predictive approaches published in the literature. The objective of this work is to enhance COSMO-RS-ES further and evaluate the model for types of data it has not been applied to before. A special emphasis is put on the improvement of the calculation of highly concentrated and non-aqueous systems. To achieve this, the following steps are taken:

1. Extension of COSMO-RS-ES: highly concentrated, mixed-solvent and non-aqueous systems

   A database of SLEs of systems containing electrolytes is to be created to extend the model to highly concentrated mixed-solvent and non-aqueous systems. Furthermore, the evaluation of the new data shall be used to find new ways to enhance the model.

2. Refinement of COSMO-RS-ES: the short-range term

   The short-range term of COSMO-RS-ES shall be analyzed and enhanced to allow for a better overall performance of the model based on the addition of a new data into the parameterization training set.

3. Refinement of COSMO-RS-ES: the long-range term

   In the literature, in most cases salt-free properties are used in the long-range description of the ion interactions. In some few cases, solution properties are taken. The long-range term of COSMO-RS-ES is to be examined to get information about how it behaves if instead of salt-free properties, the actual properties of the solution considering the influence of the salt are taken. Additionally, the inclusion

of a Born term is discussed as this term has been included into other electrolyte models in the literature.

4. Refinement of COSMO-RS-ES: the interplay of short-range and long-range interactions

   As most models in the literature, COSMO-RS-ES is a joint model combining a short-range and a long-range term. At specific system conditions this sum might reach the limit of its applicability. The interplay of both terms is to be addressed, and a way is searched to balance them in order to improve the model.

5. Experimental and computational analysis of non-aqueous liquid-liquid equilibria

   In literature very few measurements of completely non-aqueous LLEs with inorganic electrolytes can be found. In this step, an experimental method developed in this work is applied to measure this type of systems. Moreover, this data can be understood as thermodynamic information which allows to explore the limits of the model and get deep insights as to how it works for these challenging systems.

6. Application of COSMO-RS-ES for calculating free solvation energies and pKa values

   The applicability range of COSMO-RS-ES is extended further to be able to calculate free solvation energies and aqueous pKa values, which in contrast to all previously calculated data, are gas-phase related thermodynamic quantities. For this purpose, first a database including these systems is created and the model is readjusted completely to be extended to the calculation of this kind of systems.

5 Computational details and experimental methods

This chapter summarizes the computational details, analytical methods and experimental procedures applied in this work. The contents of this chapter are revised versions of the respective sections published by Müller et al.[15], Müller et al.[16] and Kröger et al.[17]

5.1 Computational details

5.1.1 COSMO-RS-ES details

There are some differences between other published COSMO-RS versions and the version used in this work. The COSMO-RS implementation used in this work is of our own programming and it employs only the first conformer in the calculations, does not have a van-der-Waals energy term and uses a different combinatorial term. For more detailed information on the differences please refer to Gerlach et al.[14] on which the version used in this work is based upon.

Table 5.1. COSMO-RS-ES general parameters and parameters referring to neutral interaction energies as defined in section 2.3.5.

Parameter	Value	Unit	Reference
a_{eff}	6.25	[Å²]	185
α'	5950	[kj Å² mol⁻¹ e⁻²]	185
c_{HB}	36700	[kJ Å² mol⁻¹ e⁻²]	185
c_{HB}^{T}	1.5	[-]	77
σ_{HB}	0.0085	[e/ Å²]	185
r_{av}	0.5	[Å]	7
f_{corr}	2.4	[-]	7
A_{norm}	79.53	[Å²]	80
z_{coord}	10	[-]	80

All the general parameters and the ones required for the interaction energy equations of the misfit interaction and the hydrogen bonding energy between neutral molecules as defined in section 2.3.5 are summarized in Table 5.1.

All the ionic interaction energy parameters as defined in Table 2.3 are summarized in Table 5.2. Additionally, the adjusted monoatomic radii relevant to this work are shown.

Table 5.2: COSMO-RS-ES parameters referring to ionic interaction energies as defined in Table 2.3, values from Gerlach et al.[14]

Parameters A [kJ Å² mol⁻¹ e⁻²]	Parameters B [kJ Å² mol⁻¹ e⁻²]	Parameters C [e Å⁻²]	Parameters D & E [-]	Cationic Radii [Å]
A_1 = 7808	B_1 = 7439	C_1 = 0.0038	D_1 = 168.5	Li = 1.746
A_2 = 37633	B_2 = 6481	C_2 = 0.0132	E_1 = 1.442	Na = 1.899
A_3 = 3106	B_3 = 12118	C_3 = 0.0145	E_2 = 1E-04	K = 2.014
A_4 = 5616	B_4 = 110		E_3 = 0.2284	Rb = 2.080
A_5 = 3672	B_5 = 12833			Cs = 2.235
A_6 = 2587	B_6 = 937			
	B_7 = 4737			
	B_8 = 5212			

5.1.2 Procedure for model parameterization and evaluation

The MATLAB program EquilProp, developed by Gerlach et al.[186], was extended to be able to:

- Evaluate salt concentration dependent dielectric decrement data
- Calculate Gibbs free energies of transfer of ions
- Calculate salt solubilities in mixed solvents
- Calculate solvation energies of ions and neutral molecules
- Calculate pKa values

The objective functions for estimating the model's parameters depend on the data type as follows:

$$F_{MIAC} = W_{type} \sum_{l} \left(ln\, \gamma_{\pm}^{(m),*,calc} - ln\, \gamma_{\pm}^{(m),*,exp} \right)^2 \tag{5.1}$$

For all alkali halides a weighting factor (W_{type}) of 40 was used. For polyatomic alkali salts a weighting factor (W_{type}) of 20 was employed. These weighting factors were chosen to give a better balance of the influences to the overall objective function in comparison to other data types.

To quantitatively evaluate the model's representation of MIAC data the average absolute deviation (AAD) and the average relative deviation (ARD) can be calculated:

$$AAD_{MIAC} = \frac{1}{N_{DP}} \sum \left| ln\left(\gamma_{\pm}^{(m),*,calc}\right) - ln\left(\gamma_{\pm}^{(m),*,exp}\right) \right| \tag{5.2}$$

$$ARD_{MIAC} = \frac{100}{N_{DP}} \sum \left(\left| 1 - \frac{\gamma_{\pm}^{(m),*,calc}}{\gamma_{\pm}^{(m),*,exp}} \right| \right) \tag{5.3}$$

For LLE systems, according to equation (2.8), there is a non-iterative way to evaluate the model based on the calculation of the partition ratio of the salt between the organic- and the salt-rich phase from the activity coefficients:

$$K_{salt}^{OS,calculated} = \frac{\gamma_{\pm}^{S}(x_{\pm}^{S,exp})}{\gamma_{\pm}^{O}(x_{\pm}^{O,exp})} \tag{5.4}$$

This way it is possible to compare the experimental partition ratio $K_{salt}^{OS,exp} = \frac{x_{\pm}^{O,exp}}{x_{\pm}^{O,exp}}$ with the calculated value $K_{salt}^{OS,calculated}$. This evaluation method has two advantages: It is computationally cheaper and independent of the convergence of the iterative algorithm.

Therefore, the following contribution to the objective function was employed:

$$F_{LLE} = \sum \left(ln\left(K_{salt}^{OS,exp}\right) - ln\left(K_{salt}^{OS,calc}\right) \right)^2 \tag{5.5}$$

While the deviation of the model for the LLE data was evaluated based on following AAD:

$$AAD_{LLE} = \frac{1}{N_{DP}} \sum \left| ln\left(K_{salt}^{OS,exp}\right) - ln\left(K_{salt}^{OS,calc}\right) \right| \tag{5.6}$$

For Gibbs free energies of transfer data, the following objective function was used:

$$F_{G-transfer} = \sum \left(\frac{\Delta G^0_{tr,ion\ w\to s}}{RT} - \ln\left(\frac{\gamma^{\infty}_{ion,s}}{\gamma^{\infty}_{ion,w}}\right)\right)^2 \tag{5.7}$$

To characterize the deviation of the model for the Gibbs free energy of transfer data the following AAD was calculated:

$$AAD_{G-transfer} = \frac{1}{N_{DP}} \sum \left| \frac{\Delta G^0_{tr,ion\ w\to s}}{RT} - \ln\left(\frac{\gamma^{\infty}_{ion,s}}{\gamma^{\infty}_{ion,w}}\right)\right| \tag{5.8}$$

To quickly evaluate the model for its predictive capability for SLE data, it is possible to calculate the expected MIAC that the model should deliver to calculate the correct solubility and compare this value to the one actually calculated.

To calculate the expected MIAC, equation (2.30) might be rearranged like so:

$$\ln \gamma^{expected}_{\pm,s} = ln\, x_{\pm,w}\gamma_{\pm,w} - \frac{\Delta G^0_{tr,salt\ w\to s}}{RT} - \ln x_{\pm,s} \tag{5.9}$$

Consequently, the deviation for the SLE systems was calculated as follows:

$$AAD_{SLE} = \frac{1}{N_{DP}} \sum \left| \ln \gamma^{s,expected}_{\pm} - \ln \gamma^{s,calc}_{\pm} \right| \tag{5.10}$$

The deviation for IDACs ($\theta = \ln \gamma^{\infty}_i$) and solvation energies ($\theta = \Delta G^{o}_{solv}$) systems was calculated as follows:

$$AAD_{\theta} = \frac{1}{N_{DP}} \sum \left| \theta^{lit} - \theta^{calc} \right| \tag{5.11}$$

Consequently, the following objective function was used for this data:

$$F_{\theta} = \sum (\theta^{lit} - \theta^{calc})^2 \tag{5.12}$$

Generally, deviations between the calculated and the experimental value for a target size θ are usually described as absolute average deviations as described above, as root mean square error (RMSE):

$$RMSE = \left(\frac{\sum_i^n (\theta_i^{calc} - \theta_i^{exp})^2}{N}\right)^{1/2} \quad (5.13)$$

or as mean signed deviation (MSD):

$$MSD = \frac{\sum_i^n (\theta_i^{calc} - \theta_i^{exp})}{N} \quad (5.14)$$

Two algorithms were used for the parametrizations: either the Nelder-Mead or the Levenberg-Marquardt.

In this work, whenever the data was used in the parameterization process, the results are considered correlations and whenever the data shown was not part of the training set the results are considered predictions.

5.1.3 Database used for model parameterization and evaluation

The database of thermodynamic and thermophysical data used in this work includes MIACs, LLEs, SLEs, Gibbs free energies of transfer, dielectric decrement data, IDACs and solvation energies.

The aqueous MIAC data used is a very similar to the MIAC data used by Gerlach et al.[14] only excluding 6 earth-alkaline systems (cf. appendix in section 8.4.1) because insufficient data was available in the database to parametrize these systems consistently. For some of the parameterizations organic MIAC data was used to evaluate the performance of the model (cf. appendix in section 8.4.2). The LLE data is composed of the data used by Gerlach et al.[14] with some additional low-permittivity systems (cf. appendix in section 8.4.3). The SLE data includes strong electrolytes in aqueous or binary solvent systems like ammonium salts and alkali metal salts with either halides, perchlorate, sulfate, nitrate or thiocyanate as the corresponding anion (cf. appendix in section 8.4.4). Gibbs free energies of transfer of alkali cations, halide anions, polyatomic anions and organic ions were also

compiled, describing the transfer from water to an organic solvent or a solvent mixture. Additional Gibbs free energies of transfer were calculated from published solubility product values of water (w) and a second solvent (s) (cf. appendix in section 8.4.5). Based on equation (2.30) it is possible to see that the Gibbs free energy of transfer of a salt can be calculated as follows:

$$\Delta G^{0}_{tr,salt\ w\to s} = RT\left(\ln K_{SP,s} - \ln K_{SP,w}\right) \tag{5.15}$$

By combination of the calculated value for the salt with the data already available in the database for single-ions, it is possible to estimate further values of Gibbs free energies of transfer of single-ions. Most of the available experimental data is commonly presented in molarity scale (c). Thus, the following scale conversion[62] had to be performed for all data points:

$$\Delta G^{0\,(x)}_{tr,w\to s} = \Delta G^{0\,(c)}_{tr,w\to s} - RT\ln\left(\frac{M_w\rho_s}{M_s\rho_w}\right) \tag{5.16}$$

Where M_i and ρ_i are the molecular mass and the density of the solvent i respectively. In other parts of this work all values presented are in mole fraction scale.

The dielectric decrement data was collected with an emphasis in representing a variety of different salts in water. Some non-aqueous systems were also found. (cf. appendix in section 8.4.6).

The infinite dilution activity coefficient data was collected from Voutsas & Tassios [187] and He [188]. The values for water as solute were however not included as it is known from the literature[187] that a systematic deviation is found for these in calculations with COSMO-RS. There are ways to get around this systematic deviation, but this further complexity was not investigated in this work.

The solvation energy data was collected from Marenich et al.[189] and contains several hundred datapoints for ionic solutes in water, methanol, DMSO and acetonitrile, as well as about 3000 datapoints for neutral molecules in a diverse range of solvents.

All systems discussed in this work were measured at 25 °C and 1 atm unless stated otherwise. The references for the complete dataset (excluding the solvation energies and the IDACs) is listed in the appendix in section 8.4.

5.2 Experimental methods

5.2.1 Preparation of chemicals

The chemicals used in this work are listed in Table 5.3.

Table 5.3: Chemicals used in the experimental measurements of the non-aqueous phase equilibria.

Chemical	Purity [wt-%]	Comment	Manufaturer
lithium chloride	99.9	anhydrous	J & K Scientific Ltd.
ethanol	99.9		Th. Geyer GmbH & Co. KG.
methanol	99.9	dried	Th. Geyer GmbH & Co. KG.
toluene	99.8	water-free	SIGMA-ALDRICH

The salt was dried in a vacuum oven of the type VT 6060 M-BL from Thermo SCIENTIFIC at 120°C under a carbon dioxide atmosphere for at least 6 hours, after which it was poured in a tightly sealed glass bottle also dried at the same time as the salt to avoid moisture.

The solvents were additionally dried using molecular sieve with a pore diameter of 3Å: a small portion of the solvent was stored with the molecular sieve inside the glass bottles before the experiments were carried out for at least a week. This ensured a water content of < 100 ppm water measured by Karl-Fisher titrator.

After drying, the salt and the solvents were kept in a desiccator to avoid moisture as much as possible.

5.2.2 Method for the measurement of the liquid-liquid phase equilibria

All sample preparation, sample taking, and weighting was done within a glove box from Labconco of the type Precise Controlled Atmosphere Glove Box. The atmosphere inside the glove box was not controlled automatically. However, silica gel particles were used to

absorb the moisture of the air up to a relative humidity of about 7 %, which was monitored closely by hygrometers from Testo of the type 174H Mini Datenlogger. Which at room temperature translates to a loading of less than 1g/kg. Weighting was performed by a scale from Mettler-Toledo (type ME 204) with an accuracy of 0.0001 grams.

The samples were prepared in such a way that the head space in the vials was minimized and then sealed with an aluminum crimp cap. Then the samples were mixed in an overhead shaker (Reax 2 from Heidolph Instruments GmbH & Co. KG).

Following the sample preparation, these were placed in a shaking water bath (OLS200 from Grant Instruments (Cambridge) Ltd). The temperature was controlled by a thermostat (RC 25 CS from LAUDA DR. R. WOBSER GmbH & Co. KG)) within a temperature range of 0.1 K.

The samples were first heated to 35 °C. After at least 3 hours the samples were then cooled to 25 °C. After at least 6 hours of shaking at 25 °C, the shaking was turned off to allow the formation of the phases for at least 24 hours.

The samples are then carefully transported to the glove box, opened and a sample is taken from each phase using a syringe. First a sample is taken from the upper phase, then the upper phase is removed to take a sample of the lower phase. The measurements were performed in triplicates.

5.2.3 Analytical methods

The salt concentration in each phase was determined with two different methods depending on the expected concentration. From previous measurements it was known that one phase mostly consisted of alcohol and salt (salt-rich phase) while the other phase contained mostly toluene with a small amount of alcohol and salt (organic phase). The salt concentration of the salt-rich phase was analyzed by drying in the vacuum oven until weight constancy. The salt concentration in the organic phase was determined by ICP-OES with an FID detector by a spectrometer from Perkin Elmer (Optima 8300 DV).

The organic solvent concentration in both phases was analyzed by a gas chromatographic method on an Agilent 7890 B using a DB255 column with a diameter of 250 µm, a length of 30 m and a stationary phase of 50% cyanopropylphenyl & 50% dimethylpolysiloxane. At the beginning of the GC method, the oven temperature was constant at 45 °C for 5 min,

after that the temperature was increased at a rate of 7 °C per minute until a temperature of 150 °C was reached. After these 15 min, the temperature was held constant at 150 °C for 7 minutes. The temperature of the detector was 320 °C while the injector was kept at 210 °C. Similar to Dong et al.[181], glass wool was put into the glass liner of the vaporizing chamber to allow the salt to crystallize there without contaminating the column. As an internal standard 1-propanol was used. Every sample was analyzed in duplicates.

The water concentration in each sample was measured using a Karl-Fisher apparatus from Mettler Toledo (V20 Volumetric KF Titrator).

6 Results and discussion

This section first shows the extension of the COSMO-RS-ES model to SLE calculations in mixed-solvents and completely non-aqueous solvents. As a first improvement the short-range term is enhanced by means of including Gibbs free energies of transfer into the training dataset. Then the long-range term is analyzed to understand the influence of using salt-free properties or the solution properties in its calculation. Furthermore, the model is improved to include the description of systems at very low permittivities by the inclusion of the effect of ion-pairing into the model. A method for measuring completely non-aqueous LLEs is developed and applied to measure two non-aqueous systems. The analysis of this data gives insights as to how to model these challenging systems. As a last extension, the model is adjusted to be able to calculate solvation energies and pKa values.

The results of this work have partially been published by Müller et al.[15], Müller et al.[16] and Kröger et al.[17] Some of the figures shown in this chapter were taken with permission from Müller et al.[15] and Müller et al.[16]

6.1 Extension of COSMO-RS-ES: highly concentrated, mixed-solvent systems

COSMO-RS-ES[14] has already been successfully applied to aqueous MIACs, mixed-solvent LLEs and VLEs. In the following, the model shall be applied to higher salt concentrations up to solubility limit in mixed-solvent and non-aqueous systems. The SLE dataset used in this section is described in more detail in section 8.4.4 of the appendix.

There are different ways to model the solubility of a salt. One method is to employ the melting enthalpy and temperature, leading to an activity coefficient with reference state pure undercooled melt. An alternative way is to employ the Gibbs free energies of formation in solution to calculate the solubility product. In this work, another approach is used. COSMO-RS-ES was created to be as predictive as possible and to be easy to apply in real life. Since it is relatively easy and fast to measure the solubility of a salt in a solvent another approach was employed in this work to model the solubility product of a salt. According to equation (2.30) the solubility product can be calculated if the experimental solubility in a reference solvent and the MIAC at this concentration is known. Then by calculating the MIAC in the other mixture with reference state infinite dilution in the reference solvent it is possible to predict the solubility. This approach assumes that the model describes the MIACs in the reference solvent quite accurately. Theoretically any solvent can be used as reference solvent, however in this work, water is used as reference solvent. This choice is done because of two reasons. Firstly, solubility measurements in water are available in literature for many salts and secondly, COSMO-RS-ES has already been shown to reliably calculate aqueous MIACs.

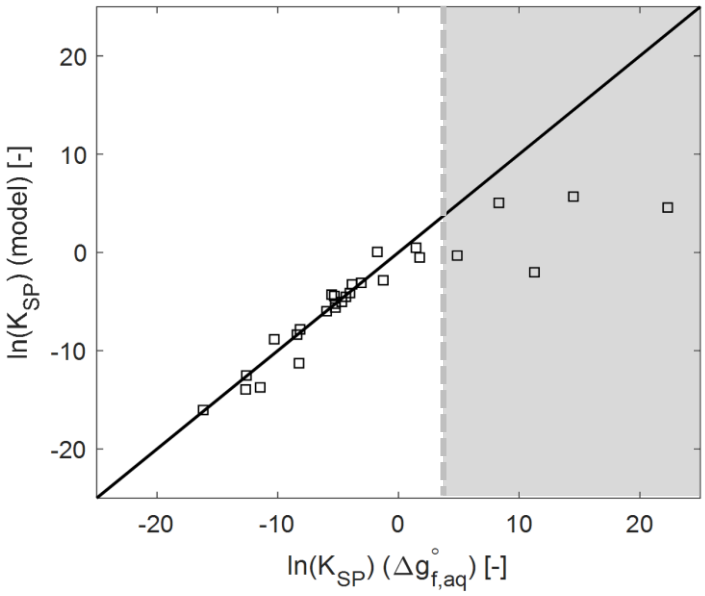

Figure 6.1: Parity plot of solubility products calculated by the model COSMO-RS-ES with the parameters published by Gerlach et al.[177] and by aqueous formation energies from the literature[4].

The solubility products calculated with COSMO-RS-ES can be expected to be as accurate as the MIACs. Figure 6.1 shows values of solubility products calculated by the model and by aqueous formation energies from the literature[4] as follows:

$$\ln(K_{sp}) = -\,\mathrm{RT}\left\{\nu_{cat}\cdot \Delta g^{\circ}_{f,cat,aq} + \nu_{an}\cdot \Delta g^{\circ}_{f,an,aq} - \Delta g^{\circ}_{f,salt,aq}\right\} \tag{6.1}$$

The calculated values can be reviewed in the appendix in section 8.1.1.

For the vast majority of electrolytes, the estimation of the solubility product by COSMO-RS-ES delivers very good results. Only for salts with very high solubilities (e.g. LiCl, LiBr, LiI, $LiClO_4$), on the right side of the figure, the values deviate from those calculated by the model. When evaluating the solubility of salts in other solvents this fact has to be taken into consideration, since the model has only been trained with data up to a molality of 6. Because of this fact, the calculation of the solubility product can be considered a predictive application of COSMO-RS-ES since for several salts, the experimental MIAC data does not reach to the solubility limit.

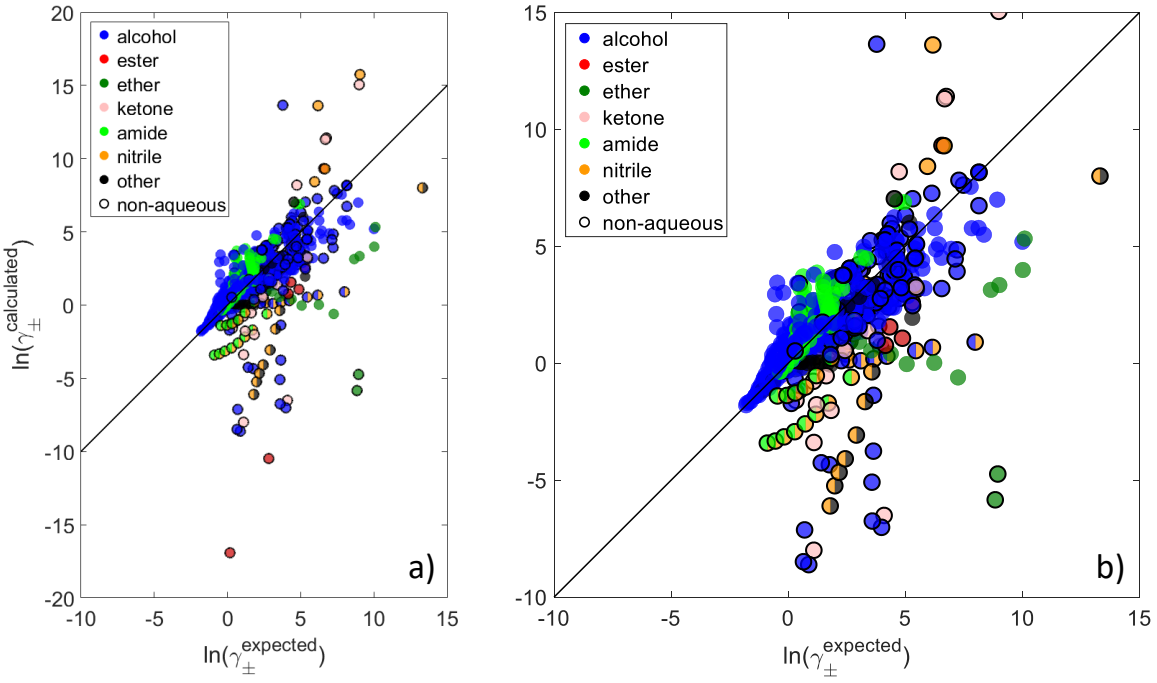

Figure 6.2: Parity plot of the calculated activity coefficient vs. the expected activity coefficient according to equation (5.9). COSMO-RS-ES calculations with the parameters published by Gerlach et al.[14] The coloring of the presented values depends on the functional groups present in the solvents of the system in question. If more than one functional group is present (e.g. 3-methoxy-1-butanol) the plot shows the system as the non-alcoholic group. Figure 6.2 a) shows all the SLE systems in the database, while Figure 6.2 b) shows an enlarged version containing most of the SLE systems. Non-aqueous systems are shown with a black circle around the markers in the plot.

After checking the ability of the model to calculate the solubility products, the model can be applied to calculating SLEs in other systems. Figure 6.2 shows the calculation of the expected activity coefficient to calculate the correct solubility as defined in equation (5.9). It is possible to see that overall the model slightly underestimates the expected values.

The overall deviation of the calculated values according to equation (5.10) is $AAD_{SLE} = 1.23$. Generally, mixed-solvent systems including water as one of the solvents (without a black circle around the marker) are represented better than non-aqueous systems. The accuracy of calculation of the water-containing systems varies depending on the co-solvent. Systems containing alcohol as the cosolvent are represented the best. This agrees with the fact that the original COSMO-RS-ES model was parametrized mainly with alcohol containing LLEs. Systems containing amide groups (in most cases with high

permittivities) are slightly overestimated. Nevertheless, these systems are calculated more accurately than systems with solvents of low permittivity.

Figure 6.3 shows the deviations of the calculation in relation to the expected value summarized according to the nature of the different ions. It can be seen that the same trend holds true as most mean signed deviations (MSDs) are negative.

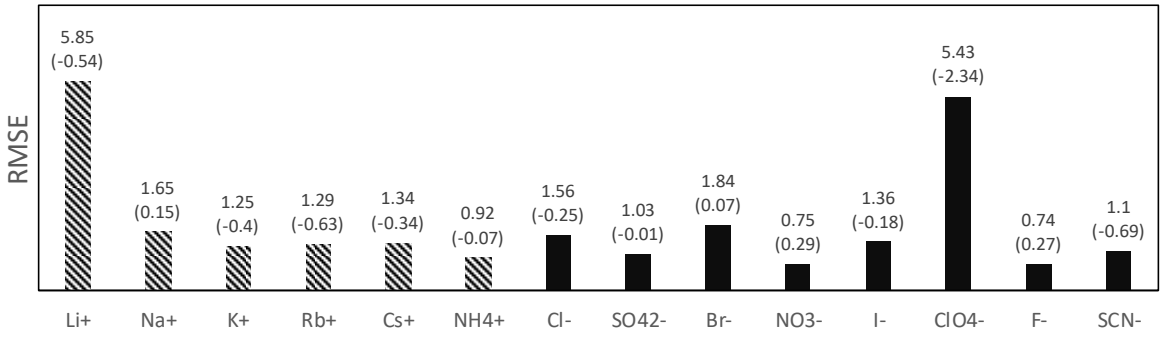

Figure 6.3: Deviations in relation to the expected value summarized according to the different ions calculated by COSMO-RS-ES using the parameters published by Gerlach et al.[14]. Values of the root mean square error (RMSE) are shown on top of every bar, while the value in the parenthesis represents the mean signed deviation (MSD) of the systems.

The deviations correlate with the size of the cation and loosely with the size of the anion. The smaller the cation and the larger the anion, the larger the deviation of the systems in question. This is due to the fact that, the solubility also correlates with the size of the ion in the same manner. Lithium salts with large anions have a very high solubility in water but also in polar organic solvents. The largest deviations can be seen for lithium and perchlorate. This is because the systems with the largest deviation (also shown in Figure 6.2 a) are the following: $LiClO_4$+diethyl ether and $LiClO_4$+ethyl acetate. Both systems are characterized by a high solubility (> than 50 wt-%) and low permittivities. At these high concentrations it is almost possible to start talking about a solvent-in-salt system. At high concentrations and low permittivities (as explained in section 2.2.1) ion-pairing becomes more prominent. This issue is addressed in more detail in section 6.4.

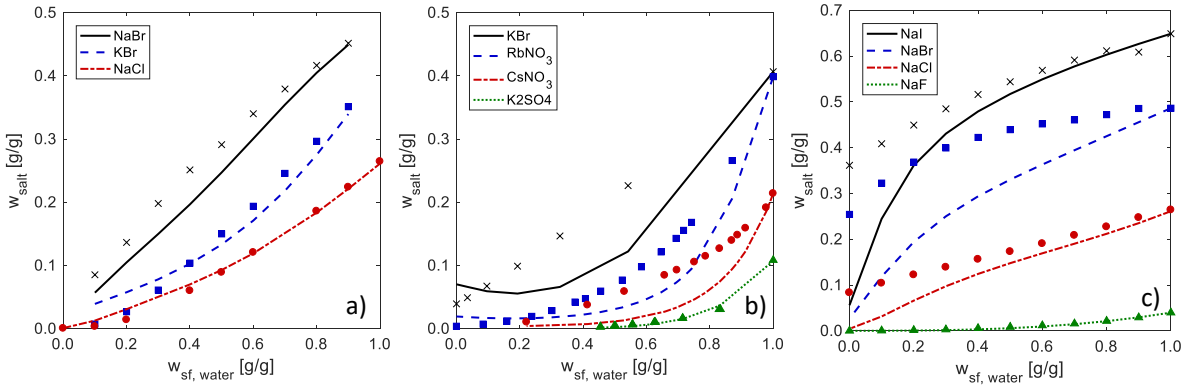

Figure 6.4: Solubilities for several systems predicted by COSMO-RS-ES using the parameters published by Gerlach et al.[14] The markers represent the experimental values, while the lines represent the calculated values. Figure 6.4 a) shows the systems NaBr + water + ethanol[190], KBr + water + ethanol[191], NaCl + water+ ethanol[192]. Figure 6.4 b) shows the systems KBr + water + 2-methoxyethanol[193], $RbNO_3$ + water + methanol[194], $CsNO_3$ + water + tert-butanol[195], K_2SO_4 in water + 1-propanol[196]. Figure 6.4 c) shows the systems (NaI, NaBr, NaCl, NaF) + water + formamide[197].

Figure 6.4 a) shows solubilities of alkali halides in aqueous alcoholic systems calculated by COSMO-RS-ES. Quantitative agreement between the predicted and experimental values can be observed. The qualitative trends are also well represented. As can be observed from Figure 6.4 b), even in systems with polyatomic anions like rubidium nitrate, cesium nitrate and the divalent potassium sulfate dissolved in different solvents, the model delivers satisfying predictions. Although the calculated values are not as quantitatively accurate as for the alkali halides, the trends are correct. The higher the solubility in pure water, the larger the underestimation of the calculated solubility becomes. This might be due to the overestimation of the activity coefficient with falling water concentration or from a wrong description of the preferential solvation. Figure 6.4 c) shows the predicted solubilities of several sodium halides in mixtures of water and formamide. There is one difference for these systems in comparison to the previously discussed. The permittivity of the co-solvent formamide is much higher than the one of water. This could have led the model to predict a higher solubility than in water. However, also in this case the model is capable of describing the trends accurately. Although the solubility is underestimated in pure formamide, the order of the predicted solubility is correct. The predictions of the model deteriorate the less water is in the system. This is

not surprising as water is taken as the reference, but it shows that the model is describing the transfer from water to the organic solvent less accurately.

To have a closer look at how the model works for organic solvents, Figure 6.5 a) shows the predicted solubility of the non-aqueous system sodium bromide in mixtures of acetonitrile and DMSO, while Figure 6.5 b) shows the corresponding calculated activity coefficients. The different contributions of the SR and the LR term to the activity coefficients are also shown. Due to the similar permittivity of both solvents ($\epsilon_{acetonitril} = 37$; $\epsilon_{DMSO} = 47$), the LR contribution does not have much influence on the overall calculated value. The SR contribution however has a large influence. Being responsible for the jump in the rightest value and on the underestimation of the activity coefficient. Keeping in mind that the reference state of the activity coefficient is infinite dilution in water, the plot hints that the calculation of the transfer of the ions from infinitely dilute in water to the system concentration is wrongly described by the model. This explains the overestimation of the solubility in this system as a deviating SR description by the model.

Figure 6.5 c) illustrates the partial calculation of the solubility of potassium chloride in mixtures of water and 1,4-dioxane, while Figure 6.5 d) shows the corresponding calculated activity coefficients. The calculation algorithm was not able to find a single solution for the solubility of the salt in high 1,4-dioxane concentrations. This system is special in the sense that both solvents are completely miscible, but the permittivity of water and 1,4-dioxane are very different ($\epsilon_{water} = 78$; $\epsilon_{1,4-dioxane} = 2$). As can be observed in Figure 6.5 d), at low dioxane concentrations the model delivers accurate activity coefficients. However, at larger dioxane concentrations, i.e. lower permittivities, the LR part of the model drifts into the wrong direction while the SR contribution would have gone into the right direction. This shows that contrary to the system shown in Figure 6.5 a), the deviation of the model is mainly due to the LR term.

The both examples described in Figure 6.5, make clear that to improve the model for the description of SLEs in mixed-solvent and non-aqueous systems, both contributions, the SR and the LR term need to be improved.

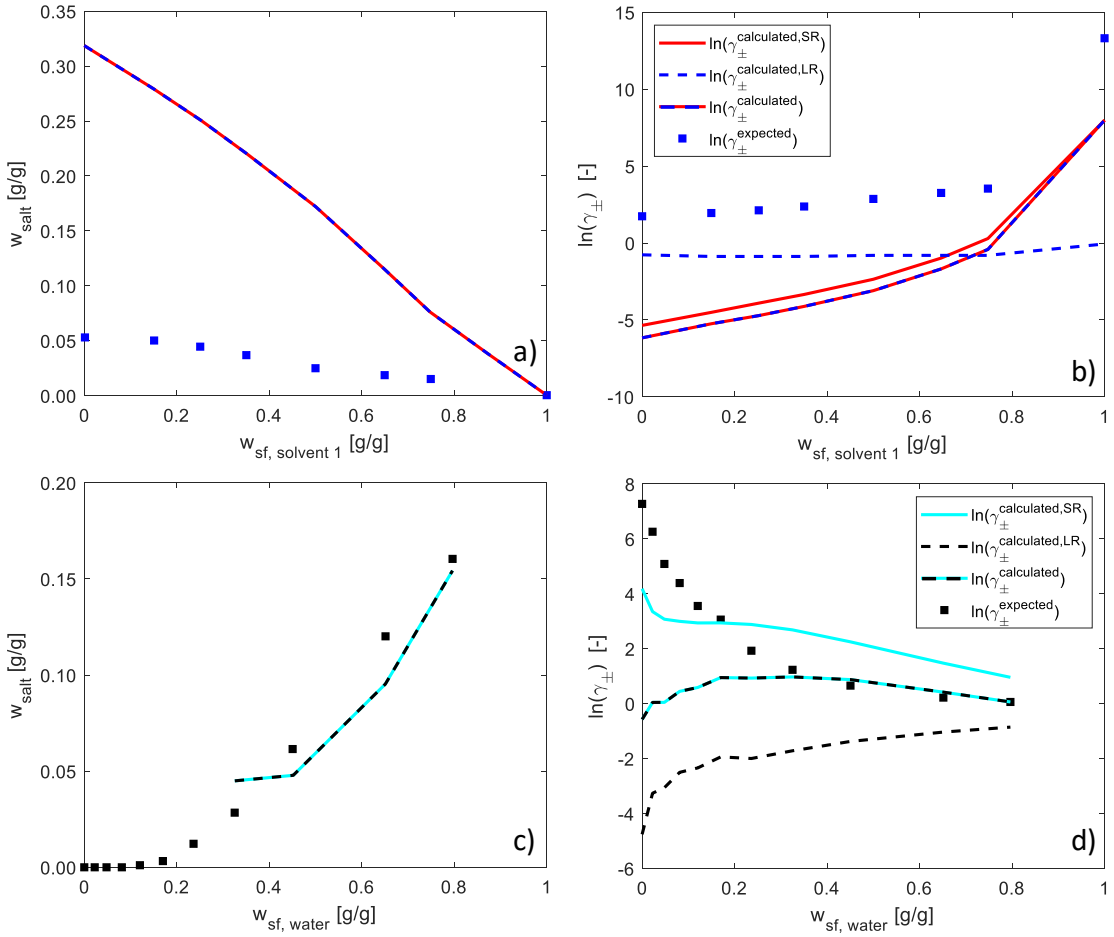

Figure 6.5: Solubilities for several systems predicted by COSMO-RS-ES using the parameters published by Gerlach et al.[14] The markers represent the experimental or expected values, while the lines represent the calculated values. Figure 6.5 a) shows the system NaBr + acetonitrile + DMSO[198] while Figure 6.5 b) shows the corresponding calculated activity coefficients. Figure 6.5 c) shows the system KCl + water + 1,4-dioxane[199] while Figure 6.5 d) shows the corresponding calculated activity coefficients.

6.2 Refinement of COSMO-RS-ES: the SR term

The improvement of the accuracy of COSMO-RS-ES for the calculation of SLE systems, as discussed in the previous section 6.1, can be done by improving the SR term of the model. In this work, the solubilities are calculated by equation (2.30). As can be seen from this equation, part of the SLE calculation includes the calculation of the Gibbs free energy of transfer of the salt. The Gibbs free energy of the transfer for the salt can be calculated as the sum of the values for the single ions according to equation (2.27). For this purpose a new dataset of Gibbs free energy of transfer of ions was created. The dataset references are listed in detail in section 8.4.5 of the appendix.

Although this data might not be considered as accurate as other thermodynamic data because of the extra-thermodynamic assumptions needed for the partitioning of the measured values for salts into the values for the single ions[200], it can deliver valuable information as to what a model is doing wrong at the moment of calculating the transfer energy needed for a salt from one solvent to another. The most commonly employed assumption for this partitioning is the TATB assumption.[20,200] TATB standing for the tetraphenylarsonium tetraphenylborate salt. As the anion and the cation are both of similar size and of low charge density, the assumption is that the Gibbs free energy of transfer for the anion is equal as for the cation.

Because the underlying uncertainty of the chosen extra-thermodynamic assumption, this data is used for evaluation of the model and also guidance for the parameters but is not included in a final parameterization of the model. In this work several parametrization strategies were tested and the most successful was based on a two-step parametrization process. In more detail this means that in a first parameterization step the MIACs, the LLEs and the Gibbs free energies of the ions are used to parametrize the model. Then in a second parameterization step, using the parameters from the first step as initial parameters, the model is parametrized only with MIACs and LLEs. The addition of these constraints in the first parametrization step is the first-time ion-specific data is used in the model parameterization. As this thermodynamic data describes the interactions of a single ion with one solvent in comparison with another solvent without the influence of

other ions, it bears valuable information for the description of the interaction energies. The inclusion of this data will be shown later to lead to a more robust model applicable predictively to a wider range of systems. To the authors knowledge, this is the first time this type of data is used to increase the performance of a predictive electrolyte g^E-model.[15]

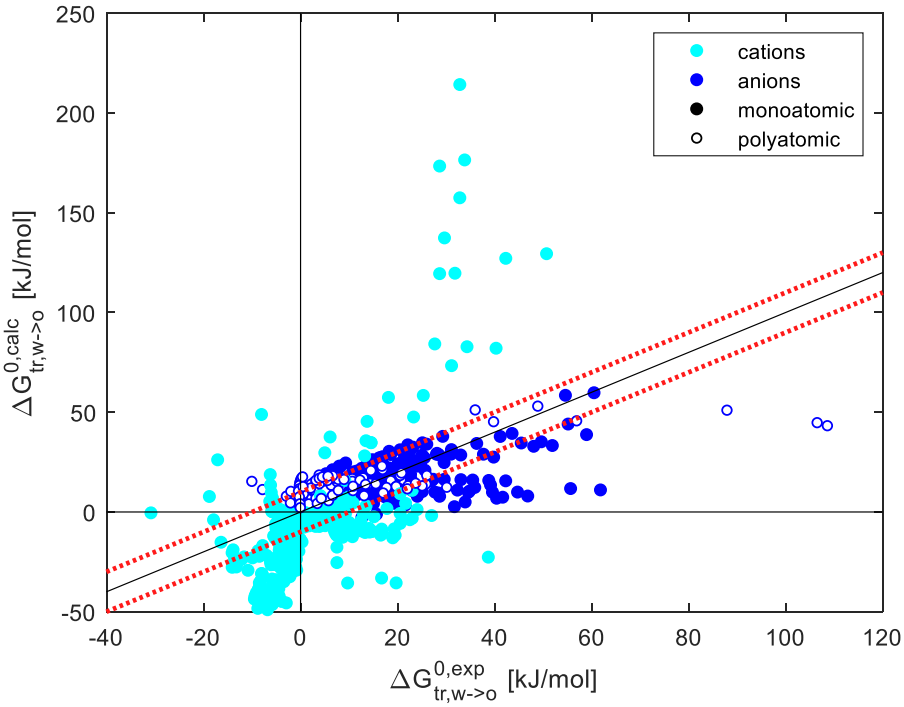

Figure 6.6: Predicted Gibbs free energies of transfer of ions calculated by COSMO-RS-ES using the parameters by Gerlach et al.[14] vs. the experimental values. The dotted red line indicates the maximum estimated experimental error ±10 kJ/mol by Kalidas et al.[201] Filled circles (•) represent monoatomic ions while open circles (○) represent polyatomic ions.

First an evaluation of the published COSMO-RS-ES version is done. Figure 6.6 shows the results of the calculation of all the Gibbs free energies of transfer of ions available in the dataset. It can be observed that most of the available data encompasses monoatomic ions. Only polyatomic anions are available in the dataset, no polyatomic cations are included.

Table 6.1 summarized the results for the evaluation of the published model. As can be seen, the calculated values for the anions already agree quite well with the experimental values. As the MSD suggests the values are evenly distributed around the parity line. Divalent polyatomic anions like thiosulfate and sulfate are the anions with the largest deviation seen on the right side of Figure 6.6. The other values for monoatomic and even polyatomic anions mostly lie within the maximum estimated experimental deviation.

In contrast to the anions, the calculated values for the cations are off by an order of magnitude in some cases. The deviation is more than twice as large as the anions (cf. Table 6.1). While Figure 6.6 at first sight suggests that the calculated values for the cations are overestimated, the MSD tells a different story: although some cationic systems are overestimated, most of them are underestimated.

Table 6.1: Summary of the deviations in $\left[\frac{kj}{mol}\right]$ of the Gibbs free energies of transfer of ions calculated by COSMO-RS-ES using the parameters by Gerlach et al.[14] and by the new Parametrization A including Gibbs free energies of transfer of ions in the training dataset.

	Published COSMO-RS-ES[14]		Parameterization A	
Data	*AAD*	*MSD*	*AAD*	*MSD*
Cations	5.86	-2.70	3.51	-1.25
Anions	2.79	0.51	2.79	0.09
Total	4.35	-1.11	3.15	-0.43

6.2.1 Parameterization A: Including Gibbs free energies of transfer

During this work two developments greatly improved the model leading to two versions of COSMO-RS-ES called Parameterization A and the later described Parameterization B. In Parameterization A the Gibbs free energies of transfer of ions were included into the training dataset. This was done by the parametrization strategy described above. Table 6.2 shows the optimized parameters of the model for the Parameterization A.

Most of the parameters do not change very much. The misfit parameter A_2 decreases by over 90% and the parameter B_6 increases by over 45% in comparison to the published values.[14] This decreases the misfit energy and increases the attractive energy between cations and organic molecules making this contact much more probable in the modeling framework. The parameters D and E also increase making the equations more dependent on the sigma descriptor than they were before. Which is a good sign, as a stronger weight is put in using this information for the calculation of the interaction energies.

From the summary of the deviations in Table 6.1 it can be seen that the cations are described much better than with the published parameters. The description of the anions stays equally as good looking at the AAD. However, the MSD shows that the cation and also the anions are described more evenly around the experimental value.

Table 6.2: COSMO-RS-ES parameters referring to ionic interaction energies as defined in Table 2.3, new values optimized including Gibbs free energies of transfer of ions in the training dataset. This parametrization is called Parametrization A. Parameters whose value increased or decreased more than 20% of their value in comparison to the values by Gerlach et al.[14] are correspondingly highlighted.

Parameters A [kJ Å² mol⁻¹ e⁻²]	Parameters B [kJ Å² mol⁻¹ e⁻²]	Parameters C [e Å⁻²]	Parameters D & E [-]	Cationic Radii [Å]
A_1 = 7178	B_1 = 6639	C_1 = 0.0020	D_1 = 562.7	Li = 1.752
A_2 = 3300	B_2 = 186	C_2 = 0.0107	E_1 = 1.747	Na = 1.901
A_3 = 2088	B_3 = 10327	C_3 = 0.0321	E_2 = 0.015	K = 2.015
A_4 = 6374	B_4 = 99		E_3 = 0.332	Rb = 2.076
A_5 = 3459	B_5 = 10613			Cs = 2.285
A_6 = 2538	B_6 = 1362			
	B_7 = 4741			
	B_8 = 4397			

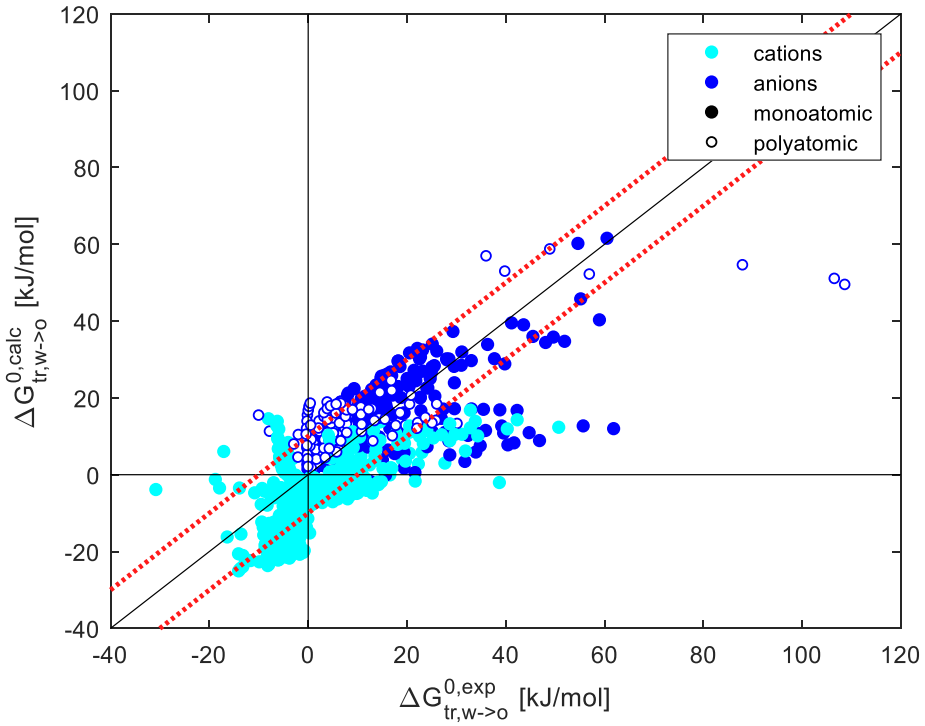

Figure 6.7: Predicted Gibbs free energies of transfer of ions calculated by COSMO-RS-ES using the values optimized including Gibbs free energies of transfer of ions in the training dataset vs. the experimental values. This parametrization is called Parametrization A. The dotted red line indicates the maximum estimated experimental error ±10 kJ/mol by Kalidas et al.[201] Filled circles (•) represent monoatomic ions while open circles (○) represent polyatomic ions.

The new Parameterization A is able to calculate the Gibbs free energies of transfer of ions much more accurate while still keeping basically the same accuracy for the MIACs ($ARD_{MIAC} = 4.37$) and LLEs ($AAD_{LLE} = 0.69$) systems as the published version.[14] Although for some systems the deviation increases slightly, for others (e.g. Figure 6.8) the LLE-calculations are improved a lot. This allows the model to reproduce trends more accurately for a more diverse set of solvents while still keeping the deviation at the same value.

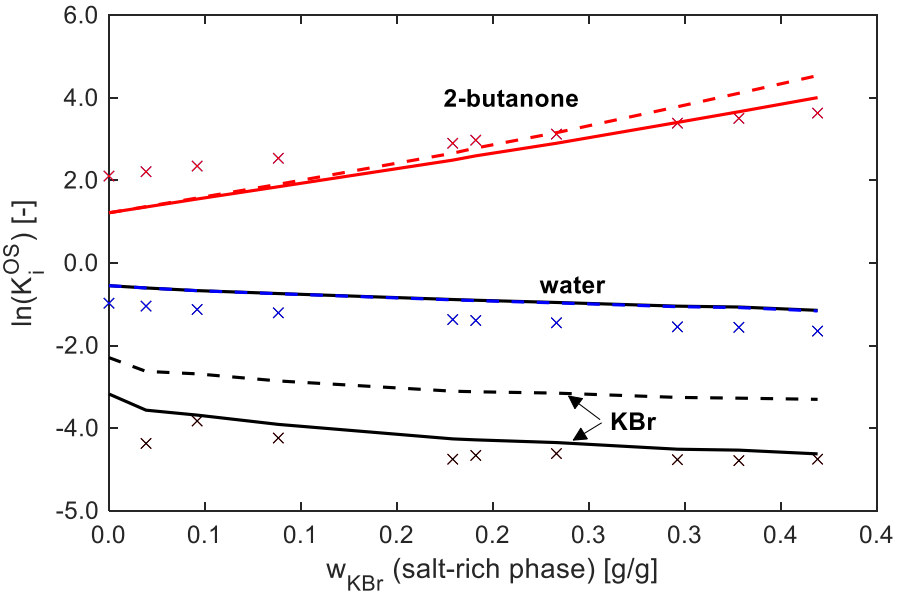

Figure 6.8:Calculation of the partition ratios of the different components in the LLE system KBr + water + 2-butanone[202] calculated according to equation (5.4). The markers correspond to the experimental values, the dashed lines represent calculations with the published parameters from Gerlach et al.[14], solid lines represent the calculated values with the new parameters from Parametrization A.

The most interesting development of the model by the addition of the Gibbs free energies of transfer of ions can be observed when looking at the predicted SLE systems. The overall deviation of the calculated values according to equation (5.10) with the parameters from Parameterization A is $AAD_{SLE} = 0.98$. This represents an improvement of about 25%. Figure 6.9 shows the calculated SLE systems with the new Parameterization A in comparison to the calculations with the published parameters by Gerlach et al.[14]

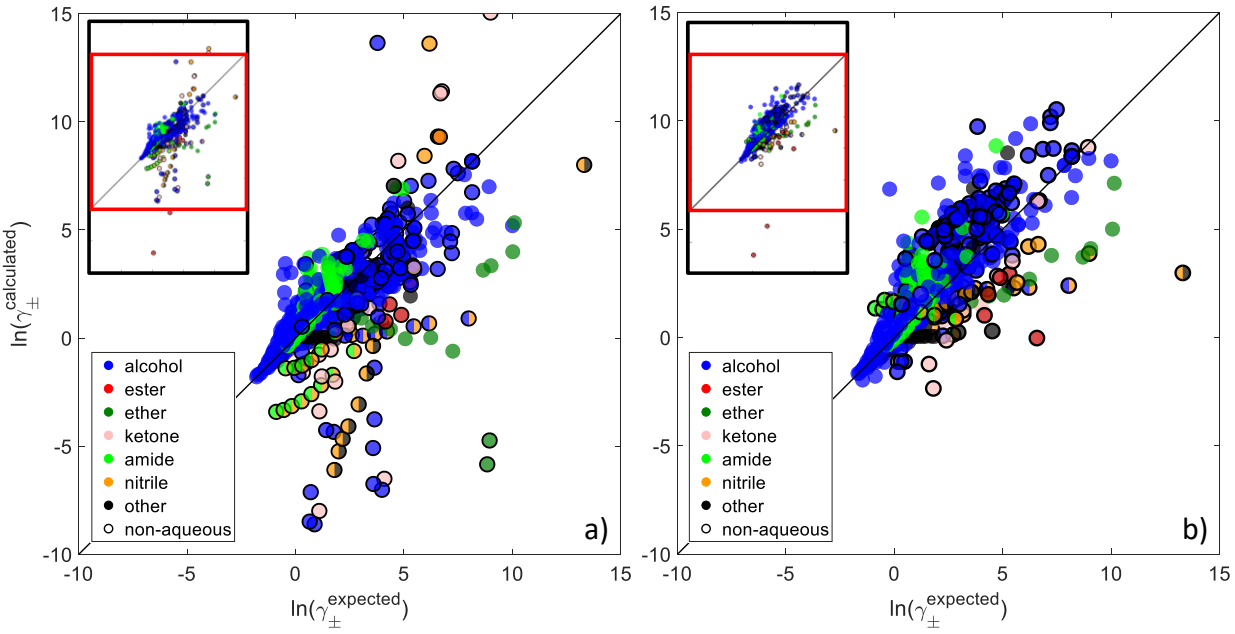

Figure 6.9:Parity plot of the calculated activity coefficient vs. the expected activity coefficient according to equation (5.9). Figure 6.9 a) shows the calculations with the parameters published by Gerlach et al.[14] while Figure 6.9 b) shows the calculations done with the Parameterization A. The coloring of the presented values depends on the functional groups present in the solvents of the system in question. If more than one functional group is present (e.g. 3-methoxy-1-butanol) the plot shows the system as the non-alcoholic group. Non-aqueous systems are shown with a black circle around the markers in the plot.

The refinement is more pronounced for the systems that were showing the largest deviation before: the non-aqueous systems. Although the additional ion-specific constraint put on the model by addition of these systems to the training dataset only is evaluated at infinite dilution, the overall performance of the model is enhanced also at high salt concentrations due to the better description of the transfer of the salt in equation (2.30). The description of the two systems at extremely high concentrations in solvents of very low permittivity were not improved. However, for almost all other systems, independently if they were overestimated or underestimated before, the model produces better results.

Figure 6.10 shows some predictions of solubilities of salts in mixed-solvent systems. For monoatomic salts like potassium bromide and even polyatomic salts like cesium nitrate

there is quantitative agreement between the predicted values and the experimental values. For the solubility of potassium chloride in 2-isopropoxyethanol, the trend is now predicted correctly over the complete concentration range of organic solvent.

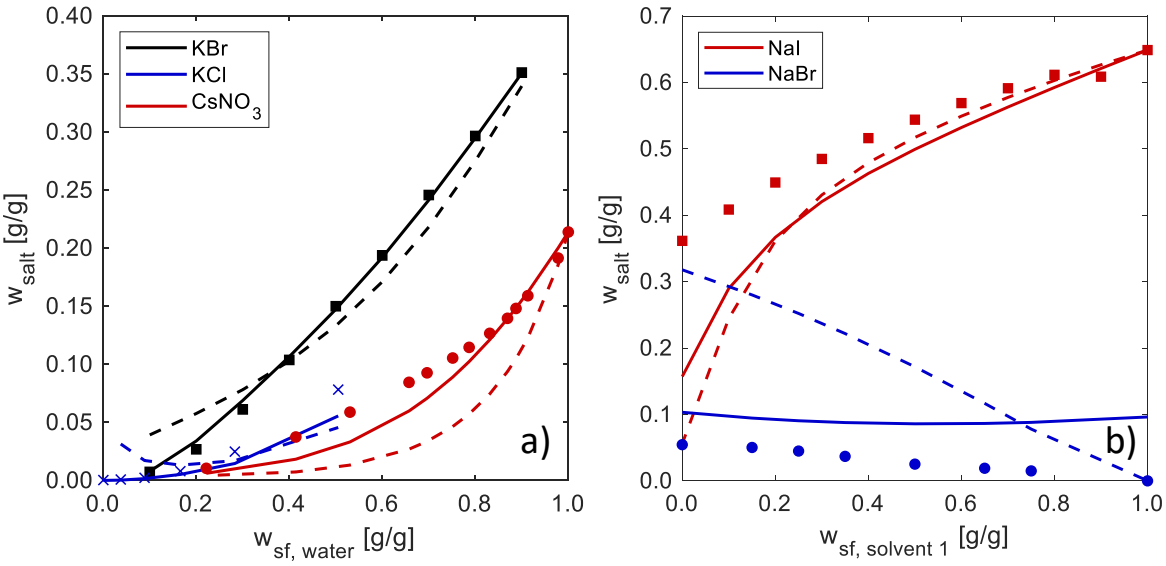

Figure 6.10: Solubilities for several systems predicted by COSMO-RS-ES. Figure 6.10 a) shows the systems KBr + water + ethanol[191], KCl + water + 2-isopropoxyethanol and $CsNO_3$ + water + tert-butanol[195]. Figure 6.10 b) shows the systems NaI + water + formamide[197] and NaBr + acetonitrile +DMSO[198]. The markers correspond to the experimental values, the dashed lines represent calculations with the published parameters from Gerlach et al.[14], solid lines represent the calculated values with Parameterization A.

For the previously shown system sodium iodide in aqueous formamide mixtures with a solubility of up to 70 wt-%, the trend is now reproduced more accurately, especially in pure formamide. While for sodium bromide in mixtures of acetonitrile and DMSO the changes produced mixed results. In pure DMSO, the solubility is predicted more accurately than before, however in pure acetonitrile the solubility is overestimated now. This last point coincides with the point with the largest deviation on the far-right side of Figure 6.9 b).

Although for some systems the improvements give mixed results, for the vast majority of systems in the database the trends and the quantitative agreement has been enhanced greatly by the addition of Gibbs free energies of transfer of ions to the training dataset.

6.3 Refinement of COSMO-RS-ES: the LR term

The improvement of the accuracy of COSMO-RS-ES for the calculation of SLE systems, as discussed in the section 6.1, can also be done by improving the LR term of the model.

In this section, a systematic analysis of the long-range term is performed. For this a sensitivity analysis is done to check the influence of the different input parameters. Furthermore, it is tested whether including the effect of dielectric decrement (cf. section 2.2.2) and a Born term leads to improvements for the model.

6.3.1 Sensitivity of the long-range term towards its input parameters

The long-range term used within the COSMO-RS-ES model is based on the theory of Pitzer-Debye-Hückel (cf. section 2.3.4). The term has basically 3 input parameters: the closest approach parameter (b), the permittivity (ϵ_r) and the density (ρ). Concerning these input parameters, so far the values used in COSMO-RS-ES[14] are equal to those used in the majority of the models in the literature. The closest approach parameter has been fixed at a value of 14.9 originally suggested by Pitzer to keep the model simple.[84] For the permittivity (ϵ_r), the salt-free value has been employed without taking into account the effect of dielectric decrement. Also, for the density the salt-free value is used. This is consistent with the theory, as in the derivation of the LR term in several steps the assumption of a salt-concentration independent density and permittivity is used (i.e. low salt concentration). It is in so far interesting that the model has been able to describe so many different phase equilibria even up to the solubility limit without taking the effect of the salt on the input properties of the LR model so accurately into account.

The closest approach parameter is a function of density and permittivity. However, since it has been considered independent of both values up until now, for the sensitivity analysis it will be treated as an independent parameter. For a 1:1-electrolyte with typical water salt-free density and permittivity at 25 °C and a closest approach value of 14.9, Figure 6.11 a) shows the sensitivity of the logarithm of the LR term activity coefficient towards the previously discussed parameters as a function of the ionic strength of the salt. It can be observed that the sensitivity of the LR term is greatest towards the closest

approach parameter. The LR term also has a strong sensitivity towards the permittivity and is almost independent of the density.

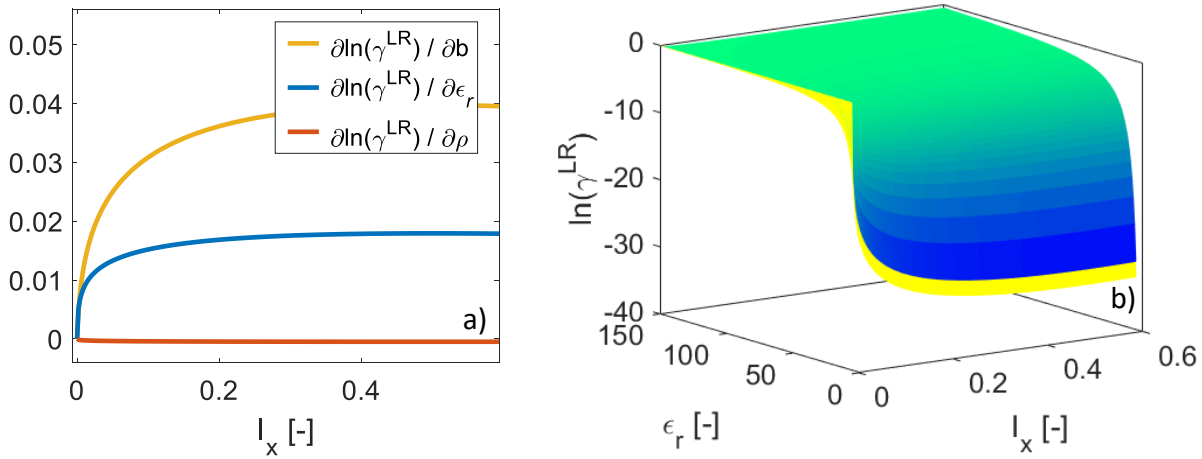

Figure 6.11: Figure 6.11 a) Sensitivity of the logarithm of the LR term activity coefficient with respect to the closest approach parameter, the permittivity and the density for a 1:1-electrolyte as a function of the ionic strength of the salt. For the calculation, the salt-free density and permittivity of water at 25 °C are used with a value for the closest approach parameter of 14.9.[84] Figure 6.11 b) shows the LR activity coefficient with the closest approach parameter calculated according to equation (6.2) as a function of the permittivity and the ionic strength for two densities (750 kg/m3 in green/blue and 1250 kg/m3 in yellow) As closest approach distance a value of 4Å was taken.

One could argue that the density dependence could be larger, as the dependency towards the closest approach parameter is so large, this value being a function of the density. Figure 6.11 b) shows the calculated LR part of activity coefficient with the closest approach parameter explicitly calculated as a function of the permittivity and the density according to equation (6.2). Within this figure it is clear that the influence of the density on the overall calculation is only clearly visible at very low permittivities, which only applied in very few of the tested systems. The low dependency of the PDH term follows from the assumptions underlying its derivation. In this work, the term is analyzed as it has been published instead of deriving a new LR term.

As the closes approach parameter and the permittivity have such a large influence on the calculated LR activity coefficient, the influence of these two parameters is investigated further, while the influence of the density is not discussed further due to its low impact on the overall calculation.

6.3.2 The influence of the closest approach parameter

The closest approach parameter has the largest influence on the calculation of the LR activity coefficient. Its value is usually fixed, although it can be calculated explicitly as follows:

$$b = a\left(\frac{2N_A\rho_s}{M_s}\frac{e^2}{\epsilon_0\epsilon_r kT}\right)^{0.5} \tag{6.2}$$

Where a is the closest approach distance.

Table 6.3 shows several values of the closest approach parameter calculated for different solvents at 25 °C with a closest approach distance of 4Å. This closest approach distance is chosen as the sum of the radii of 2 monoatomic ions lies in the range of this value. Depending on the size of the ions, its value can lay between 3Å and 10Å.

Shilov and Lyaschchenko also use the sum of the radii for 1:1-electrolytes[203,204] and 1:3-electrolytes[205], while Hsieh & Lin use the stoichiometric weighted average of the radii scaled by a factor adjusted to experimental data[12].

Table 6.3: Values of the closest approach parameter calculated for several solvents at 25 °C with a closest approach distance of 4Å. Unless specified, the experimental values were taken from the CRC Handbook of Chemistry and Physics[206].

Description	Density (ρ_s)	Permittivity (ϵ_r)	Closest approach parameter (b)
Pitzer's assumption			14.9
Water	997	78	9.79
Methanol	791	33	10.14
Ethanol	789	25	9.67
1-Pentanol	814	15	9.24
Acetone	785	21	9.46
Diethyl ether	713	4.3	17.56

From the values of the Table 6.3 it is possible to see that the influence of the permittivity on the closest approach parameter is larger than the one from the density, being especially large at very low permittivities. This becomes also clear when its influence on the LR activity coefficient is considered as shown in Figure 6.12. Although it doesn't seem like it due to the scale, the influence of the closest approach parameter on the calculation is more than tenfold on the diethyl ether system ($\epsilon_r = 4.3$) then on the water system

($\epsilon_r = 78$). Furthermore, the effect of the explicit calculation of the closest approach parameter leads to contrary trends on the shown systems: In Figure 6.12 a) the calculated absolute value becomes larger, while in Figure 6.12 b) the calculated absolute value becomes smaller.

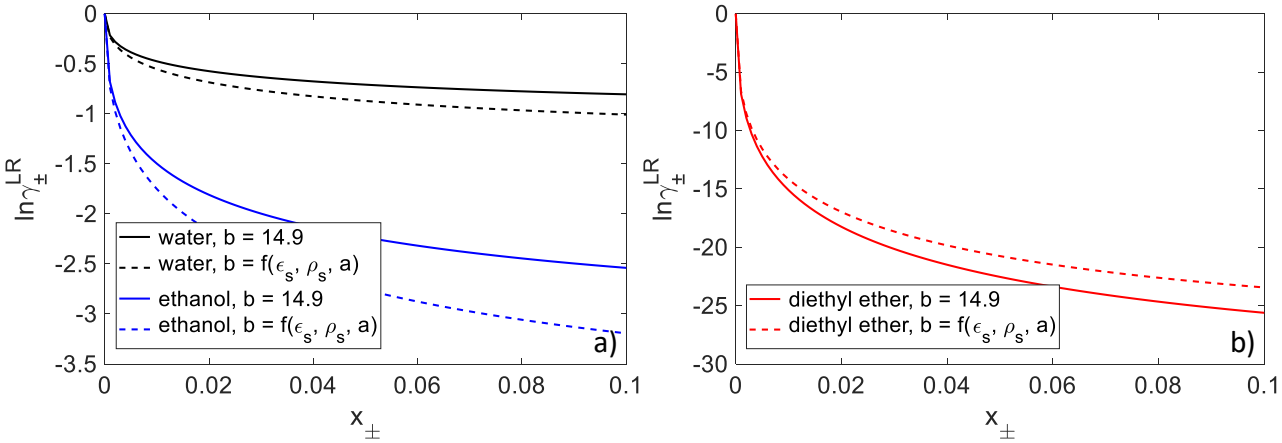

Figure 6.12: Influence of the closest approach parameter on the LR activity coefficient as a function of the salt mole fraction for a 1:1-electrolyte at 25 °C . Figure 6.12 a) shows systems with water ($\epsilon_r = 78$) and ethanol ($\epsilon_r = 25$), while Figure 6.12 b) shows a system with diethyl ether ($\epsilon_r = 4.3$). As closest approach distance a value of 4Å was taken.

To test whether COSMO-RS-ES can be made more accurate by including the explicit calculation of the closest approach parameter a new Parameterization A1 was done. This adds one additional parameter to the parameter set, namely the closest distance a from equation (6.2). It was noticed that without including the SLE data into the training set, the change did not influence very much the outcome because most of the systems with lower permittivities are of the type SLE. Therefore, the parametrization strategy was changed in contrast to Parameterization A (cf. section 6.2). In a first step, the training dataset included MIACs, LLEs and Gibbs free energies of transfer of ions and in the second step it included MIACs, LLEs and SLEs.

A comparison of the performance of Parameterization A and A1 is shown in the Table 6.4. The adjusted value of the closest distance parameter a of 5.48 Å fits very well into the theoretical value of being nearly the sum of the radii of single ions.

Table 6.4: Comparison of Parameterizations A and A1 based on the performance in calculating different thermodynamic data.

Type of data	Parameterization A	Parametrization A1
	AAD	AAD
MIAC aq [-]	0.043	0.040
MIAC org. [-]	0.78	0.84
LLE [-]	0.69	0.67
SLE [-]	0.98	0.83
$\Delta G^{0}_{tr,w\rightarrow o}$ **[kJ/mol]**	3.15	3.56

The overall performance of Parameterization A1 is a bit better than of Parameterization A. The MIACs and the LLEs are described slightly better than Parameterization A. Parameterization A1 describes SLE data much better than Parameterization A. This is expected as it was part of the training dataset. In contrast to Parameterization A where the SLEs where predicted, in this case they are correlated. This makes the comparison between both parameterizations a bit more difficult as not the same training data was employed. However, it seems that describing the closest approach parameter explicitly as a function of density, permittivity of the solvents and the adjusted closest distance has a positive impact overall.

To better analyze if the improvements achieved by this change in the model are consistent with other thermodynamic data, organic MIACs were included in the evaluation of the model. The SLEs are calculated according to equation (2.30). This means that after calculating the solubility product in water with the model, the Gibbs free energy of transfer of the salt and the activity coefficient in the other solvent has to be described correctly to calculate the right solubility. By checking the accuracy of the model for the Gibbs free energies of transfer and for organic MIACs it is then possible to assess whether the improvements achieved for the SLE calculations are consistent with other thermodynamic data. Unfortunately, for both thermodynamic data, Parameterization A1 performs poorer than Parameterization A. This means that Parameterization A1 is able to describe SLE data better than Parameterization A but at the cost of describing Gibbs free energies of transfer and MIACs in organic solvents worse. Because of this reason, this change was not included into the next developments of the COSMO-RS-ES model.

6.3.3 The influence of the permittivity and the dielectric decrement

As already introduced in section 2.2.2, the decision about what is the correct thermodynamic static permittivity to use in electrolyte systems is difficult due to the effect of kinetic depolarization. To include the salt influence on the permittivity into the modeling approach, a mathematical representation of the dielectric decrement is necessary. COSMO-RS-ES is a model meant to be applied predictively in engineering applications. Therefore, an effort is made to minimize the system-specific information needed to calculate the phase equilibria. Concerning the dielectric decrement, this means that whatever model is applied to describe this effect, it should not require much more information than already available, namely the solvent permittivity, the salt concentration, the ion radii, etc. Subsequently, three models are modified to be applicable within the COSMO-RS-ES modeling framework and tested for their applicability to include the dielectric decrement effect.

The steps followed for the implementation of such models are the following:

1. **Test the models in aqueous dielectric decrement systems**: for their ability to describe the complete range of dielectric decrement corrected for kinetic depolarization between the boundaries of no-slip and perfect-slip conditions. This is performed on aqueous data, as non-aqueous data is not as consistently available for a larger variety of electrolytes at the same conditions and up to high electrolyte concentrations to apply the correction for kinetic depolarization. Furthermore, if possible the models are extended for them to be valid not only in aqueous systems, but for them to be in principle applicable to mixed-solvent systems and up to high electrolyte concentrations.
2. **Test the extended models on the larger dataset** to find out what dielectric decrement model works best and to test the inclusion of a Born term. For this the average of the parameters found for the no-slip and the perfect-slip condition for the aqueous systems in step 1 were used as starting parameters for the dielectric decrement models.

The results of both steps are described in the following sections.

1. Test the models in aqueous dielectric decrement systems

The models discussed here were already introduced in section 2.2.2. The database of dielectric decrement data is specified in the appendix in section 8.4.6.

The extended Simonin model

The first model tested was the model by Simonin et al.[50] This model is an empirical model that just describes the dielectric decrement per se as a phenomenon without a thorough theoretical derivation. The adjustable parameters employed in the model can be determined in different ways. They can be system-specific, electrolyte-specific, solvent-specific, or ion-specific. As considering the parameters ion-specific is the only truly predictive approach, this is what is done in this work. While Zuber et al.[52] published several ion-specific parameters for each solvent, in this work we empirically extend the approach to a sum of ion-type specific parameters multiplied by the radii of the ions. This allows to predictively at least differentiate between the different ions, as the original model would not be able to do this. The version of the model by Simonin used in this work is therefore a modification of equation (2.13):

$$\epsilon_{\mathrm{r}} = \frac{\epsilon_{r,sf}}{1 +} \tag{6.3}$$

Where k refers to the ion type, meaning either cation, monoatomic anion or polyatomic anion. The sum in equation (6.3) extends over for all ions i of the ion type k. Of different expressions tried, this was the one that resulted in the best representation of the corrected dielectric decrement data. In the case of polyatomic anions, the area of a sphere with equal surface is used.

The extended Simonin model was then parametrized with the corrected dielectric decrement data once for the no-slip and once for the perfect-slip condition. Figure 6.13 shows the results for the adjustments of the corrected dielectric decrement by the extended Simonin model. The obtained parameters and the AAD of the model are also shown in the figure. For both boundary conditions, the calculation represents the data with the correct trend towards dielectric decrement. Interestingly the parameter for the monoatomic cations is negative in both cases. This is probably due to the introduced dependence of the radii. Since the radius of lithium is smaller than the one from cesium, the dielectric decrement being stronger for the one with the smaller radius, this leads to

the parameter being negative. Which also agrees with the fact that cations have a larger influence on the dielectric decrement in general than the anions.

Although systematic trends of the deviations can be observed as the size of the cation increases from top to bottom, the trends are captured good enough to be applied to testing within COSMO-RS-ES.

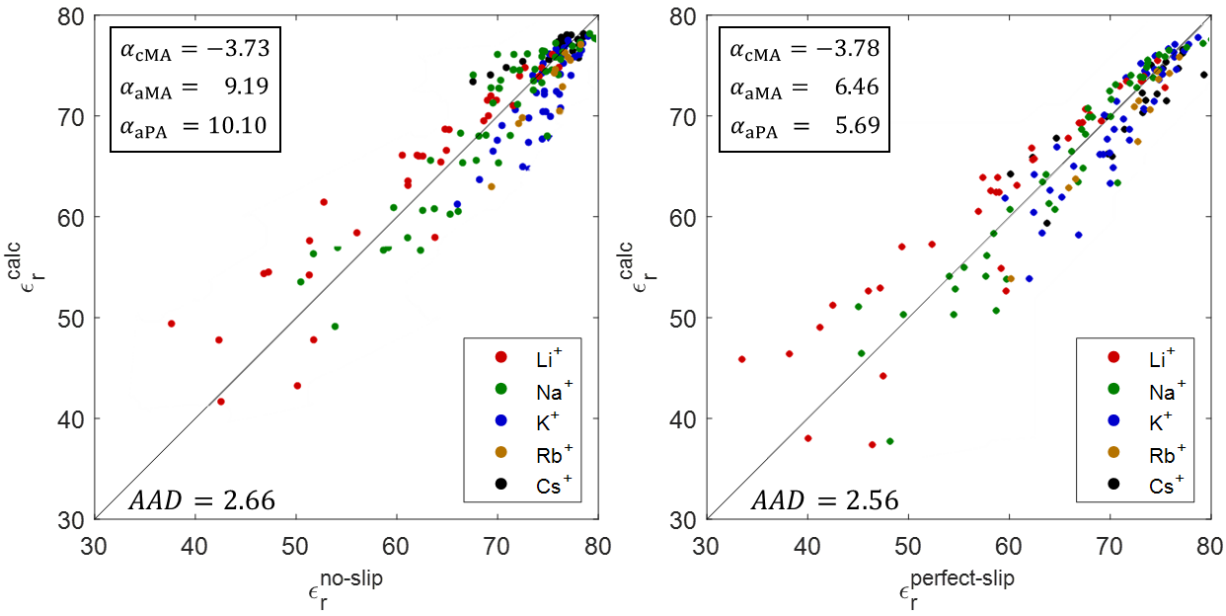

Figure 6.13: Parity plot for the corrected permittivity as calculated by the extended Simonin model vs. the corrected permittivity calculated from experimental data. Figure 6.13 a) shows the values for the no-slip condition and Figure 6.13 b) shows the values for the perfect-slip condition. The different colors denote the cations for every electrolyte. The parameters of the model and the AAD are also shown.

The extended Pottel model

The idea behind this model is to describe the dielectric decrement as a mixture of two pseudo-species: a solvent and a hydrated sphere with a permittivity with a value of two. The information needed for this model is the size of the hydration layer. As this allows calculating the size of the hydrated spheres as the sum of the radius of the ion and the hydration layer. This approach is in good agreement with experimental investigations as the dielectric decrement is described based on physical considerations, however an accurate description of the hydration shell is necessary for the model to be employed. The description by Pottel has already been employed in a variety of thermodynamic models previously[51,66,115] using different sets of radii to describe the solvation shell. Figure 6.14

shows a comparison of different sets of radii with the radii of Parameterization A. The size increase for both cationic and anionic ions is qualitatively the same and even proportional to the radii optimized for COSMO-RS-ES. However, if the radius of the hydrated sphere is taken (i.e. $r_{Marcus} + \Delta r_{Marcus,hyd}$), only for the anions the trend of the hydration sphere size is the same as for the radii optimized for COSMO-RS-ES. The trend for the cations is not monotonic and will surely depend on the solvent employed. This makes the application of this model difficult for mixed-solvent systems as a model would have to be developed for the hydration shell.

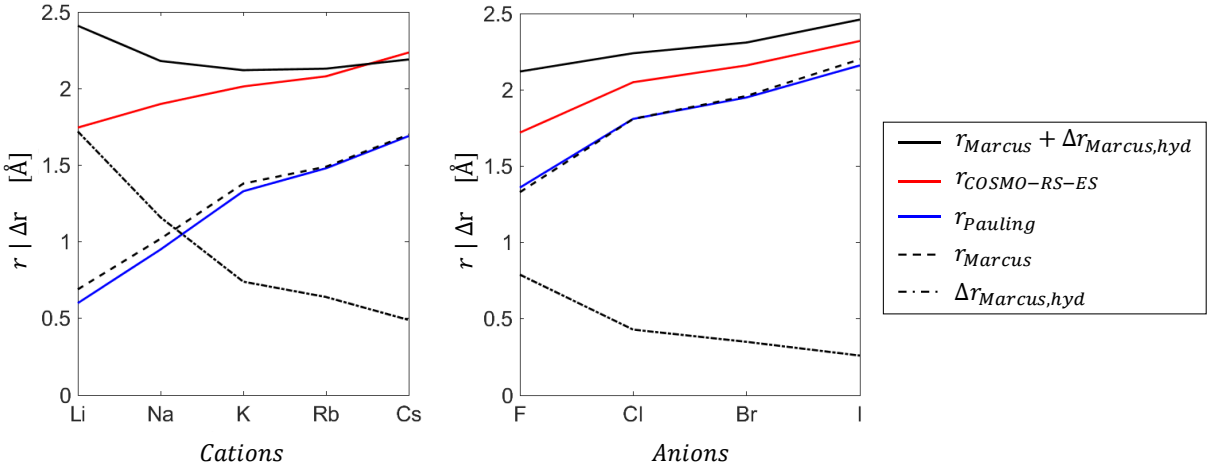

Figure 6.14: Comparison of different sets of radii of ions (by Marcus[207] and Pauling[21]) with the radii from Parameterization A and radii of the hydration shell also from Marcus.[207]

A further limitation found with the model by Pottel is that at high salt concentrations, the solvation shell is not composed only of solvent molecules, but also contains ions. The concentration dependency of the hydration shell is therefore not accounted for. It is easy to see from equation (2.14) that this can even lead to negative permittivities in systems like lithium chloride in water due to the high solubility of the salt. Exactly for this system Wey & Sridhar show that the number of water molecules in the first hydration shell drop from 7.6 at a concentration 0.55 M to 2.2 at a concentration of 13.38 M. To avoid this limitation of the model, as an empirical approach to include this effect, a concentration dependent decay was included. Substituting equation for the following:

$$\phi_{ions} = \frac{4N_A\pi\rho}{3M}\sum_{i}^{\text{ions}} x_i {r_{i,solv}}^3 \exp(-a_{\text{Pottel}} \cdot x_i) \tag{6.4}$$

Where a_{Pottel} is a universal constant having the same value for every electrolyte.

The model was then fitted to the data assuming the no-slip and the perfect-slip boundary condition. Figure 6.15 shows the resulting calculated permittivities with their corresponding model parameter and AAD. The deviation of the model is slightly larger than the extended Simonin model. As with the first model, a trend is visible for different electrolytes with the same cation. Especially for highly charged cations (e.g. lithium) the model does not perform as well as the extended model by Simonin. This model has a more thorough physical background, at the cost of using experimental hydration radii of the ions, which makes it only applicable to where this data is available.

Interestingly, as well as with the extended Simonin model, there is a trend of underestimating the dielectric decrement for lithium and overestimating the dielectric decrement for larger cations. Since this model does not use the radii of the cations but the experimental radii of the hydrated ions, it is interesting that also for this model, this effect can be observed.

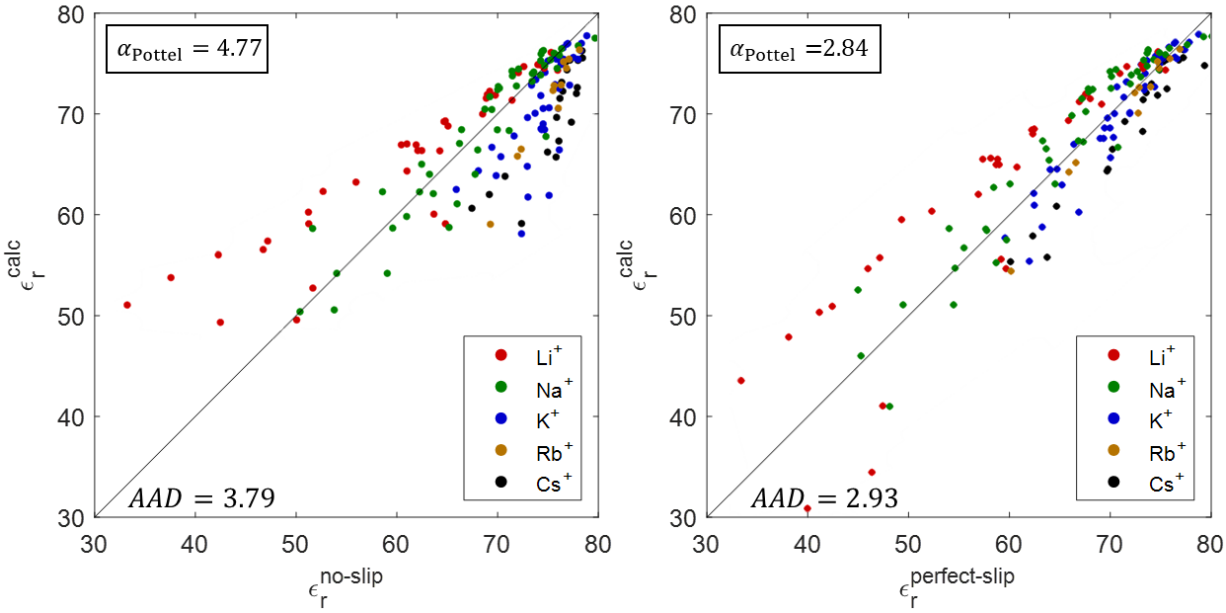

Figure 6.15: Parity plot for the corrected permittivity as calculated by the extended Pottel model vs. the corrected permittivity calculated from experimental data. Figure 6.15 a) shows the values for the no-slip condition and Figure 6.15 b) shows the values for the perfect-slip condition. The different colors denote the cations for every electrolyte. The parameters of the model and the AAD are also shown.

The model by Maribo-Mogensen

Differently than the two first models, the model of Maribo-Mogensen does not have adjustable parameters. Instead of describing "just" the dielectric decrement as a correction factor after applying a mixing rule for the permittivities of the solvents, it describes the permittivity of the mixture per se for any type of mixtures also including ions. As input parameters the pure component permittivities and the salt-free density is used. It however also requires a few other input parameters for each solvent: the permittivity at infinite frequency (as defined in section 0), the dipole moment, Kirkwood's g-factor and the fraction of molecule *i* not bound to an ion.

To keep the predictivity of the approach, the permittivity at infinite frequency is calculated from the Clausius-Mossotti relation[208]:

$$\frac{\epsilon_\infty - 1}{\epsilon_\infty + 2} = \frac{N_A}{3\epsilon_0 \nu} \sum_i x_i \alpha_{0,i} \tag{6.5}$$

The Clausius-Mossotti relation needs the molecular polarizability $\alpha_{0,i}$ as input. In this work, the molecular polarizability is calculated by the atomic contribution method of Bosque and Sales[209]. The method is able to predict the molecular polarizabilities for molecules with common atoms with an AAD of 2.31%.

The needed dipole moments were taken from the Thermophysical Properties of Chemicals and Hydrocarbons by Yaws[210], while the Kirkwood's g-factors were calculated with equation (2.16) using the corresponding pure component experimental values. The model from Maribo-Mogensen was implemented in such a way that the only information necessary additionally to what the other models require (pure component density and permittivity) are the dipole moments of the solvents. And the dipole moment is usually readily available from literature data, or otherwise it can be calculated from quantum chemistry calculations quite accurately, allowing for a completely predictive application of the model.

The only information missing for the application of the model is the fraction of molecules not bound to an ion. Unfortunately within COSMO-RS-ES something like the association calculated by the Wertheim theory, which was applied in the publication[48] of Maribo-Mogensen, does not exist. However, it is possible to calculate contact probabilities directly

from the interacting segments of two molecules i and j in the mixture according to the following equation:

$$P_{ij} = \frac{x_j}{A^i(N/n)} \sum_I \sum_J A_I^i A_J^j \Gamma_J \Gamma_I \tau_{IJ} \tag{6.6}$$

Here x_j is the mole fraction of molecule j, A^i is the area of molecule I, N the number of segments, n the number of molecules, A_I^i is the area belonging to segment I on molecule i, Γ_I is the segment activity coefficient and τ_{IJ} is the interaction parameter as calculated by equation (2.45).

As can be seen in Figure 6.16, this model also correctly predicts the trend of the permittivity with changing ion concentration towards dielectric decrement. However, as the other two models, it also predicts the reverse order for the effect as a function of the cation size, even with a larger deviation than the other two models.

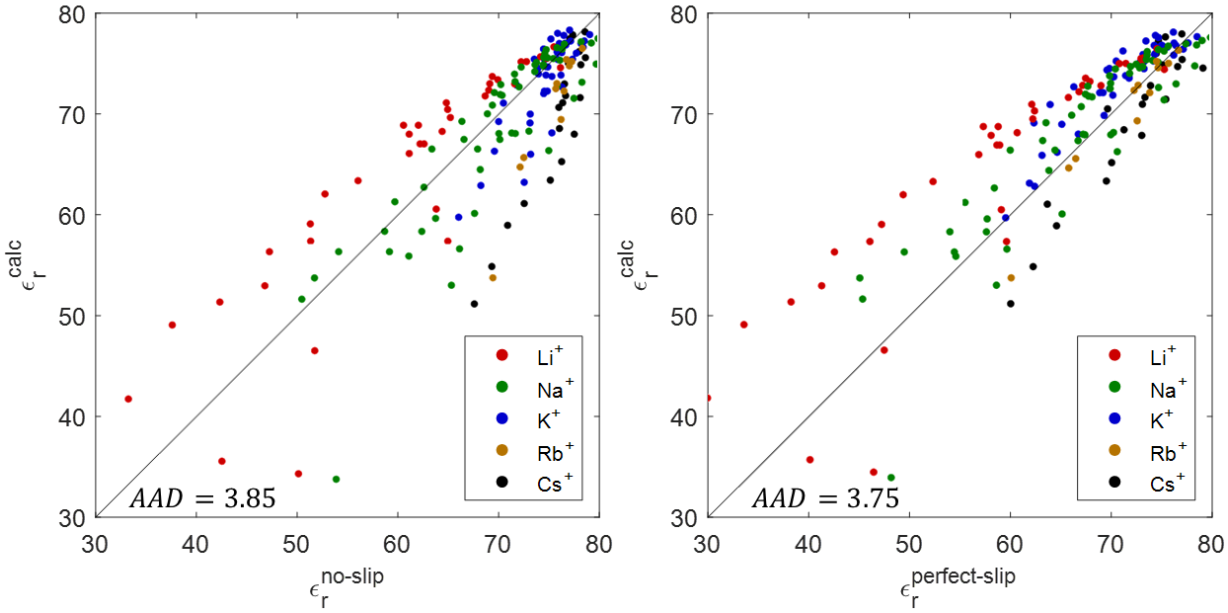

Figure 6.16: Parity plot for the corrected permittivity as calculated by the Maribo-Mogensen model vs. the corrected permittivity calculated from experimental data. Figure 6.16 a) shows the values for the no-slip condition and Figure 6.16 b) shows the values for the perfect-slip condition. The different colors denote the cations for every electrolyte.

Although assuming the calculated contact statistic according to equation (6.6) is equal to the association calculated by Wertheim's theory[211] is not correct, the trend should be

similar and the predictivity is kept as all the information needed is provided by the model itself. In the future, it might be possible to calculate something like the association calculated from Wertheim's theory. As this theory, as implemented in most thermodynamic models, describes binary association, perhaps by using the hydrogen bonding energy of two molecules calculated from COSMO-RS-ES, the model could be developed further into describing the association between a neutral molecule and an ion or to calculate the SR contribution of ion-pairing in the future. An ion-solvent, or ion-ion association constant K_{ij} could be calculated similarly to the following equation:

$$\ln K_{ij} = -\frac{\Delta G_{\text{attr}}}{RT} \tag{6.7}$$

Where ΔG_{attr} is the attractive part of the interaction energy equations.

This procedure would need the association parameters to be predicted from COSMO information. And it would be quite similar to the SEPP framework developed by Kaminski[212] where all parameters are calculated by a surrogate model based on exactly this information.

2. Test the extended models on the larger dataset

Of the three models tested, the extended Simonin model and the extended Pottel model showed the most promising results in describing the dielectric decrement. Especially the extended Simonin model was even able to describe the dielectric decrement in correct order with the cation size for the perfect-slip boundary condition. While the extended Pottel model and the extended Simonin model describe the influence of the cation on the dielectric decrement in the correct order, the model by Maribo-Mogensen as implemented in this work, does not. This can be observed in Figure 6.17. This deviation from the expected order might be due to a wrong description of the contact statistics or due to the contact statistics not describing the same as the association probability. Because of the unphysical behavior, only the first two mentioned models are used to test their applicability for thermodynamic data within the COSMO-RS-ES modeling framework.

After the dielectric decrement models have been tested and shown to be able to reproduce the data at least in a qualitative matter for aqueous systems, there are two options to include the dielectric decrement effect into the model. The first one is to use a dielectric decrement model adjusted to experimental data. And in the following step, with fixed

parameters for the dielectric decrement model to adjust all the COSMO-RS-ES parameters to fit the model to the thermodynamic data. The second one is to adjust the parameters of the dielectric decrement model at the same time as the COSMO-RS-ES parameters and later test whether the modeled dielectric decrement describes the trend as expected from experimental data.

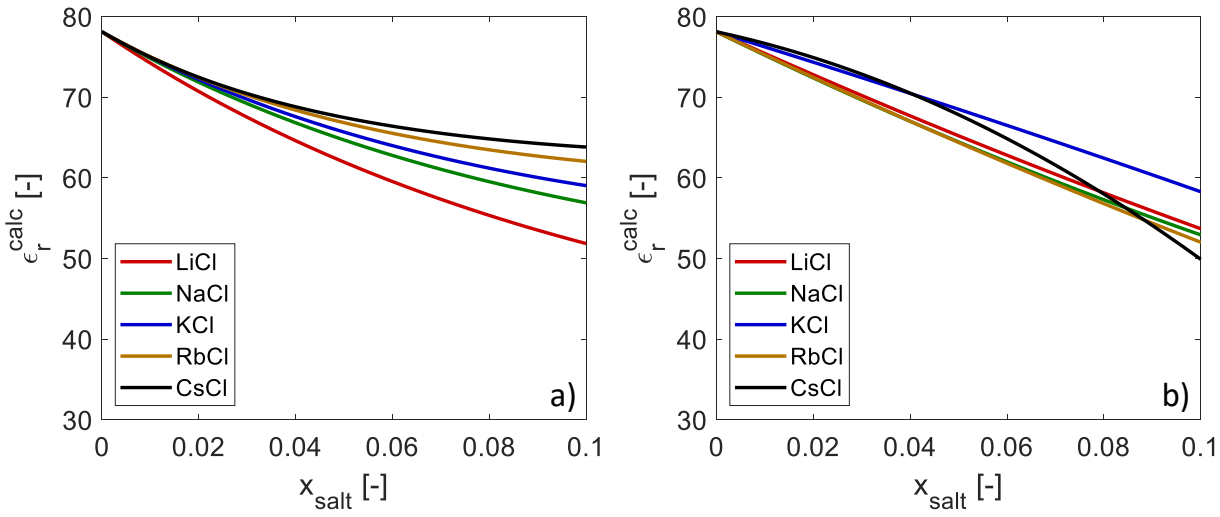

Figure 6.17: Plot of the permittivity as a function of the salt concentration. Figure 6.17 a) shows values calculated by the extended Pottel model and Figure 6.17 b) shows values calculated by the model by Maribo-Mogensen.

In this work, we decided to employ another strategy. As discussed already in section 2.2.2, dielectric decrement data is in many cases biased due the effect of kinetic depolarization. As it is not known for the majority of experimental data whether a correction has been included into the experimental data or not, the parameters of the dielectric decrement models are adjusted to thermodynamic data instead of adjusting them to the dielectric decrement data. After adjusting the parameters, the model is checked to find whether the predicted dielectric decrement makes sense.

The investigation of the permittivity influence on the model started as a way to analyze the LR term, as so far this was the only term in the COSMO-RS-ES model dependent on this property. However, reviewing the literature showed that several g^E-models[125,128,213–215] and many more EOS employ a term based on the Born model (cf. section 3.1), while a wide variety also introduce a way to describe the dielectric decrement. First Boda's group[216–219] and then Shilov & Lyaschchenko[203–205] both developed a model very similar to each other which includes a Born term. It was shown that without the need of

parameters but by using the experimental input (densities, permittivities and radii), the MIAC for several electrolytes could be calculated. Valiskó & Boda[218] even showed being able to reproduce trends of experimental single-ion activity coefficients.

If the dielectric decrement effect is included into the model in this work, an eventually included Born term would also be dependent on the salt concentration rather than just only on the concentrations of the solvents. Therefore, in this part of the work it is also tested if a Born term inclusion improves the performance of the model. Figure 6.21 shows an example for the contributions calculated by a Born term and by the LR term for the system sodium chloride in water. If a contribution to the activity coefficient is calculated from the Born term, as shown in equation (2.35), not only does the calculated permittivity has to be correct, but also the derivative with respect to the different ions. A model not describing the derivative correctly leads to non-physical trends especially for lower permittivities. It is exactly at this range where the model reacts very sensitively towards these changes.

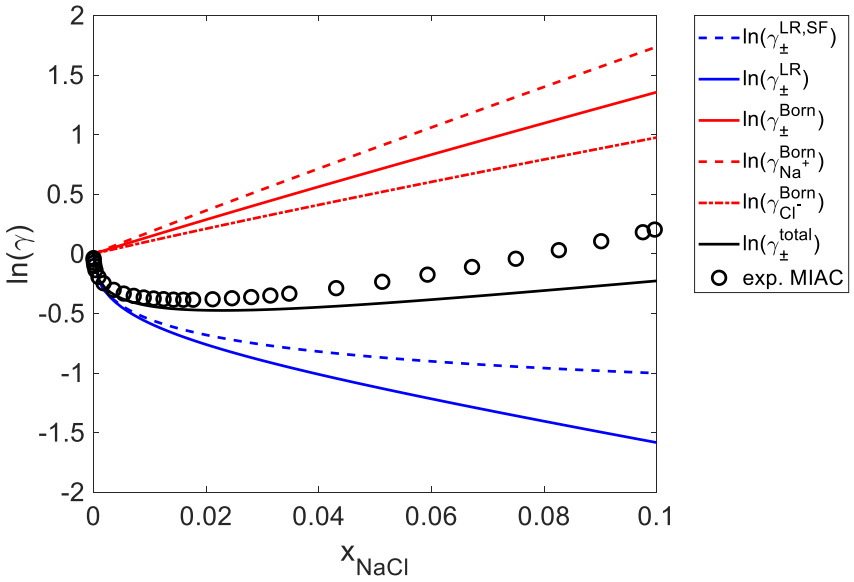

Figure 6.18: Example of the LR and Born contributions calculated for sodium chloride without the SR term. The LR term is shown, being calculated with the salt-free permittivity (blue dashed line) and with the dielectric decrement calculated with the extended Pottel model (blue solid line). The Born Term is shown with its ionic contributions (red line). The sum of the LR and the Born term is shown as the black solid line. Experimental values were taken from Hamer & Wu[220].

The extended Pottel model

This model requires experimental hydration layer sizes and is therefore only applicable for aqueous systems. However, it describes the derivative with respect to the ions correctly as opposed to the Simonin model, which showed negative parameters for the cations (cf. to step 1 from section 6.3.3). This allows to test the influence of the dielectric decrement and of the inclusion of a Born term.

The needed data for the application of the dielectric decrement model for all salts was taken from Marcus[207]. Only the empirically adjusted decay parameter and eventually the closest approach distance were adjusted additionally to the COSMO-RS-ES parameters in each of the different parameterizations based on the aqueous MIAC data available until solubility limit. For the calculation of the Born model different ionic radii can be used. Two different radii sets were tested: the same radii as the ones from Marcus[207] used in the dielectric decrement model and the radii from COSMO-RS-ES. As a starting point to better compare the other parameterizations to each other, the Parameterization A2 was performed by adjusting the model exactly as Parameterization A1, with the small change of including aqueous MIAC data up to the solubility limit. Meaning that in a first step, the training dataset included MIACs up to solubility limit, LLEs and Gibbs free energies of transfer of ions and in the second step it included MIACs, LLEs and SLEs.

Table 6.5 shows the results of the testing versions of COSMO-RS-ES with dielectric decrement and a Born term. The best result is achieved by Parameterization A2.1. Interestingly this is the only variant of the different modeling approaches that brings a performance improvement for the model in comparison to Parameterization A2. While it is clearly visible that the Born term performs better with the radii from Marcus[207], none of the parameterizations including a Born term achieve a better result than the model without changes. Looking at Figure 6.21, this could have been expected as for some aqueous systems the sum of the LR term plus the Born term (without the SR term!) gave results closer to the experimental values, giving the SR term more flexibility to adjust better to the experimental data. This is however not the case for all systems and therefore in average the Born term does not lead to an improvement of the COSMO-RS-ES model.

Table 6.5: Comparison of the parametrizations using the dielectric decrement model (extended Pottel) in aqueous MIAC data. Columns show whether the closest distance parameter of the LR term was adjusted, whether the dielectric decrement (DD) was used in the LR term, whether the Born term was used and what radii were used in the Born term.

Name	Adjusted a	Use DD in LR	Use Born term	Radii for Born term	AAD [-]	a_{Pottel}
A2	Yes	No	No	-	**0.050**	-
A2.1	Yes	Yes	No	-	**0.048**	4.84
A2.2	Yes	Yes	Yes	COSMO-RS-ES	**0.194**	5.03
A2.3	Yes	Yes	Yes	Marcus[207]	**0.133**	6.64
A2.4	Yes	No	Yes	COSMO-RS-ES	**0.222**	5.21
A2.5	Yes	No	Yes	Marcus[207]	**0.134**	6.91

The extended Simonin model

The extended Pottel model can be employed to calculate a Born contribution but was only applicable to aqueous systems due to the need of the hydration radii. In contrast to this, the extended Simonin model is applicable to non-aqueous systems, but it cannot be used to calculate a Born term due to the wrong description of the derivative of the permittivity with respect to the cations. However, since the evaluation of the extended Pottel model already showed that the inclusion of a Born term does not lead to an improvement of COSMO-RS-ES for the aqueous systems, this is not a development pursued further anyway.

To test the performance of the extended Simonin model a new Parameterization A3 was done. It was done in a two-step strategy similarly to Parameterization A2. In the first step, the training dataset included MIACs up to solubility limit, LLEs and Gibbs free energies of transfer of ions and in the second step it included MIACs, LLEs and SLEs. The only difference to Parameterization A2 was that the extended Simonin model was used to describe the dielectric decrement in the LR term.

Table 6.8 shows a comparison of Parameterization A1, A2 and A3. The values show that Parameterization A3 performs better for all evaluated thermodynamic data in comparison with Parameterization A2. It even performs as well as Parameterization A1

Table 6.6: Comparison of Parametrizations A1, A2 and A3 based on the performance in calculating different thermodynamic data.

Type of data	Parametrization A1	Parameterization A2	Parametrization A3
	AAD	AAD	AAD
MIAC aq. [-]	0.040[a]	0.050[b]	0.040[b]
MIAC org. [-]	0.84	0.89	0.51
LLE [-]	0.67	0.70	0.66
SLE [-]	0.83	0.77	0.74
$\Delta G^0_{tr,w\to o}$ [kJ/mol]	3.56	3.82	3.29

[a]up to a concentration of 6 m, [b]up to the solubility limit

for aqueous MIAC systems even though a larger concentration range is evaluated until the solubility limit. Especially the organic MIACs are calculated much more accurately than before. It seems that including the dielectric decrement effect allows the model to describe trends it was unable to account for so far.

Unfortunately, the model does not reproduce experimental trends for the dielectric decrement at all (cf. Figure 6.22), meaning that some other effect is fitted into the extended Simonin model. Instead of describing dielectric decrement for the non-aqueous systems, the model calculates dielectric increment in most cases. Only for the aqueous systems (around $\epsilon_r = 78$), some systems show dielectric decrement while others present dielectric increment. For the calculated values, disregarding in which solvent, it seems that the larger the cation the stronger is the described shift towards larger permittivities. The trend seems to be equal for the anions in the non-aqueous systems, while it is reversed in water.

What the above-described trends following ion sizes mean for the model is another question altogether. For most non-aqueous systems, the permittivity is increased, which causes a lower influence of the LR term as its absolute value is reduced. The trends might hint towards effects like the tendency to form ion-pairs as has been shown by Mazzini & Craig[221]. As the dielectric decrement model is a function of the ionic size, another possible interpretation may be that the corrections brough about by the dielectric decrement model are in fact accounting for ion-size effects that a restricted model like the PDH is not able to account for.

Although the inclusion of the extended Simonin model leads to improvements for the calculation of thermodynamic data, the trends described for the dielectric decrement are non-physical. Therefore, including this effect in this way into the model is not advisable.

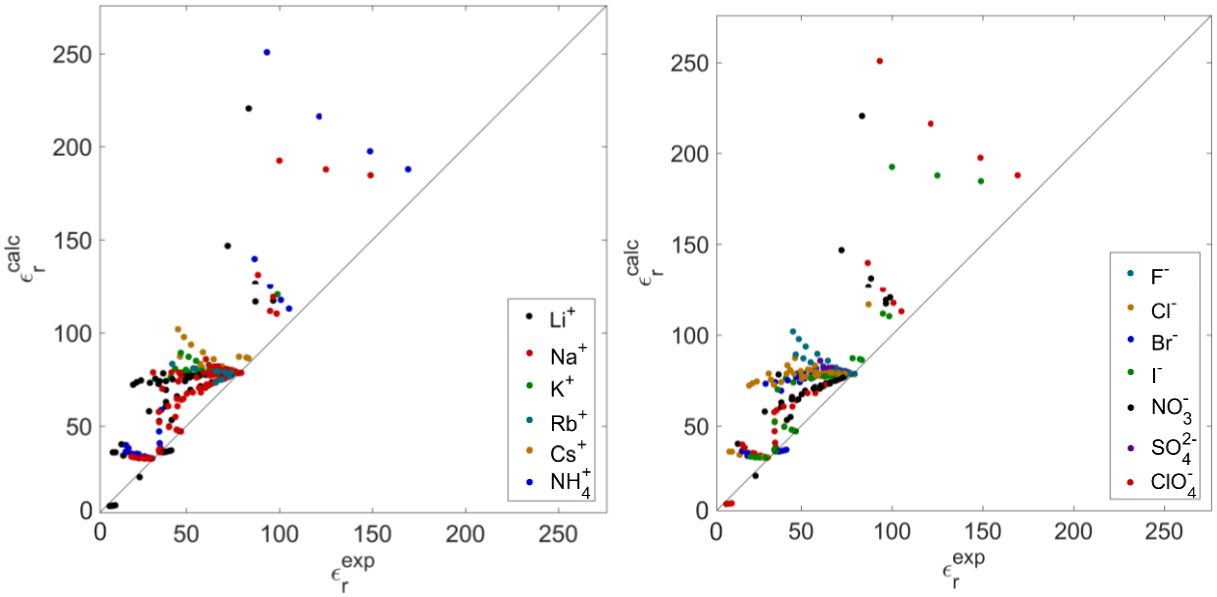

Figure 6.19: Plot of the permittivity calculated from the extended Simonin model from Parameterization A3 as a function of the experimental permittivity. Figure 6.19 a) shows values colored by cation while Figure 6.19 b) shows colored by anion.

6.3.4 Summary and important considerations for the improvement of the long-rang term

In section 6.3 several improvements were tested for the LR term implemented in the COSMO-RS-ES model. As a first step, a sensitivity analysis was performed towards the input values of the model: the closest approach parameter, the permittivity and the density. As the salt-free permittivity and density are employed so far in the model, a particular interest of this section was to test the use of the actual solution properties instead of the salt-free properties.

The sensitivity towards the density is low compared with the two other parameters, which is also partly due to the underlying assumptions when deriving the model in its present form. For this reason, only the other two are further analyzed.

Although the explicit calculation of the closest approach parameter with the inclusion of one additional universal parameter leads to improvements for the SLE systems, this enhancement comes at a cost of describing other thermodynamic data less accurately.

The LR term is quite sensitive towards the permittivity. Two ways to include this information into the model were tested: as a salt concentration dependent dielectric decrement and a Born term. For the three models tested, no enhancement of the predictive capabilities could be achieved by the inclusion of these modifications that would lead to a model improvement for all data types.

No development from this section influenced the model in a way leading to a performance improvement. However, some important considerations were discovered while testing the different approaches:

1. To include the density and permittivity dependence of the salt-concentration, the model should be derived taking these dependencies into account. Otherwise, it might lead to the model losing its sensitivity towards a specific property (e.g. density) or to unphysical behavior.
2. If the inclusion of a Born term is considered, the model describing the dielectric decrement needs to describe the derivative with respect to the ion concentrations correctly.
3. The model by Maribo-Mogensen shows the highest predictivity at describing the permittivity of a mixture. Including the effect of dielectric decrement is possible, however a better way has to be found to describe the bounding of dipolar molecules to the ions from the COSMO-RS-ES information.
4. The adjustment of a dielectric decrement model for non-aqueous systems based on thermodynamic data showed that the influence of the LR is reduced in almost all cases for these systems.

The SR and the LR term of COSMO-RS-ES were analyzed independently in the previous chapters and improvements were done where possible. As a next step, the interplay of both contributions are examined in the following section.

6.4 Refinement of COSMO-RS-ES: the interplay of SR and LR interactions

In a predictive model like COSMO-RS-ES, composed of two contributions, the balance between the SR and the LR term is an important topic. Especially if the application of this model is to be extended to the complete concentration range. The question whether LR interactions happen in very concentrated electrolyte solutions e.g. ionic liquids or to what extend these happen, has been discussed in recent literature. For large ions, e.g. for ionic liquids[222–230], the role of the LR interactions was found to be less important than for lower electrolyte concentrations. This interesting behavior was also observed for smaller inorganic ions[231–233]. As the two contributions to COSMO-RS-ES have been investigated independently in previous sections of this work, in this section the interplay of both is studied to find conditions for which the application of the LR contribution would be inappropriate.

COSMO-RS-ES (Parameterization A) has been shown to be able to predict solubilities quite accurately in many cases (cf. section 6.2). However, for some systems very large negative deviations were observed. Figure 6.20 shows the signed deviation of the SLE systems as calculated by COSMO-RS-ES (Parameterization A). It is clearly visible that the systems with very negative deviations are of salts with a high solubility in low-permittivity solvents.

Ion-pairing is a phenomenon that happens at these conditions. As explained in section 2.2.1, ion-pairing happens when it becomes more energetically favorable to form clusters of 2 or more ions than for them to be surrounded by a solvation shell of their own. Ion-pairing is also an explanation for the seemingly low importance of the LR term for very concentrated electrolyte solutions. Implicitly being a way to influence the balancing between the SR and the LR term of the COSMO-RS-ES model.

For other systems in the dataset some underestimations are found, including e.g. the SLE *KCl + water + 1,4-dioxane* ($\epsilon_{1,4-dioxane} = 2$) shown already shown in Figure 6.5 d) and the LLE *LiCl + water + 2-methyl-2-butanol* ($\epsilon_{2\text{-}methyl\text{-}2\text{-}butanol} = 5.8$). Large

underestimations as seen in these systems are in most cases due to the underestimation of the LR term. This can be followed from a comparison of how the LR term behaves at very low permittivities (cf. Figure 6.11 b) with Figure 6.20. At the same time from the analysis of Parameterization A for these systems it is known that the deviation of the Gibbs free energies of transfer of the ions is about an order of magnitude smaller than the deviations observed for the SLE systems also indicating a systematic underestimation of the LR term.

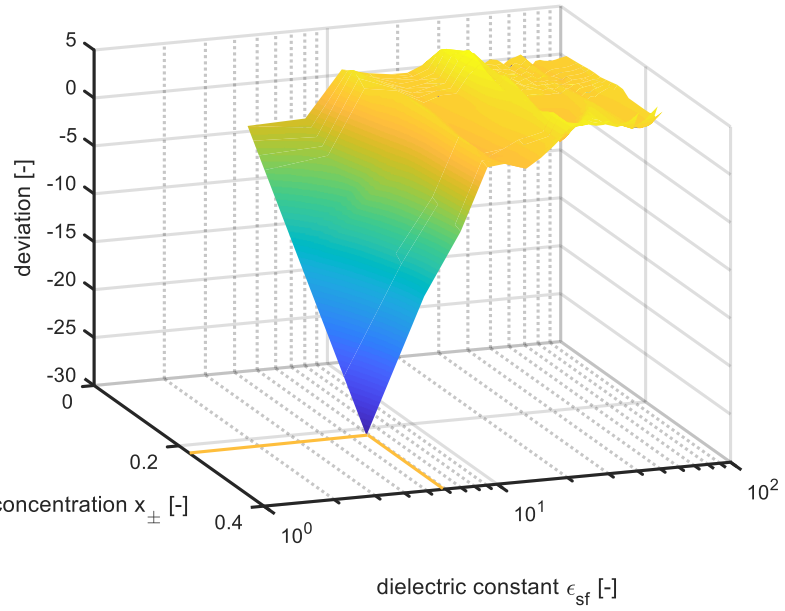

Figure 6.20: Signed deviation of the activity coefficients for the SLE systems according to equation (5.10) plotted as a function of the salt-concentration and the salt-free dielectric constant calculated with COSMO-RS-ES (Parameterization A). Large deviations can be observed for systems with high solubilities and low-permittivities.

To include the effect of ion-pairing into the model this can be done by describing the process as an equilibrium reaction between the free ions and the ion-pair. All electrolytes are assumed to be treated equally as symmetric electrolytes with only one dissociation step, as treating several dissociation steps would be computationally very expensive. Based on the equation (2.10), on a mole fraction basis, this reaction can be described by:

$$K_A = \frac{(1-\alpha)\gamma_{IP}}{\alpha^{\nu} x_{\pm}^{\nu-1} \gamma_{\pm}{}^{\nu}} \tag{6.8}$$

Where γ_{IP} is the activity coefficient of the ion-pair, α is the dissociation degree and K_A is the mole fraction-based association constant. The activity of the ion-pair γ_{IP} could be described explicitly within the COSMO-RS-ES framework, however this would need the introduction of new interaction energy equations and a way to calculate the sigma-profile of an ion-pair. However, calculating the sigma-profile of an ion-pair is not trivial due to the dependence on the chosen distance between the ions. Because of this, the activity coefficient of the ion-pair is set to unity as a first attempt to include this effect into the model[27]. The association constant can be described by many models. In this work the model by Fuoss and the model by Bjerrum are tested (cf. section 2.3.6). Both of the models only need two input parameters: the permittivity of the solvent and the closest approach distance, a parameter describing the distance defining the point at which two close ions are considered paired. Both of the models allow the calculation of concentration-based association constants ($K_A^{(c)}$). These can be transformed into mole fraction-based association constant as follows:

$$K_A = K_A^{(c)} \cdot \left(\frac{\rho_s}{M_s}\right)^{\nu} \tag{6.9}$$

As the density ρ_s would increase with the salt concentration similarly as the molar mass M_s, the quotient stays roughly the same. Therefore, the salt-free values are employed here.

If the association constant is known, equation (6.8) can be solved for the dissociation degree α. Under the assumption that only free ions contribute to the LR term, with the dissociation degree α, it is possible to correct the concentration used in the calculation of the LR term. Instead of employing the total ionic strength I, the effective ionic strength is used $I_{eff} = I \cdot \alpha$.

The mean ionic activity coefficient $\gamma_{\pm}$ in equation (6.8) is a function of the SR and the LR term (cf. equation (2.56)). As the concentrations of free ions is not equal to the overall salt concentration, being now a function of the dissociation degree α, this calculation becomes iterative. The iterative calculation of the LR term is not very demanding. However, it is quite expensive for the SR calculation, which needs to be performed several times for different concentrations for each data point in the training dataset. A scheme using a non-linear interpolation based on already calculated SR values was developed to speed up this process until convergence is reached with a threshold of $|\alpha_i - \alpha_{i-1}| \leq 0.005$ for the dissociation degree.

6.4.1 Evaluation of the description of ion-pairing by Fuoss and by Bjerrum

Firstly, both models are tested to see which one of them deliver better results within the COSMO-RS-ES framework. The only bigger difference between them, as can be seen in Figure 2.11, is how the model behaves at very high permittivities. So, the largest differences between both models applied on the training dataset are expected to be noticeable for the aqueous MIAC systems. This can indeed be observed in the results shown in Table 6.7.

As already explained in the previous section, a full optimization of all parameters is very computationally demanding due to the iterative calculation of the dissociation degree. For this reason, to test whether the model by Fuoss or by Bjerrum perform better a non-iterative approximation was employed, keeping the SR term constant and adjusting only the concentration of the LR term. This was done by adjusting only the closest distance parameter to the MIAC, LLE and SLE data and taking Parameterization A as starting point.

As can be noted in Table 6.7, both ion-pairing models improve the description of the SLE systems. As these are the systems with the lower permittivities this agrees with the fact that both models have a larger influence at low permittivities. For the other data however, the model by Fuoss does not improve the description of the systems, it even worsens the results in comparison to Parameterization A. Especially the MIAC systems have a deviation 50 % larger than with the ion-pair treatment by Bjerrum. The Bjerrum treatment performs better for all three system types. This is probably due to the different limiting behavior at high permittivities.

Table 6.7: Comparison of Parameterizations A and its modifications including two different ion-pairing models based on the performance in calculating different thermodynamic data.

Type of data	Parameterization A	Parametrization A + ion-pairing (Fuoss)	Parametrization A + ion-pairing (Bjerrum)
	AAD	AAD	
MIAC aq. [-]	0.043	0.062	0.041
LLE [-]	0.69	0.73	0.62
SLE [-]	0.98	0.86	0.76
Closest approach distance [Å]	-	2.5	13.6

The closest approach distances of both models are in the correct order of magnitude. In comparison to what would be expected for the typical ionic sizes (4-6Å) the value for the Fuoss model seems to be small while the model for Bjerrum seems to be quite large.

Figure 6.21 shows how the models behave depending on the permittivity with the values of the closest approach distance optimized to the experimental data (cf. Table 6.7).

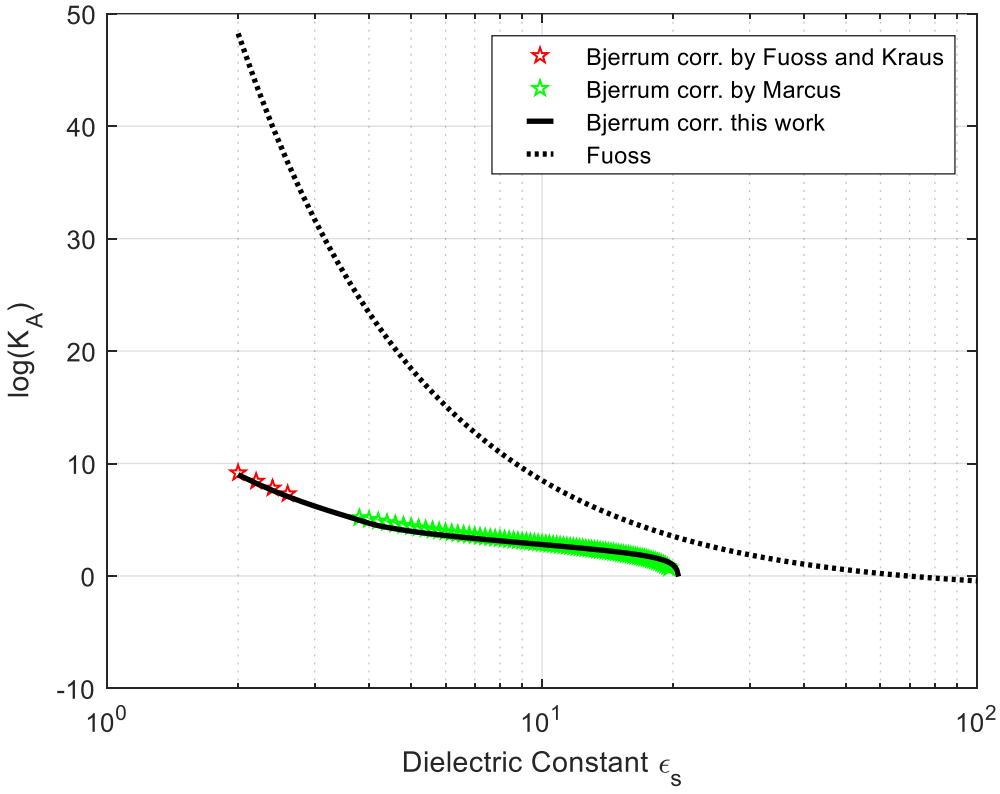

Figure 6.21: Dependency of the association constant with regards to the permittivity for a fixed closest approach distance of 13.6 Å as calculated by the Bjerrum model (solid line), and a fixed closest approach distance of 2.5 Å as calculated by the Fuoss model[89] (dashed line). The correlations for the Bjerrum model by Fuoss and Kraus[28] and by [Marcus: personal communication][90], only valid for a specific permittivity range, are also shown here for comparison with the correlation developed in this work valid for the complete permittivity range.

Interestingly, the models deliver quite different results for the dissociation constant and are still able to represent the experimental data. While the Bjerrum model describes the ion-pairing with a cutoff at a permittivity of about 20, the Fuoss model predicts existing association up to very high permittivities.

6.4.2 Parameterization B: Inclusion of ion-pairing according to Bjerrum

Due to the better performance of the Bjerrum treatment for describing the ion-pairing effect, this model is used for the iterative parameterization. Some new SLE systems were added into the evaluation database to add more data points with solvents with very low permittivities. With this addition, the SLE database contains 43 data point of permittivity 15 or lower.

While testing different parameterization strategies to include the ion-pairing effect two further improvements were made along the way:

Firstly, the interaction energy equations were changed to include thresholds for the solvents in almost all the interactions (cf. Table 6.8). This makes sense as only the segments patches on the surface of the solvents with higher screening charge density would interact in an attractive manner with the ions. In the case of the interactions of ions with water, the normal hydrogen bonding threshold was used, while for interactions with organic molecules one threshold was adjusted. Only for the interactions of the organic molecules with the cations this threshold did not seem to be necessary, giving better results leaving the equation unchanged.

Secondly, the closest approach distance is not adjusted as one parameter for all electrolytes. The parameter is instead calculated for every electrolyte as a scaled function of the sum of the radii of the ions as follows:

$$a = f_{scale}(r_{cation} + r_{anion}) \tag{6.10}$$

Due to the large sensitivity of the objective function towards the closest approach distance a variety of strategies were tried. A three-step parameterization procedure was found to deliver the best results. In the first parameterization step a fixed value for the f_{scale} parameter of 0.76 is used and all the SR parameters are adjusted using Parameterization A as starting point. The starting value of f_{scale} comes from a correlation of experimental ionic radii in solution by Marcus[23] and the corresponding ionic radii from the COSMO structure. In the case of polyatomic i.e. non-spherical ions, the radius was calculated from a sphere of equal area. In the second parameterization step, the interaction parameters are fixed and the monoatomic radii and the f_{scale} parameters are optimized. In a last step, all the parameters are adjusted at the same time to improve the result even further.

Table 6.8: Interaction energy equations for ionic interactions in the short-range contribution of COSMO-RS-ES for Parameterization B. Added threshold values in comparison to the interaction energy equations of Parameterization A shown in Table 2.3 are highlighted in red.

Type of contact	Misfit factor	Ionic interaction energy term	
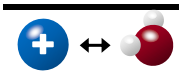 cation – H_2O	A_1	$E^{ion}_{cat-H_2O} = \frac{a_{eff}}{2} B_1 \sigma_{cat} \max(0, \sigma_{H_2O} - \sigma_{HB})$	(6.11)
 cation – org. mol.	A_2	$E^{ion}_{cat-om} = \frac{a_{eff}}{2} B_2 \sigma_{cat} \max(0, \sigma_{om})$	(6.12)
 cation - halide	0	$E^{ion}_{cat-hal} = \frac{a_{eff}}{2} B_3 \min\left(0, \sigma_{cat}\left(1 - D_1 \lvert\sigma_{cat}\rvert^{E_1}\right)\right) \sigma_{hal}$	(6.13)
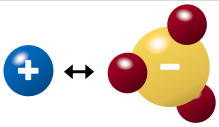 cation – polyat. an.	0	$E^{ion}_{cat-pa} = \frac{a_{eff}}{2} B_4 \min\left(0, \sigma_{cat}\left(1 - D_1 \lvert\sigma_{cat}\rvert^{E_1}\right)\right) \max(0, \sigma_{pa})^{E_2}$	(6.14)
 halide - H_2O	A_3	$E^{ion}_{hal-H_2O} = \frac{a_{eff}}{2} B_5 \min(0, \sigma_{H_2O} + \sigma_{HB}) \max(0, \sigma_{hal})$	(6.15)
 halide – org. mol.	A_4	$E^{ion}_{hal-om} = \frac{a_{eff}}{2} B_6 \min(0, \sigma_{om} + C_1) \max(0, \sigma_{hal} - C_2)^{E_3}$	(6.16)
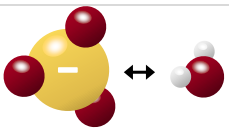 polyat. an. - H_2O	A_5	$E^{ion}_{pa-H_2O} = \frac{a_{eff}}{2} B_7 \min(0, \sigma_{H_2O} + \sigma_{HB}) \max(0, \sigma_{pa})$	(6.17)
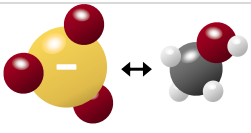 polyat. an. - org. mol.	A_6	$E^{ion}_{pa-om} = \frac{a_{eff}}{2} B_8 \min(0, \sigma_{om} + C_1) \max(0, \sigma_{pa})$	(6.18)

The resulting parameters of Parameterization B using the three-step parameterization strategy are listed in Table 6.9.

As for almost all interactions with ions, threshold values were added or reparametrized, most of the A & B parameters change greatly to adjust the representation of the training dataset. In some cases, the parameters change by even more than 100% in comparison to the values of Parameterization A. The parameters B2 and B4 used to describe the attractive interactions of cation-organic molecule and cation-polyatomic anion respectively are quite low in comparison to other parameters. This is probably due to not using a threshold value for the interacting segments. Parameters C1 and C2 could be merged to one, although a more thorough analysis of this interaction is needed. The exponent E2 is so small that it might be possible to eliminate this parameter from the model setting it to zero. This however would mean that the interaction between the cation and the polyatomic anion can be calculated solely as a function of the screening charge density of the cation. If this is really true needs to be tested in the future. The scaling parameter for calculating the closest approach distance between two pairing ions also lies in a range that shows that the radii optimized for the cations are close to values measured in the literature.

Table 6.9: COSMO-RS-ES parameters referring to ionic interaction energies as defined in Table 2.3, new values optimized including Gibbs free energies of transfer of ions in the training dataset. This parametrization is called Parametrization B. Parameters whose value increased or decreased more than 20% of their value in comparison to the values of Parameterization B are correspondingly highlighted.

Parameters A [kJ Å² mol⁻¹ e⁻²]	Parameters B [kJ Å² mol⁻¹ e⁻²]	Parameters C [e Å⁻²]	Parameters D & E [-]	Cationic Radii [Å]
A_1 = 5515	B_1 = 13554	C_1 = 0.0096	D_1 = 1852	Li = 1.697
A_2 = 4151	B_2 = 166	C_2 = 0.0097	E_1 = 2.075	Na = 1.874
A_3 = 3965	B_3 = 3795		E_2 = 5E-06	K = 1.993
A_4 = 3294	B_4 = 30		E_3 = 0.036	Rb = 2.071
A_5 = 3459	B_5 = 20497			Cs = 2.231
A_6 = 3802	B_6 = 789			
	B_7 = 12302		$f_{scale} = 0.824$	
	B_8 = 13624			

Table 6.10: Comparison of Parameterizations A and Parameterization B based on the performance in calculating different thermodynamic data.

Type of data	Parameterization A	Parametrization B
	AAD	AAD
MIAC [-]	0.043	0.043
LLE [-]	0.69	0.52
SLE [-]	0.98	0.89

The evaluation of Parameterization B is shown in Table 6.10. As the comparison with Parameterization A shows, the MIAC systems are calculated equally as good while the LLE and the SLE systems are greatly improved. Especially the AAD of the LLE systems is reduced by about 25%. The improvements in Parameterization B have mainly two reasons. The first is the introduction of the new threshold values for the interactions of the ions with the neutral molecules. This improves mainly systems of alkali halides in mixtures of water and acetonitrile. One example of this improvement is depicted in Figure 6.22 marked with a blue oval. Another example that is enhanced slightly by this is the interaction of the electrolytes with mixtures of water and ketones. The red oval in Figure 5.22 signalizes some of these systems.

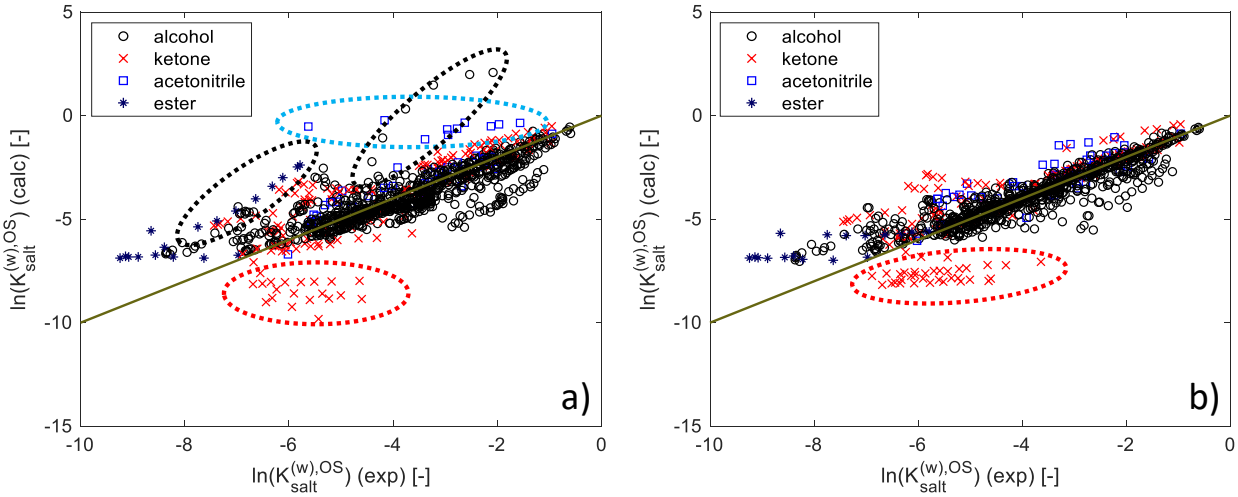

Figure 6.22: Parity plots of the logarithmic partition coefficients of the salts for the SLE systems in the training database calculated with equation (5.4). Figure 6.22 a) Shows calculations performed with Parameterization A. Figure 6.22 b) Shows calculations performed with Parameterization B. Black ovals: outliers due to the occurrence of ion-pairing. Blue oval: outliers due to the description of the SR term having deficiencies. Red oval: outliers due to a systematic deviation in the description of the salt-free system.

It can also be seen that for these systems a systematic deviation can be observed. This is due to the water-ketone system already being described wrongly, as can be appreciated in Figure 6.23. The figure shows the MIBK concentration in the aqueous phase for the systems: LiCl + MIBK + water and Na_2SO_4 + MIBK + water. The ePC-SAFT model is compared to the Parameterization B. Qualitatively both models represent the experimental data quite accurately. ePC-SAFT agrees better with the data using binary interaction parameters while the data calculated with COSMO-RS-ES shows a systematic deviation already in the salt-free system, however without using binary interaction parameters.

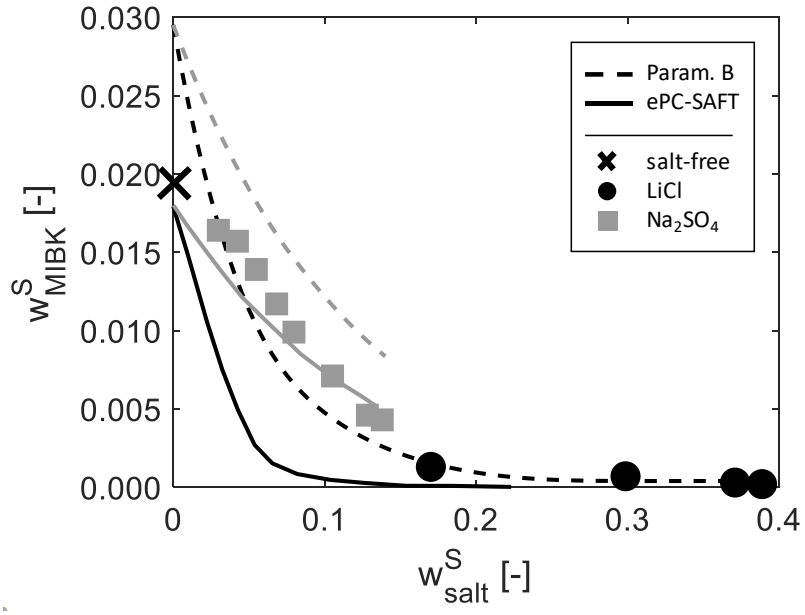

Figure 6.23: Weight fraction of MIBK in the salt-rich phase vs. salt weight fraction in the salt-rich phase. Circles (LiCl + MIBK + water) and squares (Na_2SO_4 + MIBK + water) are experimental results from Mohammad et al.[234] while the cross (MIBK + water) is the experimental value for the salt-free system from Yang et al.[235] Full lines are modeling results with ePC-SAFT[234] and dashed lines are calculations with Parameterization B. Grey lines: Na_2SO_4, black lines: LiCl

Because the activity coefficients are not independent (cf. the Gibbs Duhem equation (2.6)), it makes sense having a look at the activity coefficients of the organic solvents in the LLE systems to make sure that the better description of the partitioning of the salts was not achieved by a worse description of the partitioning of the organic solvents. Indeed, Figure 6.24 shows that the enhancements made in this work in most cases lead to an even better description of the partitioning of the organic solvents than in the original publication.[14]

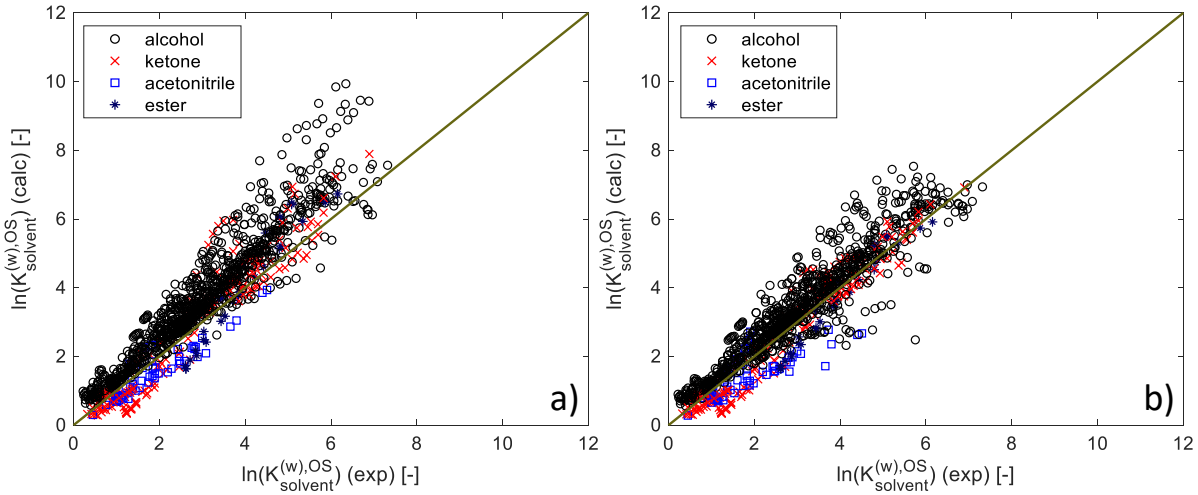

Figure 6.24: Parity plots of the logarithmic partition coefficients of the organic solvents for the SLE systems in the training database calculated according to equation (5.4). Figure 6.24 a) Shows calculations performed with COSMO-RS-ES with the parameters by Gerlach et al.[14] Figure 6.24 b) Shows calculations performed with Parameterization B.

This suggests that the advancements made in the modeling approach in this work are thermodynamically consistent in the sense that by adjusting the model to ion related data also the description of the neutral components is improved in most electrolyte systems.

The second reason for the better representation of the systems is the introduction of ion-pairing to describe the partial association in systems with lower permittivities. The use of an effective concentration in the LR term leads to the term having a lower influence in the case of highly associated electrolytes. A system within the training dataset for which the ion-pairing becomes very important for a correct calculation is the LLE system KNO_3 + water + 2-methyl-2-butanol ($\epsilon_r = 5.8$). Figure 6.25 shows the evolution of this system from using the published parameters[14] to the Parameterization A to the Parameterization B. Although an improvement can already be seen for when the system is calculated employing Parameterization A instead of the parameters by Gerlach et al.[14], the largest improvement in the calculation of this system is achieved with the introduction of Parameterization B. The change is so large that the trend of the partitioning of the salt with increasing salt concentration is correctly changed from preferring the organic-rich phase to the salt-rich-phase. The model predicts basically complete dissociation in the salt-rich phase while in the organic-rich phase almost complete association is calculated.

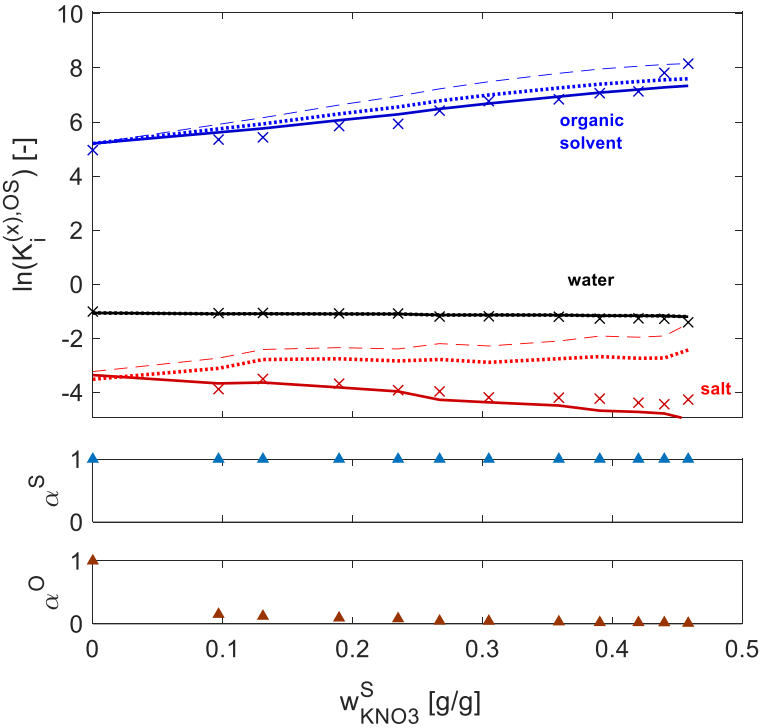

Figure 6.25: Logarithmic partition ratios calculated according to equation (5.4) for the system KNO_3 + water + 2-methyl-2-butanol. In the upper plot, calculated values are represented by lines and experimental by markers (×). Dashed line: calculated with parameters from Gerlach et al[14]. Dotted line: calculated with Parameterization A. Solid line: calculated with Parameterization B. The two subplots show the calculated dissociation degree α for the salt in the organic (O) and salt-rich (S) phases.

Although these trends would probably be close to reality, these dissociation degrees are still something that would need to be regarded as a model improvement rather than an accurate depiction of the actual dissociation phenomena. The inclusion of the Bjerrum association treatment already enhances the models capabilities, however a more complete ion-pairing model would also have to include SR terms to reproduce the law of matching water affinities[236,237] which is also applicable in many cases to the ion-pairing tendency in non-aqueous systems[34].

Whether the trend change of the salt partitioning coefficient at the highest salt concentrations is an experimental error or due to the ion-pairing increasing the affinity of the salt for the organic phase, as described in literature[1,27], cannot be said. However, for the majority of LLE systems the ion-pairing treatment by Bjerrum improves the predictivity of the model. The same can be said about the prediction of SLEs.

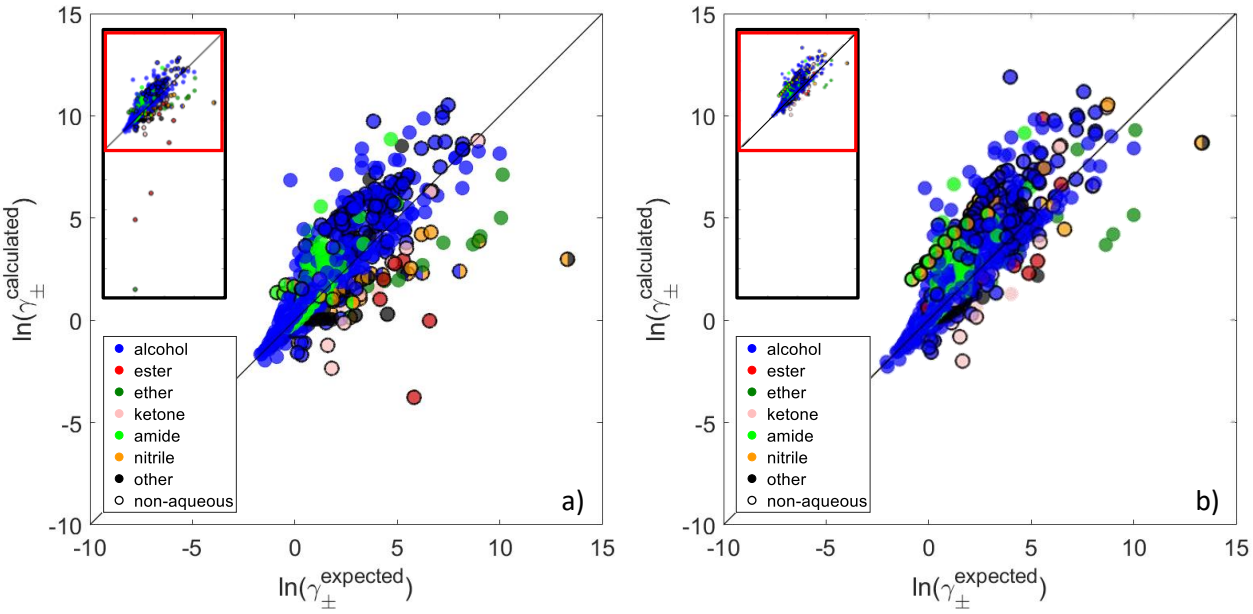

Figure 6.26: Parity plot of the calculated activity coefficient vs. the expected activity coefficient according to equation (5.9). Figure 6.9 a) shows the calculations with the Parameterization A while Figure 6.9 b) shows the calculations done with the Parameterization B. The coloring of the presented values depends on the functional groups present in the solvents of the system in question. If more than one functional group is present (e.g. 3-methoxy-1-butanol) the plot shows the system as the non-alcoholic group. Non-aqueous systems are shown with a black circle around the markers in the plot.

Figure 6.26 shows a comparison of the predicted activity coefficients for the SLE systems in the evaluation database calculated with Parameterization A and Parameterization B. Contrary to the LLE systems, the improvements for the SLE systems are mainly driven by the correction of the LR term. The small overview plots inside Figure 6.26 have limits of -35 to +15 on the y-axis. Since this is a plot of the logarithm of the activity coefficient, the model was still underestimating systems with low permittivities by orders of magnitude with the improved Parameterization A. However, with the inclusion of ion-pairing all systems in the evaluation dataset are visible on the Figure 6.26 b), showing the vast progress achieved by this development. Salts with a small cation and large anions, like $LiClO_4$ tend to exhibit very large solubilities (up to 50 wt%[238]) in polar solvents even for very low permittivities. Agreeing with experimental evidence[239], these systems are now modeled mainly as ion-pairs. At these high concentrations, the assumption that the ion-pair activity coefficient is unity should be revised in the future. Including a new interaction equation for an ion-pair with the other species is straightforward within the COSMO-RS-ES framework. It might be possible to calculate a sigma profile for the ion-pair

based on the sigma profile from the composing ions and some geometrical considerations taking the charge of the ion-pair as additional constraint. The problem is that it is difficult to verify the correctness of the calculated activity coefficient for the ion-pair, although Marcus & Hefter[27] give a theoretical approach that could be used to at least verify the overall trend of symmetrical ion-pairs.
From Figure 6.26 b) it is possible to see that for the values calculated with Parameterization B, most of the systems are overestimated slightly. This has probably following reasons. Either, now the influence of the LR term is being underestimated due to the model assuming ion-pairing where the formation of pairs is unlikely, or the deviations are now mainly due to the SR term.

The evaluation of Parameterization B has shown that parametrizing the interactions of the neutral components has become as important as parameterizing the interactions of the ions. This is especially clear looking at the calculation of the LLE systems. It might be of advantage for the further development of the model to parameterize neutral interactions first. After this, as a second step, the equations for the ionic interactions can be adjusted to the electrolyte data.

As the largest deviations for the calculation of SLE systems are now addressed, it should now be possible to include this data along with the organic MIACs into the training dataset to improve the model descriptions for these challenging systems even further.

As expected from the improvement in the prediction of the activity coefficients, for the calculation of actual solubilities the model also shows a higher predictivity as Parameterization A. Figure 6.27 show several SLE systems calculated with Parameterization A (dashed line) and with Parameterization B (solid line). As shown for most systems, independently of the salt or solvents in question, the model develops towards a better quantitative prediction of the solubilities. It is possible to see that the model still has problems describing completely non-aqueous solvents. However, one has to keep in mind that the model is expected to describe the transfer of the ions from infinite dilution in water to a finite concentration in a non-aqueous mixture. This is very challenging for any kind of model. Nonetheless, the predictive application of the model to these systems shows the power that lies behind using general polarity descriptors to describe the interactions within the COSMO-RS-ES modeling framework.

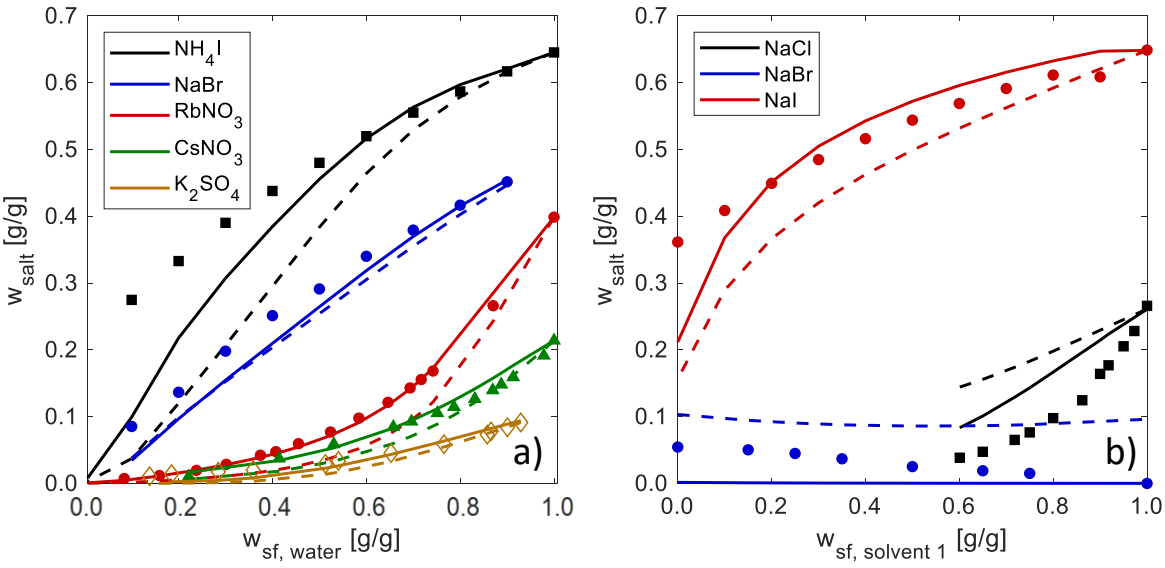

Figure 6.27: Solubility predictions at 25°C plotted as function of the salt-free concentration of the first solvent mentioned. Markers correspond to the experimental values; dashed lines correspond to calculations performed with Parameterization A and solid lines correspond to values calculated with Parameterization B. Figure 6.27 a) shows the solubilities of the following systems: NH_4I + water + ethanol[240]; NaBr + water + ethanol[190]; $RbNO_3$ + water + methanol[194]; $CsNO_3$ + water + tert-butanol[241]; K_2SO_4 + water + chloral-hydrate[242]. Figure 6.27 b) shows the solubilities of the following systems: NaI + water + formamide[197]; NaCl + water + DMSO[158]; NaBr + acetonitrile + DMSO[198].

6.5 Experimental and computational analysis of non-aqueous LLE

Completely non-aqueous LLEs are an interesting datatype to evaluate the model. This is because a salt-concentration dependent partitioning of the ions between two relatively different non-aqueous phases represents thermodynamic information with which the model has not been analyzed before. Predicting phase equilibria is quite demanding for any kind of g^E-model. However, applying the best version of COSMO-RS-ES so far (Parameterization B) to this new data will allow to take the model at its limits and see where it can be improved further.

As discussed in section 3.2, in literature very few examples of measurements of completely non-aqueous LLEs with electrolytes can be found. To find systems where an LLE might occur, different mixtures of 1-alkanols and toluene were prepared. Then lithium chloride was added until either a two-phase system formed, or the salt started crystalizing. Figure 6.28 shows the SLEs measured while searching for LLE systems.

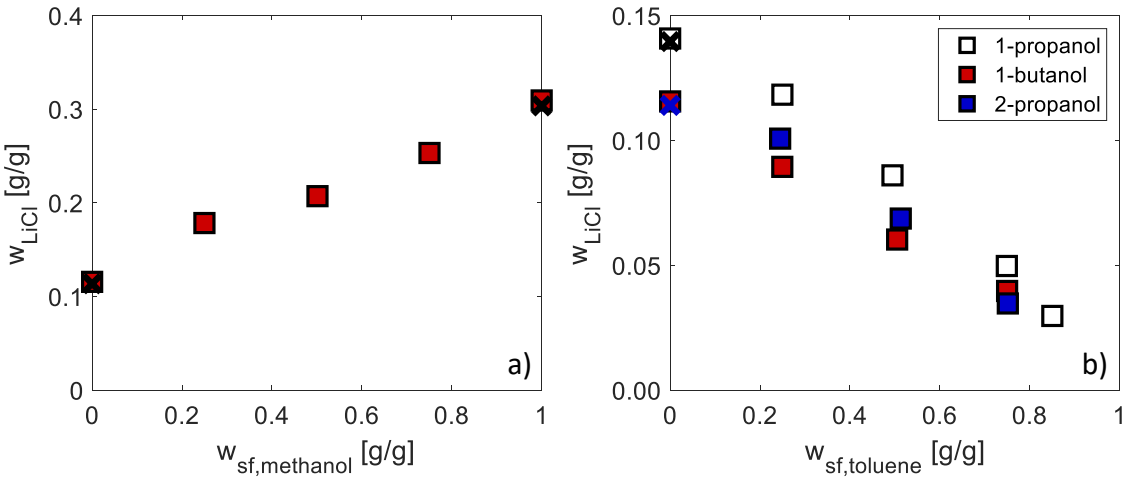

Figure 6.28: Solubility measurements of lithium chloride in binary non-aqueous systems at 25°C. Figure 6.28 a) shows the system lithium chloride + 1-butanol + methanol. Crosses denote respective solubility measurements from the literature for lithium chloride in 1-butanol[243] and in methanol[244]. Figure 6.28 b) shows the systems lithium chloride + 1-butanol + toluene, lithium chloride + 1-propanol + toluene and lithium chloride +

2-propanol + toluene. Crosses denote respective solubility measurements from the literature for lithium chloride in 1-propanol[245] and in 2-propanol[245].

As can be seen from the crosses representing literature values in Figure 6.28, the method used to measure the solubility is in very good agreement with literature data. The experimental values may be found in the appendix in section 8.3.

The solubilities for the measured systems calculated by COSMO-RS-ES with Parameterization B are shown in Figure 6.29. The model describes the trends correctly in all cases but underestimates the solubilities. As the solubility is antiproportional to the activity coefficient, this means that the activity coefficient is overestimated. This agrees with the results of section 6.4.2 where most activity coefficients are shown to be slightly overestimated. Nevertheless, it is remarkable that the model is able to describe the relative difference between 1-propanol and 2-propanol quite similarly to the experimental trend, although the difference in the sigma profile is very small and the steric information is lost in the COSMO-RS calculations. The solubility in 2-propanol is predicted first being lower than in 1-butanol, then with rising toluene concentration in the mixture it is predicted higher than 1-butanol equally as in the experimental data.

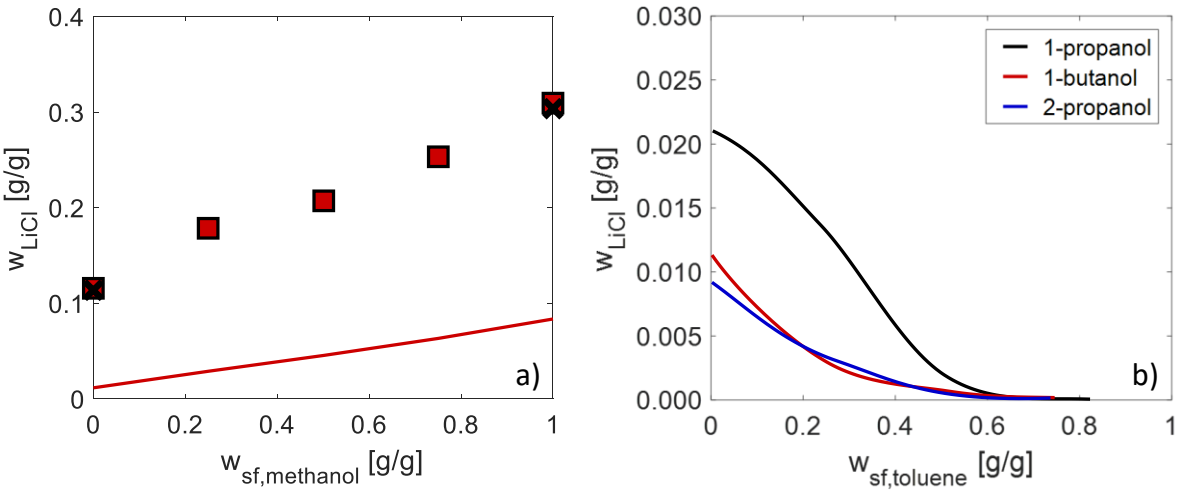

Figure 6.29: Solubilities of lithium chloride in the different systems calculated by COSMO-RS-ES using Parameterization B. Figure 6.29 a) shows the system lithium chloride + 1-butanol + methanol. Crosses denote respective solubility measurements from the literature for lithium chloride in 1-butanol[243] and in methanol[244]. The red squares show the measured experimental data. Figure 6.29 b) shows the systems lithium chloride +

1-butanol + toluene, lithium chloride + 1-propanol + toluene and lithium chloride + 2-propanol + toluene.

For the smaller 1-alkanols (ethanol and methanol) an LLE could be measured. Figure 6.30 and Figure 6.31 depict enlarged versions showing the important sections of the ternary LLE systems lithium chloride + ethanol + toluene and lithium chloride + ethanol + toluene respectively. The experimental values may be found in the appendix in section 8.3.

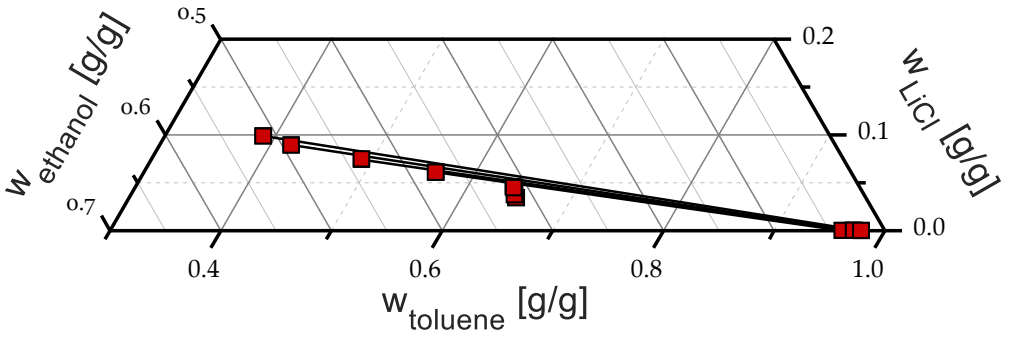

Figure 6.30: Enlarged portion of the ternary plot for the non-aqueous liquid-liquid system lithium chloride + ethanol + toluene. Squares denote the measured concentrations in both phases while the lines represent the tie-lines. The square at the lowest lithium chloride concentration represents an initial mixture for which no phase separation was found.

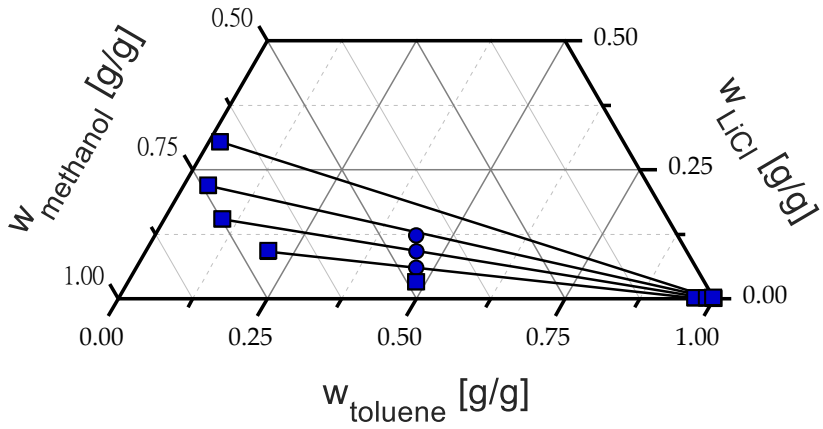

Figure 6.31: Enlarged portion of the ternary plot for the non-aqueous liquid-liquid system lithium chloride + methanol + toluene. Circles denote the initial mixtures. Squares denote the measured concentrations in both phases while the lines represent the tie-lines.

The square at the lowest lithium chloride concentration represents an initial mixture for which no phase separation was found.

The experimental measurement of the system with ethanol was much more challenging than in the system with methanol. The mass balance could also not be closed as accurately as with the methanol system. Only for a small range of lithium chloride concentrations (5-13 wt-%) a phase separation was found before the salt started crystallizing. For both systems the tie-line at the highest salt concentration already is a SLLE. The salt concentration in the organic phase could not be determined for the ethanol system because its concentration was below the detection limit of the measuring method employed. Interestingly, for the system with methanol the mole fraction based partitioning ratio of the salt seems to be quite constant (cf. Figure 6.32 b), independent of the overall salt concentration in the system.

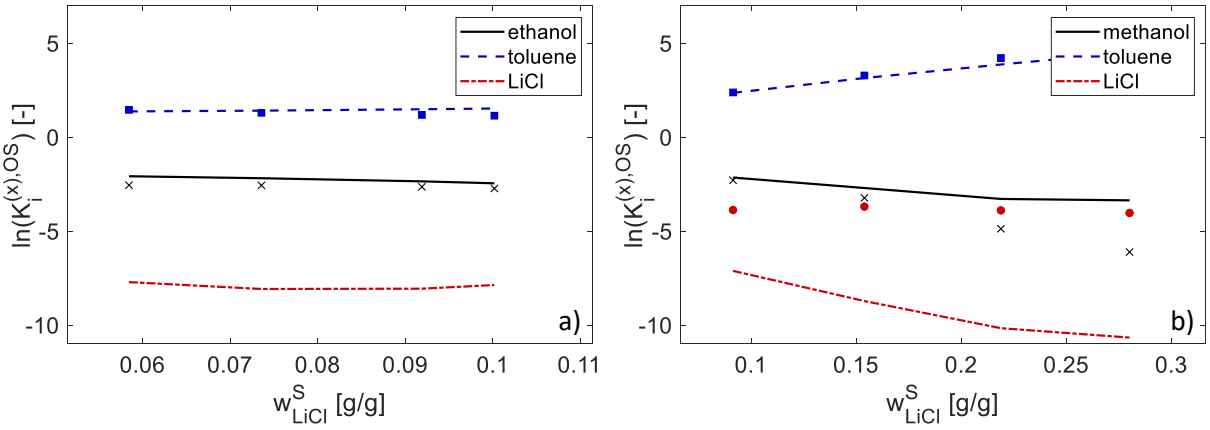

Figure 6.32: Logarithmic partition ratios calculated according to equation (5.4). Figure 6.32a) shows the system lithium chloride + ethanol + toluene and Figure 6.32 b) shows the system lithium chloride + methanol + toluene. Calculated values are represented by lines and experimental values by markers.

Figure 6.32 shows the calculated partition ratios as calculated by COSMO-RS-ES with Parameterization B. The trends for the partitioning of the organic solvents are predicted quite accurately. For the system in Figure 6.32 b), only at higher salt concentrations a larger deviation of the predicted value for the partitioning of methanol can be observed. The salt partitioning however is underestimated by several orders of magnitude with a much higher preference for the methanol-rich phase than the experimental partitioning.

This discrepancy shows how valuable this type of measurements can be to assess the limits of a model and develop ideas to further improve it.

To analyze this system further, Figure 6.33 shows the partition ratios for the methanol system with some additional details. The permittivity of both phases is very low, being around a value of $\epsilon_r = 3$ for the toluene phase and close to a value of $\epsilon_r = 29$ for the methanol phase.

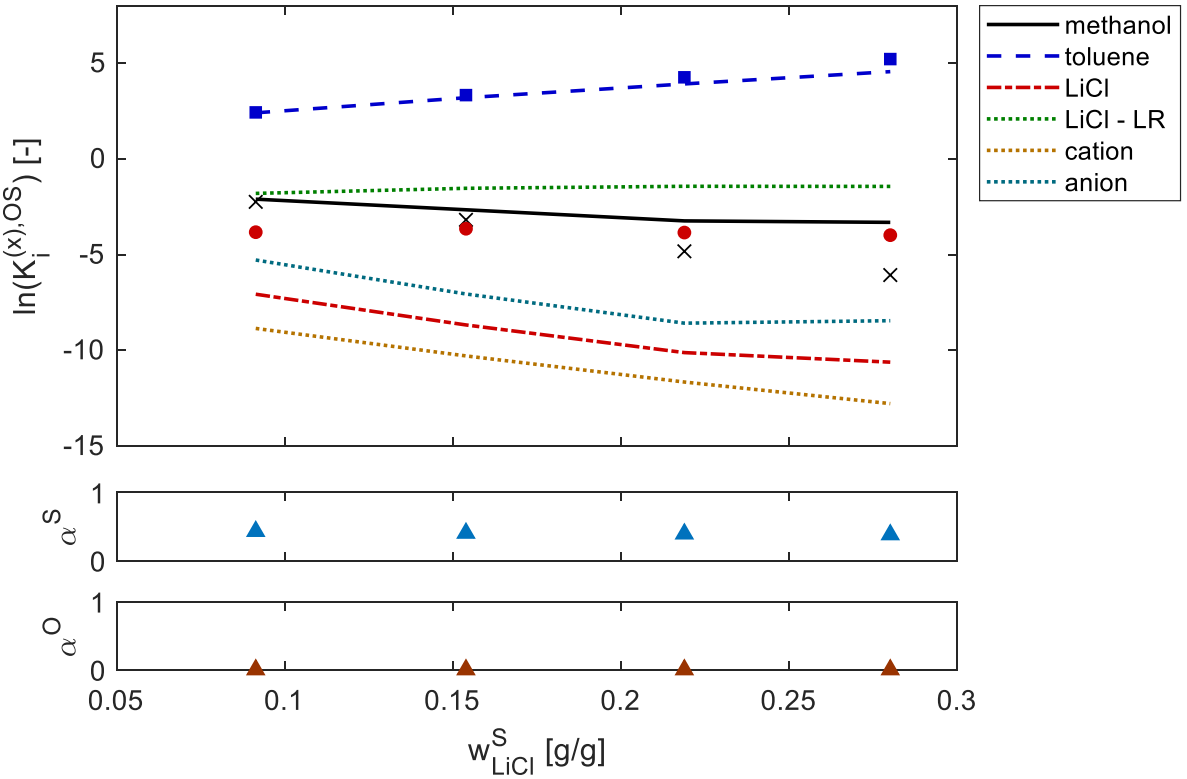

Figure 6.33: Logarithmic partition ratios calculated according to equation (5.4). for the system lithium chloride + methanol + toluene. In the upper plot, calculated values are represented by lines and experimental values by markers. The dotted lines represent different contributions to the overall salt partition ratio. The two subplots show the calculated dissociation degree α for the salt in the organic (O) and salt-rich (S) phases.

Based on these permittivities, one could postulate that the underestimation of the partition ratio of the salt is due to an underestimation of the LR contribution to the partitioning. However, as can be seen in Figure 6.33, the dissociation degree in the toluene phase is basically zero, meaning that the little amount of salt in this phase is completely associated while the dissociation degree in the methanol-rich phase is close to 0.5. This decrease in the free-ion concentration leads to the decrease of the influence of the LR contribution to the partitioning (green dotted line). In fact, by comparing the LR

contribution and the calculated partition ratio for the salt it becomes clear that the SR contribution dominates and is about twice the size of the LR contribution. From the experience gained for the calculation of LLEs in aqueous systems it is known that if the partitioning of the salt is wrong, in most cases also the partitioning of the solvent whose interactions with the salt are not described correctly is also calculated with a higher deviation from the experiment. This insight is also in accordance with the Gibbs-Duhem equation. Because methanol is the solvent whose calculated partition ratio has the largest deviation to the measured values, it is likely that the interactions of the salt with methanol have to be improved to describe this system better. Both ions prefer the methanol phase. As this behavior is expected for ions in this kind of systems, it is not clear whether the interaction of one of the ions is being described more accurately as the other.

This finding is in agreement with an additional evaluation made of experimental SLE data. As can be observed in equation (2.30), the solubility calculation has three contributions: the activity in water at the solubility limit, the transfer at infinite dilution from water to the system in question and activity at solubility limit in the system to be calculated. If the relative size of these three contributions is compared for several alkali salts, the largest portion of these three with an average of 47% is the Gibbs free energy of transfer of the salt at infinite dilution from water to the solvent in questions (cf. Table A-2 in the appendix). In the future, more emphasis has to put into describing the Gibbs free energies of transfer more accurately.

Although these very challenging systems show the limits of the predictive COSMO-RS-ES model, valuable understandings with these measurements could be gained for the further development and improvement of it. To the authors knowledge no other predictive electrolyte model has been applied to this type of data before.

6.6 Application of COSMO-RS-ES for calculating free solvation energies and pKa values

In this section, the applicability range of COSMO-RS-ES is extended further to be able to calculate solvation energies and aqueous pKa values, which in contrast to all data before, are gas phase related thermodynamic quantities.

pKa values for an acid (HA) can be calculated as a function of the Gibbs free energies of formation of the neutral acid and its respective dissociated ions:

$$pKa = \frac{1}{RTln(10)}\left[\Delta G_f(H^+) + \Delta G_f(A^-) - \Delta G_f(AH)\right] \tag{6.19}$$

where the Gibbs free energies of formation ΔG_f is calculated from the gaseous Gibbs free energies of formation and the free solvation energy of each species. The value $\Delta G_f(H^+)$ cannot be calculated explicitly, however for its solvation energy the theoretically calculated value from Zhan & Dixon[246] is used. Following Klamt et al.[247], the difference in the Gibbs free energies of formation of the anion and the neutral species is summarized into the dissociation energy ΔG_{diss}:

$$pKa = \frac{1}{RTln(10)}\left[\Delta G_f(H^+) + \Delta G_{diss}\right] \tag{6.20}$$

Several steps must be followed to be able to calculate the solvation energies. First the model needs to be able to describe the solvation energies of neutral components as well as the thermodynamics of neutral molecules quite accurately. This means that the neutral parameters need to be adjusted. After this, the parameters for the interactions of ions with the solvents can be adjusted. This would also be the first step for a complete reparameterization of the COSMO-RS-ES model, which would also start at the parameterization of the neutral interactions. In this work, this development will be termed Parameterization C.

The adjustment of the parameters describing the neutral interactions starts with the determination of the parameters for the combinatorial term. As already shown by Soares[248], the modified Stavermann-Guggenheim expression provides better results than

the normal Stavermann-Guggenheim expression used so far. In the modified version the following equation is used in the determination of the normalized volume fraction adding one additional parameter (the exponent p) to the combinatorial model:

$$\phi_i = \frac{x_i r_i^p}{\sum_j x_j^p r_j} \tag{6.21}$$

The rest of the expression to calculate the combinatorial contribution to the IDAC stays the same as in equation (2.48). In this work it could also be corroborated that for the calculation of IDACs in binary hydrocarbon systems with very low polarity, the modified expression provides better results (cf. Figure 8.1 in the appendix). The found parameters (listed in Table 6.11) and the deviation ($AAD_{\ln\gamma^\infty} = 0.037$) are very similar to the values found by Soares[248].

Following the adjustment of the combinatorial term, the residual COSMO-RS term was adjusted to IDACs and solvation energies. Section 5.1.3 describes the references for the thermodynamic data used and the definition of the objective functions optimized.

The solvation energies were calculated similarly to proposed by Klamt et al.[7]:

$$\Delta G^{o}_{solv} = E_{diel} + \Delta G^{o,cav+vdw}_{solv} + \Delta G^{o,COSMO-RS}_{solv} + \Delta G^{o,corr}_{solv} \tag{6.22}$$

The first term represents the transfer of the solute from ideal gas to the ideal conductor as calculated by the COSMO model. The second term is proportional to the area of the solute and describes the cavity formation. However, by making the term a function of the atom the area belongs to, effects related to the van der Waals interactions can be correlated delivering better results. The third term is calculated using COSMO-RS and it describes the transfer from ideal conductor to the real solution. This is the term that allows to use solvation energies to parameterize the model. The last term includes an adjustment of the reference state of the calculation from ideal gas to the liquid, a small empirical correction for molecules with rings in their structure and one additional parameter. Therefore, in more detail the solvation, the equation might be rewritten as follows:

$$\Delta G^{o}_{solv} = E_{diel} - \sum_{\alpha} \tau_\alpha A_\alpha + RT ln\gamma^{\infty,cosmo} - RT ln \frac{v_{IG}}{v_{liquid}} - \omega_{ring} n_{ring} - \eta_{type} \tag{6.23}$$

The second term is calculated as the area of an atom on the solute A_α multiplied by a factor depending on the atom α in question τ_α. ν_i stands for the molar volume of the respective phase *i*. ω_{ring} is an adjustable parameter while n_{ring} describes the number of atoms of a solute molecule that belong to a ring. η_{type} is the additional parameter that only depends on the type of the solute (cation, anion or neutral).

The parameter related to the misfit energy α' from equation (2.39) and the parameter for the hydrogen bonding energy c_{HB} from equation (2.42) were adjusted to the experimental data. As only data at temperatures close to 25 °C were considered, the temperature dependence of the hydrogen-bonding term was kept with the values previously used. Table 6.11 list the adjusted parameters for the first parameterization of COSMO-RS-ES using neutral data: Parameterization C.

Table 6.11. COSMO-RS-ES general parameters and parameters referring to neutral interaction energies for Parameterization C. The parameters τ_α depend on the atomic number α of the atom in question.

Parameter	Value	Unit
A_{norm}	116.85	[Å²]
α'	4583.86	$[\frac{kJ}{mol\ Å^2}]$
c_{HB}	19616.22	$[\frac{kJ}{mol\ Å^2}]$
p	0.645	[-]
ω_{ring}	0.77	$[\frac{kJ}{mol}]$
τ_α	$\tau_1 = 1.50 \cdot 10^{-1}, \tau_6 = 1.32 \cdot 10^{-1}, \tau_7 = 0.61 \cdot 10^{-4}$ $\tau_8 = 0.17 \cdot 10^{-6}, \tau_9 = 7.39 \cdot 10^{-2}, \tau_{15} = 1.02 \cdot 10^{-1}$ $\tau_{16} = 1.70 \cdot 10^{-1}, \tau_{17} = 1.84 \cdot 10^{-1}, \tau_{15} = 1.99 \cdot 10^{-1}$	$[\frac{kJ}{mol\ Å^2}]$
$\eta_{neutral}$	25.17	$[\frac{kJ}{mol}]$

The results of the calculation of IDACs using COSMO-RS-ES with Parameterization C are depicted in Figure 6.34. The overall deviation for the IDAC calculation of $AAD_{\ln\gamma^\infty} = 0.69$ is within the range of other COSMO-RS implementations[249] using almost the same dataset.

For the hydrocarbons or halogenated hydrocarbons in water the model calculates the IDAC with very high accuracy (cf .Figure 6.34 a). However, for more polar substances like alcohols, ketones, esters and ethers, the model overestimates the IDAC.

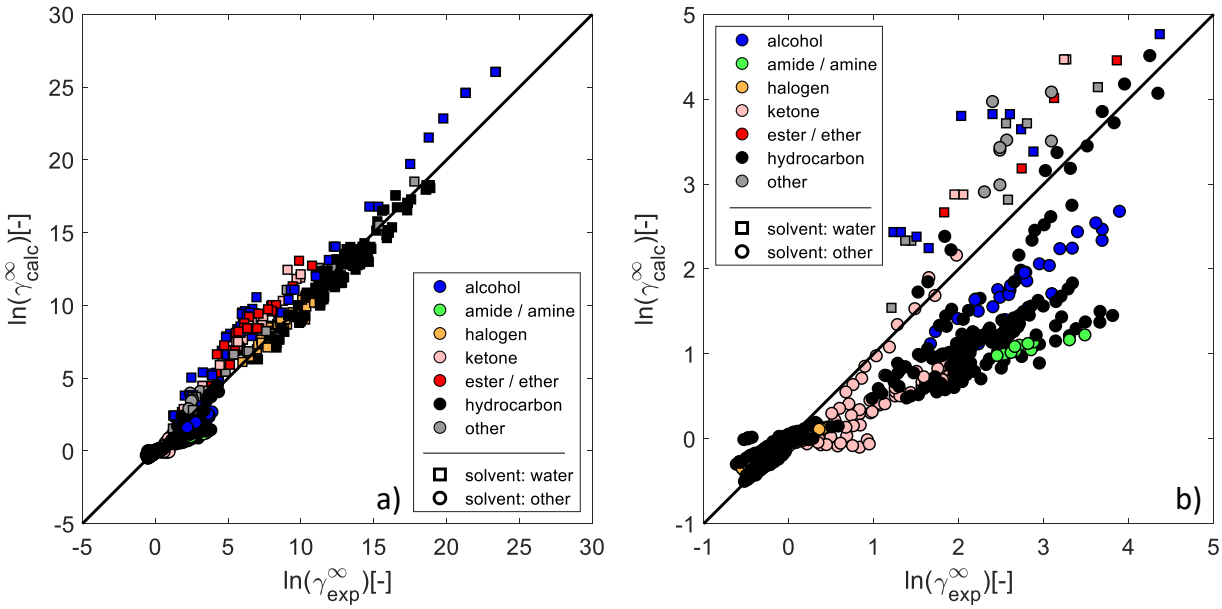

Figure 6.34: Calculated logarithmic infinite dilution activity coefficients vs. the experimental values. Figure 6.34 a) shows all the systems in the database allowing an evaluation of the data with water as the solvent. Figure 6.34 b) shows a zoomed version reporting mainly the systems with other solvents than water.

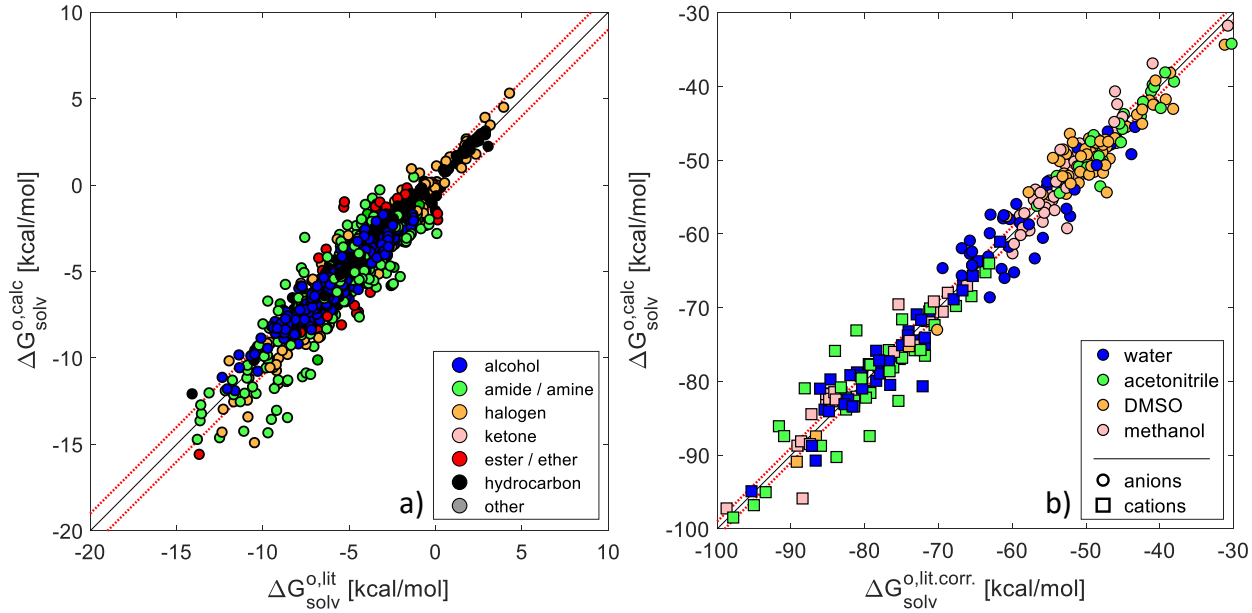

Figure 6.35: Calculated solvation energies vs. the experimental values. Figure 6.35 a) shows the calculations for all the systems with neutral solutes. Figure 6.35 b) shows the calculations for all the systems with ionic solutes including the correction of the literature values described in the text. The dotted red line denotes a deviation of 1 kcal/mol from the parity line.

For the non-aqueous systems most of the calculated values are underestimated (cf. Figure 6.34 b), showing that the model behaves quite similar to the implementation of Gerber & Soares[249]. This behavior might be due to underestimating the strength of the hydrogen bonding energy from the solute with water in comparison of the interactions of the solute with itself. This is especially interesting for alcohols, as these should behave quite similar as they possess a hydrogen bond donor and an acceptor. The other groups only have an oxygen that acts as a hydrogen bond acceptor which could explain the behavior of the model.

Table 6.12: Interaction energy equations for ionic interactions in the short-range contribution of COSMO-RS-ES for Parameterization C. Added threshold values and additional changes in comparison to the interaction energy equations of Parameterization B shown in Table 6.8 are highlighted in red.

Type of contact	Misfit factor	Ionic interaction energy term	
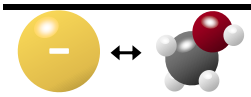 halide – org. mol.	A_4	$E^{ion}_{hal-om} = \frac{a_{eff}}{2} B_6 \min(0, \sigma_{om}) \max(0, \sigma_{hal})$	(6.24)
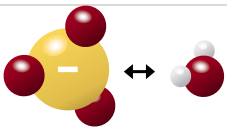 polyat. an. - H_2O	A_5	$E^{ion}_{pa-H_2O} = \frac{a_{eff}}{2} B_7 \min(0, \sigma_{H_2O} + \sigma_{HB}) \max(0, \sigma_{pa} - \sigma_{HB})$	(6.25)
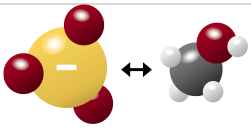 polyat. an. - org. mol.	A_6	$E^{ion}_{pa-om} = \frac{a_{eff}}{2} B_8 \min(0, \sigma_{om} + C_4) \max(0, \sigma_{pa} - C_3)$	(6.26)
 polyat. cat. – H_2O	A_7	$E^{ion}_{pc-H_2O} = \frac{a_{eff}}{2} B_9 \min(0, \sigma_{pc} + \sigma_{HB}) \max(0, \sigma_{H_2O} - \sigma_{HB})$	(6.27)
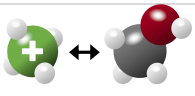 polyat. cat. - org. mol	A_8	$E^{ion}_{pc-om} = \frac{a_{eff}}{2} B_{10} \min(0, \sigma_{pc} + C_5) \max(0, \sigma_{om} - \sigma_{HB})$	(6.28)

For the solvation energies of the neutral molecules a very good correlation could be achieved with an average deviation of $AAD_{\Delta G^o_{solv}} = 0.55 \frac{kcal}{mol}$. It can be observed from Figure 6.35 a) that the solvation energies for most systems lies within what is considered chemical accuracy ($1 \frac{kcal}{mol}$) of the literature value from Marenich et al.[189] Only for solutes with amines/amides, esters/ethers and halogens a few outliers exist.

Ideally at this point the remaining equations for the ions would be adjusted to all the available electrolyte data in the database. However, to get a first glimpse at what the model is capable of accomplishing regarding the calculation of solvation energies of ionic solutes, the model is adjusted only to the target data. This is leads to a less generally applicable parameterization but allows to test how well the model can be tuned to be able to calculate solvation energies and by extension pKa values. Furthermore, it allows to test the needed interaction equations as a new type of interaction has to be introduced into the model, namely the two equations for polyatomic cations and water or an organic solvent. Table 6.12 shows the interaction energy equations employed in Parameterization C.

The solvation energy of ionic solutes cannot be determined directly, as discussed by Kröger et al.[17] The largest error source in the calculation of the solvation energy of the literature data lies in the estimation of the solvation energy of the proton (H^+). To account for this error, the literature data is corrected by a value $\delta_{H^+}^{solvent}$ which is dependent on the solvent of the system in question. This value is subtracted or added from the literature value of the solvation energy depending on the charge of the ion.

The same τ_α parameters for the calculation of the solvation energies of the neutral solutes are applied for the ionic solutes. The remaining parameters introduced in Table 6.12, the values of η_{type} for the anions / cations and the correction values $\delta_{H^+}^{solvent}$ were optimized based on the literature data leading to the parameters in Table 6.13.

As can be seen in Figure 6.35 b), this especially tuned version of COSMO-RS-ES allows the calculation of solvation energies of polyatomic anions and cations with a relatively high accuracy. The average deviation of $AAD_{\Delta G^o_{solv}} = 2.04 \frac{kcal}{mol}$ is four times larger than for the neutral molecules. However, this average deviation is about half the size of the deviation calculated by the SM8 model presented in the same publication[189] where the literature

data was taken from. If the four correction terms $\delta_{H^+}^{solvent}$ are taken as solvent specific parameters, this shows that this approach delivers better results with fewer solvent specific parameters than the SM8 model. Kröger et al.[17] show that by combining the cluster-continuum approach with the BP-TZVPD-FINE parameterization of COSMOtherm (BP_TZVP_FINE_C30_1701) it is possible to calculate the solvation energies with similar accuracy as COSMO-RS-ES with the Parameterization C. This approach is, however, much more computationally intensive and difficult to apply for a screening with a large database of solvents as for each solute several quantum chemistry calculations would be necessary for every solvent. The question needs to be addressed as to how many solvent molecules to use to the explicit solvation and the formation of the cluster. Furthermore, finding the most stable conformation has to be considered to know the starting geometry for the quantum chemical calculations.

Table 6.13. COSMO-RS-ES general parameters and parameters referring to ionic interaction energies for Parameterization C. Correction values $\delta_{H^+}^{solvent}$ are shown in kcal/mol because the literature data is in the same unit.

Parameters A [kJ/Å² mol⁻¹ e⁻²]	Parameters B [kJ/Å² mol⁻¹ e⁻²]	Parameters C [e/Å⁻²]	η_{type} [kJ/mol]	$\delta_{H^+}^{solvent}$ [kcal/mol]
A_4 = 15080	B_6 = 4566	C_3 = 0,0175	$\eta_{anion} = 68.85$	$\delta_{H^+}^{H2O} = 9.53$
A_5 = 473	B_7 = 25454	C_4 = 0,0094	$\eta_{cation} = 82.11$	$\delta_{H^+}^{methanol} = 11.86$
A_6 = 5408	B_8 = 143278	C_5 = 0,2112		$\delta_{H^+}^{DMSO} = 5.54$
A_7 = 5794	B_9 = 404			$\delta_{H^+}^{acetonitrile} = 4.48$
A_8 = 10869	B_{10} = 135177			

Although the performance of the model is quite satisfying, it is interesting to see that a peculiar trend might be observed for the calculated values. Whenever the deviation for a cation is particularly low in one specific solvent, the deviation for this solvent for the anions is large and vice versa. As an example, the values for cations solubilized in acetonitrile show the largest deviation while the values for anions in acetonitrile are calculated very accurately. The other way around, while the values for the anions in DMSO are calculated with a larger deviation, for the cations the values calculated have a deviation even lower than the ones of the neutral solutes. This systematic deviation might hint that the correction of the literature value lead to this behavior.

Now that the model has been adjusted to solvation data of neutral and ionic solutes, it can be applied to the prediction of pKa values. Figure 6.36 shows the same experimental pKa

values from Klamt et al.[247] as a function of the dissociation energy as defined in equation (6.20). a clear correlation as a function of the dissociation energy is visible (pKa = 0.0976 ΔG_{diss} – 2.82). The RMSE of the calculated values with respect to the correlation is about 1.1 pKa units. This deviation is somewhat larger than what Klamt et al.[247] found. As can be seen from the figure, this is most likely because of just calculating the formation energy for the first conformer not including the conformer equilibrium. So far COSMO-RS-ES has not included the conformer equilibrium as it adds further calculations increasing the computational cost and a test on the IDAC dataset with COSMOtherm showed a very small impact (cf. Figure 8.2 in the appendix).

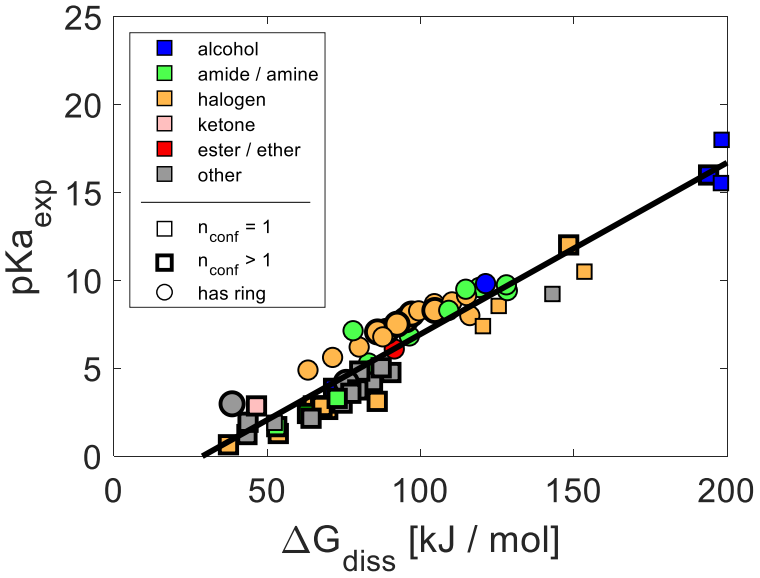

Figure 6.36: Calculated pKa values vs the dissociation energy predicted from COSMO-RS-ES with the Parameterization C. The markers with a larger border indicate that for the neutral component several conformers are available. If the marker is a circle, the neutral molecule has a ring in its structure.

For the calculation of Gibbs free energies of formation or gas-phase related energies in general the conformer equilibrium seems to be more important than for the chemical potential in the liquid phase unless intramolecular hydrogen-bonding is possible. This is due to the fact that the sigma-profiles of conformers are very similar to each other in most cases other than when intramolecular hydrogen-bonding is present. As several of the outliers refer to acids with a similar structure to acetic acid, the hypothesis was tested on this solute for which two conformers exist in our database. It could be confirmed by a COSMOtherm (BP_TZVP_FINE_C30_1701) calculation that the solvation energy of the two

conformers in water differs by about 5 kcal/mol (ca. 20 kJ/mol), which in the calculation of the pKa value leads to a shift of up to 0.3 pKa units.

As it is possible to calculate solvation energies in different solvents with the Parameterization C, in the future it could be tested whether the model is able to calculate pKa values in different solvents, however first the conformer equilibrium should be implemented.

7 Conclusions

COSMO-RS-ES, which was further developed in this work, is one of the most predictive electrolyte g^E-models available to date as it does not need binary interaction parameters, instead using the sigma-profile as first-principle input to describe the interactions. It has been successfully applied to a wide range of different thermodynamic data in mixed-solvent systems including MIACs, LLEs and VLEs in ternary and even quaternary systems.

In this work, the applicability range of the model was extended further to highly concentrated and non-aqueous systems. To achieve this goal a new database of SLE data concentrating on mixed-solvent and completely non-aqueous solvents was created to evaluate the model. Usually to model these systems the fusion temperature and enthalpy of the solutes are necessary. Instead, in this work the way proposed to calculate the solubilities of these systems is through the knowledge of the experimental solubility in a reference solvent (in this case water), which is generally easier to measure. Then, for the calculation of the solubility, the model is used to describe the transfer of the salt from the reference solvent to the system in question. COSMO-RS-ES was shown to be able to predict SLEs in a variety of systems. However, the evaluation also revealed some systematic deviations especially for salts with very high solubilities and for systems with very low permittivity. The model is a sum of two contributions, the short-range and the long-range contribution, these were thoroughly analyzed. It could be shown that the deviations originated from deficiencies in the description of both terms.

For the SLE calculation the model implicitly has to describe the Gibbs free energy of transfer between water and the system in question. To test whether the model was describing this data correctly on a qualitative basis a database of Gibbs free energies of ions was created. The calculation of this data showed that the transfer of anions was already been calculated quite accurately while for the transfer of the monoatomic cations the model calculated the transfer energy with large deviations from the experimental values. As a next step to improve the short-range contribution of the model, the Gibbs free energies of transfer of ions was included into the training dataset leading to Parameterization A. As expected, the inclusion of this data type improved the model's

ability to reproduce this data, especially for the cations. At the same time, the accuracy of the prediction for SLEs was greatly enhanced.

As the next step the long-range contribution of the model was systematically analyzed. As a first step the sensitivity of the model towards its different input parameters was calculated. It was found that the Pitzer-Debye-Hückel term is most sensitive towards the closest approach parameter. While the sensitivity towards the permittivity was also found to be quite high, the model is least sensitive towards the density. So far, a fixed closest approach parameter, the salt-free permittivity and density had been used as input for the long-range contribution. In this work, firstly it was tested if the explicit calculation of the closest approach parameter leads to a better description of the experimental data. Secondly, it was tested whether using the permittivity of the solution rather than the salt-free permittivity by including the description of the dielectric decrement effect through the ions has an influence on the overall performance of the model. Thirdly, introducing the salt influence on the permittivity of the solution also allowed to test a Born term contribution, as included in other models. For all the three changes tested, improvements could be observed for some of the thermodynamic data evaluated. However, when having a closer look at the complete dataset it was found that either these changes lead to other thermodynamic data being misrepresented or the changes lead to trends that were unphysical. Important insights could be gained from these tests. It was found that already in the derivation of the long-range model, the salt dependency of the properties needs to be properly considered for the model to be correctly applied using these properties. It is not enough to apply a model with salt-dependent properties when it was derived to be used with salt-free properties. If the inclusion of a Born term is considered the model describing the permittivity of the solution has to represent the derivative of the permittivity towards the ion concentration correctly.

Besides systematically evaluating the short-term and the long-range term, the balance between both terms was addressed. For the calculation of SLEs in highly concentrated systems and low permittivities very high deviations were found. For these conditions, ion-pairing becomes increasingly important. In the literature, for the calculations it is mainly assumed that all ions are free ions. Especially at low permittivities this assumption is not valid. Therefore, in this work the effect of ion-pairing was introduced into the model leading to Parameterization B. To calculate the association constant, two models with

different behaviors at high permittivities, namely the models by Fuoss and by Bjerrum were tested. It was found that the model by Bjerrum delivers better results for the calculations with COSMO-RS-ES. The description of this effect not only improved the overall performance of the model for the calculation of SLE systems but also for some LLE systems with low permittivities. For some ketone containing systems it was found that the model shows deviations in the salt free systems already. This systematic deviation is then carried over to the calculation of the salt distribution in these systems. This shows that maybe a point is reached where the model describes the ionic interactions accurate enough to begin thinking of improving the model's calculations for neutral molecules.

During this work, two salt-containing non-aqueous LLEs were measured: methanol + toluene + lithium chloride and ethanol + toluene + lithium chloride. The evaluation of this newly gained unique experimental data using COSMO-RS-ES with the Parameterization B showed that the model describes the relative trends in the correct order while underestimating the solubility in the SLE systems and the partition ratio in the LLE systems. This challenging type of data is very valuable to test the boundaries of the model and to gain valuable understandings. In this case it could be shown that the underestimation of the partitioning in the LLE systems is mainly due to the short-range contribution of the model. This agrees with an evaluation of experimental SLE data which shows that in the future more emphasis has to be put into describing the Gibbs free energies of transfer correctly, as this is the largest contribution to the calculation of SLE systems.

Further, the model was applied to the calculation of solvation energies and pKa values. As these are gas-phase related quantities, the model needed to be reparametrized from the bottom up. After adjusting it to IDACs and solvation energies of neutral and ionic solutes, the model was able to predict pKa values. It was found that for the calculation of pKa values for the systems tested, the inclusion of the conformer equilibrium is more important than for the calculation of thermodynamics in liquid phases unless intramolecular hydrogen-bonding exists.

In summary in this work, COSMO-RS-ES was extended and refined for the use with highly concentrated salt systems in mixed- and non-aqueous solvents. By the introduction of new thermodynamic data into the training dataset and including the effect of ion-pairing,

the model could be enhanced consistently for a wide variety of systems. New insights have been gained as to how improve the model further and directions are proposed which could lead to an even more generally applicable predictive model.

8 Appendix

8.1 Complementary evaluations

8.1.1 Solubility products

Table A-1: Calculated solubility products using two different methods: COSMO-RS-ES with the parameters published by Gerlach et al.[14] and based on aqueous free formation energies according to equation (6.1).

Salt	$ln\ (K_{SP})$	
	COSMO-RS-ES (Gerlach et al. [14])	Aqueous free formation energies
Cs_2SO_4	-11.9221	-10.0365
CsBr	-6.61525	-6.10877
$CsClO_4$	-13.5759	-13.568
CsCl	-5.08211	-4.51607
CsI	-7.55789	-6.81878
$CsNO_3$	-9.58268	-9.31594
K_2SO_4	-16.0386	-16.1766
KBr	-5.61145	-5.22528
$KClO_4$	-12.5236	-12.5957
KCl	-5.98587	-5.95224
KF	-0.51399	1.757882
KI	-4.13461	-4.01906
KNO_3	-7.83123	-8.15006
KSCN	-3.09646	-3.08313
Li_2SO_4	-11.2766	-8.23731
LiBr	5.682037	14.49379
$LiClO_4$	-2.02223	11.26241
LiCl	5.043128	8.316651
LiI	4.566441	22.30799
$LiNO_3$	0.475764	1.451285
$(NH_4)_2SO_4$	-13.7376	-11.4525
NH_4Br	-5.03584	-4.6968

NH_4ClO_4	-8.36685	-8.40421
NH_4Cl	-5.21833	-5.23416
NH_4I	-3.24764	-3.84156
NH_4NO_3	-4.43199	-5.31403
Na_2SO_4	-13.9464	-12.6588
NaBr	-2.83747	-1.25767
$NaClO_4$	0.050859	-1.74984
NaCl	-4.52147	-4.35672
NaF	-8.83868	-10.2902
NaI	-0.31691	4.866217
$NaNO_3$	-4.29114	-5.5339
Rb_2SO_4	-14.5855	-13.861
RbBr	-5.84127	-5.51978
$RbClO_4$	-13.8102	-13.8463
RbCl	-5.55963	-5.05262
RbI	-5.36116	-5.35438
$RbNO_3$	-8.14934	-8.26705

8.1.2 Infinite dilution activity coefficients for hydrocarbons

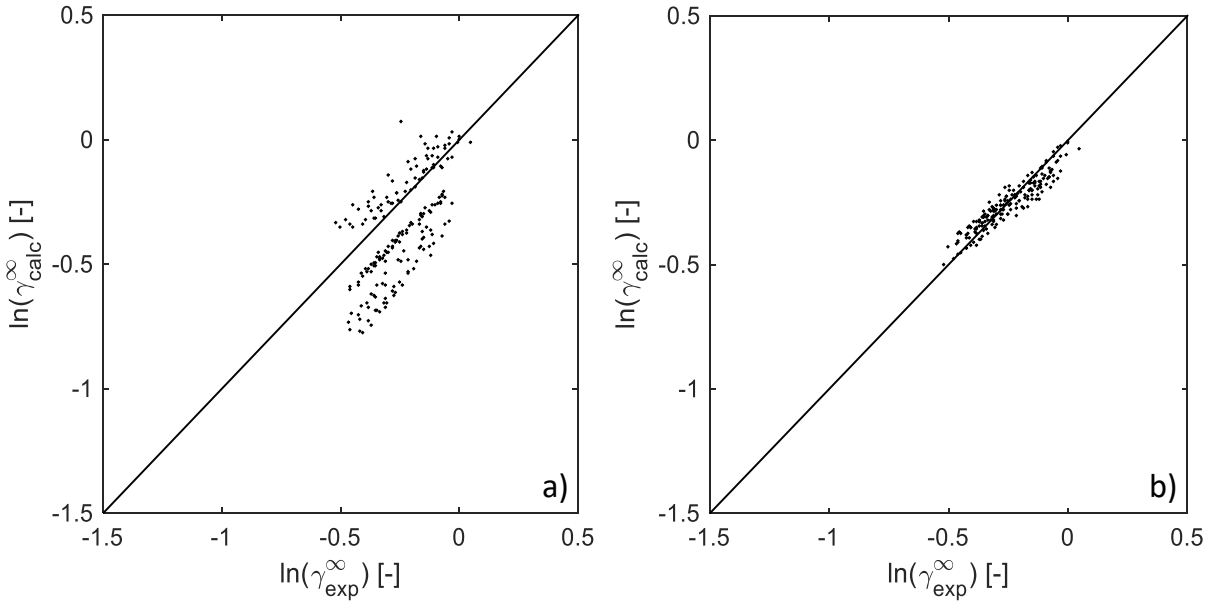

Figure 8.1: Parity plot of the calculated infinite dilution activity coefficient against the experimental values for binary mixtures of hydrocarbons. Figure 8.1 a) shows the values calculated with the Staverman-Guggenheim expression i.e. equation (2.48). Figure 8.1 b) shows the values calculated with the modified Staverman-Guggenheim expression as discussed in section 6.6.

8.1.3 Evaluation conformer equilibrium

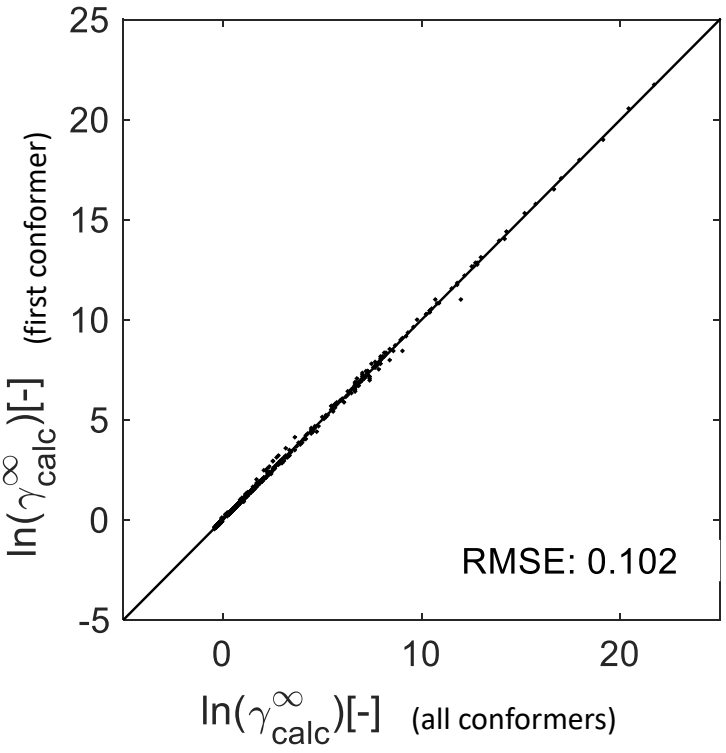

Figure 8.2: Parity plot of the calculated infinite dilution activity coefficients calculated with only the first conformer against the calculated values including the conformer equilibrium. Values calculated by COSMOtherm (BP_TZVP_FINE_C30_1701).

8.1.4 Evaluation of relative importance in the terms of the SLE calculation

Table A-2: Relative importance of the three terms in equation (2.30) used for the calculation of the SLE systems in this work. As reference solvent water was taken. The table is sorted by the fourth column which shows the sum of the solubilities in water and the other solvent in the mole-fraction scale. The relative importance is measured as the absolute value of the term divided by the sum of the absolute values of the three terms. All values are calculated from experimental data.

cation	anion	solvent	$x_{\pm,w} + x_{\pm,s}$	$\left\lvert\frac{\Delta G^0_{t,salt\ w\to s}}{RT}\right\rvert$	$\lvert \nu\, ln\, x_{\pm,w}\gamma^w_{\pm}\rvert$	$\lvert \nu\, ln\, x_{\pm,s}\gamma^s_{\pm}\rvert$
sodium	fluoride	methanol	0.0173	31%	23%	46%
potassium	bromide	methanol	0.0915	35%	20%	44%
sodium	chloride	methanol	0.0961	38%	18%	44%
sodium	chloride	methanol	0.0961	38%	18%	44%
sodium	chloride	methanol	0.0961	38%	18%	44%
rubidium	iodide	methanol	0.1278	37%	21%	42%
sodium	bromide	ethanol	0.1352	53%	7%	39%
sodium	nitrate	ethanol	0.1390	42%	13%	44%
lithium	perchlorate	acetonitrile	0.1403	58%	8%	35%
sodium	chloride	formamide	0.1500	28%	33%	40%
sodium	bromide	methanol	0.1733	48%	12%	40%
sodium	bromide	formamide	0.2390	50%	43%	8%
lithium	bromide	acetonitrile	0.2397	56%	20%	24%
sodium	iodide	methanol	0.2810	78%	7%	15%
sodium	perchlorate	methanol	0.2970	52%	16%	32%
lithium	nitrate	ethanol	0.3010	75%	1%	24%
lithium	nitrate	methanol	0.3400	73%	2%	25%
lithium	perchlorate	methanol	0.3461	35%	13%	53%
lithium	chloride	ethanol	0.3830	65%	27%	8%
lithium	chloride	ethanol	0.3840	65%	27%	8%
lithium	bromide	methanol	0.3990	29%	37%	33%
lithium	chloride	methanol	0.4060	48%	36%	16%
lithium	chloride	methanol	0.4080	47%	36%	16%
lithium	bromide	ethanol	0.4100	41%	27%	32%
lithium	iodide	methanol	0.4480	23%	28%	49%
lithium	bromide	methanol	0.4520	28%	36%	36%
			average	47%	21%	32%

8.2 Solving Bjerrum's integral

The evaluation of Bjerrum's equation is easier by employing the approximation also developed by Fuoss & Kraus[28], changing equation (2.72) to:

$$\mathrm{K}_{\mathrm{A}}^{(c)} = 4\pi N_A \cdot 1000 \cdot \left(\frac{2q}{a}\right)^3 \cdot \int_2^{2q/a} \frac{\exp(u)}{u^{-4}}\, du \tag{8.1}$$

where $u = \frac{2q}{r}$ and the integral that be approximated from tabulated values or by the following truncated expansion:

$$\begin{gathered}\int_a^B \frac{\exp(u)}{u^{-4}}\, du = -\left(\frac{\exp(u)}{3u^3}\middle|\begin{matrix}B\\2\end{matrix}\right) - \left(\frac{\exp(u)}{6u^2}\middle|\begin{matrix}B\\2\end{matrix}\right) - \left(\frac{\exp(u)}{6u}\middle|\begin{matrix}B\\2\end{matrix}\right) + \cdots \\ \frac{1}{6}\cdot\left[\sum_{i=2}^{i=4}\left(\frac{\exp(u)}{u^i}\cdot(i-1)!\middle|\begin{matrix}B\\2\end{matrix}\right) + abs\left(\frac{\exp(u)}{u^5}\cdot(5-1)!\right)\right]\end{gathered} \tag{8.2}$$

where $B = \frac{2q}{a}$ and the convention $\left(f(u)\,|_2^B\right)$ expresses the evaluation $f(B) - f(2)$.

8.3 Experimental data for non-aqueous phase equilibria

Table A-3: Experimental data for the SLE system X (1) + toluene (2) + lithium chloride (3) at temperature T = 25 °C and pressure p = 0.1 MPa. The salt-free concentration of the first solvent $w_{1,sf}$ and the solubility of the salt are shown.

first solvent (X)	$w_{1,sf}$	w_3
1-butanol	1.0000	0.1156
	0.7505	0.0894
	0.4950	0.0603
	0.2504	0.0397
1-propanol	1.0000	0.1408
	0.7503	0.1183
	0.5054	0.0860
	0.2510	0.0497
	0.1498	0.0297
2-propanol	1.0000	0.1140
	0.7553	0.1007
	0.4870	0.0687
	0.2488	0.0347

The standard uncertainties are within u(T) = 0.1 K, u(p) = 10 kPa, $u(w_{1,sf}) = 0.0001$ g/g, $u(w_{2,sf}) = 0.0001$ g/g, $u(w_3) = 0.0010$ g/g. Water concentration in the samples was always lower than 0.15 wt%.

Table A-4: Experimental data for the SLE system methanol (1) + 1-butanol (2) + lithium chloride (3) at temperature T = 25 °C and pressure p = 0.1 MPa. The salt-free concentration of the first solvent $w_{1,sf}$ and the solubility of the salt are shown.

$w_{1,sf}$	w_3
0.0000	0.1156
0.2498	0.1784
0.5013	0.2071
0.7505	0.2532
1.0000	0.3093

The standard uncertainties are within u(T) = 0.1 K, u(p) = 10 kPa, $u(w_{1,sf}) = 0.0001$ g/g, $u(w_{2,sf}) = 0.0001$ g/g, $u(w_3) = 0.0010$ g/g. Water concentration in the samples was always lower than 0.18 wt%.

Table A-5: Experimental data for the LLE system methanol (1) + toluene (2) + lithium chloride (3) at temperature T = 25 °C and pressure p = 0.1 MPa.

organic phase			salt-rich phase			
w_1	w_2	w_3	w_1	w_2	w_3	Type
0.0297	0.9696	0.0008	0.6962	0.2124	0.0914	LLE
0.0108	0.9878	0.0014	0.7451	0.1010	0.1539	LLE
0.0019	0.9966	0.0015	0.7373	0.0437	0.2188	LLE
0.0005	0.9978	0.0016	0.6723	0.0192	0.3040	SLLE

The standard uncertainties are within u(T) = 0.1 K, u(p) = 10 kPa, $u(w_1^O) = 0.002$ g/g, $u(w_2^O) = 0.003$ g/g, $u(w_3^O) = 0.001$ g/g, $u(w_1^S) = 0.020$ g/g, $u(w_2^S) = 0.020$ g/g and $u(w_3^S) = 0.001$ g/g. Water concentration in the samples was always lower than 0.11 wt% in the salt-rich phase and lower than 0.01% in the organic phase.

Table A-6: Experimental data for the LLE system ethanol (1) + toluene (2) + lithium chloride (3) at temperature T = 25 °C and pressure p = 0.1 MPa.

organic phase[b]			salt-rich phase			
w_1	w_2	w_3	w_1	w_2	w_3	Type
0.0258	0.9397	0.0000[a]	0.5613	0.3716	0.0579	LLE
0.0225	0.9495	0.0000[a]	0.4888	0.4344	0.0733	LLE
0.0178	0.9552	0.0000[a]	0.4226	0.4946	0.0928	LLE
0.0153	0.9670	0.0000[a]	0.3906	0.5141	0.1007	SLLE

The standard uncertainties are within u(T) = 0.1 K, u(p) = 10 kPa, $u(w_1^O) = 0.023$ g/g , $u(w_2^O) = 0.029$ g/g $u(w_1^S) = 0.001$ g/g, $u(w_2^S) = 0.001$ g/g and , $u(w_3^S) = 0.007$ g/g,. Water concentration in the samples was always lower than 0.16 wt% in the salt-rich phase and lower than 0.01% in the organic phase. [a]Value was below the detection limit.

8.4 Dataset used with COSMO-RS-ES for training and evaluation

8.4.1 MIAC (aqueous) dataset at 298.15 K

System	Reference
Cs_2SO_4	Goldberg, 1981[250]
CsBr	Hamer & Wu, 1972[220]
$CsClO_4$	Justice, Bury & Justice, 1971[251]
CsCl	Hamer & Wu, 1972[220]
CsF	Hamer & Wu, 1972[220]
CsI	Hamer & Wu, 1972[220]
$CsNO_3$	Hamer & Wu, 1972[220]
K_2HPO_4	Goldberg, 1981[250]
K_2SO_4	Goldberg, 1981[250]
KBr	Hamer & Wu, 1972[220]
$KClO_4$	Justice, Bury & Justice, 1971[251]
KCl	Hamer & Wu, 1972[220]
KF	Hamer & Wu, 1972[220]
KH_2PO_4	Hamer & Wu, 1972[220]
KI	Hamer & Wu, 1972[220]
KNO_3	Hamer & Wu, 1972[220]
Li_2SO_4	Goldberg, 1981[250]
LiBr	Hamer & Wu, 1972[220]
$LiClO_4$	Hamer & Wu, 1972[220]
LiCl	Hamer & Wu, 1972[220]
LiI	Hamer & Wu, 1972[220]
$LiNO_3$	Hamer & Wu, 1972[220]
$(NH_4)_2HPO_4$	Goldberg, 1981[250]
$(NH_4)_2SO4$	Robinson & Stokes, 1970[2]
NH_4Br	Lobo & Quaresma, 1989[252]
NH_4ClO_4	Hamer & Wu, 1972[220]
NH_4Cl	Hamer & Wu, 1972[220]
NH_4NO_3	Hamer & Wu, 1972[220]
Na_2HPO_4	Goldberg, 1981[250]
$Na_2S_2O_3$	Goldberg, 1981[250]
Na_2SO_3	Goldberg, 1981[250]
Na_2SO_4	Goldberg, 1981[250]
NaBr	Hamer & Wu, 1972[220]
$NaClO_4$	Hamer & Wu, 1972[220]
NaCl	Hamer & Wu, 1972[220]
NaF	Hamer & Wu, 1972[220]
NaH_2PO_4	Hamer & Wu, 1972[220]

NaI	Hamer & Wu, 1972[220]
$NaNO_3$	Hamer & Wu, 1972[220]
Rb_2SO_4	Goldberg, 1981[250]
RbBr	Hamer & Wu, 1972[220]
$RbClO_4$	Justice, Bury & Justice, 1971[251]

8.4.2 MIAC (organic) dataset at 298.15 K

System	Reference
methanol + LiCl	Bonner, 1987[253]
ethanol + LiCl	Safarov et al., 2006[254]
2-propanol + LiCl	Zafarani-Moattar & Aria, 2001[255]
methanol + LiBr	Nasirzadeh et al., 2004[256]
ethanol + LiBr	Nasirzadeh et al., 2004[256]
2-propanol + LiBr	Nasirzadeh et al., 2005[257]
acetone + LiBr	Barthel et al., 1999[258]
acetonitrile + LiBr	Kunz et al., 1991[259]
methanol + LiI	Held et al., 2011[260]
ethanol + LiI	Safarov et al., 2005[261]
methanol + $LiClO_4$	Barthel et al., 1998[262] + Nasirzadeh & Neueder, 2004[263]
ethanol + $LiClO_4$	Barthel et al., 1998[262]
2-propanol + $LiClO_4$	Barthel et al., 1998[262]
acetonitrile + $LiClO_4$	Barthel et al., 1999[264]
acetone + $LiClO_4$	Barthel et al., 1999[264]
DME + $LiClO_4$	Barthel et al., 1999[264]
methanol + $LiNO_3$	Nasirzadeh & Neueder, 2004[263]
ethanol + $LiNO_3$	Verevkin et al., 2006[265]
2-propanol + $LiNO_3$	Zafarani-Moattar & Aria, 2001[255]
methanol + KI	Barthel et al., 1985[266]
methanol + KBr	Barthel et al., 1985[266]
methanol + KSCN	Nasirzadeh & Zafarani-Moattar 2004[267]
methanol + NaBr	Ye et al., 1994[268]
ethanol + NaBr	Ye et al., 1994[268]
formamide + NaBr	Hernández-Luis, 2011[269]
methanol + NaCl	Barthel et al., 1985[266]
formamide + NaCl	Hernández-Luis, 2011[270]
N-methylformamide + NaCl	Hernández-Luis, 2009[271]
ethanol + NaI	Barthel et al., 1993[272]
methanol + NaI	Hernández-Luis, 2009[271]
2-propanol + NaI	Barthel & Lauermann, 1986[273]
ethanol + $NaNO_3$	Bonner, 1987[253]
methanol + NaSCN	Nasirzadeh & Salabat, 2003[274]
methanol + NH_4SCN	Nasirzadeh & Zafarani-Moattar, 2004[267]
methanol + RbI	Barthel et al., 1993[272]
methanol + $NaClO_4$	Barthel et al., 1993[272]
acetonitrile + NaI	Barthel et al., 1993[272]

8.4.3 LLE dataset

System	Temperature[K]	Reference
LiCl + water + *n*-butanol	298	243
LiCl + water + 1-pentanol	298	275
LiCl + water + 2-pentanol	298	275
LiCl + water + 3-pentanol	298	275
LiCl + water + 2-methyl-1-butanol	298	275
LiCl + water + 2-methyl-2-butanol	298	275
LiCl + water + 2-butanone	298	276
LiCl + water + acetonitrile	298	277
Li_2SO_4 + water + *n*-propanol	298-308	278
Li_2SO_4 + water + 2-propanol	298-308	279
Li_2SO_4 + water + acetonitrile	298	277
Li_2SO_4 + water + methyl isobutyl ketone	298	234
$LiNO_3$ + water + methyl isobutyl ketone	298	234
NaCl + water + ethanol + *n*-butanol	298	280,281
NaCl + water + ethanol + 1-pentanol	298	282
NaCl + water + ethanol + 3-methyl-1-butanol	298	280
NaCl + water + ethanol + acetone	298	281
NaCl + water + *n*-propanol	298	283
NaCl + water + 2-propanol	298	284–286
NaCl + water + *n*-butanol	293-303	202,284,287
NaCl + water + *sec*-butanol	298	284,288
NaCl + water + *tert*-butanol	298	284,288
NaCl + water + isobutanol	298	284,288
NaCl + water + 1-pentanol	298	283
NaCl + water + 2-pentanol	298	283
NaCl + water + 3-pentanol	298	283
NaCl + water + 2-methyl-1-butanol	298	283
NaCl + water + 2-methyl-2-butanol	298	283
NaCl + water + 2-butanone	298	202
NaCl + water + acetone	298	281
NaCl + water + acetone + *n*-butanol	298	289
NaCl + water + methyl isobutyl ketone	298	234
NaBr + water + *n*-propanol	298	285
NaBr + water + *n*-butanol	298	243
NaBr + water + 2-butanone	298	276
NaBr + water + ethyl acetate	298	276
NaBr + water + acetonitrile	298	290
Na_2SO_4 + water + 2-propanol	308	291
Na_2SO_4 + water + *tert*-butanol	308	291
Na_2SO_4 + water + acetone	308	291
Na_2SO_4 + water + acetonitrile	298	292
Na_2SO_4 + water + methyl isobutyl ketone	298	234
Na_2SO_3 + water + *n*-propanol	298	293
Na_2SO_3 + water + 2-propanol	298-308	291,293
Na_2SO_3 + water + *tert*-butanol	298-308	291,293
Na_2SO_3 + water + acetone	308	291
$Na_2S_2O_3$ + water + ethanol	298	294
$Na_2S_2O_3$ + water + *n*-propanol	298	294
$Na_2S_2O_3$ + water + 2-propanol	298	294
$Na_2S_2O_3$ + water + *sec*-butanol	298	294

$Na_2S_2O_3$ + water + *tert*-butanol	298	294
$Na_2S_2O_3$ + water + acetonitrile	298	292
$NaNO_3$ + water + *n*-butanol	298-308	295
$NaNO_3$ + water + 1-pentanol	298-308	296
$NaNO_3$ + water + 2-pentanol	298	297
$NaNO_3$ + water + 3-pentanol	298	297
$NaNO_3$ + water + 2-methyl-1-butanol	298	297
$NaNO_3$ + water + acetonitrile	298	290
$NaNO_3$ + water + methyl isobutyl ketone	298	234
NaH_2PO_4 + water + ethanol	298-308	298
KF + water + *n*-propanol	298-308	299
KF + water + 2-propanol	298-308	299
KF + water + acetonitrile	298	300
KCl + water + ethanol + *n*-butanol	298	301
KCl + water + ethanol + 1-pentanol	298	280
KCl + water + *n*-propanol	298	286,285
KCl + water + *n*-butanol	293-298	202,288
KCl + water + *sec*-butanol	298	288
KCl + water + *tert*-butanol	298	288
KCl + water + isobutanol	298	288
KCl + water + 2-butanone	298	202
KCl + water + methyl isobutyl ketone	298	234
KBr + water + ethanol + 1-pentanol	298	280
KBr + water + *n*-butanol	298	202,243
KBr + water + *n*-butanol + *tert*-butanol	293	302
KBr + water + 2-butanone	298	202
KBr + water + acetonitrile	298	300
KI + water + *n*-butanol	298	243
KI + water + 2-butanone	298	276
KI + water + ethyl acetate	298	276
K_2SO_4 + water + ethanol + 1-pentanol	298	280
K_2HPO_4 + water + methanol	298-308	298
K_2HPO_4 + water + ethanol	298-308	298
K_2HPO_4 + water + *n*-propanol	298-308	303
K_2HPO_4 + water + 2-propanol	298-308	303
KNO_3 + water + 1-pentanol	298	297
KNO_3 + water + 2-pentanol	298	297
KNO_3 + water + 2-methyl-1-butanol	298	297
KNO_3 + water + 2-methyl-2-butanol	298	297
CsCl + water + *n*-propanol	298-308	304
CsCl + water + 2-propanol	298-308	304
Cs_2SO_4 + water + ethanol	303	305
NH_4Cl + water + *n*-butanol	298-308	306
$(NH_4)_2SO_4$ + water + acetonitrile	298	292
$(NH_4)_2HPO_4$ + water + *n*-propanol	298	307
$(NH_4)_2HPO_4$ + water + 2-propanol	298	307
$(NH_4)_2HPO_4$ + water + acetonitrile	298	290,308
NH_4NO_3 + water + acetonitrile	298	290
$NH_4H_2PO_4$ + water + *n*-propanol	298	307
$CaCl_2$ + water + ethanol + *n*-butanol	298	280
$CaCl_2$ + water + ethanol + 3-methyl-1-butanol	298	280

8.4.4 SLE dataset at 298.15 K

System	Reference
Cs_2SO_4 + methanol	Stenger, 1996[309]
Cs_2SO_4 + water + methanol	Hu, et al, 2004[310]
CsBr + methanol	Stenger, 1996[309]
CsBr + water	CRC Handbook, 1998[311]
CsCl + acetonitrile	IUPAC-NIST Solubility Data Series 78, 2002[312]
CsCl + acetonitrile + methanol	IUPAC-NIST Solubility Data Series 83, 2007[198]
CsCl + methanol	Stenger, 1996[309]
CsCl + water	CRC Handbook, 1998[311]
$CsClO_4$ + acetone	Willard & Smith, 1923[238]
$CsClO_4$ + ethanol	Willard & Smith, 1923[238]
$CsClO_4$ + isobutanol	Willard & Smith, 1923[238]
$CsClO_4$ + methanol	Willard & Smith, 1923[238]
$CsClO_4$ + n-butanol	Willard & Smith, 1923[238]
$CsClO_4$ + n-propanol	Willard & Smith, 1923[238]
$CsClO_4$ + water	Willard & Smith, 1923[238]
CsI + acetonitrile + N,N-dimethylformamide	IUPAC-NIST Solubility Data Series 83, 2007[198]
CsI + water	CRC Handbook, 2005[206]
$CsNO_3$ + methanol	Stenger, 1996[309]
$CsNO_3$ + water + 2-propanol	Hu et al., 2005[241]
$CsNO_3$ + water + ethanol	Hu et al., 2005[241]
$CsNO_3$ + water + methanol	Hu et al., 2005[241]
$CsNO_3$ + water + n-propanol	Hu et al., 2005[241]
$CsNO_3$ + water + tert-butanol	Hu et al., 2005[241]
K_2SO_4 + methanol	Stenger, 1996[309]
K_2SO_4 + water	Wang et al, 2011[313]
K_2SO_4 + water + 1-propanol	Taboada, 2002[196]
K_2SO_4 + water + acetone	Fox and Gauge, 1910[242]
K_2SO_4 + water + chloralhydrate	Fox and Gauge, 1910[242]
K_2SO_4 + water + ethanol	Fox and Gauge, 1910[242]
K_2SO_4 + water + ethylene glycol	Fox and Gauge, 1910[242]
K_2SO_4 + water + glycerol	Fox and Gauge, 1910[242]
K_2SO_4 + water + pyridine	Fox and Gauge, 1910[242]
KBr + ethanol	Pinho & Macedo, 2002[191]
KBr + methanol	Pinho & Macedo, 2002[191]
KBr + methanol + ethanol	Pinho & Macedo, 2002[191]
KBr + water	Pinho & Macedo, 2002[191]
KBr + water + 2-butoxyethanol	Chiavone-Filho & Rasmussen, 1993[193]
KBr + water + 2-methoxyethanol	Chiavone-Filho & Rasmussen, 1993[193]
KBr + water + acetone	Wang et al, 2008[314]
KBr + water + ethanol	Pinho & Macedo, 2002[191]
KBr + water + methanol	Pinho & Macedo, 2002[191]
KCl + ethanol	Li et al, 2010[244]

KCl + methanol	Li et al, 2010[244]
KCl + methanol + ethanol	Pinho & Macedo, 2005[190]
KCl + water	Wang et al, 2011[313]
KCl + water + 1,2-ethanediol	Chiavone-Filho & Rasmussen, 1993[193]
KCl + water + 1,4-dioxane	Eysseltová & Málková, 2006[199]
KCl + water + 1-butanol	Gomis et al, 1996[288]
KCl + water + 1-methoxy-2-propanol	Chiavone-Filho & Rasmussen, 1993[193]
KCl + water + 2-butanol	Gomis et al, 1996[288]
KCl + water + 2-ethoxyethanol	Chiavone-Filho & Rasmussen, 1993[193]
KCl + water + 2-isopropoxyethanol	Chiavone-Filho & Rasmussen, 1993[193]
KCl + water + 2-methoxyethanol	Chiavone-Filho & Rasmussen, 1993[193]
KCl + water + 2-methyl-1-propanol	Gomis et al, 1996[288]
KCl + water + 2-methyl-2-propanol	Gomis et al, 1996[288]
KCl + water + 2-propanol	Gomis et al, 1994[288]
KCl + water + DMSO	Mohs et al, 2011[158]
KCl + water + ethanol	Pinho & Macedo, 2005[190]
KCl + water + glycerol	Wang et al, 2011[313]
KCl + water + methanol	Pinho & Macedo, 1996[192]
KCl + water + n-propanol	Gomis et al, 1994[286]
$KClO_4$ + acetone	Willard & Smith, 1923[238]
$KClO_4$ + ethanol	Willard & Smith, 1923[238]
$KClO_4$ + ethyl acetate	Willard & Smith, 1923[238]
$KClO_4$ + isobutanol	Willard & Smith, 1923[238]
$KClO_4$ + methanol	Willard & Smith, 1923[238]
$KClO_4$ + n-butanol	Willard & Smith, 1923[238]
$KClO_4$ + n-propanol	Willard & Smith, 1923[238]
$KClO_4$ + water	Willard & Smith, 1923[238]
KF + methanol	Stenger, 1996[309]
KF + water	CRC Handbook, 2005[206]
KI + 1-propanol	Long et al, 2012[315]
KI + acetone	Long et al, 2012[315]
KI + acetonitrile	IUPAC-NIST Solubility Data Series 78, 2002[312]
KI + ethanol	Long et al, 2012[315]
KI + water	CRC Handbook, 2005[206]
KNO_3 + aceticacid	Davidsson and Geer, 1933[316]
KNO_3 + methanol	Stenger, 1996[309]
KNO_3 + water	Davidsson and Geer, 1933[316]
KSCN + n-butanol	IUPAC-NIST Solubility Data Series 79, 2004[317]
KSCN + water	IUPAC-NIST Solubility Data Series 79, 2004[317]
Li_2SO_4 + methanol	Stenger, 1996[309]
Li_2SO_4 + water	CRC Handbook, 2005[206]
LiBr + 1-butanol	Li et al, 2011[318]
LiBr + 1-propanol	Li et al, 2011[318]

LiBr + 2-propanol	Li et al, 2011[318]
LiBr + acetonitrile	IUPAC-NIST Solubility Data Series 78, 2002[312]
LiBr + ethanol	Li et al, 2011[318]
LiBr + methanol	Li et al, 2010[244]
LiBr + propylene carbonate	Harris, 1958[319]
LiBr + water	Boryta, 1970[320]
LiCl + 1-pentanol	Gomis et al, 2004[321]
LiCl + acetone	Li et al, 2010[244]
LiCl + ethanol	Li et al, 2010[244]
LiCl + methanol	Li et al, 2010[244]
LiCl + water	CRC Handbook, 2005[206]
LiCl + water + 2-methyl-1-butanol	Gomis et al, 2004[275]
LiCl + water + 2-pentanol	Gomis et al, 2004[275]
$LiClO_4$ + acetone	Willard & Smith, 1923[238]
$LiClO_4$ + acetonitrile	IUPAC-NIST Solubility Data Series 78, 2002[312]
$LiClO_4$ + diethyl ether	Willard & Smith, 1923[238]
$LiClO_4$ + ethanol	Willard & Smith, 1923[238]
$LiClO_4$ + ethyl acetate	Willard & Smith, 1923[238]
$LiClO_4$ + isobutanol	Willard & Smith, 1923[238]
$LiClO_4$ + methanol	Willard & Smith, 1923[238]
$LiClO_4$ + n-butanol	Willard & Smith, 1923[238]
$LiClO_4$ + 2-butanol	IUPAC-NIST Solubility Data Series 61, 1996[322]
$LiClO_4$ + n-propanol	Willard & Smith, 1923[238]
$LiClO_4$ + t-butanol	IUPAC-NIST Solubility Data Series 61, 1996[322]
$LiClO_4$ + water	Willard & Smith, 1923[238]
LiI + methanol	Stenger, 1996[309]
LiI + i-pentanol	Turner & Bisset, 1913[323]
LiI + water	CRC Handbook, 2005[206]
$LiNO_3$ + 1-butanol	Li et al, 2011[318]
$LiNO_3$ + 1-propanol	Li et al, 2011[318]
$LiNO_3$ + 2-propanol	Li et al, 2011[318]
$LiNO_3$ + ethanol	Li et al, 2011[318]
$LiNO_3$ + methanol	Li et al, 2011[318]
$LiNO_3$ + water	CRC Handbook, 2005[206]
LiSCN + water	IUPAC-NIST Solubility Data Series 79, 2004[317]
Na_2SO_4 + methanol	Stenger, 1996[309]
Na_2SO_4 + water	CRC Handbook, 2005[206]
Na_2SO_4 + water + 2-propanol	Brenner et al, 1992[324]
NaBr + acetonitrile + DMSO	IUPAC-NIST Solubility Data Series 83, 2007[198]
NaBr + ethanol	Pinho & Macedo, 2005[190]
NaBr + methanol	Pinho & Macedo, 2005[190]
NaBr + methanol + ethanol	Pinho & Macedo, 2005[190]
NaBr + water	Pinho & Macedo, 2005[190]
NaBr + water + ethanol	Pinho & Macedo, 2005[190]
NaBr + water + formamide	Hernández-Luis, et al, 2016[197]

NaBr + water + methanol	Pinho & Macedo, 2005[190]
NaBr + water + n-methylformamide	Hernández-Luis, et al, 2016[197]
NaCl + ethanol	Pinho & Macedo, 2005[190]
NaCl + methanol	Pinho & Macedo, 2005[190]
NaCl + methanol + ethanol	Pinho & Macedo, 2005[190]
NaCl + water	Pinho & Macedo, 2005[190]
NaCl + water + 1,2-propanediol	Raridon and Kraus, 1971[325]
NaCl + water + 1,3-butanediol	Raridon and Kraus, 1971[325]
NaCl + water + 1,3-propanediol	Raridon and Kraus, 1971[325]
NaCl + water + 1,4-butanediol	Raridon and Kraus, 1971[325]
NaCl + water + 1,4-dioxane	Eysseltová & Málková, 2006[199]
NaCl + water + 1,5-pentanediol	Raridon and Kraus, 1971[325]
NaCl + water + 1-pentanol	Gomis et al., 1999[283]
NaCl + water + 1-propanol	Gomis et al., 1994[286]
NaCl + water + 2-butanol	Gomis et al, 1996[288]
NaCl + water + 2-butoxyethane-1-ol	Raridon and Kraus, 1971[325]
NaCl + water + 2-ethoxyethan-1-ol	Raridon and Kraus, 1971[325]
NaCl + water + 2-methoxyethane-1-ol	Raridon and Kraus, 1971[325]
NaCl + water + 2-methyl-1-butanol	Gomis et al., 1999[283]
NaCl + water + 2-methyl-1-propanol	Gomis et al, 1996[288]
NaCl + water + 2-methyl-2-butanol	Gomis et al., 1999[283]
NaCl + water + 2-methyl-2-propanol	Gomis et al., 1996[288]
NaCl + water + 2-methylpentane-2,4-diol	Raridon and Kraus, 1971[325]
NaCl + water + 2-pentanol	Gomis et al., 1999[283]
NaCl + water + 2-propanol	Gomis et al, 1994[286]
NaCl + water + 3-pentanol	Gomis et al., 1999[283]
NaCl + water + bis(2-hydroxyethyl)ether	Raridon and Kraus, 1971[325]
NaCl + water + DMSO	Mohs et al, 2011[158]
NaCl + water + ethanol	Pinho & Macedo, 1996[192]
NaCl + water + ethylen glycol	Zeng & Li, 2015[326]
NaCl + water + formamide	Hernández-Luis, et al, 2016[197]
NaCl + water + glycerol	Marcolli & Krieger, 2006[327]
NaCl + water + hexane-2,5-diol	Raridon and Kraus, 1971[325]
NaCl + water + methanol	Pinho & Macedo, 1996[192]
NaCl + water + n-methylformamide	Hernández-Luis, et al, 2016[197]
NaCl + water + n-propanol	Gomis et al, 1994[286]
$NaClO_4$ + acetone	Willard & Smith, 1923[238]
$NaClO_4$ + ethanol	Willard & Smith, 1923[238]

$NaClO_4$ + ethyl acetate	Willard & Smith, 1923[238]
$NaClO_4$ + ethylene glycol	IUPAC-NIST Solubility Data Series 61, 1996[322]
$NaClO_4$ + isobutanol	Willard & Smith, 1923[238]
$NaClO_4$ + methanol	Willard & Smith, 1923[238]
$NaClO_4$ + n-butanol	Willard & Smith, 1923[238]
$NaClO_4$ + n-propanol	Willard & Smith, 1923[238]
$NaClO_4$ + water	Willard & Smith, 1923[238]
NaF + water + formamide	Hernández-Luis, et al, 2016[197]
NaF + water + n-methylformamide	Hernández-Luis, et al, 2016[197]
NaI + methanol	Stenger, 1996[309]
NaI + water + formamide	Hernández-Luis, et al, 2016[197]
NaI + water + n-methylformamide	Hernández-Luis, et al, 2016[197]
NaI + n-propanol	Turner & Bisset, 1913[323]
NaI + water	Stephen & Stephen, 1963[328]
$NaNO_3$ + acetic acid	Davidsson and Geer, 1933[316]
$NaNO_3$ + methanol	Stenger, 1996[309]
$NaNO_3$ + water	Davidsson and Geer, 1933[316]
NaSCN + 2-butanone	IUPAC-NIST Solubility Data Series 79, 2004[317]
NaSCN + acetone	IUPAC-NIST Solubility Data Series 79, 2004[317]
NaSCN + water	CRC Handbook, 2005[206]
NH_4Br + methanol	Stenger, 1996[309]
NH_4Br + water	CRC Handbook, 2005[206]
NH_4Cl + methanol	Stenger, 1996[309]
NH_4Cl + water	CRC Handbook, 2005[206]
NH_4ClO_4 + acetone	Willard & Smith, 1923[238]
NH_4ClO_4 + ethanol	Willard & Smith, 1923[238]
NH_4ClO_4 + ethyl acetate	Willard & Smith, 1923[238]
NH_4ClO_4 + isobutanol	Willard & Smith, 1923[238]
NH_4ClO_4 + n-butanol	Willard & Smith, 1923[238]
NH_4ClO_4 + n-propanol	Willard & Smith, 1923[238]
NH_4ClO_4 + water	CRC Handbook, 2005[206]
NH_4I + water + ethanol	Seidell, 1919[329]
NH_4NO3 + methanol	Stenger, 1996[309]
NH_4NO3 + water	Seidell, 1919[329]
NH_4SCN + methanol	IUPAC-NIST Solubility Data Series 79, 2004[317]
NH_4SCN + water	IUPAC-NIST Solubility Data Series 79, 2004[317]
Rb_2SO_4 + methanol	Stenger, 1996[309]
Rb_2SO_4 + water	CRC Handbook, 2005[206]
RbBr + methanol	Stenger, 1996[309]
RbBr + water	CRC Handbook, 2005[206]
RbCl + ethanol	Seidell, 1919[329]
RbCl + methanol	Seidell, 1919[329]
RbCl + n-propanol	Seidell, 1919[329]
RbCl + water	CRC Handbook, 2005[206]

$RbClO_4$ + acetone	Willard & Smith, 1923[238]
$RbClO_4$ + ethanol	Willard & Smith, 1923[238]
$RbClO_4$ + ethyl acetate	Willard & Smith, 1923[238]
$RbClO_4$ + isobutanol	Willard & Smith, 1923[238]
$RbClO_4$ + methanol	Willard & Smith, 1923[238]
$RbClO_4$ + n-butanol	Willard & Smith, 1923[238]
$RbClO_4$ + n-propanol	Willard & Smith, 1923[238]
$RbClO_4$ + water	Willard & Smith, 1923[238]
RbI + acetonitrile	IUPAC-NIST Solubility Data Series 78, 2002[312]
RbI + acetonitrile + n,n-dimethylformamide	IUPAC-NIST Solubility Data Series 83, 2007[198]
RbI + methanol	Stenger, 1996[309]
RbI + water	Seidell & Linke, 1940[240]
$RbNO_3$ + methanol	Stenger, 1996[309]
$RbNO_3$ + water + ethanol	Li et al, 2005[194]
$RbNO_3$ + water + methanol	Li et al, 2005[194]
RbSCN + ethanol	IUPAC-NIST Solubility Data Series 79, 2004[317]
RbSCN + methanol	IUPAC-NIST Solubility Data Series 79, 2004[317]
RbSCN + water	IUPAC-NIST Solubility Data Series 79, 2004[317]

8.4.5 Gibbs free energy of transfer of ions dataset at 298.15 K

System	Reference
ammonium ion + 2-propanol + water	calculated in this work
ammonium ion + ethanol + water	calculated in this work
ammonium ion + methanol + water	calculated in this work
ammonium ion + t-butanol + water	Kalidas et al. 2000[201]
bromide ion + 1,1-dichloroethane + water	Marcus, 1983[330]
bromide ion + 1,2-dichloroethane + water	Marcus, 1983[330]
bromide ion + 1,4-dioxane + water	Marcus. 2007[62]
bromide ion + 2-propanol + water	Marcus. 2007[62]
bromide ion + DME + water	Marcus. 2007[62]
bromide ion + DMSO + water	Marcus. 2007[62]
bromide ion + NMP + water	Marcus, 1983[330]
bromide ion + nitromethane + water	Marcus, 2007[62]
bromide ion + THF + water	Marcus. 2007[62]
bromide ion + acetone + water	Marcus. 2007[62]
bromide ion + acetonitrile + water	Marcus, 2007[62]
bromide ion + ethanol + water	Marcus. 2007[62]
bromide ion + ethylene glycol + water	Marcus. 2007[62]
bromide ion + formamide + water	Marcus. 2007[62]
bromide ion + methanol + water	Marcus. 2007[62]
bromide ion + n-butanol + water	Marcus, 2015[20]
bromide ion + n,n-dimethylacetamide + water	Marcus, 2007[62]

bromide ion + n,n-dimethylformamide + water	Marcus, 2007[62]
bromide ion + n-propanol + water	Marcus, 2007[62]
bromide ion + pyridine + water	Marcus, 2007[62]
bromide ion + t-butanol + water	Marcus. 2007[62]
caesium ion + 1,1-dichloroethane + water	Marcus, 1983[330]
caesium ion + 1,2-dichloroethane + water	Marcus, 1983[330]
caesium ion + 12propanediol + water	Kalidas et al. 2000[201]
caesium ion + 1,4-dioxane + water	Kalidas et al. 2000[201]
caesium ion + DMSO + water	Kalidas et al. 2000[201]
caesium ion + NMP + water	Marcus, 1983[330]
caesium ion + n-methylformamide + water	Kalidas et al. 2000[201]
caesium ion + nitromethane + water	Marcus, 2015[20]
caesium ion + acetone + water	Kalidas et al. 2000[201]
caesium ion + acetonitrile + water	Kalidas et al. 2000[201]
caesium ion + ethanol + water	Kalidas et al. 2000[201]
caesium ion + formamide + water	Kalidas et al. 2000[201]
caesium ion + methanol + water	Kalidas et al. 2000[201]
caesium ion + n-butanol + water	Marcus, 2015[20]
caesium ion + nitrobenzene + water	Marcus, 2015[20]
caesium ion + n,n-dimethylacetamide + water	Kalidas et al. 2000[201]
caesium ion + n,n-dimethylformamide + water	Kalidas et al. 2000[201]
caesium ion + n-propanol + water	Kalidas et al. 2000[201]
caesium ion + pyridine + water	Marcus, 2015[20]
caesium ion + t-butanol + water	Kalidas et al. 2000[201]
chlorate ion + 2-propanol + water	Marcus. 2007[62]
chlorate ion + formamide + water	Marcus. 2007[62]
chloride ion + 1,1-dichloroethane + water	Marcus, 1983[330]
chloride ion + 1,2-dichloroethane + water	Marcus, 1983[330]
chloride ion + 12propanediol + water	Marcus. 2007[62]
chloride ion + 1,4-dioxane + water	Marcus. 2007[62]
chloride ion + 2-methoxyethanol + water	Marcus. 2007[62]
chloride ion + 2-propanol + water	Marcus. 2007[62]
chloride ion + DME + water	Marcus. 2007[62]
chloride ion + DMSO + water	Marcus. 2007[62]
chloride ion + NMP + water	Marcus, 1983[330]
chloride ion + nitromethane + water	Marcus, 2007[62]
chloride ion + THF + water	Marcus. 2007[62]
chloride ion + acetone + water	Marcus. 2007[62]
chloride ion + acetonitrile + water	Marcus. 2007[62]
chloride ion + ethanol + water	Marcus. 2007[62]
chloride ion + ethylene glycol + water	Marcus. 2007[62]
chloride ion + formamide + water	Marcus, 2007[62]
chloride ion + methanol + water	Marcus. 2007[62]
chloride ion + n-butanol + water	Marcus, 2015[20]
chloride ion + n,n-dimethylacetamide + water	Marcus, 2007[62]
chloride ion + n,n-dimethylformamide + water	Marcus. 2007[62]

chloride ion + n-propanol + water	Marcus, 2007[62]
chloride ion + pyridine + water	Marcus, 2007[62]
chloride ion + t-butanol + water	Marcus. 2007[62]
fluoride ion + 2-methoxyethanol + water	Marcus. 2007[62]
fluoride ion + acetone + water	Marcus. 2007[62]
fluoride ion + acetonitrile + water	Marcus, 2007[62]
fluoride ion + ethanol + water	Marcus. 2007[62]
fluoride ion + ethylene glycol + water	Marcus. 2007[62]
fluoride ion + formamide + water	Marcus. 2007[62]
fluoride ion + methanol + water	Marcus. 2007[62]
fluoride ion + n,n-dimethylformamide + water	Marcus, 2007[62]
fluoride ion + t-butanol + water	Marcus. 2007[62]
iodide ion + 1,1-dichloroethane + water	Marcus, 1983[330]
iodide ion + 1,2-dichloroethane + water	Marcus, 1983[330]
iodide ion + 2-methoxyethanol + water	Marcus. 2007[62]
iodide ion + 2-propanol + water	Marcus. 2007[62]
iodide ion + DME + water	Marcus. 2007[62]
iodide ion + DMSO + water	Marcus. 2007[62]
iodide ion + NMP + water	Marcus, 1983[330]
iodide ion + nitromethane + water	Marcus, 2007[62]
iodide ion + acetone + water	Marcus. 2007[62]
iodide ion + acetonitrile + water	Marcus, 2007[62]
iodide ion + ethanol + water	Marcus. 2007[62]
iodide ion + ethylene glycol + water	Marcus. 2007[62]
iodide ion + formamide + water	Marcus. 2007[62]
iodide ion + methanol + water	Marcus. 2007[62]
iodide ion + n-butanol + water	Marcus, 2015[20]
iodide ion + n,n-dimethylacetamide + water	Marcus, 2007[62]
iodide ion + n,n-dimethylformamide + water	Marcus, 2007[62]
iodide ion + n-propanol + water	Marcus, 2007[62]
iodide ion + pyridine + water	Marcus, 2007[62]
iodide ion + t-butanol + water	Marcus. 2007[62]
lithium ion + 1,4-dioxane + water	Kalidas et al. 2000[201]
lithium ion + DMSO + water	Kalidas et al. 2000[201]
lithium ion + NMP + water	Marcus, 1983[330]
lithium ion + n-methylformamide + water	Kalidas et al. 2000[201]
lithium ion + nitromethane + water	Marcus, 2015[20]
lithium ion + THF + water	Kalidas et al. 2000[201]
lithium ion + acetone + water	Kalidas et al. 2000[201]
lithium ion + acetonitrile + water	Kalidas et al. 2000[201]
lithium ion + ethanol + water	Kalidas et al. 2000[201]
lithium ion + ethylene glycol + water	Kalidas et al. 2000[201]
lithium ion + formamide + water	Marcus, 1983[330]
lithium ion + methanol + water	Kalidas et al. 2000[201]
lithium ion + nitrobenzene + water	Marcus, 2015[20]
lithium ion + n,n-dimethylacetamide + water	Kalidas et al. 2000[201]

lithium ion + n,n-dimethylformamide + water	Kalidas et al. 2000[201]
lithium ion + n-propanol + water	Kalidas et al. 2000[201]
lithium ion + t-butanol + water	Kalidas et al. 2000[201]
nitrate ion + 1,2-dichloroethane + water	Marcus, 1983[330]
nitrate ion + acetone + water	Marcus. 2007[62]
nitrate ion + acetonitrile + water	calculated in this work
nitrate ion + ethanol + water	Marcus. 2007[62]
nitrate ion + methanol + water	Marcus. 2007[62]
perchlorate ion + 1,1-dichloroethane + water	Marcus, 1983[330]
perchlorate ion + 1,2-dichloroethane + water	Marcus, 1983[330]
perchlorate ion + 12propanediol + water	Marcus. 2007[62]
perchlorate ion + 2-propanol + water	Marcus. 2007[62]
perchlorate ion + DMSO + water	calculated in this work
perchlorate ion + NMP + water	Marcus, 1983[330]
perchlorate ion + nitromethane + water	Marcus, 2015[20]
perchlorate ion + acetonitrile + water	Marcus, 2007[62]
perchlorate ion + ethanol + water	Marcus. 2007[62]
perchlorate ion + formamide + water	Marcus. 2007[62]
perchlorate ion + methanol + water	Marcus. 2007[62]
perchlorate ion + n-butanol + water	Marcus, 2015[20]
perchlorate ion + n,n-dimethylformamide + water	Marcus, 2015[20]
perchlorate ion + n-propanol + water	Marcus, 2015[20]
perchlorate ion + pyridine + water	Marcus, 2015[20]
perchlorate ion + t-butanol + water	Marcus. 2007[62]
potassium ion + 1,1-dichloroethane + water	Marcus, 1983[330]
potassium ion + 1,2-dichloroethane + water	Marcus, 1983[330]
potassium ion + 12propanediol + water	Kalidas et al. 2000[201]
potassium ion + 1,4-dioxane + water	Kalidas et al. 2000[201]
potassium ion + 2-propanol + water	Kalidas et al. 2000[201]
potassium ion + DMSO + water	Kalidas et al. 2000[201]
potassium ion + NMP + water	Marcus, 1983[330]
potassium ion + n-methylformamide + water	Kalidas et al. 2000[201]
potassium ion + nitromethane + water	Marcus, 2015[20]
potassium ion + THF + water	Kalidas et al. 2000[201]
potassium ion + acetone + water	Kalidas et al. 2000[201]
potassium ion + acetonitrile + water	Kalidas et al. 2000[201]
potassium ion + ethanol + water	Kalidas et al. 2000[201]
potassium ion + ethylene glycol + water	Kalidas et al. 2000[201]
potassium ion + formamide + water	Kalidas et al. 2000[201]
potassium ion + methanol + water	Kalidas et al. 2000[201]
potassium ion + n-butanol + water	Marcus, 2015[20]
potassium ion + nitrobenzene + water	Marcus, 2015[20]
potassium ion + n,n-dimethylacetamide + water	Kalidas et al. 2000[201]
potassium ion + n,n-dimethylformamide + water	Kalidas et al. 2000[201]
potassium ion + n-propanol + water	Kalidas et al. 2000[201]
potassium ion + pyridine + water	Marcus, 2015[20]

potassium ion + t-butanol + water	Kalidas et al. 2000[201]
rubidium ion + 1,1-dichloroethane + water	Marcus, 1983[330]
rubidium ion + 1,2-dichloroethane + water	Marcus, 1983[330]
rubidium ion + 1,4-dioxane + water	Kalidas et al. 2000[201]
rubidium ion + 2-propanol + water	Kalidas et al. 2000[201]
rubidium ion + DMSO + water	Kalidas et al. 2000[201]
rubidium ion + NMP + water	Marcus, 1983[330]
rubidium ion + n-methylformamide + water	Kalidas et al. 2000[201]
rubidium ion + nitromethane + water	Marcus, 2015[20]
rubidium ion + THF + water	Kalidas et al. 2000[201]
rubidium ion + acetone + water	Kalidas et al. 2000[201]
rubidium ion + acetonitrile + water	Kalidas et al. 2000[201]
rubidium ion + ethanol + water	Kalidas et al. 2000[201]
rubidium ion + formamide + water	Kalidas et al. 2000[201]
rubidium ion + methanol + water	Kalidas et al. 2000[201]
rubidium ion + n-butanol + water	Marcus, 2015[20]
rubidium ion + nitrobenzene + water	Marcus, 2015[20]
rubidium ion + n,n-dimethylacetamide + water	Kalidas et al. 2000[201]
rubidium ion + n,n-dimethylformamide + water	Kalidas et al. 2000[201]
rubidium ion + n-propanol + water	Kalidas et al. 2000[201]
rubidium ion + pyridine + water	Marcus, 2015[20]
rubidium ion + t-butanol + water	Kalidas et al. 2000[201]
sodium ion + 1,1-dichloroethane + water	Marcus, 1983[330]
sodium ion + 1,2-dichloroethane + water	Marcus, 1983[330]
sodium ion + 1,4-dioxane + water	Kalidas et al. 2000[201]
sodium ion + DMSO + water	Kalidas et al. 2000[201]
sodium ion + NMP + water	Marcus, 1983[330]
sodium ion + n-methylformamide + water	Kalidas et al. 2000[201]
sodium ion + nitromethane + water	Marcus, 2015[20]
sodium ion + THF + water	Kalidas et al. 2000[201]
sodium ion + acetone + water	Kalidas et al. 2000[201]
sodium ion + acetonitrile + water	Kalidas et al. 2000[201]
sodium ion + ethanol + water	Kalidas et al. 2000[201]
sodium ion + ethylene glycol + water	Kalidas et al. 2000[201]
sodium ion + formamide + water	Kalidas et al. 2000[201]
sodium ion + methanol + water	Kalidas et al. 2000[201]
sodium ion + n-butanol + water	Marcus, 2015[20]
sodium ion + nitrobenzene + water	Marcus, 2015[20]
sodium ion + n,n-dimethylacetamide + water	Kalidas et al. 2000[201]
sodium ion + n,n-dimethylformamide + water	Kalidas et al. 2000[201]
sodium ion + n-propanol + water	Kalidas et al. 2000[201]
sodium ion + pyridine + water	Marcus, 2015[20]
sodium ion + t-butanol + water	Kalidas et al. 2000[201]
sulfate ion + n-methylformamide + water	Marcus, 2015[20]
sulfate ion + acetone + water	Marcus, 2015[20]
sulfate ion + ethanol + water	Marcus. 2007[62]

sulfate ion + ethylene glycol + water	Marcus, 2015[20]
sulfate ion + methanol + water	Marcus. 2007[62]
sulfate ion + n,n-dimethylformamide + water	Marcus, 2015[20]
thiocyanate ion + 1,4-dioxane + water	Marcus. 2007[62]
thiocyanate ion + DMSO + water	Marcus, 2015[20]
thiocyanate ion + NMP + water	Marcus, 1983[330]
thiocyanate ion + nitromethane + water	Marcus, 2015[20]
thiocyanate ion + acetone + water	Marcus. 2007[62]
thiocyanate ion + acetonitrile + water	Marcus, 2015[20]
thiocyanate ion + ethanol + water	Marcus. 2007[62]
thiocyanate ion + ethylene glycol + water	Marcus, 2015[20]
thiocyanate ion + formamide + water	Marcus, 2015[20]
thiocyanate ion + methanol + water	Marcus. 2007[62]
thiocyanate ion + n,n-dimethylacetamide + water	Marcus, 2015[20]
thiocyanate ion + n,n-dimethylformamide + water	Marcus, 2015[20]
thiocyanate ion + pyridine + water	Marcus, 2015[20]
thiosulfate ion + ethanol + water	Marcus, 2007[62]

8.4.6 Dielectric decrement dataset at 198.15 K

Overview of the aqueous dielectric constant data used in this work.

Salt	Reference
CsBr	Barthel, 1977 [331]
CsCl	Wei et al. 1992 [332]
CsF	Loginova et al. 2006 [333]
CsI	Pottel and Lossen 1967 [334], Barthel, 1977 [331]
$CsNO_3$	Barthel et al. 1970 [335]
KBr	Barthel, 1977 [331]
KCl	Barthel et al. 1970 [335], Haggis et al. 1952 [336], Harris and O'Konski, 1957[47], Hasted et al. 1948 [46]
KF	Buchner et al. 1994 [337], Haggis et al. 1952 [336], Hasted et al. 1948 [46], Harris and O'Konski, 1957[47], Loginova et al. 2006 [333]
KI	Barthel, 1977 [331], Hasted et al. 1948 [46], Harris and O'Konski, 1957 [47]
KNO_3	Barthel et al. 1970 [335]
LiBr	Barthel, 1977 [331], Harris and O'Konski, 1957 [47]
LiCl	Harris and O'Konski, 1957[47], Hasted et al. 1948 [46], Haggis et al. 1952 [336], Wei and Sridhar, 1990 [29]
$LiClO_4$	Barthel, 1977 [331]
LiI	Pottel and Lossen 1967 [334]
$LiNO_3$	Barthel et al. 1970 [335]
$NaSO_4$	Barthel et al. 1992 [338], Hasted et al. 1948 [46]
NaBr	Haggis et al. 1952 [336], Harris and O'Konski, 1957 [47]
NaCl	Haggis et al. 1952 [336], Hasted and Roderick, 1958 [339], Harris and O'Konski, 1957[47], Barthel, 1977 [331]

$NaClO_4$	Harris and O'Konski, 1957[47], Barthel, 1977 [331]
NaF	Buchner et al. 1994 [337], Haggis et al. 1952 [336], Hasted et al. 1948 [46]
NaI	Haggis et al. 1952 [336], Hasted et al. 1948 [46], Harris and O'Konski, 1957 [47]
$NaNO_3$	Barthel et al. 1970 [335], Harris and O'Konski, 1957 [47]
RbCl	Haggis et al. 1952 [336], Wei et al. 1992 [332]
$RbNO_3$	Barthel et al. 1970 [335]

Overview of the non-aqueous dielectric constant data used in this work.

System	Reference
$LiNO_3$ – acetone	Behret, 1975 [340]
LiBr – acetonitrile	Barthel et al. 1995 [341]
$NaClO_4$ – acetonitrile	Barthel et al. 1995 [341]
NaI – acetonitrile	Barthel et al. 1995 [341]
$LiClO_4$ – dimethyl carbonate	Delsignore et al. 1985 [342]
LiCl – dimethyl sulfoxide	Winsor and Cole 1982 [343]
$LiNO_3$ – dimethyl sulfoxide	Behret, 1975 [340]
NaI – dimethyl sulfoxide	Winsor and Cole 1982 [343]
$NaNO_3$ – dimethyl sulfoxide	Behret, 1975 [340]
KNO_3 – formamide	Behret, 1975 [340]
LiCl – formamide	Behret, 1975 [340]
$LiNO_3$ – formamide	Behret, 1975 [340]
$NaNO_3$ – formamide	Behret, 1975 [340]
$NaClO_4$ – formamide	Barthel et al. 1995 [344]
NaI – formamide	Winsor and Cole 1982 [343]
KI – methanol	Kaatze et al. 1980 [345], Pottel 1989 [346]
LiCl – methanol	Kaatze et al. 1980 [345], Pottel 1989 [346], Behret, 1975 [340], Barthel et al. 1971 [347]
$LiClO_4$ – methanol	Badiali et al. 1967 [348]
LiI – methanol	Pottel 1989 [346]
$LiNO_3$ – methanol	Behret, 1975 [340]
NaBr – methanol	Maribo-Mogensen[349]
NaCl – methanol	Maribo-Mogensen[349]
$NaClO_4$ – methanol	Badiali et al. 1967 [348]
NaI – methanol	Kaatze et al. 1980 [345]
$LiClO_4$ – methyl acetate	Salomon et al. 1989 [39]
$LiNO_3$ – n-methyl formamide	Behret, 1975 [340]
$NaClO_4$ – n-methyl formamide	Barthel et al. 1995 [344]
NaI – n-methyl formamide	Winsor and Cole 1982 [343]

9 Bibliography

1. Kontogeorgis GM, Maribo-Mogensen B, Thomsen K. The Debye-Hückel theory and its importance in modeling electrolyte solutions. *Fluid Phase Equilibria*. Published online January 2018. doi:10.1016/j.fluid.2018.01.004

2. Robinson RA, Stokes RH. *Electrolyte Solutions*. 2nd rev. ed. Dover Publications; 2002.

3. Prausnitz JM. *Molecular Thermodynamics of Fluid-Phase Equilibria*. 3rd ed. Prentice Hall PTR; 1999.

4. Mohs A, Gmehling J. A revised LIQUAC and LIFAC model (LIQUAC*/LIFAC*) for the prediction of properties of electrolyte containing solutions. *Fluid Phase Equilibria*. 2013;337:311-322. doi:10.1016/j.fluid.2012.09.023

5. Ganbavale G, Zuend A, Marcolli C, Peter T. Improved AIOMFAC model parameterisation of the temperature dependence of activity coefficients for aqueous organic mixtures. *Atmospheric Chem Phys*. 2015;15(1):447-493. doi:10.5194/acp-15-447-2015

6. Klamt A. Conductor-like screening model for real solvents: a new approach to the quantitative calculation of solvation phenomena. *J Phys Chem*. 1995;99(7):2224–2235.

7. Klamt A, Jonas V, Bürger T, Lohrenz JC. Refinement and parametrization of COSMO-RS. *J Phys Chem A*. 1998;102(26):5074–5085.

8. Diedenhofen M, Klamt A. COSMO-RS as a tool for property prediction of IL mixtures—A review. *Fluid Phase Equilibria*. 2010;294(1-2):31-38. doi:10.1016/j.fluid.2010.02.002

9. González de Castilla A, Bittner JP, Müller S, Jakobtorweihen S, Smirnova I. Thermodynamic and Transport Properties Modeling of Deep Eutectic Solvents: A Review on gE-Models, Equations of State, and Molecular Dynamics. *J Chem Eng Data*. Published online September 26, 2019. doi:10/ggcgvq

10. Ingram T, Gerlach T, Mehling T, Smirnova I. Extension of COSMO-RS for monoatomic electrolytes: Modeling of liquid–liquid equilibria in presence of salts. *Fluid Phase Equilibria*. 2011;314:29-37. doi:10.1016/j.fluid.2011.09.021

11. Toure O, Audonnet F, Lebert A, Dussap C-G. COSMO-RS-PDHS: A new predictive model for aqueous electrolytes solutions. *Chem Eng Res Des*. 2014;92(12):2873-2883. doi:10.1016/j.cherd.2014.06.020

12. Hsieh M-T, Lin S-T. A predictive model for the excess gibbs free energy of fully dissociated electrolyte solutions. *AIChE J*. 2011;57(4):1061-1074. doi:10/c9mjjd

13. S. Wang, Y. Song, C. C. Chen. Extension of COSMO-SAC solvation model for electrolytes. Published online February 25, 2014. http://www.google.com/patents/US8660831

14. Gerlach T, Müller S, Smirnova I. Development of a COSMO-RS based model for the calculation of phase equilibria in electrolyte systems. *AIChE J*. 2018;64(1):272-285. doi:10.1002/aic.15875

15. Müller S, González de Castilla A, Taeschler C, Klein A, Smirnova I. Evaluation and refinement of the novel predictive electrolyte model COSMO-RS-ES based on solid-liquid equilibria of salts and Gibbs free energies of transfer of ions. *Fluid Phase Equilibria*. 2018;483:165-174. doi:10/gfgw8n

16. Müller S, González de Castilla A, Taeschler C, Klein A, Smirnova I. Calculation of thermodynamic equilibria with the predictive electrolyte model COSMO-RS-ES: Improvements for low permittivity systems. *Fluid Phase Equilibria*. 2020;506:112368. doi:10/gf98vf

17. Kröger LC, Mueller S, Smirnova I, Leonhard K. Prediction of Solvation Free Energies of Ionic Solutes in Neutral Solvents. *J Phys Chem A*. Published online April 27, 2020:acs.jpca.0c01606. doi:10.1021/acs.jpca.0c01606

18. Marcus Y. Electrostriction, Ion Solvation, and Solvent Release on Ion Pairing. *J Phys Chem B*. 2005;109(39):18541-18549. doi:10.1021/jp051505k

19. Marcus Y. Effect of Ions on the Structure of Water: Structure Making and Breaking. *Chem Rev*. 2009;109(3):1346-1370. doi:10.1021/cr8003828

20. Marcus Y. *Ions in Solution and Their Solvation*. John Wiley & Sons; 2015.

21. Pauling L. THE SIZES OF IONS AND THE STRUCTURE OF IONIC CRYSTALS. *J Am Chem Soc*. 1927;49(3):765-790. doi:10.1021/ja01402a019

22. Shannon RD, Prewitt CT. Effective ionic radii in oxides and fluorides. *Acta Crystallogr B*. 1969;25(5):925-946. doi:10.1107/S0567740869003220

23. Marcus Y. Ionic radii in aqueous solutions. *Chem Rev*. 1988;88(8):1475–1498.

24. Schmid R, Miah AM, Sapunov VN. A new table of the thermodynamic quantities of ionic hydration: values and some applications (enthalpy–entropy compensation and Born radii). *Phys Chem Chem Phys*. 2000;2(1):97-102. doi:10.1039/a907160a

25. Ahrens LH. The use of ionization potentials Part 1. Ionic radii of the elements. *Geochim Cosmochim Acta*. 1952;2(3):155-169. doi:10.1016/0016-7037(52)90004-5

26. Han S. Dynamic features of water molecules in superconcentrated aqueous electrolytes. *Sci Rep*. 2018;8(1):1-10. doi:10/gdr4rr

27. Marcus Y, Hefter G. Ion Pairing. *Chem Rev*. 2006;106(11):4585-4621. doi:10.1021/cr040087x

28. Fuoss RM, Kraus CA. Properties of Electrolytic Solutions. III. The Dissociation Constant. *J Am Chem Soc*. 1933;55(3):1019-1028. doi:10/bgqgrf

29. Wei Y, Sridhar S. Dielectric spectroscopy up to 20 GHz of LiCl/H2O solutions. *J Chem Phys*. 1990;92(2):923-928. doi:10/fntxv9

30. Baer MD, Fulton JL, Balasubramanian M, Schenter GK, Mundy CJ. Persistent Ion Pairing in Aqueous Hydrochloric Acid. *J Phys Chem B*. 2014;118(26):7211-7220. doi:10/f59kzx

31. Ball P. Water as an Active Constituent in Cell Biology. *Chem Rev*. 2008;108(1):74-108. doi:10.1021/cr068037a

32. Mazzini V, Liu G, Craig VSJ. Probing the Hofmeister series beyond water: Specific-ion effects in non-aqueous solvents. *J Chem Phys*. 2018;148(22):222805. doi:10/gdq2bj

33. Mazzini V, Craig VSJ. Specific-ion effects in non-aqueous systems. *Curr Opin Colloid Interface Sci*. 2016;23:82-93. doi:10/f84xv8

34. Mazzini V. Specific ion effects in non-aqueous solutions. Published online 2017. Accessed March 27, 2019. https://doi.org/10.25911/5d67b788c55de

35. Marcus Y. Electrostriction in Electrolyte Solutions. *Chem Rev*. 2011;111(4):2761-2783. doi:10/bbj9c6

36. Liszi J, Felinger A, Kristóf EH. Static relative permittivity of electrolyte solutions. *Electrochimica Acta*. 1988;33(9):1191-1194. doi:10/bjvczj

37. Franks F. *Water: A Comprehensive Treatise. Volume 3, Aqueous Solutions of Simple Electrolytes*. Plenum; 1973.

38. De Ninno A, Nikollari E, Missori M, Frezza F. Dielectric permittivity of aqueous solutions of electrolytes probed by THz time-domain and FTIR spectroscopy. *ArXiv191008159 Cond-Mat Physicsphysics*. Published online October 14, 2019. Accessed October 25, 2019. http://arxiv.org/abs/1910.08159

39. Salomon M, Uchiyama M, Xu M, Petrucci S. Structure, dynamics, and molecular association of lithium hexafluoroarsenate and lithium perchlorate in methyl acetate at 25.degree.C. *J Phys Chem*. 1989;93(10):4374-4382. doi:10.1021/j100347a092

40. Buchner R, Barthel J. Dielectric relaxation in solutions. *Annu Rep Sect C Phys Chem*. Unassigned/0;97(1):349-382. doi:10/cfm8q5

41. Buchner R, Hefter GT, May PM. Dielectric Relaxation of Aqueous NaCl Solutions. *J Phys Chem A*. 1999;103(1):1-9. doi:10.1021/jp982977k

42. Kaatze U. Bound water: Evidence from and implications for the dielectric properties of aqueous solutions. *J Mol Liq*. 2011;162(3):105-112. doi:10/dkfcd3

43. Hubbard J, Onsager L. Dielectric dispersion and dielectric friction in electrolyte solutions. I. *J Chem Phys*. 1977;67(11):4850-4857. doi:10.1063/1.434664

44. Hubbard JB. Dielectric dispersion and dielectric friction in electrolyte solutions. II. *J Chem Phys*. 1978;68(4):1649-1664. doi:10/fgs4m6

45. Barthel J, Krüger J, Schollmeyer E. Untersuchungen zur Dispersion der komplexen Dielektrizitätskonstante wäßriger und nichtwäßriger Elektrolytlösungen. *Z Für Phys Chem*. 1977;104(1-3):59–72. doi:10/cghg86

46. Hasted JB, Ritson DM, Collie CH. Dielectric Properties of Aqueous Ionic Solutions. Parts I and II. *J Chem Phys*. 1948;16(1):1-21. doi:10.1063/1.1746645

47. Harris FE, O'Konski CT. Dielectric Properties of Aqueous Ionic Solutions at Microwave Frequencies. *J Phys Chem*. 1957;61(3):310-319. doi:10/frszx4

48. Maribo-Mogensen B, Kontogeorgis GM, Thomsen K. Modeling of Dielectric Properties of Aqueous Salt Solutions with an Equation of State. *J Phys Chem B*. 2013;117(36):10523-10533. doi:10.1021/jp403375t

49. Hückel E. Zur Theorie konzentrierter wässeriger Lösungen starker Electrolyte. *Phys Z*. 1925;26:93-147.

50. Simonin J-P, Bernard O, Blum L. Ionic Solutions in the Binding Mean Spherical Approximation: Thermodynamic Properties of Mixtures of Associating Electrolytes. *J Phys Chem B*. 1999;103(4):699-704. doi:10/cxjd55

51. Inchekel R, de Hemptinne J-C, Fürst W. The simultaneous representation of dielectric constant, volume and activity coefficients using an electrolyte equation of state. *Fluid Phase Equilibria*. 2008;271(1):19-27. doi:10/cd69cw

52. Zuber A, Cardozo-Filho L, Cabral VF, Checoni RF, Castier M. An empirical equation for the dielectric constant in aqueous and nonaqueous electrolyte mixtures. *Fluid Phase Equilibria*. 2014;376:116-123. doi:10.1016/j.fluid.2014.05.037

53. Zuber A, Checoni RF, Castier M. Thermodynamic properties of aqueous solutions of single and multiple salts using the Q-electrolattice equation of state. *Fluid Phase Equilibria*. 2014;362:268-280. doi:10.1016/j.fluid.2013.10.021

54. Zuo Y-X, Fürst W. Prediction of vapor pressure for nonaqueous electrolyte solutions using an electrolyte equation of state. *Fluid Phase Equilibria*. 1997;138(1):87-104. doi:10/cv8sn8

55. Fürst W, Renon H. Representation of excess properties of electrolyte solutions using a new equation of state. *AIChE J*. 1993;39(2):335-343. doi:10/dpg258

56. Onsager L. Electric Moments of Molecules in Liquids. *J Am Chem Soc*. 1936;58(8):1486-1493. doi:10/fqjvx7

57. Kirkwood JG. The Dielectric Polarization of Polar Liquids. *J Chem Phys*. 1939;7(10):911-919. doi:10/fsnfc4

58. Frohlich H. *Theory of Dielectrics: Dielectric Constant and Dielectric Loss*. 2 edition. Oxford University Press; 1987.

59. Maribo-Mogensen B, Kontogeorgis GM, Thomsen K. Modeling of Dielectric Properties of Complex Fluids with an Equation of State. *J Phys Chem B*. 2013;117(12):3389-3397. doi:10.1021/jp310572q

60. Akhadov YY. *Dielectric Properties of Binary Solutions: A Handbook*. Pergamon Press; 1981.

61. McQuarrie DA, Simon JD. *Physical Chemistry a Molecular Approach*. Univ. Science Books; 2000.

62. Marcus Y. Gibbs Energies of Transfer of Anions from Water to Mixed Aqueous Organic Solvents. *Chem Rev*. 2007;107(9):3880-3897. doi:10.1021/cr068045r

63. Mie G. Zur kinetischen Theorie der einatomigen Körper. *Ann Phys*. 1903;316(8):657-697. doi:10/fpvskc

64. Atkins PW, De Paula J. *Elements of Physical Chemistry*. 5th ed. Oxford University Press; 2009.

65. Izutsu K. *Electrochemistry in Nonaqueous Solutions*. 2., rev.enlarged ed. Wiley-VCH Verlag GmbH & Co. KGaA; 2009. doi:10.1002/3527600655

66. Ahmed S, Ferrando N, Hemptinne J-C de, Simonin J-P, Bernard O, Baudouin O. Modeling of mixed-solvent electrolyte systems. *Fluid Phase Equilibria*. 2018;459:138-157. doi:10.1016/j.fluid.2017.12.002

67. Klamt A, Schüürmann G. COSMO: a new approach to dielectric screening in solvents with explicit expressions for the screening energy and its gradient. *J Chem Soc Perkin Trans 2*. 1993;(5):799–805.

68. Klamt A. The COSMO and COSMO-RS solvation models. *Wiley Interdiscip Rev Comput Mol Sci*. 2011;1(5):699-709. doi:10.1002/wcms.56

69. Tomasi J, Mennucci B, Cammi R. Quantum Mechanical Continuum Solvation Models. *Chem Rev*. 2005;105(8):2999-3094. doi:10/btqxrg

70. Klamt A. *COSMO-RS: From Quantum Chemistry to Fluid PhaseThermodynamics and Drug Design*. 1. ed. Elsevier; 2005.

71. Klamt A, Moya C, Palomar J. A Comprehensive Comparison of the IEFPCM and SS(V)PE Continuum Solvation Methods with the COSMO Approach. *J Chem Theory Comput*. 2015;11(9):4220-4225. doi:10/f7rcb5

72. Kono H, Ohtsuki Y, Abe T. Electrostatic Free Energy of Solvation of an Arbitrary Charge Distribution in the Block–Walker Inhomogeneous Dielectric. *J Phys Chem*. 1996;100(23):9935-9942. doi:10/fb4pd6

73. Tomasi J, Persico M. Molecular Interactions in Solution: An Overview of Methods Based on Continuous Distributions of the Solvent. *Chem Rev*. 1994;94(7):2027-2094. doi:10/ddnqq7

74. Cramer CJ, Truhlar DG. Continuum Solvation Models: Classical and Quantum Mechanical Implementations. In: *Reviews in Computational Chemistry*. Vol 6. John Wiley & Sons, Ltd; 1995:1-72. doi:10.1002/9780470125830.ch1

75. Bienert K, Klamt A, Krockenberger D, Nader F, Sewekow B, Wittlinger R. Zum Bioakkumulationspotential von Chlororganika. *Umweltwissenschaften Schadst-Forsch*. 1993;5(4):228-234. doi:10/bf4dxn

76. Maaßen S, Arlt W, Klamt A. Vorhersage von Gaslöslichkeiten und Verteilungskoeffizienten aufgrund von Molekülorbitalrechnungen (COSMO) unter Berücksichtigung des Lösungsmitteleinflusses. *Chem Ing Tech*. 1995;67(4):476-479. doi:10/bgckrb

77. Klamt A, Eckert F. COSMO-RS: a novel and efficient method for the a priori prediction of thermophysical data of liquids. *Fluid Phase Equilibria*. 2000;172(1):43–72. doi:10.1016/S0378-3812(00)00357-5

78. Klamt A, Eckert F. Prediction, fine tuning, and temperature extrapolation of a vapor liquid equilibrium using COSMOtherm. *Fluid Phase Equilibria*. 2007;260(2):183-189. doi:10.1016/j.fluid.2007.07.055

79. Klamt A, Krooshof GJ, Taylor R. COSMOSPACE: Alternative to conventional activity-coefficient models. *AIChE J*. 2002;48(10):2332–2349.

80. Lin S-T, Sandler SI. A Priori Phase Equilibrium Prediction from a Segment Contribution Solvation Model. *Ind Eng Chem Res*. 2002;41(5):899-913. doi:10.1021/ie001047w

81. Larsen BL, Rasmussen P, Fredenslund A. A modified UNIFAC group-contribution model for prediction of phase equilibria and heats of mixing. *Ind Eng Chem Res*. 1987;26(11):2274-2286. doi:10.1021/ie00071a018

82. Pitzer KS. Electrolyte theory-improvements since Debye and Hückel. *Acc Chem Res*. 1977;10(10):371–377.

83. Pitzer KS. Thermodynamics of electrolytes. I. Theoretical basis and general equations. *J Phys Chem*. 1973;77(2):268–277.

84. Pitzer KS. Electrolytes. From dilute solutions to fused salts. *J Am Chem Soc*. 1980;102(9):2902–2906.

85. Chen C-C, Britt HI, Boston JF, Evans LB. Local composition model for excess Gibbs energy of electrolyte systems. Part I: Single solvent, single completely dissociated electrolyte systems. *AIChE J*. 1982;28(4):588–596.

86. Chen C-C, Song Y. Generalized electrolyte-NRTL model for mixed-solvent electrolyte systems. *AIChE J*. 2004;50(8):1928-1941. doi:10.1002/aic.10151

87. Bollas GM, Chen CC, Barton PI. Refined electrolyte-NRTL model: Activity coefficient expressions for application to multi-electrolyte systems. *AIChE J*. 2008;54(6):1608-1624. doi:10.1002/aic.11485

88. Bjerrum N. UNTERSUCHUNGEN ÜBER IONENASSOZIATION. I. Der Einfluss der Ionenassoziation auf die Aktivität der Ionen bei Mittleren Assoziationsgraden. *Kgl Dan Vidensk Selsk Math-Fys Meddelelser*. 1926;VII(9).

89. Fuoss RM. Ionic Association. III. The Equilibrium between Ion Pairs and Free Ions. *J Am Chem Soc*. 1958;80(19):5059-5061. doi:10.1021/ja01552a016

90. Marcus Y. Private Communication. Published online November 21, 2017.

91. Simon H-G, Kistenmacher H, Prausnitz JM, Vortmeyer D. An equation of state for systems containing electrolytes and nonelectrolytes. *Chem Eng Process Process Intensif*. 1991;29(3):139-146. doi:10/dzk26h

92. Zuo JY, Zhang D, Fürst W. Extension of the electrolyte EOS of Fürst and Renon to mixed solvent electrolyte systems. *Fluid Phase Equilibria*. 2000;175(1):285-310. doi:10/bg5sjn

93. Zuo JY, Zhang D, Fürst W. Predicting LLE in mixed-solvent electrolyte systems by an electrolyte EOS. *AIChE J*. 2000;46(11):2318-2329. doi:10.1002/aic.690461122

94. Kiepe J, Horstmann S, Fischer K, Gmehling J. Application of the PSRK Model for Systems Containing Strong Electrolytes. *Ind Eng Chem Res*. 2004;43(20):6607-6615. doi:10/fj52w9

95. Collinet E, Gmehling J. Prediction of phase equilibria with strong electrolytes with the help of the volume translated Peng-Robinson group contribution equation of state (VTPR). *Fluid Phase Equilibria*. 2006;246(1):111-118. doi:10.1016/j.fluid.2006.05.033

96. Krotov D. Weiterentwicklung der Gruppenbeitragszustandsgleichung VTPR zur Beschreibung von Elektrolyt- und Polymersystemen. Published online 2014. Accessed December 18, 2019. http://oops.uni-oldenburg.de/1968/

97. Wu J, Prausnitz JM. Phase Equilibria for Systems Containing Hydrocarbons, Water, and Salt: An Extended Peng–Robinson Equation of State. *Ind Eng Chem Res*. 1998;37(5):1634-1643. doi:10/cz6bvh

98. Maribo-Mogensen B, Thomsen K, Kontogeorgis GM. An electrolyte CPA equation of state for mixed solvent electrolytes. *AIChE J*. 2015;61(9):2933-2950. doi:10.1002/aic.14829

99. Sun L, Liang X, von Solms N, Kontogeorgis GM. Modeling Tetra-n-butyl ammonium halides aqueous solutions with the electrolyte CPA equation of state. *Fluid Phase Equilibria*. Published online December 28, 2018. doi:10/gfsvb5

100. Schlaikjer A, Thomsen K, Kontogeorgis GM. eCPA: An ion-specific approach to parametrization. *Fluid Phase Equilibria*. Published online December 12, 2017. doi:10/gc4jh2

101. Schlaikjer A, Thomsen K, Kontogeorgis GM. Simultaneous Description of Activity Coefficients and Solubility with eCPA. *Ind Eng Chem Res*. 2017;56(4):1074-1089. doi:10.1021/acs.iecr.6b03333

102. Galindo A, Gil-Villegas A, Jackson G, Burgess AN. SAFT-VRE: Phase Behavior of Electrolyte Solutions with the Statistical Associating Fluid Theory for Potentials of Variable Range. *J Phys Chem B*. 1999;103(46):10272-10281. doi:10/ddmkv3

103. GIL-VILLEGAS A, GALINDO A, JACKSON G. A statistical associating fluid theory for electrolyte solutions (SAFT-VRE). *Mol Phys*. 2001;99(6):531-546. doi:10/cfdhp3

104. Patel BH, Paricaud P, Galindo A, Maitland GC. Prediction of the Salting-Out Effect of Strong Electrolytes on Water + Alkane Solutions. *Ind Eng Chem Res*. 2003;42(16):3809-3823. doi:10/brj8pp

105. Behzadi B, Patel BH, Galindo A, Ghotbi C. Modeling electrolyte solutions with the SAFT-VR equation using Yukawa potentials and the mean-spherical approximation. *Fluid Phase Equilibria*. 2005;236(1):241-255. doi:10/dvb84d

106. Schreckenberg JMA, Dufal S, Haslam AJ, Adjiman CS, Jackson G, Galindo A. Modelling of the thermodynamic and solvation properties of electrolyte solutions with the statistical associating fluid theory for potentials of variable range. *Mol Phys*. 2014;112(17):2339-2364. doi:10.1080/00268976.2014.910316

107. Selam MA, Economou IG, Castier M. A thermodynamic model for strong aqueous electrolytes based on the eSAFT-VR Mie equation of state. *Fluid Phase Equilibria*. 2018;464:47-63. doi:10/gc4mz7

108. Cameretti LF, Sadowski G, Mollerup JM. Modeling of Aqueous Electrolyte Solutions with Perturbed-Chain Statistical Associated Fluid Theory. *Ind Eng Chem Res*. 2005;44(9):3355-3362. doi:10.1021/ie0488142

109. Held C, Cameretti LF, Sadowski G. Modeling aqueous electrolyte solutions. *Fluid Phase Equilibria*. 2008;270(1-2):87-96. doi:10.1016/j.fluid.2008.06.010

110. Held C, Sadowski G. Modeling aqueous electrolyte solutions. Part 2. Weak electrolytes. *Fluid Phase Equilibria*. 2009;279(2):141-148. doi:10.1016/j.fluid.2009.02.015

111. Held C, Reschke T, Mohammad S, Luza A, Sadowski G. ePC-SAFT revised. *Chem Eng Res Des*. 2014;92(12):2884-2897. doi:10.1016/j.cherd.2014.05.017

112. Reschke T, Brandenbusch C, Sadowski G. Modeling aqueous two-phase systems: I. Polyethylene glycol and inorganic salts as ATPS former. *Fluid Phase Equilibria*. 2014;368:91-103. doi:10.1016/j.fluid.2014.02.016

113. Reschke T, Brandenbusch C, Sadowski G. Modeling aqueous two-phase systems: II. Inorganic salts and polyether homo- and copolymers as ATPS former. *Fluid Phase Equilibria*. 2014;375:306-315. doi:10/f6bkr3

114. Reschke T, Brandenbusch C, Sadowski G. Modeling aqueous two-phase systems: III. Polymers and organic salts as ATPS former. *Fluid Phase Equilibria*. 2015;387:178-189. doi:10/f69fht

115. Rozmus J, de Hemptinne J-C, Galindo A, Dufal S, Mougin P. Modeling of Strong Electrolytes with ePPC-SAFT up to High Temperatures. *Ind Eng Chem Res*. 2013;52(29):9979-9994. doi:10.1021/ie303527j

116. Ji X, Adidharma H. Ion-Based SAFT2 to Represent Aqueous Single- and Multiple-Salt Solutions at 298.15 K. *Ind Eng Chem Res*. 2006;45(22):7719-7728. doi:10.1021/ie060649y

117. Ji X, Adidharma H. Ion-based SAFT2 to represent aqueous multiple-salt solutions at ambient and elevated temperatures and pressures. *Chem Eng Sci*. 2008;63(1):131-140. doi:10/fdvhqq

118. Jiang H, Adidharma H. Prediction of hydrate dissociation conditions for alkanes in the presence of alcohol and electrolyte solutions using ion-based statistical associating fluid theory. *Chem Eng Sci*. 2012;82:14-21. doi:10/ggfrzb

119. Jiang H, Adidharma H. Modeling of Hydrate Dissociation Conditions for Alkanes in the Presence of Single and Mixed Electrolyte Solutions Using Ion-Based Statistical Associating Fluid Theory. *Ind Eng Chem Res*. 2012;51(16):5818-5825. doi:10/ggfrx9

120. Valavi M, Dehghani MR, Shahriari R. Application of modified PHSC model in prediction of phase behavior of single and mixed electrolyte solutions. *Fluid Phase Equilibria*. 2013;344:92-100. doi:10/f4tx35

121. Zuber A, Checoni RF, Mathew R, Santos JPL, Tavares FW, Castier M. Thermodynamic Properties of 1:1 Salt Aqueous Solutions with the Electrolattice Equation of State. *Oil Gas Sci Technol – Rev D'IFP Energ Nouv*. 2013;68(2):255-270. doi:10.2516/ogst/2012088

122. Lazarou G. Development of the SAFT-γ Mie equation of state for predicting the thermodynamic behaviour of strong and weak electrolyte solutions. Published online September 2017. Accessed December 17, 2019. https://doi.org/10.25560/60588

123. Di Lecce S, Lazarou G, Khalit SH, et al. Modelling and prediction of the thermophysical properties of aqueous mixtures of choline geranate and geranic acid (CAGE) using SAFT-γ Mie. *RSC Adv*. 2019;9(65):38017-38031. doi:10.1039/C9RA07057E

124. Ahmed S. Thermodynamic modeling of mixed-solvent electrolytes for process simulators. Published online March 1, 2018. Accessed December 17, 2019. https://tel.archives-ouvertes.fr/tel-02049398

125. Cruz J-L, Renon H. A new thermodynamic representation of binary electrolyte solutions nonideality in the whole range of concentrations. *AIChE J*. 1978;24(5):817-830. doi:10/ct2k3n

126. Chen C-C, Evans LB. A local composition model for the excess Gibbs energy of aqueous electrolyte systems. *AIChE J*. 1986;32(3):444–454.

127. Mock B, Evans LB, Chen C-C. Thermodynamic representation of phase equilibria of mixed-solvent electrolyte systems. *AIChE J*. 1986;32(10):1655-1664. doi:10/ffk3bx

128. Austgen DM, Rochelle GT, Peng X, Chen CC. Model of vapor-liquid equilibria for aqueous acid gas-alkanolamine systems using the electrolyte-NRTL equation. *Ind Eng Chem Res*. 1989;28(7):1060-1073. doi:10/cwt46w

129. Chen C-C, Mathias PM, Orbey H. Use of hydration and dissociation chemistries with the electrolyte–NRTL model. *AIChE J*. 1999;45(7):1576–1586.

130. Chen C-C, Bokis CP, Mathias P. Segment-based excess Gibbs energy model for aqueous organic electrolytes. *AIChE J*. 2001;47(11):2593-2602. doi:10.1002/aic.690471122

131. Chen C-C, Song Y. Extension of Nonrandom Two-Liquid Segment Activity Coefficient Model for Electrolytes. *Ind Eng Chem Res*. 2005;44(23):8909-8921. doi:10.1021/ie0503592

132. Song Y, Chen C-C. Symmetric Electrolyte Nonrandom Two-Liquid Activity Coefficient Model. *Ind Eng Chem Res*. 2009;48(16):7788-7797. doi:10.1021/ie9004578

133. Song Y, Chen C-C. Symmetric Nonrandom Two-Liquid Segment Activity Coefficient Model for Electrolytes. *Ind Eng Chem Res*. 2009;48(11):5522-5529. doi:10.1021/ie900006g

134. Hossain N, Bhattacharia SK, Chen C-C. Temperature dependence of interaction parameters in electrolyte NRTL model. *AIChE J*. 2016;62(4):1244-1253. doi:10.1002/aic.15080

135. Hossain N, Ravichandran A, Khare R, Chen C-C. Revisiting electrolyte thermodynamic models: Insights from molecular simulations. *AIChE J*. 2018;64(10):3728-3734. doi:10.1002/aic.16327

136. Tanveer S, Chen C-C. A comprehensive thermodynamic model for high salinity produced waters. *AIChE J*. 2020;n/a(n/a):e16818. doi:10.1002/aic.16818

137. Liu Y, Harvey AH, Prausnitz JM. THERMODYNAMICS OF CONCENTRATED ELECTROLYTE SOLUTIONS. *Chem Eng Commun*. 1989;77(1):43-66. doi:10.1080/00986448908940172

138. Liu Y, Wimby M, Grén U. An activity-coefficient model for electrolyte systems. *Comput Chem Eng*. 1989;13(4):405-410. doi:10/cmwc84

139. Kuramochi H, Osako M, Kida A, et al. Determination of Ion-Specific NRTL Parameters for Predicting Phase Equilibria in Aqueous Multielectrolyte Solutions. *Ind Eng Chem Res*. 2005;44(9):3289-3297. doi:10/b9pmwk

140. Christensen C, Sander B, Fredenslund Aa, Rasmussen P. Towards the extensionof UNIFAC to mixtures with electrolytes. *Fluid Phase Equilibria*. 1983;13:297-309. doi:10/bz6853

141. Sander B, Fredenslund A, Rasmussen P. Calculation of vapour-liquid equilibria in mixed solvent/salt systems using an extended UNIQUAC equation. *Chem Eng Sci*. 1986;41(5):1171-1183. doi:10.1016/0009-2509(86)87090-7

142. Nicolaisen H, Rasmussen P, Sørensen JM. Correlation and prediction of mineral solubilities in the reciprocal salt system (Na+, K+)(Cl−, SO2−4)−H2O at 0–100°C. *Chem Eng Sci*. 1993;48(18):3149-3158. doi:10/cmq5p7

143. Thomsen K, Rasmussen P, Gani R. Correlation and prediction of thermal properties and phase behaviour for a class of aqueous electrolyte systems. *Chem Eng Sci*. 1996;51(14):3675-3683. doi:10/btn3z6

144. Lu X, Maurer G. Model for describing activity coefficients in mixed electrolyte aqueous solutions. *AIChE J*. 1993;39(9):1527-1538. doi:10/fggwvp

145. Lee CS, Park SB, Shim YS. A Unified and Predictive Model for Mixed-Electrolyte, Aqueous Mixed-Solvent Systems Using Parameters for Ions and Solvents. *Ind Eng Chem Res*. 1996;35(12):4772-4780. doi:10.1021/ie960294q

146. Messnaoui B, Ouiazzane S, Bouhaouss A, Bounahmidi T. A modified electrolyte-Uniquac model for computing the activity coefficient and phase diagrams of electrolytes systems. *Calphad*. 2008;32(3):566-576.

147. Thomsen K, C. Iliuta M, Rasmussen P. Extended UNIQUAC model for correlation and prediction of vapor–liquid–liquid–solid equilibria in aqueous salt systems containing non-electrolytes. Part B. Alcohol (ethanol, propanols, butanols)–water–salt systems. *Chem Eng Sci*. 2004;59(17):3631-3647. doi:10/fjrbrc

148. Thomsen K. Modeling electrolyte solutions with the extended universal quasichemical (UNIQUAC) model. *Pure Appl Chem*. 2005;77(3):531–542. doi:10/ckr6pb

149. Chiavone Filho O, Rasmussen P. Modeling of salt solubilities in mixed solvents. *Braz J Chem Eng*. 2000;17(2). doi:10.1590/S0104-66322000000200001

150. Iliuta MC, Thomsen K, Rasmussen P. Extended UNIQUAC model for correlation and prediction of vapour–liquid–solid equilibria in aqueous salt systems containing non-electrolytes. Part A. Methanol–water–salt systems. *Chem Eng Sci*. 2000;55(14):2673-2686. doi:10/c2wdsv

151. Li J, Polka H-M, Gmehling J. A gE model for single and mixed solvent electrolyte systems: 1. Model and results for strong electrolytes. *Fluid Phase Equilibria*. 1994;94:89–114.

152. Polka H-M, Li J, Gmehling J. A gE model for single and mixed solvent electrolyte systems: 2. Results and comparison with other models. *Fluid Phase Equilibria*. 1994;94:115-127. doi:10/ft4nkz

153. Rose C. Vorausberechnung des Einflusses starker Elektrolyte -Salzeffekt- auf das Phasengleichgewichtsverhalten von Lösungsmittelgemischen. Published online 2001. Accessed December 15, 2019. http://oops.uni-oldenburg.de/345/

154. Li J, Lin Y, Gmehling J. A gE Model for Single- and Mixed-Solvent Electrolyte Systems. 3. Prediction of Salt Solubilities in Aqueous Electrolyte Systems. *Ind Eng Chem Res*. 2005;44(5):1602-1609. doi:10/fpb8rk

155. Kiepe J, Noll O, Gmehling J. Modified LIQUAC and Modified LIFAC A Further Development of Electrolyte Models for the Reliable Prediction of Phase Equilibria with Strong Electrolytes. *Ind Eng Chem Res*. 2006;45(7):2361-2373. doi:10.1021/ie0510122

156. Li M-Y, Wang L-S, Jiang B, Gmehling J. Generalized LIQUAC model for the single- and mixed-solvent strong electrolyte systems. *AIChE J*. 2011;57(9):2535-2546. doi:10.1002/aic.12445

157. Mohs A. Weiterentwicklung eines auf der LIQUAC-und LIFAC-Methode basierenden Modells zur Berechnung von Salzlöslichkeiten in Lösungsmittelgemischen. Published online 2011. Accessed April 11, 2015. http://oops.uni-oldenburg.de/1144/

158. Mohs A, Decker S, Gmehling J. The solid–liquid equilibrium of the binary system H2O–DMSO and the influence of a salt (NaCl, KCl) on the thermodynamic behavior: Correlations using a revised LIQUAC model. *Fluid Phase Equilibria*. 2011;304(1–2):12-20. doi:10.1016/j.fluid.2011.01.026

159. Wang P, Anderko A, Young RD. A speciation-based model for mixed-solvent electrolyte systems. *Fluid Phase Equilibria*. 2002;203(1):141-176. doi:10/bmrbqw

160. Wang P, Anderko A. Computation of dielectric constants of solvent mixtures and electrolyte solutions. *Fluid Phase Equilibria*. 2001;186(1-2):103-122. doi:10.1016/S0378-3812(01)00507-6

161. Wang P, Springer RD, Anderko A, Young RD. Modeling phase equilibria and speciation in mixed-solvent electrolyte systems. *Fluid Phase Equilibria*. 2004;222-223:11-17. doi:10.1016/j.fluid.2004.06.008

162. Wang P, Anderko A, Springer RD, Young RD. Modeling phase equilibria and speciation in mixed-solvent electrolyte systems: II. Liquid–liquid equilibria and properties of associating electrolyte solutions. *J Mol Liq*. 2006;125(1):37-44. doi:10/d7qmtn

163. Kosinski JJ, Wang P, Springer RD, Anderko A. Modeling acid–base equilibria and phase behavior in mixed-solvent electrolyte systems. *Fluid Phase Equilibria*. 2007;256(1):34-41. doi:10/bzt7b5

164. Kikic I, Fermeglia M, Rasmussen P. Unifac prediction of vapor—liquid equilibria in mixed solvent—salt systems. *Chem Eng Sci*. 1991;46(11):2775-2780. doi:10.1016/0009-2509(91)85146-O

165. Achard C, Dussap CG, Gros JB. Representation of vapour-liquid equilibria in water-alcohol-electrolyte mixtures with a modified UNIFAC group-contribution method. *Fluid Phase Equilibria*. 1994;98:71-89. doi:10/cthg6w

166. Aznar M, Telles AS. Prediction of electrolyte vapor-liquid equilibrium by UNIFAC-Dortmund. *Braz J Chem Eng*. 2001;18(2):127-137. doi:10/bs2j8z

167. Kim SH, Anantpinijwatna A, Kang JW, Gani R. Analysis and modeling of alkali halide aqueous solutions. *Fluid Phase Equilibria*. 2016;412:177-198. doi:10/f8bdzw

168. Erdakos GB, Asher WE, Seinfeld JH, Pankow JF. Prediction of activity coefficients in liquid aerosol particles containing organic compounds, dissolved inorganic salts, and water—Part 1: Organic compounds and water by consideration of short- and long-range effects using X-UNIFAC.1. *Atmos Environ*. 2006;40(33):6410-6421. doi:10.1016/j.atmosenv.2006.04.030

169. Chang EI, Pankow JF. Prediction of activity coefficients in liquid aerosol particles containing organic compounds, dissolved inorganic salts, and water—Part 2: Consideration of phase separation effects by an X-UNIFAC model. *Atmos Environ*. 2006;40(33):6422-6436. doi:10.1016/j.atmosenv.2006.04.031

170. Erdakos GB, Chang EI, Pankow JF, Seinfeld JH. Prediction of activity coefficients in liquid aerosol particles containing organic compounds, dissolved inorganic salts, and water—Part 3: Organic compounds, water, and ionic constituents by consideration of short-, mid-, and long-range effects using X-UNIFAC.3. *Atmos Environ*. 2006;40(33):6437-6452. doi:10.1016/j.atmosenv.2006.04.001

171. Bakhshi H, Mobalegholeslam P. Phase equilibria calculations of electrolyte solutions containing water- polymer- salt using a new thermodynamic model, applicable in aqueous two phase systems. *Fluid Phase Equilibria*. 2017;434:222-232. doi:10.1016/j.fluid.2016.11.033

172. Yan W, Topphoff M, Rose C, Gmehling J. Prediction of vapor–liquid equilibria in mixed-solvent electrolyte systems using the group contribution concept. *Fluid Phase Equilibria*. 1999;162(1-2):97-113. doi:10/bjvs6d

173. Zuend A. Modelling the thermodynamics of mixed organic-inorganic aerosols to predict water activities and phase separations. Published online 2007. doi:10.3929/ethz-a-005582922

174. Zuend A, Marcolli C, Luo BP, Peter T. A thermodynamic model of mixed organic-inorganic aerosols to predict activity coefficients. *Atmospheric Chem Phys*. 2008;8(16):4559–4593.

175. Zuend A, Marcolli C, Booth AM, et al. New and extended parameterization of the thermodynamic model AIOMFAC: calculation of activity coefficients for organic-inorganic mixtures containing carboxyl, hydroxyl, carbonyl, ether, ester, alkenyl, alkyl, and aromatic functional groups. *Atmospheric Chem Phys*. 2011;11(17):9155-9206. doi:10.5194/acp-11-9155-2011

176. Ganbavale G. Temperature dependence of activity coefficients in organic aerosols. Published online 2014. doi:10.3929/ethz-a-010109026

177. Gerlach T, Ingram T, Sieder G, Smirnova I. Modeling the solubility of CO2 in aqueous methyl diethanolamine solutions with an electrolyte model based on COSMO-RS. *Fluid Phase Equilibria*. 2018;461:39-50. doi:10/gcz7k5

178. Toure O, Lebert A, Dussap C-G. Extension of the COSMO-RS-PDHS model to the prediction of activity coefficients in concentrated {water-electrolyte} and {water-polyol} solutions. *Fluid Phase Equilibria*. 2016;424:90-104. doi:10.1016/j.fluid.2015.11.005

179. Eckfeldt EL, Lucasse WW. The Liquid–Liquid Phase Equilibria of the System Cyclohexane–Methyl Alcohol in the Presence of Various Salts as Third Components. *J Phys Chem*. 1943;47(2):164-183. doi:10/cvwgg2

180. Andrade EF, Igarashi-Mafra L, Mafra MR, Corazza ML. (Liquid+liquid) equilibrium for the system {ethyl stearate(1)+ethanol(2)+glycerol(3)}. *J Chem Thermodyn*. 2012;47:213-218. doi:10/d662wn

181. Dong H, Yang X, Zhang J. Liquid–Liquid Equilibria for Benzene + Cyclohexane + N,N-Dimethylformamide + Potassium Thiocyanate. *J Chem Eng Data*. 2010;55(9):3972-3975. doi:10/ftrw4s

182. Dong H, Yang X, Yue G, Cao W, Zhang J. Liquid–Liquid Equilibria for Benzene + Cyclohexane + N,N-Dimethylformamide + Ammonium Thiocyanate. *J Chem Eng Data*. 2011;56(5):2664-2668. doi:10/d9rpw7

183. Dong H, Yang X, Yue G, Zhang W, Zhang J. (Liquid+liquid) equilibria for benzene+cyclohexane+N,N-dimethylformamide+sodium thiocyanate. *J Chem Thermodyn*. 2013;63:169-172. doi:10/f43czb

184. Song S, Lin C, You N. Phase equilibria Study of the (benzene+ cyclohexane+N,N-dimethylformamide+ potassium thiocyanate) quaternary systems. *Fluid Phase Equilibria*. 2014;376:154-158. doi:10/f6djqs

185. Eckert F, Klamt A. Fast solvent screening via quantum chemistry: COSMO-RS approach. *AIChE J*. 2002;48(2):369–385.

186. Gerlach T. Electrolyte systems in separation processes: development of a COSMO-RS based model and experimental investigation. Published online 2019.

187. Klamt A. Prediction of the mutual solubilities of hydrocarbons and water with COSMO-RS. *Fluid Phase Equilibria*. 2003;206(1-2):223-235. doi:10.1016/S0378-3812(02)00322-9

188. He J, Zhong C. A QSPR study of infinite dilution activity coefficients of organic compounds in aqueous solutions. *Fluid Phase Equilibria*. 2003;205(2):303-316. doi:10.1016/S0378-3812(02)00296-0

189. Marenich AV, Olson RM, Kelly CP, Cramer CJ, Truhlar DG. Self-Consistent Reaction Field Model for Aqueous and Nonaqueous Solutions Based on Accurate Polarized Partial Charges. *J Chem Theory Comput*. 2007;3(6):2011-2033. doi:10/dxjt9d

190. Pinho SP, Macedo EA. Solubility of NaCl, NaBr, and KCl in Water, Methanol, Ethanol, and Their Mixed Solvents. *J Chem Eng Data*. 2005;50(1):29-32. doi:10.1021/je049922y

191. Pinho SP, Macedo EA. Experimental measurement and modelling of KBr solubility in water, methanol, ethanol, and its binary mixed solvents at different temperatures. *J Chem Thermodyn*. 2002;34(3):337-360. doi:10.1006/jcht.2001.0856

192. Pinho SP, Macedo EA. Proceedings of the Seventh International Conference on Fluid Properties and Phase Equilibria for Chemical Process DesignRepresentation of salt solubility in mixed solvents: A comparison of thermodynamic models. *Fluid Phase Equilibria*. 1996;116(1):209-216. doi:10.1016/0378-3812(95)02889-7

193. Chiavone-Filho O, Rasmussen P. Solubilities of salts in mixed solvents. *J Chem Eng Data*. 1993;38(3):367–369.

194. Li S-N, Hu M-C, Jin L-H, Zhang X-L, Jiang Y-C. Solubility of Rubidium Nitrate in CH3OH or C2H5OH Aqueous Solutions at Different Temperatures. *Chin J Chem*. 2005;23(10):1348–1354.

195. HU M, ZHANG X, LI S, ZHAI Q, JIANG Y, LIU Z. Solubility and refractive index for the ternary system propanol-rubidium nitrate-water at 25,35, and 45°C
. *Russ J Inorg Chem*. 2005;50(9):1434-1440.

196. Taboada ME, Véliz DM, Galleguillos HR, Graber TA. Solubilities, Densities, Viscosities, Electrical Conductivities, and Refractive Indices of Saturated Solutions of Potassium Sulfate in Water + 1-Propanol at 298.15, 308.15, and 318.15 K. *J Chem Eng Data*. 2002;47(5):1193-1196. doi:10/c573zp

197. Hernández-Luis F, Rodríguez-Raposo R, Galleguillos HR, Morales JW. Solubility of Sodium Halides in Aqueous Mixtures with ε-Increasing Cosolvents: Formamide, *N* -Methylformamide, and *N* -Methylacetamide at 298.15 K. *Ind Eng Chem Res*. 2016;55(3):812-819. doi:10.1021/acs.iecr.5b04614

198. Skrzecz A, Lisov NI, Sazonov NV. IUPAC-NIST Solubility Data Series. 83. Acetonitrile: Ternary and Quaternary Systems. *J Phys Chem Ref Data*. 2007;36(3):733-1131. doi:10/b3k9qb

199. Eysseltová J, Málková Z. Solubility in the Systems MCl (M = Na, K)–1,4-Dioxane–Water at 25 ^C. *J Solut Chem*. 2006;35(9):1329-1334. doi:10/fwd4wq

200. Marcus Y. Thermodynamic functions of transfer of single ions from water to nonaqueous and mixed solvents: Part 4-The selection of extra thermodynamic assumptions. *Pure Appl Chem*. 1986;58(12):1721-1736.

201. Kalidas C, Hefter G, Marcus Y. Gibbs Energies of Transfer of Cations from Water to Mixed Aqueous Organic Solvents. *Chem Rev*. 2000;100(3):819-852. doi:10.1021/cr980144k

202. Li Z, Tang Y, Liu Y, Li Y. Salting effect in partially miscible systems of n-butanol/water and butanone/water 1. Determination and correlation of liquid-liquid equilibrium data. *Fluid Phase Equilibria*. 1995;103(1):143-153.

203. Shilov IYu, Lyashchenko AK. The Role of Concentration Dependent Static Permittivity of Electrolyte Solutions in the Debye–Hückel Theory. *J Phys Chem B*. 2015;119(31):10087-10095. doi:10.1021/acs.jpcb.5b04555

204. Shilov IYu, Lyashchenko AK. Modeling activity coefficients in alkali iodide aqueous solutions using the extended Debye-Hückel theory. *J Mol Liq*. 2017;240:172-178. doi:10.1016/j.molliq.2017.05.010

205. Shilov IYu, Lyashchenko AK. Activity Coefficient Modeling for Aqueous Aluminum Salt Solutions in Terms of the Generalized Debye–Hückel Theory. *Russ J Inorg Chem*. 2019;64(9):1186-1189. doi:10/gf9wkq

206. Chemical Rubber Company, Lide DR, eds. *CRC Handbook of Chemistry and Physics: A Ready-Reference Book of Chemical and Physical Data*. 86. ed. CRC Press; 2005.

207. Marcus Y. Thermodynamics of solvation of ions. Part 5.—Gibbs free energy of hydration at 298.15 K. *J Chem Soc Faraday Trans*. 1991;87(18):2995–2999. doi:10/cjz9gb

208. Scaife BKP. *Principles of Dielectrics*. Clarendon Press; 1989.

209. Bosque R, Sales J. Polarizabilities of solvents from the chemical composition. *J Chem Inf Comput Sci*. 2002;42(5):1154–1163.

210. Yaws CL. *Thermophysical Properties of Chemicals and Hydrocarbons*. Second edition. Elsevier; 2014.

211. Kontogeorgis GM. Association theories for complex thermodynamics. *Chem Eng Res Des*. 2013;91(10):1840-1858. doi:10.1016/j.cherd.2013.07.006

212. Kaminski S. Quantum-mechanics-based prediction of SAFT parameters for non-associating and associating molecules containing carbon, hydrogen, oxygen, and nitrogen. Published online 2019. doi:37997

213. Brandani V, del Re G, di Giacomo G. Thermodynamics of hydrothermal solutions: Calcium carbonate and calcium sulphate solubility in a four-phase system. *Chem Eng J*. 1986;32(3):145-150. doi:10/dpx33c

214. Chen J-F, Choppin GR. Activity coefficients of single electrolytes in concentrated solutions derived from a quasi-lattice model. *J Solut Chem*. 1995;24(5):465–484.

215. Pérez-Salado Kamps Á. Model for the Gibbs Excess Energy of Mixed-Solvent (Chemical-Reacting and Gas-Containing) Electrolyte Systems. *Ind Eng Chem Res*. 2005;44(1):201-225. doi:10/bv7t8w

216. Vincze J, Valiskó M, Boda D. The nonmonotonic concentration dependence of the mean activity coefficient of electrolytes is a result of a balance between solvation and ion-ion correlations. *J Chem Phys*. 2010;133(15):154507. doi:10/d362c8

217. Valiskó M, Boda D. The effect of concentration- and temperature-dependent dielectric constant on the activity coefficient of NaCl electrolyte solutions. *J Chem Phys*. 2014;140(23):234508. doi:10/gcx9b3

218. Valiskó M, Boda D. Unraveling the Behavior of the Individual Ionic Activity Coefficients on the Basis of the Balance of Ion–Ion and Ion–Water Interactions. *J Phys Chem B*. 2015;119(4):1546-1557. doi:10.1021/jp509445k

219. Valiskó M, Boda D. Activity coefficients of individual ions in LaCl3 from the II+IW theory. *Mol Phys*. 2017;115(9-12):1245-1252. doi:10.1080/00268976.2016.1276640

220. Hamer WJ, Wu Y-C. Osmotic Coefficients and Mean Activity Coefficients of Uni-univalent Electrolytes in Water at 25°C. *J Phys Chem Ref Data*. 1972;1(4):1047. doi:10.1063/1.3253108

221. Mazzini V, Craig VSJ. Volcano Plots Emerge from a Sea of Nonaqueous Solvents: The Law of Matching Water Affinities Extends to All Solvents. *ACS Cent Sci*. 2018;4(8):1056-1064. doi:10/gd5vrk

222. Gebbie MA, Valtiner M, Banquy X, Fox ET, Henderson WA, Israelachvili JN. Ionic liquids behave as dilute electrolyte solutions. *Proc Natl Acad Sci*. 2013;110(24):9674-9679. doi:10.1073/pnas.1307871110

223. Gebbie MA, Dobbs HA, Valtiner M, Israelachvili JN. Long-range electrostatic screening in ionic liquids. *Proc Natl Acad Sci*. 2015;112(24):7432-7437. doi:10.1073/pnas.1508366112

224. Kirchner B, Malberg F, Firaha DS, Hollóczki O. Ion pairing in ionic liquids. *J Phys Condens Matter*. 2015;27(46):463002. doi:10.1088/0953-8984/27/46/463002

225. Lee AA, Vella D, Perkin S, Goriely A. Are Room-Temperature Ionic Liquids Dilute Electrolytes? *J Phys Chem Lett*. 2015;6(1):159-163. doi:10.1021/jz502250z

226. Sha M, Dong H, Luo F, Tang Z, Zhu G, Wu G. Dilute or Concentrated Electrolyte Solutions? Insight from Ionic Liquid/Water Electrolytes. *J Phys Chem Lett*. 2015;6(18):3713-3720. doi:10.1021/acs.jpclett.5b01513

227. Smith AM, Lee AA, Perkin S. The Electrostatic Screening Length in Concentrated Electrolytes Increases with Concentration. *J Phys Chem Lett*. 2016;7(12):2157-2163. doi:10.1021/acs.jpclett.6b00867

228. Gebbie MA, Smith AM, Dobbs HA, et al. Long range electrostatic forces in ionic liquids. *Chem Commun*. 2017;53(7):1214-1224. doi:10.1039/C6CC08820A

229. Goodwin ZAH, Kornyshev AA. Underscreening, overscreening and double-layer capacitance. *Electrochem Commun*. 2017;82(Supplement C):129-133. doi:10.1016/j.elecom.2017.07.008

230. Rotenberg B, Bernard O, Hansen J-P. Underscreening in ionic liquids: a first principles analysis. *J Phys Condens Matter*. 2018;30(5):054005. doi:10/gdwtpn

231. Lee AA, Perez-Martinez CS, Smith AM, Perkin S. Underscreening in concentrated electrolytes. *Faraday Discuss*. 2017;199(0):239-259. doi:10.1039/C6FD00250A

232. Lee AA, Perez-Martinez CS, Smith AM, Perkin S. Scaling Analysis of the Screening Length in Concentrated Electrolytes. *Phys Rev Lett*. 2017;119(2):026002. doi:10.1103/PhysRevLett.119.026002

233. Smith AM, Maroni P, Trefalt G, Borkovec M. Unexpectedly Large Decay Lengths of Double Layer Forces in Solutions of Symmetric, Multivalent Electrolytes. *J Phys Chem B*. Published online January 29, 2019. doi:10/gft5r7

234. Mohammad S, Held C, Altuntepe E, et al. Salt influence on MIBK/water liquid–liquid equilibrium: Measuring and modeling with ePC-SAFT and COSMO-RS. *Fluid Phase Equilibria*. 2016;416:83-93. doi:10.1016/j.fluid.2015.11.018

235. Yang C, Jiang Y, Zhang L, Qian Y. Liquid−Liquid Equilibria for the Ternary System Methyl Isobutyl Ketone + Water + Hydroquinone. *J Chem Eng Data*. 2006;51(6):2107-2109. doi:10/fnp4bj

236. Morris DFC. Ionic radii and enthalpies of hydration of ions. In: Jørgensen CK, Neilands JB, Nyholm RS, Reinen D, Williams RJP, eds. *Structure and Bonding*. Structure and Bonding. Springer; 1969:157-159. doi.org/10.1007/BFb0118857

237. Collins KD. Charge density-dependent strength of hydration and biological structure. *Biophys J*. 1997;72(1):65-76. doi:10/fpkr6m

238. Willard HH, Smith GF. THE PERCHLORATES OF THE ALKALI AND ALKALINE EARTH METALS AND AMMONIUM. THEIR SOLUBILITY IN WATER AND OTHER SOLVENTS. *J Am Chem Soc*. 1923;45(2):286-297. doi:10.1021/ja01655a004

239. James DW, Mayes RE. Ion-ion-solvent interactions in solution. II. Solutions of LiClO4 in diethyl ether. *Aust J Chem*. 1982;35(9):1785-1792. doi:10/bztqxz

240. Seidell A. Solubilities of Inorganic and Metal Organic Compounds. Third edition (Seidell, A.). *J Chem Educ*. 1941;18(8):399. doi:10.1021/ed018p399.2

241. Hu M, Jin L, Jiang Y, Li S, Zhai Q. Solubility of Cesium Nitrate in Aqueous Alcohol Solutions at (25, 35, and 45) °C. *J Chem Eng Data*. 2005;50(4):1361-1364. doi:10.1021/je050072b

242. Fox JJ, Gauge AJH. XLII.—The solubility of potassium sulphate in concentrated aqueous solutions of non-electrolytes. *J Chem Soc Trans*. 1910;97(0):377-385. doi:10/cb4kb7

243. Al-Sahhaf TA, Kapetanovic E. Salt Effects of Lithium Chloride, Sodium Bromide, or Potassium Iodide on Liquid−Liquid Equilibrium in the System Water + 1-Butanol. *J Chem Eng Data*. 1997;42(1):74-77. doi:10.1021/je960234r

244. Li M, Constantinescu D, Wang L, Mohs A, Gmehling J. Solubilities of NaCl, KCl, LiCl, and LiBr in Methanol, Ethanol, Acetone, and Mixed Solvents and Correlation Using the LIQUAC Model. *Ind Eng Chem Res*. 2010;49(10):4981-4988. doi:10.1021/ie100027c

245. Gomis V, Ruiz F, Asensi JC, Cayuela P. Liquid-liquid-solid equilibria for the ternary systems water-lithium chloride-1-propanol or 2-propanol at 25 °C. *Fluid Phase Equilibria*. 1996;119(1):191-195. doi:10/dzbcfn

246. Zhan C-G, Dixon DA. Absolute Hydration Free Energy of the Proton from First-Principles Electronic Structure Calculations. *J Phys Chem A*. 2001;105(51):11534-11540. doi:10/ds84wr

247. Klamt A, Eckert F, Diedenhofen M, Beck ME. First Principles Calculations of Aqueous p K_a Values for Organic and Inorganic Acids Using COSMO−RS Reveal an Inconsistency in the Slope of the p K_a Scale. *J Phys Chem A*. 2003;107(44):9380-9386. doi:10.1021/jp034688o

248. Soares R de P. The Combinatorial Term for COSMO-Based Activity Coefficient Models. *Ind Eng Chem Res*. 2011;50(5):3060-3063. doi:10.1021/ie102087p

249. Gerber RP, Soares R de P. Prediction of Infinite-Dilution Activity Coefficients Using UNIFAC and COSMO-SAC Variants. *Ind Eng Chem Res*. 2010;49(16):7488-7496. doi:10.1021/ie901947m

250. Goldberg RN. Evaluated activity and osmotic coefficients for aqueous solutions: thirty-six uni-bivalent electrolytes. *J Phys Chem Ref Data*. 1981;10(3):671-764. doi:10.1063/1.555646

251. Justice M-C, Bury R, Justice J-C. Determination conductimétrique des coefficients d'activitè: sels alcalins à anions oxygènés dans l'eau a 25°C. *Electrochimica Acta*. 1971;16(6):687-700. doi:10.1016/0013-4686(71)85037-5

252. Lobo VMM, Quaresma JL. *Handbook of Electrolyte Solutions*. Elsevier; 1989.

253. Bonner OD. The colligative properties of certain electrolytes and non-electrolytes in methanol. *J Solut Chem*. 1987;16(4):307-314. doi:10.1007/BF00646122

254. Safarov JT. Vapor pressures of lithium bromide or lithium chloride and ethanol solutions. *Fluid Phase Equilibria*. 2006;243(1–2):38-44. doi:10.1016/j.fluid.2006.02.012

255. Zafarani-Moattar MT, Aria M. Isopiestic determination of osmotic and activity coefficients for solutions of LiCl, LiBr, and LiNO3 in 2-propanol at 25° C. *J Solut Chem*. 2001;30(4):351–363.

256. Nasirzadeh K, Papaiconomou N, Neueder R, Kunz W. Vapor pressures, osmotic and activity coefficients of electrolytes in protic solvents at different temperatures. 1. Lithium bromide in methanol. *J Solut Chem*. 2004;33(3):227–245.

257. Nasirzadeh K, Neueder R, Kunz W. Vapor Pressures, Osmotic and Activity Coefficients of Electrolytes in Protic Solvents at Different Temperatures. 3. Lithium Bromide in 2-Propanol. *J Solut Chem*. 2005;34(1):9-24. doi:10.1007/s10953-005-2024-9

258. Barthel J, Neueder R, Poepke H, Wittmann H. Osmotic Coefficients and Activity Coefficients of Nonaqueous Electrolyte Solutions. Part 4. Lithium Bromide, Tetrabutylammonium Bromide, and Tetrabutylammonium Perchlorate in Acetone. *J Solut Chem*. 1999;28(12):1277-1287. doi:10.1023/A:1021791823158

259. Kunz W, Barthel J, Klein L, Cartailler T, Turq P, Reindl B. Lithium bromide in acetonitrile: thermodynamics, theory, and simulation. *J Solut Chem*. 1991;20(9):875–891.

260. Held C, Prinz A, Wallmeyer V, Sadowski G. Measuring and modeling alcohol/salt systems. *Chem Eng Sci*. 2011;68(1):328-339. doi:10.1016/j.ces.2011.09.040

261. Safarov JT. Vapor Pressure Measurements of LiI + C2H5OH Solutions. *Z Für Phys Chem*. 2005;219(8):1133–1144. doi:10.1524/zpch.2005.219.8.1133

262. Barthel J, Neueder R, Poepke H, Wittmann H. Osmotic and activity coefficients of nonaqueous electrolyte solutions. 1. Lithium perchlorate in the protic solvents methanol, ethanol, and 2-propanol. *J Solut Chem*. 1998;27(12):1055–1066.

263. Nasirzadeh K, Neueder R. Measurement and correlation of osmotic coefficients and evaluation of vapor pressure for electrolyte solutions of LiClO4 and LiNO3 in methanol at 25 °C. *J Mol Liq*. 2004;113(1-3):13-20. doi:10.1016/j.molliq.2004.02.028

264. Barthel J, Neueder R, Poepke H, Wittmann H. Osmotic coefficients and activity coefficients of nonaqueous electrolyte solutions. Part 2. Lithium perchlorate in the aprotic solvents acetone, acetonitrile, dimethoxyethane, and dimethylcarbonate. *J Solut Chem*. 1999;28(5):489–503.

265. Verevkin S, Safarov J, Bich E, Hassel E, Heintz A. Study of vapour pressure of lithium nitrate solutions in ethanol. *J Chem Thermodyn*. 2006;38(5):611-616. doi:10.1016/j.jct.2005.07.015

266. Barthel J, Neueder R, Lauermann G. Vapor pressures of non-aqueous electrolyte solutions. Part 1. Alkali metal salts in methanol. *J Solut Chem*. 1985;14(9):621-633. doi:10.1007/BF00646055

267. Nasirzadeh K, Zafarani-Moattar MT. Isopiestic determination of osmotic coefficients and evaluation of vapor pressures for solutions of KI, NH4SCN and KSCN in methanol at 25 °C. *J Mol Liq*. 2004;111(1-3):7-13. doi:10.1016/j.molliq.2003.08.021

268. Ye S, Xans P, Lagourette B. Modification of the Pitzer model to calculate the mean activity coefficients of electrolytes in a water-alcohol mixed solvent solution. *J Solut Chem*. 1994;23(12):1301-1315. doi:10.1007/BF00974183

269. Hernández-Luis F, Rodríguez-Raposo R, Grandoso D. Activity Coefficients of NaBr in Aqueous Mixtures with High Relative Permittivity Cosolvent: Formamide + Water at 298.15 K. *J Chem Eng Data*. 2011;56(10):3940-3948. doi:10.1021/je200805d

270. Hernández-Luis F, Rodríguez-Raposo R, Ruiz-Cabrera G. Activity coefficients of NaCl in aqueous mixtures with ε-increasing co-solvent: N-methylformamide–water mixtures at 298.15K. *Fluid Phase Equilibria*. 2011;310(1-2):182-191. doi:10.1016/j.fluid.2011.08.018

271. Hernández-Luis F, Galleguillos HR, Fernández-Mérida L, González-Díaz O. Activity coefficients of NaCl in aqueous mixtures with ε-increasing co-solvent: Formamide–water mixtures at 298.15K. *Fluid Phase Equilibria*. 2009;275(2):116-126. doi:10.1016/j.fluid.2008.10.001

272. Barthel JMG, Neueder RMA, Deutsche Gesellschaft für Chemisches Apparatewesen, Chemische Technik und Biotechnologie, Universität Regensburg, eds. *Conductivities, Transference Numbers, Limiting Ionic Conductivities of Ethanol Solutions: Tables, Diagrams, Correlations and Literature Survey*. DECHEMA; 1993.

273. Barthel J, Lauermann G. Vapor pressure measurements on non-aqueous electrolyte solutions. Part 3: Solutions of sodium lodide in ethanol, 2-propanol, and acetonitrile. *J Solut Chem*. 1986;15(10):869-877. doi:10.1007/BF00646093

274. Nasirzadeh K, Salabat A. Isopiestic determination of osmotic coefficients and evaluation of vapor pressures for solutions of sodium bromide and sodium thiocyanate in methanal at 25 °C. *J Mol Liq*. 2003;106(1):1-14. doi:10.1016/S0167-7322(03)00016-3

275. Gomis V, Ruiz F, Boluda N, Saquete MD. Liquid–liquid–solid equilibria for ternary systems water + lithium chloride + pentanols. *Fluid Phase Equilibria*. 2004;215(1):79-83. doi:10.1016/S0378-3812(03)00361-3

276. Al-Sahhaf TA, Kapetanovic E, Kadhem Q. Salt effects on liquid–liquid equilibria in the partially miscible systems water+2-butanone and water+ethyl acetate. *Fluid Phase Equilibria*. 1999;157(2):271-283. doi:10.1016/S0378-3812(99)00040-0

277. Renard JA, Heichelheim HR. Ternary systems water-acetonitrile-salts. *J Chem Eng Data*. 1967;12(1):33-36. doi:10.1021/je60032a009

278. Taboada ME. Liquid–liquid and solid–liquid equilibrium of the 1-propanol+ lithium sulfate+ water system at 25, 35 and 45 C. *Fluid Phase Equilibria*. 2003;204(1):155–165.

279. Zafarani-Moattar MT, Nemati-Kande E, Soleimani A. Study of the liquid–liquid equilibrium of 1-propanol+manganese sulphate and 2-propanol+lithium sulphate aqueous two-phase systems at different temperatures: Experiment and correlation. *Fluid Phase Equilibria*. 2012;313:107-113. doi:10.1016/j.fluid.2011.10.004

280. Aznar M, Araújo RN, Romanato JF, Santos GR, d'Ávila SG. Salt Effects on Liquid−Liquid Equilibrium in Water + Ethanol + Alcohol + Salt Systems. *J Chem Eng Data*. 2000;45(6):1055-1059. doi:10.1021/je000029i

281. Marcilla A, Ruiz F, García AN. Liquid-liquid-solid equilibria of the quaternary system water-ethanol-acetone-sodium chloride at 25 °C. *Fluid Phase Equilibria*. 1995;112(2):273-289. doi:10.1016/0378-3812(95)02804-N

282. Olaya MM, Botella A, Marcilla A. Liquid–liquid–solid equilibria for the quaternary system water+ ethanol+ 1-pentanol+ sodium chloride at 25° C. *Fluid Phase Equilibria*. 1999;157(2):197–211.

283. Gomis V, Ruiz F, Boluda N, Saquete MD. Liquid−Liquid−Solid Equilibria for Ternary Systems Water + Sodium Chloride + Pentanols. *J Chem Eng Data*. 1999;44(5):918-920. doi:10.1021/je990071h

284. De Santis R, Marrelli L, Muscetta PN. Liquid—liquid equilibria in water—aliphatic alcohol systems in the presence of sodium chloride. *Chem Eng J*. 1976;11(3):207-214. doi:10.1016/0300-9467(76)80042-1

285. Chou T-J, Tanioka A, Tseng H-C. Salting Effect on the Liquid−Liquid Equilibria for the Partially Miscible Systems of n-Propanol−Water and i-Propanol−Water. *Ind Eng Chem Res*. 1998;37(5):2039-2044. doi:10.1021/ie9707578

286. Gomis V, Ruiz F, De Vera G, López E, Saquete MD. Liquid-liquid-solid equilibria for the ternary systems water-sodium chloride or potassium chloride-1-propanol or 2-propanol. *Fluid Phase Equilibria*. 1994;98:141–147.

287. De Santis R, Marrelli L, Muscetta PN. Influence of temperature on the liquid-liquid equilibrium of the water-n-butyl alcohol-sodium chloride system. *J Chem Eng Data*. 1976;21(3):324-327. doi:10.1021/je60070a008

288. Gomis V, Ruiz F, Asensi JC, Saquete MD. Liquid-liquid-solid equilibria for the ternary systems butanols+ water+ sodium chloride or+ potassium chloride. *J Chem Eng Data*. 1996;41(2):188–191.

289. Olaya MM, García AN, Marcilla A. Liquid-liquid-solid equilibria for the quaternary system water+ acetone+ 1-butanol+ sodium chloride at 25 C. *J Chem Eng Data*. 1996;41(4):910–917.

290. Renard JA, Heichelheim HR. Ternary systems. Water-acetonitrile-salts. *J Chem Eng Data*. 1968;13(4):485–488.

291. Lynn S, Schiozer AL, Jaecksch WL, Cos R, Prausnitz JM. Recovery of anhydrous Na2SO4 from SO2-scrubbing liquor by extractive crystallization: Liquid-liquid equilibria for aqueous solutions of sodium carbonate, sulfate, and/or sulfite plus acetone, 2-propanol, or tert-butyl alcohol. *Ind Eng Chem Res*. 1996;35(11):4236–4245.

292. Renard JA. Ternary Systems Water-Acetonitrile-Salts. *J Chem Eng Data*. 1966;11(2):169–171.

293. Nemati-Kande E, Shekaari H, Jafari SA. Liquid–liquid equilibrium of 1-propanol, 2-propanol, 2-methyl-2-propanol or 2-butanol+sodium sulfite+water aqueous two phase systems. *Fluid Phase Equilibria*. 2012;329:42-54. doi:10.1016/j.fluid.2012.05.012

294. Nemati-Knade E, Shekaari H, Jafari SA. Thermodynamic study of aqueous two phase systems for some aliphatic alcohols+sodium thiosulfate+water. *Fluid Phase Equilibria*. 2012;321:64-72. doi:10.1016/j.fluid.2012.02.015

295. Pirahmadi F, Dehghani MR, Behzadi B, Seyedi SM, Rabiee H. Experimental and theoretical study on liquid–liquid equilibrium of 1-butanol+water+NaNO3 at 25 and 35°C. *Fluid Phase Equilibria*. 2010;299(1):122-126. doi:10.1016/j.fluid.2010.09.013

296. Pirahmadi F, Behzadi B, Dehghani MR. Experimental measurement and thermodynamic modeling of liquid–liquid equilibrium for 1-pentanol+water+NaNO3 at 298.15 and 308.15K. *Fluid Phase Equilibria*. 2011;307(1):39-44. doi:10.1016/j.fluid.2011.05.003

297. El-Dossoki FI. The influence of cation, anion and temperature on the liquid–liquid equilibrium of some pentanols–water system. *Fluid Phase Equilibria*. 2011;305(2):161-168. doi:10.1016/j.fluid.2011.03.018

298. Katayama H, Miyahara M. Liquid−Liquid Phase Equilibria of (Ethanol or Methanol + Water) Containing either Dipotassium Hydrogen Phosphate or Sodium Dihydrogen Phosphate. *J Chem Eng Data*. 2006;51(3):914-918. doi:10.1021/je050408h

299. Wang J, Zhang Y, Wang Y. Liquid−Liquid Equilibria for 1-Propanol (or 2-Propanol)−Water Systems Containing Potassium Fluoride. *J Chem Eng Data*. 2002;47(1):110-112. doi:10.1021/je015506r

300. Renard JA, Oberg AG. Ternary Systems: Water-Acetonitrile-Salts. *J Chem Eng Data*. 1965;10(2):152-155. doi:10.1021/je60025a025

301. Olaya MM, Conesa JA, Marcilla A. Salt effect in the quaternary system water+ ethanol+ 1-butanol+ potassium chloride at 25 C. *J Chem Eng Data*. 1997;42(5):858–864.

302. Pereira MAP, Aznar M. Salt effect on (liquid+liquid) equilibrium of (water+tert-butanol+1-butanol) system: Experimental data and correlation. *J Chem Thermodyn*. 2006;38(1):84-89. doi:10.1016/j.jct.2005.03.025

303. Katayama H, Kitagawa K. Liquid−Liquid Phase Equilibria of (1-Propanol or 2-Propanol + Water) Containing Dipotassium Hydrogen Phosphate. *J Chem Eng Data*. 2006;51(6):2103-2106. doi:10.1021/je060232z

304. Hu M, Jin L, Li S 'ni, Jiang Y. Equilibrium Phase Behavior of Water + Propan-1-ol or Propan-2-ol + Cesium Chloride at (298.15, 308.15, and 318.15) K. *J Chem Eng Data*. 2005;50(6):2049-2052. doi:10.1021/je050265z

305. Hu M, Zhai Q, Liu Z, Xia S. Liquid−Liquid and Solid−Liquid Equilibrium of the Ternary System Ethanol + Cesium Sulfate + Water at (10, 30, and 50) °C. *J Chem Eng Data*. 2003;48(6):1561-1564. doi:10.1021/je0301803

306. Pirahmadi F, Dehghani MR, Behzadi B. Experimental and theoretical study on liquid–liquid equilibrium of 1-butanol+water+NH4Cl at 298.15, 308.15 and 318.15K. *Fluid Phase Equilibria*. 2012;325:1-5. doi:10.1016/j.fluid.2012.03.026

307. Zafarani-Moattar MT, Gasemi J. Phase Diagrams of Some Aliphatic Alcohols + Ammonium Dihydrogen Phosphate or Diammonium Hydrogen Phosphate + Water. *J Chem Eng Data*. 2002;47(3):525-528. doi:10.1021/je0102863

308. Cannon SL, Bethea RM, Heichelheim HR. Ternary liquid-liquid equilibrium by infrared spectrometry. *J Chem Eng Data*. 1970;15(3):419–421.

309. Stenger VA. Solubilities of various alkali metal and alkaline earth metal compounds in methanol. *J Chem Eng Data*. 1996;41(5):1111–1113.

310. Hu M, Zhai Q, Jiang Y, Liu Z. Solid−Liquid Phase Equilibria of Some Aliphatic Alcohols + Cesium Sulfate + Water. *J Chem Eng Data*. 2004;49(4):1070-1073. doi:10.1021/je049914h

311. Lide DR, ed. *CRC Handbook of Chemistry and Physics*. 79th edition. CRC-Press; 1998.

312. Volume Editors, Sazonov VP, Shaw DG, et al. IUPAC-NIST Solubility Data Series. 78. Acetonitrile Binary Systems. *J Phys Chem Ref Data*. 2002;31(4):989-1133. doi:10.1063/1.1494086

313. Wang L-X, Xia Q, Kang J, Du M-X, Zhang G-L, Zhang F-B. Measurement and Correlation of Solubilities of Potassium Chloride and Potassium Sulfate in Aqueous Glycerol Solutions. *J Chem Eng Data*. 2011;56(10):3813-3817. doi:10.1021/je200238s

314. Wang Y, Sha Z, Wang Y, Zheng Q. Solubility of KBr in Binary Solvents Formed by Acetone and Water in the Temperature Range between (288.15 and 313.15) K. *J Chem Eng Data*. 2008;53(11):2547-2549. doi:10.1021/je8003639

315. Long B, Zhao D, Liu W. Thermodynamics Studies on the Solubility of Inorganic Salt in Organic Solvents: Application to KI in Organic Solvents and Water–Ethanol Mixtures. *Ind Eng Chem Res*. 2012;51(28):9456-9467. doi:10.1021/ie301000b

316. Davidson AW, Geer HA. The Solubility of Nitrates in Anhydrous Acetic Acid. *J Am Chem Soc*. 1933;55(2):642-649. doi:10/dcn5vh

317. Hála J. IUPAC-NIST Solubility Data Series. 79. Alkali and Alkaline Earth Metal Pseudohalides. *J Phys Chem Ref Data*. 2004;33(1):1-176. doi:10.1063/1.1563591

318. Li M-Y, Wang L-S, Wang K-P, Jiang B, Gmehling J. Experimental measurement and modeling of solubility of LiBr and LiNO3 in methanol, ethanol, 1-propanol, 2-propanol and 1-butanol. *Fluid Phase Equilibria*. 2011;307(1):104-109. doi:10.1016/j.fluid.2011.03.017

319. Harris WS. *Electrochemical Studies in Cyclic Esters*. Univ. of California, Berkeley, CA (United States); 1958. doi:10.2172/4305596

320. Boryta DA. Solubility of lithium bromide in water between -50.deg. and +100.deg. (45 to 70% lithium bromide). *J Chem Eng Data*. 1970;15(1):142-144. doi:10/dwvn37

321. Gomis V, Ruiz F, Boluda N, Saquete MD. Liquid–liquid–solid equilibria for ternary systems water + lithium chloride + pentanols. *Fluid Phase Equilibria*. 2004;215(1):79-83. doi:10.1016/S0378-3812(03)00361-3

322. Chan, C.-Y. C, Khoo, K.H. M, Gryzlova, E.S. DG, Saugier-Cohen Adad, M.T. IUPAC-NIST Solubility Data Series. 61. Alkali Metal and Ammonium Perchlorates, Part I: Lithium and Sodium Perchlorates. Published online 1996:286.

323. Turner WES, Bissett CC. CCIV.—The solubilities of alkali haloids in methyl, ethyl, propyl, and isoamyl alcohols. *J Chem Soc Trans*. 1913;103(0):1904-1910. doi:10/dhbrxh

324. Brenner DK, Anderson EW, Lynn S, Prausnitz JM. Liquid-liquid equilibria for saturated aqueous solutions of sodium sulfate + 1-propanol, 2-propanol, or 2-methylpropan-2-ol. *J Chem Eng Data*. 1992;37(4):419-422. doi:10.1021/je00008a011

325. Raridon RJ, Kraus KA. Properties of organic-water mixtures. Activity coefficients of sodium chloride at saturation in aqueous solutions of some oxy-oxa compounds at 25.deg. *J Chem Eng Data*. 1971;16(2):241-243. doi:10/bght6n

326. Zeng Y, Li Z. Solubility Measurement and Modeling for the NaCl–NH4Cl–Monoethylene Glycol–H2O System from (278 to 353) K. *J Chem Eng Data*. 2015;60(8):2248-2255. doi:10/f7nt5r

327. Marcolli C, Krieger UK. Phase Changes during Hygroscopic Cycles of Mixed Organic/Inorganic Model Systems of Tropospheric Aerosols. *J Phys Chem A*. 2006;110(5):1881-1893. doi:10/bp94x4

328. Stephen H, Stephen T. *Solubilities of Inorganic and Organic Compounds. Volume 1, Part 2 Volume 1, Part 2*.; 1963. Accessed August 27, 2019. http://public.eblib.com/choice/publicfullrecord.aspx?p=1822014

329. Seidell A. *Solubilities of Inorganic and Organic Compounds; a Compilation of Quantitative Solubility Data from the Periodical Literature*. 2nd ed. New York, Van Nostrand; 1919. Accessed January 25, 2018. http://archive.org/details/solubilitiesino04seidgoog

330. Marcus Y. Thermodynamic functions of transfer of single ions from water to nonaqueous and mixed solvents: Part I - Gibbs free energies of transfer to nonaqueous solvents. *Pure Appl Chem*. 1983;55(6):977–1021. doi:10.1351/pac198355060977

331. Barthel J J|Schollmeyer,E. Untersuchungen zur Dispersion der komplexen Dielektrizitätskonstante wäßriger und nichtwäßriger Elektrolytlösungen. *Z Für Phys Chem*. 1977;104(1-3):59-72.

332. Wei Y, Chiang P, Sridhar S. Ion size effects on the dynamic and static dielectric properties of aqueous alkali solutions. *J Chem Phys*. 1992;96(6):4569-4573. doi:10.1063/1.462792

333. Loginova DV, Lileev AS, Lyashchenko AK. Microwave dielectric properties of aqueous solutions of potassium and cesium fluorides. *Russ J Phys Chem*. 2006;80(10):1626-1633. doi:10.1134/S003602440610013X

334. Pottel R, Lossen. Die komplexe Dielektrizitätskonstante wäßriger Lösungen einiger 1-1-wertiger Elektrolyte (Salze) im Frequenzbereich 0,5 bis 38 GHz. *Berichte Bunsenges Für Phys Chem*. 1967;71(2):135-146.

335. Barthel J, Schmithals F, Behret H. Untersuchungen zur Dispersion der komplexen Dielektrizitätskonstante wäßriger und nichtwäßriger Elektrolytlösungen. *Z Für Phys Chem*. 1970;71(1_3):115–131. doi:10/d5r342

336. Haggis GH, Hasted JB, Buchanan TJ. The Dielectric Properties of Water in Solutions. *J Chem Phys*. 1952;20(9):1452-1465. doi:10.1063/1.1700780

337. Buchner R, T. Hefter G, Barthel J. Dielectric relaxation of aqueous NaF and KF solutions. *J Chem Soc Faraday Trans*. 1994;90(17):2475-2479. doi:10/cdttz8

338. Barthel J, Hetzenauer H, Buchner R. Dielectric relaxation of aqueous electrolyte solutions. I. Solvent relaxation of 1:2, 2:1, and 2:2 electrolyte solutions. *Berichte Bunsenges Für Phys Chem*. 1992;96(8):988-997. doi:10.1002/bbpc.19920960807

339. Hasted JB, Roderick GW. Dielectric Properties of Aqueous and Alcoholic Electrolytic Solutions. *J Chem Phys*. 1958;29(1):17-26. doi:10.1063/1.1744418

340. Behret H F|Barthel,J. Untersuchungen zur Dispersion der komplexen Dielektrizitätskonstante wäßriger und nichtwäßriger Elektrolytlösungen. *Z Für Phys Chem*. 1975;96(1-3):73-88.

341. Barthel J, Kleebauer M, Buchner R. Dielectric relaxation of electrolyte solutions in acetonitrile. *J Solut Chem*. 1995;24(1):1-17. doi:10.1007/BF00973045

342. Delsignore M, Farber H, Petrucci S. Ionic conductivity and microwave dielectric relaxation of lithium hexafluoroarsenate (LiAsF6) and lithium perchlorate (LiClO4) in dimethyl carbonate. *J Phys Chem*. 1985;89(23):4968-4973. doi:10.1021/j100269a017

343. Winsor P, Cole RH. Dielectric properties of electrolyte solutions. 1. Sodium iodide in seven solvents at various temperatures. *J Phys Chem*. 1982;86(13):2486-2490. doi:10.1021/j100210a049

344. Barthel J, Bachhuber K, Büchner R. Dielectric Relaxation of NaClO4Solutions in Formamide, N-Methylformamide, and N,N-Dimethylformamide. *Z Für Naturforschung A*. 1995;50(1). doi:10.1515/zna-1995-0109

345. Kaatze U, Adolph D, Gottlob D, Pottel R. Static Permittivity and Dielectric Relaxation of Solutions of Ions in Methanol. *Berichte Bunsenges Für Phys Chem*. 1980;84(12):1198-1203. doi:10.1002/bbpc.19800841203

346. Pottel R E|Eck,R|Tresp,V. Dielectric Relaxation Rate and Static Dielectric Permittivity of Water and Aqueous Solutions at High Pressures. *Berichte Bunsenges Für Phys Chem*. 1989;93(6):676-681.

347. Barthel J, Behret H, Schmithals F. Dielectric Behaviour of solutions of Alkali Chlorides and Nitrates in the Microwave Region. *Berichte Bunsenges Für Phys Chem*. 1971;75(3-4):305-309.

348. Badiali J-P, Cachet H, Cyrot A, Lestrade J-C. Dielectric properties of electrolyte solutions. Lithium perchlorate solutions in tetrahydrofuran + benzene mixtures. *J Chem Soc Faraday Trans 2*. 1973;69:1339. doi:10.1039/f29736901339

349. Maribo-Mogensen B. Personal communication: Dielectric constants in non-aqueous systems. Published online March 14, 2018.

Relevant publications

- L. Kröger, S. Müller, I. Smirnova, and K. Leonhard

  Prediction/Modeling of Solvation Free Energies of Ionic Solutes in Neutral Solvents to be submitted

- S. Müller, A. González de Castilla, C. Taeschler, A. Klein, I. Smirnova

  Calculation of thermodynamic equilibria with the predictive electrolyte model COSMO-RS-ES: Improvements for low permittivity systems

  Fluid Phase Equilib. 2020, 506, 112368

- S. Müller, A. González de Castilla, C. Taeschler, A. Klein, I. Smirnova

  Evaluation and refinement of the novel predictive electrolyte model COSMO-RS-ES based on solid-liquid equilibria of salts and Gibbs free energies of transfer of ions

  Fluid Phase Equilib. 2019, 483, 165-174

- T. Gerlach, S. Müller, I. Smirnova

  Development of a COSMO-RS based model for the calculation of phase equilibria in electrolyte systems

  AIChE J. 2018, 64, 272-285

Student theses

Several project theses, bachelor theses and master theses were supervised in the context of this Ph.D. thesis. The results of the following theses have been partially or completely used in the present work:

- Andrés González de Castilla Mena, "*Evaluation of the applicability of COSMO-RS for the calculation of Salt Solubilities in Pure and Mixed Solvents*", Project thesis, 2017
- Andrés González de Castilla Mena, "*Analysis and Refinement of the COSMO-RS-ES Model Based on Free Energies of Transfer of Ions and Electrolyte Solubility Data*", Master thesis, 2018
- Kathrin Eckert, "*Löslichkeitsbestimmung und Untersuchung des Einflusses von Lithiumsalzen auf das Phasengleichgewicht in binären Lösungsmittelgemischen*", Bachelor thesis, 2018
- Jan Philipp Bittner, "*Systematical investigation of the influence of permittivity and density on the modeling of mean ionic activity coefficients using COSMO-RS-ES*", Master thesis, 2018
- Marian Nassar, "*Consistent Temperature-dependent Mean Ionic Activity Coefficients for Aqueous Systems: Evaluation & Refinement with COSMO-RS-ES*", Master thesis, 2019
- Tim Julian Brandt, "*Evaluierung von COSMO-RS-ES zur Berechnung von Setschenow-Konstanten*", Bachelor thesis, 2019

The results from the works of the following student assistants also contributed to this work: Arlette Flores Orozco, Florian Lorenzen, Hassan Raza, Lena Marie Ränger and Mónica Cornejo Infante.